# To Develop a Universal Gamut Mapping Algorithm

*Ján Morovič*

A thesis submitted
in partial fulfilment
of the requirements
of the University of Derby
for the degree of
Doctor of Philosophy

**October 1998**

**Note:** The formatting of this copy of the thesis is different from the formatting of the copies which were officially submitted and is not in accordance with the regulations of the University of Derby. If you refer to specific pages in this edition please include "Condensed format edition" in the reference.

# Abstract

When a colour image from one colour reproduction medium (e.g. nature, a monitor) needs to be reproduced on another (e.g. on a monitor or in print) and these media have different colour ranges (gamuts), it is necessary to have a method for mapping between them. If such a gamut mapping algorithm can be used under a wide range of conditions, it can also be incorporated in an automated colour reproduction system and considered to be in some sense universal.

In terms of preliminary work, a colour reproduction system was implemented, for which a new printer characterisation model (including grey–scale correction) was developed. Methods were also developed for calculating gamut boundary descriptors and for calculating gamut boundaries along given lines from them.

The gamut mapping solution proposed in this thesis is a gamut compression algorithm developed with the aim of being accurate and universally applicable. It was arrived at by way of an evolutionary gamut mapping development strategy for the purposes of which five test images were reproduced between a CRT and printed media obtained using an inkjet printer. Initially, a number of previously published algorithms were chosen and psychophysically evaluated whereby an important characteristic of this evaluation was that it also considered the performance of algorithms for individual colour regions within the test images used. New algorithms were then developed on their basis, subsequently evaluated and this process was repeated once more. In this series of experiments the new GCUSP algorithm, which consists of a chroma–dependent lightness compression followed by a compression towards the lightness of the reproduction cusp on the lightness axis, gave the most accurate and stable performance overall. The results of these experiments were also useful for improving the understanding of some gamut mapping factors – in particular gamut difference.

In addition to looking at accuracy, the pleasantness of reproductions obtained using various algorithms was also looked at and a strong and positive correlation was found between these two properties. It was also shown that the reproductions made with GCUSP were pleasant in isolation, which makes it a very good candidate for a standard universal gamut mapping algorithm.

# Errata

Equation 7.2.1 on page 108 is the corrected form of the equation given in the original version of the thesis (thanks to Gus Brown (RIT) for pointing out the problem with the original equation). Note that this change does not affect the rest of the thesis as the actual mapping of images using GCUSP was carried out correctly.

# Acknowledgements

Firstly, I would like to express my deepest gratitude to Prof. Ronnier Luo, my Director of Studies. His initial encouragement, continuous support and true friendship were essential to the coming about of this thesis. I would also like to thank Prof. Tony Johnson for sharing his valuable experience and for his constructive comments during our regular review meetings. Further, I would like to thank Dr. Peter Rhodes for his untiring support in both scientific and linguistic terms. Here I would also like to thank my external examiner Prof. Mark Fairchild as well as my internal examiner Prof. Lindsay MacDonald for their excellent questions and comments.

Thanks also go to Hewlett Packard for supporting this project in terms of financial and technological donations alike. Here I would particularly like to thank Mike Stokes of HP Boise and Jay Gondek of HP Vancouver.

Next, I would like to thank my colleagues at the Design Research Centre and later the Colour & Imaging Institute as well as all other observers for their patient participation in my psychophysical experiments, without which the majority of this work would not have been. More importantly, however, I would like to thank them for their friendship. Disregarding the risk of forgetting somebody, here is an alphabetical list: Ambrosia, Dr. Paula Bourges, Geoff Broadway, Angela Carr, Chun–Di (Vick) Chen, Wen-Lung Chou, Dr. Graham Finlayson, Dr. Shing-Sheng Guan, Dr. Guowei Hong, Steve Hordley, Lu-Yin (Grace) Juan, Hsiao–Pei (Alex) Lee, Robert Liang, Helen Lin, Maryliza Mazijoglou, Gerald Schaefer, Suchitra Sueeprason, Dr. Hong Xu and Peggy Zhu. I would also like to thank Anne Naylor and Suki Atwal for their valuable help.

Thanks also go to everybody from the Focolare and all my friends I didn't mention by name – I hope they can forgive this audacity :o). A special thanks also goes to Komerzialrat Eduard Harant for his magnanimous support throughout my studies.

Unspeakable thanks go to my entire family – first and foremost to my parents, my brother Peter and my sisters Monika and Beatka but also to my grandparents and other members of the family. Finally, I would like to thank God, who is Love.

# Contents

# List of Tables

# List of Figures

# Chapter 1

# Introduction

*Communication of all kinds is like painting –*
*a compromise with impossibilities.*
*Samuel Butler (II)*

## 1.1 Background

***Figure 1.1.1*** *Cave–wall painting from Lascaux, France.*

Colour image reproduction has always been about reproducing scenes between dissimilar media. Early on, the colour of animal skin was simulated with earth based pigments on stone walls (Figure 1.1.1). Later, more sophisticated colorants were used to create and subsequently copy illustrations in sacred manuscripts and with time more and more elaborate techniques were developed.

However, throughout history the art of simulating real life scenes or creating new images altogether on paper, leather, canvas, walls, wood or other materials was superimposed on a trial and error approach to colour image reproduction. The situation only began to change in this century with rapid advances in science and technology, which resulted in the development of colour printing and computing on the one hand and a better understanding of colour on the other.

Developing a complete scientifically based colour image reproduction system is now an aim towards which a sizeable research effort is directed. In this context, the aim of the present study is to provide this system with a universally applicable method for transforming colours from one medium so that they can be reproduced on another medium, which has a different colour range (this technique is generally referred to as **gamut mapping**).

The importance of having a gamut mapping algorithm, which gives good results for a wide range of original images and original and reproduction media combinations is becoming ever more important as the means for colour reproduction are becoming more and more wide–spread. This trend implies that colour reproduction is no longer a domain of specially–trained experts but is a facility required by a large audience. Hence, it is of importance to provide a transparent and unobtrusive system for colour reproduction and any such system will necessarily have to include gamut mapping as an essential feature. In this setting the availability of a universally applicable gamut mapping algorithm is of paramount importance as potential users would not have the skills for choosing among a number of algorithms intended only for application in specific situations and neither would having to make such a choice be acceptable. Furthermore a universal algorithm is also of use in a professional environment, as it can be used as a default method, which can be supplemented with proprietary gamut mapping algorithms designed for the reproduction of special images or for image reproduction with special intents.

How gamut mapping fits into colour reproduction as a whole, what the overall approach is to solving this problem and what is assumed while carrying out this study will be introduced in this chapter.

## 1.2 Cross–Media Colour Image Reproduction

Cross–media colour image reproduction, as understood today, is a process, which includes three essential elements: device characterisation, colour appearance modelling and gamut mapping, which can be combined into a **five–stage–transform** (MacDonald, 1993) for the reproduction of colour images (Figure 1.2.1).

Initially the description of an original image is available in a way, which is specific to the medium in which it is present. To be able to transfer colour information between different media, it is first best to describe different media in some medium–independent way. To this end, **device characterisation** describes colour reproduction media by relating their device–dependent colour specification to the characteristics of the resulting visual stimulus in terms of how it excites the eye. However, this alone is not sufficient for colour communication, as a given excitation of the eye can result in different colour appearances depending on viewing conditions. Further it is necessary to understand the perceptual attributes of a colour (e.g. lightness, chroma and hue), as it is these, which need to be communicated rather than some characteristics of stimuli depending only on the receptors in the eye and not on subsequent processing by the visual system. Hence, **colour appearance models** link the description of the stimulus to the perceptual attributes it has when seen in a given environment. These two elements (device characterisation and colour appearance modelling) would be sufficient for colour image reproduction if all media could reproduce the same set of colours. As this is not the case, there is a need for a way of overcoming any differences, which might exist between the sets of colours obtainable on different media, i.e. it is necessary to have an algorithm for mapping between their gamuts (Figure 1.2.2) – a **gamut mapping algorithm** (**GMA**).

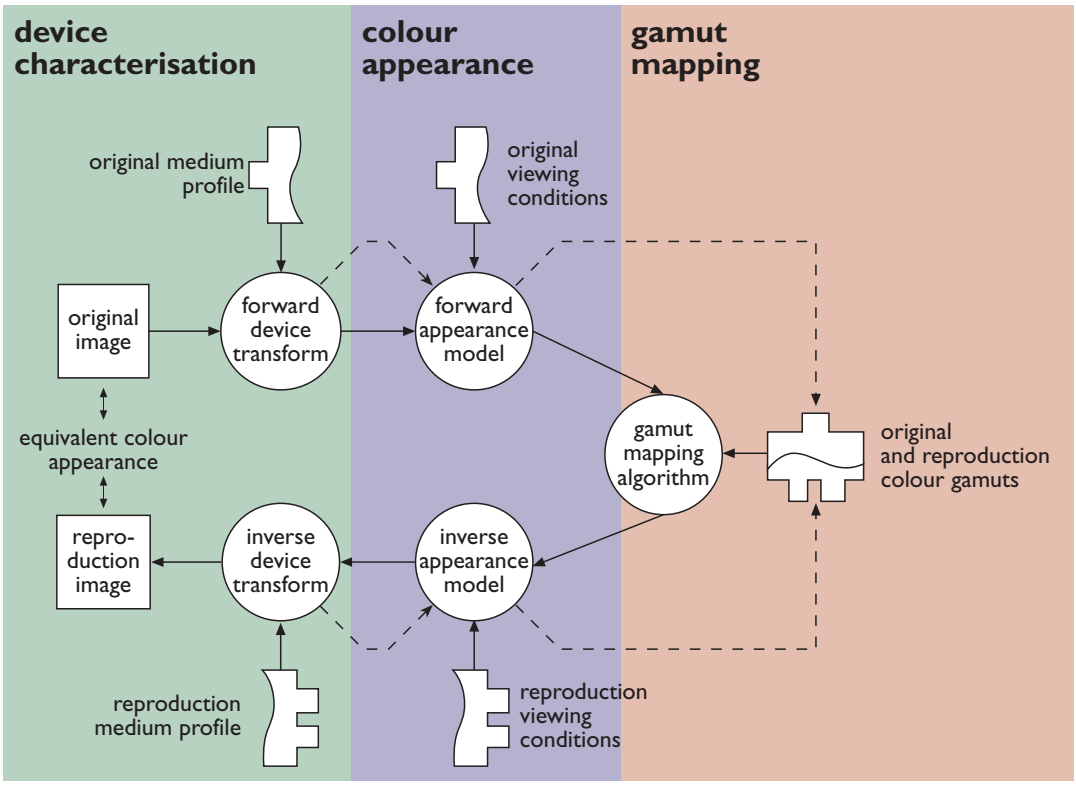


***Figure 1.2.1*** *Five–stage colour reproduction system*
*(dashed lines represent the data–flow for calculating the original and reproduction gamuts (Chapter 4)).*

The above is only a brief overview of colour reproduction, necessary for understanding the object of this study, and the state–of–the–art of its three elements will be dealt with in more detail in Chapter 2.

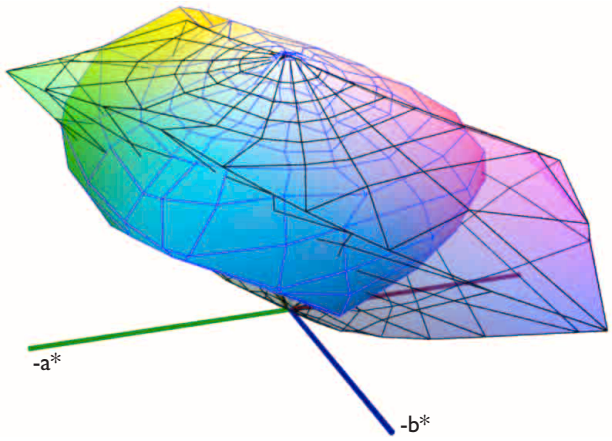


***Figure 1.2.2*** *Colour gamuts of a printed medium (solid) and a monitor (transparent).*

## 1.3 Assumptions and Aims

As with any subject, there is a range of possible interpretations of the basic terms used in gamut mapping as well. Therefore, to avoid misunderstandings, their definitions will be given next, whereby the definitions of an image were given by Braun *et al.* (1996), those of accuracy and pleasantness by Morovic and Luo (1998b) and the others by Morovic and Luo (1998d):

An **image** is a two–dimensional stimulus containing pictorial or graphical information whereby the **original** image is the image to which its **reproduction**s are compared in terms of some characteristic (e.g. accuracy).

A **colour reproduction medium** is a medium for displaying or capturing colour information, e.g. a CRT monitor, a digital camera or a scanner. Note, that in the case of printing, the colour reproduction medium is not the printer but the combination of printer, colorants and substrate. For the sake of conformity with accepted terminology, however, the term *device characterisation* will be used in this thesis, even though it would more correctly be labelled as medium characterisation.

A **colour gamut** is a range of colours achievable on a given colour reproduction medium (or present in an image on that medium) under a given set of viewing conditions – it is a volume in colour space (Figure 1.2.2). The **gamut boundary** is then a surface determined by its extremes.

**Colour gamut mapping** is a method for assigning colours from the reproduction medium to colours from the original medium or image (i.e. a mapping in colour space). As a number of solutions are possible, various colour reproductions intents can be pursued by gamut mapping. The most generic ones of these are accuracy and pleasantness but it is also possible to define others for specific applications (e.g. to provide an accurate reproduction of corporate identity colours while giving pleasant results for others).

The **accuracy** of a reproduction describes the degree of similarity between the original image and a reproduction of it. Note, that this characteristic is intrinsically relative (i.e. reproduction v. original)

**Pleasantness** on the other hand is a vaguer criterion, which will be used here to describe the degree to which an image is pleasant in isolation. To clarify the preceding circular definition, it can be said that pleasantness represents correspondence with preconceived ideas of how a given image should look according to an individual whereby this criterion encompasses contrast, lack of artefacts, sharpness, etc. Note, that unlike accuracy, pleasantness is absolute – at least as far as a given observer understands it at a given moment.

In the context of the above definitions, the development of algorithms described in this study assumes that the appearance of the original image is what needs to be reproduced and that the original image has a pleasant appearance. Hence the algorithms aim at an **accurate reproduction** and have no image enhancing intents. One could argue that it is often a pleasant reproduction, which is needed and as this is an important question, the relationship between the pleasantness and accuracy of reproductions made with GMAs dealt with here was investigated in Experiment 4 and will be described in Chapter 11.

It further needs to be noted that this study focuses on **gamut compression** – i.e. gamut mapping from a larger to a smaller gamut, as this is most often needed in situations where a universal gamut mapping would be used at present. As the reproduction gamuts in this study were not smaller than the original gamuts in all parts of colour space, gamut mapping was only applied in the areas where it was necessary and no changes were made to original colours when the reproduction gamut was larger or equal to the original gamut along a given line of compression. In the context of accurate reproduction it was though to be more important to focus on gamut compression. For an investigation of gamut expansion (gamut mapping from a smaller to a larger gamut) refer to Hoshino (1991).

Before going into the details of this study, it is of great importance to clearly understand its aim – a **universal gamut mapping algorithm**. Here it will be defined as a gamut mapping algorithm, which gives consistently good results for a wide range of media combinations and original images. It is not meant to be a method, which gives the best result for every image under every possible set of conditions. Instead, it ought to be seen as a default method, which can be used for the majority of images and media combinations and which can be supplemented by proprietary solutions for use in special applications.

Further it needs to be noted that no claims are made about the universality of algorithms developed in this study, as this would require far more extensive testing than is practical in the period of time available and as this would also require the investigation of gamut expansion and the use of a larger variety of test images. The use of the term "universal" in the title of this thesis denotes its aim rather than a label for its outcomes.

## 1.4 A Method for Developing GMAs

Various methods have previously been used for developing GMAs whereby in a small number of cases the starting point was a set of experimental data, which was then modelled. However, in the majority of studies a model was first formulated and then tested experimentally (or the model's parameters were established on that basis).

The approach taken in this study is a combination of these two styles whereby the starting point is a selection of existing GMAs, which are then experimentally evaluated. The experimental method used in most experiments of this study has a special feature, which is that in addition to evaluating the overall image, individual regions within the image are also evaluated. As in the paper by MacDonald and Morovic (1995), these **image regions** are chosen so as to have characteristic colours and their evaluation therefore gives information about the performance of GMAs in different parts of colour space. This kind of information is a solid and quantitative basis for making alterations to GMAs.

The results of the evaluation of existing GMAs then serve as a starting point for the development of new algorithms and as can be seen from its description, this method fundamentally lends itself to iteration. This study therefore has two main parts – psychophysical experimentation and gamut mapping algorithm development – which alternate (Figure 1.4.1). Note, that the nature of this method is in some ways analogous to evolution, whereby individuals are substituted by GMAs and

natural selection by their performance in terms of psychophysical evaluation. This is also why the "generation" of an algorithm is referred to in the context of this study.

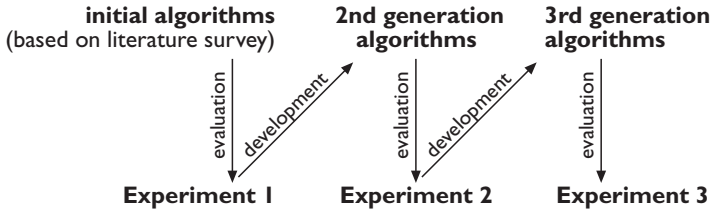


***Figure 1.4.1*** *Overview of gamut mapping development.*

Three of the four Experiments (1–3) in this study are parts of the above process and Experiment 4 is an investigation of the relationship between accuracy and pleasantness. In Experiment 1, previously proposed algorithms were compared amongst each other by psychophysical means and on its basis new algorithms were developed. These were subsequently evaluated in relationship to each other and to a selection of initial algorithms in Experiment 2. A set of new algorithms was again developed after Experiment 2 and they were tested in Experiment 3.

## 1.5 Thesis Outline

After the present chapter, which intends to be an introduction to this study, Chapter 2 will give an overview of previous work done in this subject and of work on which this study builds. This will include an introduction to colorimetry, psychophysical methods, colour appearance, colour reproduction media and their characterisation and calibration and, most importantly, gamut mapping.

Chapter 3 describes the colour reproduction system implemented for the purposes of this study, including details of work carried out on printer characterisation. Chapter 4 contains instructions for using the gamut boundary calculation methods developed for this study. This is followed by Chapter 5, which deals with the experimental methods used for the evaluation of GMAs and gives details of data analysis procedures as well.

Chapter 6 describes the set of previously published algorithms, which were evaluated in Experiment 1. This chapter also contains the results of Experiment 1, which served as the basis for developing the set of second generation GMAs described in Chapter 7.

Chapter 8 is an overview of Experiment 2, where second generation algorithms were evaluated alongside two of the initial GMAs. The algorithms developed from these results are then described in Chapter 9. The final evaluation of GMAs from all three generations, which is done using two different printed media, is described in Chapter 10.

Chapter 11 then presents Experiment 4, which was carried out to investigate the relationship between the accuracy of GMAs evaluated in Experiment 2 and their pleasantness when seen in isolation.

Finally, Chapter 12 compares the results from the individual experiments and summarises the findings of this study.

## 1.6 Summary

The context in which this study is set and on which it builds was introduced in this chapter alongside a discussion of the importance of this study's aim – a universal gamut mapping algorithm. Definitions were given of basic terminology and the assumptions and aims were also given. With the understanding of the above points it is now possible to proceed with the description of the development of universal gamut mapping algorithms as carried out in this study.

# Chapter 2

# Literature Survey

*Nature has given to men one tongue,*
*but two ears, that we may hear from others*
*twice as much as we speak.*

*Epictetus*

# 2.1 Colorimetry

Human vision relies on the stimulation of receptors in the retina of the eye. There are two types of receptors: **rods**, which give monochromatic vision under low levels of illumination and **cones**, which give colour vision under normal levels of illumination and of which there are three kinds. Colour sensation then arises when **electromagnetic radiation** with wavelengths of between approximately 380 nm and 780 nm is incident on these receptors and this stimulation is processed and interpreted by the human visual system. As a result of this, colour stimuli can be described by their *spectral power distribution* (SPD). However, as the human visual system only uses three kinds of cones it can also be described by a set of three values, which are the multiples of the SPD and a set of weighting functions (one for each kind of receptor). Two sets of standard weighting functions – for samples subtending 2° and 10° – have been defined by the CIE (*Commission Internationale de l'Éclairage*) in 1931 and 1964 as the *Standard Colorimetric Observer* and *Supplementary Standard Colorimetric Observer* colour matching functions respectively and are denoted by $\bar{x}(\lambda),\bar{y}(\lambda),\bar{z}(\lambda)$ and $\bar{x}_{10}(\lambda),\bar{y}_{10}(\lambda),\bar{z}_{10}(\lambda)$ respectively (Figure 2.1.1).

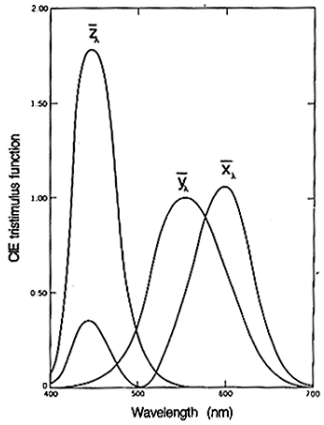


***Figure 2.1.1*** *CIE 1931 Standard Colorimetric Observer's colour matching functions (reproduced from Jackson et al. (1994)).*

It is important to note that these are not the actual response characteristics of the cones, but linear transformations of them, so that the $\bar{y}_\lambda$ function is identical to the V(λ) function and thereby represents perceived luminance. Furthermore, the three numbers representing the cone responses are only representations of the total SPD of the light incident on the retina. As this is made up of the characteristics of the **illuminant** and the **illuminated object**, a pair of stimuli could match under one illuminant but mismatch under another, whereby such a pair is called *metameric*.

This makes the specification of the illuminant equally important as the specification of the cone responses for quantifying colour. To this end, the CIE has specified a range of standards, of which the most important for industrial applications are the illuminants A (tungsten light), D50 (daylight with a *correlated colour temperature* (CCT) of 5000K) and D65 (6500K) (Hunt, 1995). In addition to these illuminants, a daylight illuminant with the CCT of 9300K is widely used for defining the white point of CRTs. A very good overview of CIE colorimetry (CIE, 1986) is given by Hunt (1995) and most of the present summary is based on that source (all quotes, figures and formulæ are taken from there, unless stated otherwise).

## 2.1.1 CIE 1931 XYZ Colour Space

The set of three numbers mentioned above constitutes the units of the first CIE colour space – CIE XYZ, whose coordinates are referred to as **tristimulus values** and can be calculated using the following formulæ:

$$X = k \sum \bar{x}_\lambda P_\lambda \Delta\lambda$$
$$Y = k \sum \bar{y}_\lambda P_\lambda \Delta\lambda \qquad (2.1.1)$$
$$Z = k \sum \bar{z}_\lambda P_\lambda \Delta\lambda$$

Here $P_\lambda$ stands for the power of the stimulus at wavelength $\lambda$ and $k$ is a scaling constant. All other CIE–defined colour spaces are derived from this one by various transformations.

For plotting the position of individual colours, a two dimensional chromaticity diagram was also derived from XYZ and its axes are defined as:

$$x = \frac{X}{X+Y+Z};\ y = \frac{Y}{X+Y+Z} \qquad (2.1.2)$$

Even though the XYZ colour space is very useful for quantifying colour stimuli, it has one serious shortcoming: equal distances in various parts of the colour space represent different perceptual colour differences as shown in Wright's results (Figure 2.1.2). It can be seen that, for example, the length of segments, which represent equal perceived difference from the blue region differ from those in the green region by a factor of five (Figure 2.1.2a). In a **uniform colour space** they ought to have the same length.

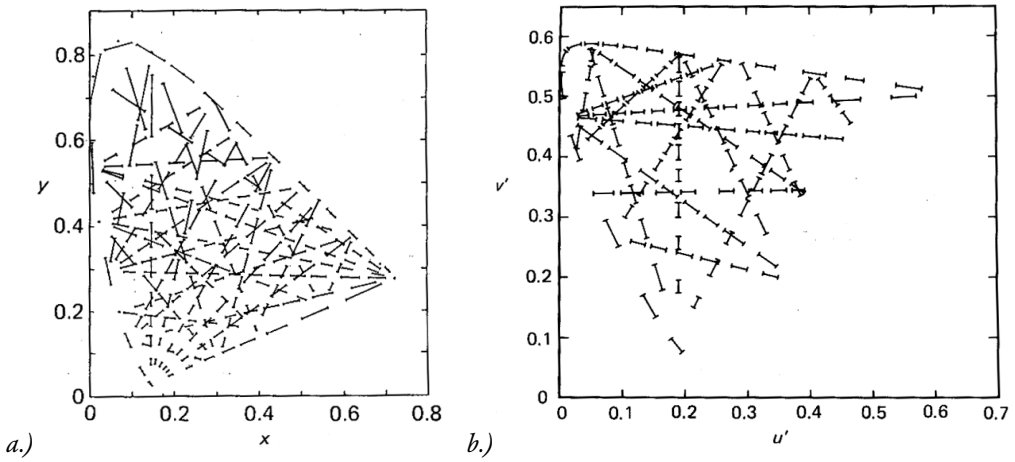


***Figure 2.1.2*** *a.) xy and b.) u'v' chromaticity diagrams (line segments represent equal perceptual colour differences).*

## 2.1.2 CIE 1976 Uniform Colour Spaces

To correct this, a new chromaticity diagram (the *CIE 1976 uniform chromaticity scale diagram)* was derived, whereby its axes are defined as follows:

$$u' = \frac{4X}{X+15Y+3Z};\ v' = \frac{9Y}{X+15Y+3Z} \qquad (2.1.3)$$

### *2.1.2.1 CIELUV*

This chromaticity diagram was further developed into the *CIE 1976 (L*u*v*) uniform colour space* – CIELUV (Hunt, 1987, pp. 114), which is one of the attempts to define a perceptually uniform colour space. It has the property that straight lines from the *xy* chromaticity diagram are mapped onto straight lines in the *u'v'* diagram as well as the CIELUV space itself. This colour space is mainly used for the lighting, CRT and television industries as well as applications involving additive mixing. It is shown in Figure 2.1.3 where its axes are defined as:

$$
\begin{aligned}
L^* &= 116(Y/Y_n)^{1/3} - 16 \quad \text{if } (Y/Y_n) > 0.008856 \\
L^* &= 903.3(Y/Y_n) \qquad\quad \text{if } (Y/Y_n) \le 0.008856 \\
u^* &= 13L^*(u' - u'_n) \\
v^* &= 13L^*(v' - v'_n)
\end{aligned}
\tag{2.1.4}
$$

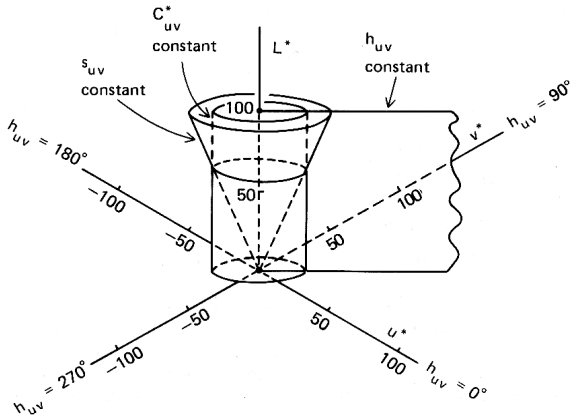


***Figure 2.1.3*** *The CIE 1976 L*u*v* colour space.*

In the above formulæ the index *n* denotes the coordinates of the reference white, which can either be the *perfect diffuser* or *transmitter* under the light source used (**absolute colorimetry**) or the white point of the medium on which a colour is presented (**relative colorimetry**). L* predicts the *lightness* of a given colour, which is on a scale from 0 (black) to 100 (white). Further, it is also possible to calculate predictors of other perceptual attributes of a colour:

*CIELUV hue–angle* $h_{uv} = \arctan(v^*/u^*)$ (2.1.5) predicts a colour's hue, which ranges from 0° to 360° following the colours of the spectrum.

*CIELUV chroma* $C^*_{uv} = (u^{*2} + v^{*2})^{1/2}$ (2.1.6) describes the chromatic content of a colour and is on an open–ended scale where chroma increases from 0 (achromatic colours).

*CIELUV saturation* $s_{uv} = C^*_{uv} / L^*$ (2.1.7) describes the strength of a colour and is again on an open–ended scale.

Given the above formulæ of CIELUV's predictors, a colour stimulus can be described using three perceptual attributes: lightness (L*), hue ($h_{uv}$) and chroma ($C^*_{uv}$). To understand the descriptions of the above predictors more clearly, it is also necessary to know the definitions of the perceptual attributes they predict. These are again based on Hunt (1995) and are the following:

- **Lightness** is the brightness of a colour relative to the brightness of the reference white (whereby **brightness** is the "attribute of visual sensation according to which an area appears to exhibit more or less light")
- **Hue** is the "attribute of a visual sensation according to which an area appears to be similar to one, or to proportions of two, of the perceived colours red, yellow, green and blue."
- **Chroma** is "the colourfulness of an area judged in proportion to the brightness of a similarly illuminated area that appears to be white or clearly transmitting."
- **Saturation** is "the colourfulness of an area judged in proportion to its brightness."
- **Colourfulness** is the "attribute of a visual sensation according to which an area appears to exhibit more or less of its hue".

In addition to the predictors of perceptual attributes, a way of quantifying colour difference is also needed. This was defined by the CIE as the Euclidean distance between two colours under comparison – therefore the *CIELUV colour difference* ($\Delta E^*_{uv}$) is defined as $\Delta E^*_{uv} = [(\Delta L^*)^2 + (\Delta u^*)^2 + (\Delta v^*)^2]^{1/2}$ (2.1.8).

### 2.1.1.2 CIELAB

An additional colour space was defined by the CIE at the same time as CIELUV and for the same purpose of uniformity – *CIE 1976 (L*a*b*) uniform colour space* – CIELAB. It is currently used by the colorant and graphic arts industries as well as for other applications of subtractive mixing (e.g. surface colour industries) and its coordinates are defined by the following transformation of XYZ:

$$L^* = 116\,(Y/Y_n)^{1/3} - 16 \text{ if } Y/Y_n > 0.008856$$
$$L^* = 903.3\,(Y/Y_n) \text{ if } Y/Y_n \le 0.008856$$
$$a^* = 500\,[f(X/X_n) - f(Y/Y_n)]$$
$$b^* = 200\,[f(Y/Y_n) - f(Z/Z_n)]$$
where if $f(N/N_n) > 0.008856\ (N \in \{X,Y,Z\})$ then
$$f(N/N_n) = (N/N_n)^{1/3},$$
otherwise
$$f(N/N_n) = 7.787(N/N_n) + 16/116 \qquad (2.1.9)$$

$X_nY_nZ_n$ represent the reference white, $h_{ab}$, $C^*_{ab}$ and $\Delta E^*_{ab}$ can be calculated from formulas (2.1.5), (2.1.6) and (2.1.8) respectively by substituting a* for u* and b* for v*. There is no chromaticity diagram associated with this colour space and saturation is not defined in CIELAB either, due to the non–linear nature of the a* and b* formulæ.

In literature, the CIE colour spaces are referred to as **device independent** as they do not depend on any particular input or output device, i.e. scanner, camera, monitor, printer or transparency. The characteristic of what are referred to as **device dependent** colour spaces is, that they are intrinsically linked to a particular device. These colour spaces are at least three dimensional, limited by the maximum amounts of the device's colorants and device gamuts are cubes (or hyper–cubes) in them.

Both the CIELAB and CIELUV colour spaces are imperfect attempts to define a perceptually uniform colour space as they each have different deficiencies and neither of them is generally considered as superior to the other. Nonetheless, they both offer significant improvements over using the XYZ tristimulus colour space for gamut mapping.

## 2.1.3 Colour Difference Formulæ

Determining the difference between two stimuli is of significant importance in colorimetry and the main objective for designing colour difference formulæ is to make their results as close to human judgements as possible. The simplest forms of colour difference ($\Delta E^*_{ab}$ and $\Delta E^*_{uv}$), which were already presented consider the distance between the coordinates of two stimuli in a given colour space to be their colour difference. However, due to the non–uniformity of colour spaces, advanced colour difference formulæ were developed, which more accurately predict human judgements. There are many different formulæ which have been developed to this end and work is still being carried out to improve them (Luo, 1995).

In addition to the two advanced colour difference formulae, which will be presented next, it is useful to be aware of the development of models for the calculation of colour differences between complex images which take into account their **spatial characteristics**. An example of such a model is **S–CIELAB** (Zhang and Wandell, 1996) where images are first transformed into an *opponent colour space* (whose dimensions are *luminance*, *redness–greenness* and *yellowness–blueness*) where each of the three channels is blurred in a way which corresponds to the spatial sensitivity of the human visual system to the given channel (i.e. the luminance channel is blurred least and the yellowness–blueness channel is blurred most). Finally, CIELAB coordinates are computed for each pixel of the filtered images and colour difference, which now takes into account spatial characteristics, is

calculated as in CIELAB. Even though this model is an advance compared to colour difference formulae, which are designed for uniform colour patches, it still needs to be improved significantly before it can reliably predict the results of psychophysical experiments.

### 2.1.1.1 CMC(l:c)

Among the most widely used advanced colour difference formulæ is the CMC(l:c) colour difference formula which apart form improving accuracy also provides a means for changing the relative importance of lightness and chroma. The $\Delta E_{CMC(l:c)}$ colour difference can be calculated using the following formulæ (Clarke *et al.*, 1984):

$$\Delta E_{CMC(l:c)} = \sqrt{\left(\frac{\Delta L^*}{lS_L}\right)^2 + \left(\frac{\Delta C^*}{cS_C}\right)^2 + \left(\frac{\Delta H^*}{S_H}\right)^2}$$

where $S_L = 0.040975L^*_1/(1+ 0.01765L^*_1)$
unless $L^*_1<16$ then $S_L=0.511$
$S_C = 0.0638C^*_1/(1+0.0131C^*_1) + 0.638$
$S_H = S_C(Tf + 1 - f)$ (2.1.10)

$$f = \sqrt{\frac{C_1^{*4}}{C_1^{*4} + 1900}}$$

$T = 0.36 + |0.4\cos(h_1 + 35)|$
unless $h_1$ (the hue angle of the first colour) is between 164° and 345°, when:
$T = 0.56 + |0.2\cos(h_1 + 168)|$

Here $L^*_1$, $C^*_1$ and $h_1$ represent the standard from which the colour difference is determined and $\Delta L^*$, $\Delta C^*$ and $\Delta H^*$ are calculated as in CIELAB. When the *l:c* ratio is set to 1:1, the $\Delta E$ values are meant to represent the **perceptibility** of colour difference whereas if set to 2:1 they stand for **acceptability**.

### 2.1.1.2 CIE94

Another colour difference formula currently used is the CIE94 colour difference formula shown in Equation 2.1.11.

$$\Delta E = \sqrt{\Delta L^{*2} + \left(\frac{\Delta C^*}{1 + 0.045C_1^*}\right)^2 + \left(\frac{\Delta H^*}{1 + 0.015C_1^*}\right)^2} \quad (2.1.11)$$

However, the CMC formula described above will be used in this study.

## 2.2 Psychophysics

As was pointed out above, colour is a phenomenon, which arises when electromagnetic radiation interacts with the human visual system. In this context, the previous section focused on quantifying the stimulus in terms directly related to its physical properties. However, it also described methods for predicting some perceptual attributes (e.g. lightness, chroma and hue) of these physical quantities. This was done on the basis of psychophysics, which according to Fairchild (1998, pp. 43) "is the scientific study of the relationships between the physical measurements of stimuli and the sensations and perceptions that those stimuli evoke."

The importance of understanding psychophysics follows already from this and is further strengthened as it is a tool for verifying the accuracy of previous modelling and for assessing such properties which have not been modelled at all or which have not been modelled satisfactorily. For the pur-

poses of the present study, psychophysics was used to determine the accuracy and pleasantness of reproductions made using different gamut mapping algorithms and the present overview of psychophysics is done with this in mind and is not intended as an overview of the entire field.

Most of modern experimental psychology has its origins in the work of Weber (whose law states that the ratio of $\Delta I/I$ is constant, whereby $I$ is stimulus intensity and $\Delta I$ is the change in stimulus intensity needed for achieving a just noticeable difference) and Fechner (whose law states that the relationship between the magnitudes of physical stimuli and resulting perceptions is logarithmic) in the nineteenth century and Stevens (whose law states that this relationship is exponential) in the present century.

For the purposes of the present study the most relevant part of psychophysics are the methods used for scaling perceptual characteristics of stimuli, three of which are introduced next. However, it is first necessary to have an understanding of the kinds of **scales**, which can result from these methods. They are presented in ascending order of how much they say about what they describe and each of these scales also has the properties of the preceding scales in the list. The simplest scale is the **nominal** scale, which results in a naming or labelling of what it is applied to. In the case of an **ordinal** scale, its members are either in ascending or descending order in terms of the characteristic scaled, but it does not provide information about the magnitude of differences between individual scale values. With an **interval** scale, the differences between scale values represent equal differences in terms of the scaled characteristic and a **ratio** scale also has a meaningful zero–point.

### 2.1.1 Pair Comparison

The most important psychophysical method for this study is the pair comparison technique, which will be dealt with in detail in Chapter 5. Here it suffices to note that it can be used for quantifying properties of stimuli on an interval scale. These scale values are obtained on an experimental basis whereby each pair combination of a set of stimuli is shown to observers in isolation or alongside a reference stimulus. Observers are then asked to chose the stimulus which exhibits more of the property being evaluated and when the experiment is not forced–choice, observers are also allowed to judge both of a pair of stimuli to be equal. With the help of Thurstone's **Law of Comparative Judgement** (Thurstone, 1927), data collected in this way can then be transformed into interval scale data where scores represent the distance of a given stimulus from the mean score of the set of stimuli being evaluated.

### 2.1.2 Category Judgement

Category judgement, which will also be dealt with in more detail in Chapter 5, is a method where a property's possible magnitudes are represented by an equi–interval scale of categories and observers are asked to judge into which category a particular stimulus belongs. Based on the **Law of Categorical Judgement** (Torgerson, 1954) this data can then be transformed into an interval scale where scores are based on the relative position of stimuli with respect to category boundaries rather than with respect to one another (Bartleson, 1984).

### 2.1.3 Magnitude Estimation

In this method observers are asked to judge the extent to which a stimulus exhibits a given property and can directly result in a ratio scale.

For more details on psychophysics in general and these methods in particular see the work of Thurstone (1927), Torgerson (1954), Stevens (1975), Gescheider (1976), Bartleson (1984), Kavsek (1993) and Fairchild (1998).

### 2.1.4 Summary

The three scaling methods described above can all be used to evaluate properties of visual stimuli, including the accuracy and pleasantness of reproductions investigated in this study. Note, that the above methods were presented in order of complexity for the observer (the first method involves only a relative binary or ternary choice, the second involves an absolute choice from a fixed set of possibilities and the third requires a direct quantification of a given property) and hence also in order of reliability. However, reliability comes at the expense of time as the pair comparison experiment requires significantly longer to carry out than category judgement or magnitude estimation. In spite of this, it is the method chosen for most of the experimental work in this study as it requires the least amount of training (which could also introduce bias to the results) and is also the simplest.

## 2.3 Colour Appearance

The appearance of a given stimulus (as specified in terms of XYZ tristimulus values) depends on the **context** in which it is seen. This is of particular importance for colour reproduction, where in most practical situations the aim is to reproduce the **appearance** of colours or colour images and not some **physical properties** of stimuli (more on this in Section 2.4.3). As the CIE XYZ system only deals with quantities derived from physical properties of stimuli and not their appearance and as it only deals with individual stimuli, it is necessary to have some way of deriving their perceptual attributes and take into account the influence of the environment in which they are seen. The list of phenomena not taken into account in the XYZ system is fairly extensive, hence only phenomena which are most relevant to complex images will be discussed next. Note, that this overview is based primarily on the work of Hunt (1995) and Fairchild (1998) and will be followed by an overview of three of the colour appearance models most relevant to colour image reproduction in general and to this study in particular.

### 2.3.1 Colour Appearance Phenomena

As far as the global conditions under which a colour is viewed are concerned, there are a number of factors affecting its appearance. Firstly, the level of illumination has an effect on apparent colourfulness and contrast, whereby an increase in luminance level results in an increase in colourfulness – **Hunt effect** (Hunt, 1987) – as well as contrast – **Stevens effect**. Secondly, changes in the light source's chromaticity do not always result in corresponding changes of a stimulus' perceptual attributes – this is referred to as **chromatic adaptation** and is due to sensory as well as cognitive factors (Fairchild, 1992). When the chromaticity of the illuminant is similar to the locus of Planckian radiators, the colour of the illuminant is significantly discounted and non–selective samples (i.e. ones where spectral reflectance or transmittance is wavelength–independent) appear neutral. However, if it is different, these samples are tinged with the hue of the light source when they are light and dark colours have a bias towards the complementary hue – **Helson–Judd effect**. While considering these phenomena, it ought to be kept in mind that the extent of their effect is also influenced by the kind of object considered. For example, the colours of some objects like skin, grass and the sky, which are called **memory colours** (Hering, 1920) are less susceptible to change than other colours.

As for the effect of a colour's local surroundings, the **simultaneous contrast** phenomenon is most prominent. It is used for describing the situation whereby a colour appears lighter when seen against a dark background and *vice versa*. The hue and saturation of the observing field also have a similar effect by changing the central colour in the direction complementary to the surround's attribute (however, the opposite happens when the central colour is below approximately 1/3° of angular subtense in which case **assimilation** – also known as *spreading* – occurs). Another similar

phenomenon is **crispening** whereby the difference between similar colours increases when seen against a background similar to them. The lightness of the **surround** also influences image contrast, which is smaller when it is dim or dark, and colourfulness, which is larger against a dim or dark surround (Bartleson and Breneman, 1967; MacDonald *et al.*, 1990).

Finally, it is important to note, that even if all of the above phenomena were modelled perfectly, such a model would only make predictions, which would apply to a theoretical observer and an individual's perception of a colour stimulus would most probably differ from it at a given moment, just as it would differ from the perception the same stimulus evokes in another observer. On the one hand this can be seen as a problem, however, on the other this also means that a model can be considered to be of use if it does not differ from a group of observers more than individual observers differ from each other. Under such conditions its predictions can be considered to be as reliable as the predictions of an individual observer.

### 2.3.2 The Observing Field

As could be seen from the above section, the environment in which a colour is seen has an effect on how it appears. However, different parts of this environment – the observing field affect the central colour to different degrees. This is also taken into account in the following colour appearance models whereby it is useful to consider the following classification of the observing field given by Hunt (1995):

- *Colour Element* – central area of the observing field typically subtending 2° of angular subtense.
- *Proximal Field* – immediate environment of the colour element extending typically for about 2° from the edge of the colour element in all or most directions.
- *Background* – environment of the colour element extending typically for about 10° from the edge of the proximal field. When the proximal field has the same colour as the background, the latter is taken as extending from the edge of the colour element.
- *Surround* – field outside the background.
- *Adapting Field* – total environment of the colour element – including proximal field, background and surround and extending to the limit of vision in all directions.

It can be seen that this classification is primarily intended for the modelling of uniform colour patches, but it is also of use in modelling the appearance of individual colours in complex images as it includes some of the most important factors affecting colour appearance.

### 2.3.3 RLAB

This colour appearance model (Fairchild and Berns, 1993; Fairchild, 1994; Fairchild, 1998) is aimed at applications where the speed of transformation is important and where complex images are considered instead of simple colour patches. The model consists of two stages: first the tristimulus coordinates of a colour are transformed into a set of reference viewing conditions (D65, 2° observer, 318 cd/m$^2$ illumination and hard copy medium) using a chromatic adaptation transform which can allow for incomplete adaptation when visual display units (VDUs) are viewed. Then, appearance attributes are calculated from the adapted cone responses and to obtain tristimulus values for another set of viewing conditions, the model is analytically reversed. To predict the appearance attributes of a colour, the following parameters are required:

- *adopted white under source viewing conditions* $X_W Y_W Z_W$
- *absolute luminance of adopted white* $Y_n$
- *sample under source viewing conditions* $XYZ$
- *information about the medium and the nature of the surround*

Note, that $X_W Y_W Z_W$ is the adopted white in terms of relative tristimulus values (scaled so that $Y_W$=100). The following steps then describe the implementation of the model:

*Step 1 Fundamental tristimulus values*

$$\begin{bmatrix} L \\ M \\ S \end{bmatrix} = \mathbf{M} \begin{bmatrix} X \\ Y \\ Z \end{bmatrix}; \; M = \begin{bmatrix} 0.3897 & 0.6890 & -0.0787 \\ -0.2298 & 1.1834 & 0.0464 \\ 0.0 & 0.0 & 1.0000 \end{bmatrix} \tag{2.3.1}$$

The elements in the matrix are normalised so as to give equal cone responses (L=M=S=100) for the equi–energy illuminant $S_E$ (X=Y=Z=100). Note, that this transformation is also carried out for the adopted white, which results in $L_W M_W S_W$.

*Step 2 Chromatic adaptation*

$$\mathbf{A} = \begin{bmatrix} a_L & 0 & 0 \\ 0 & a_M & 0 \\ 0 & 0 & a_S \end{bmatrix}$$

$$a_L = \frac{p_L + D(1.0 - p_L)}{L_n}; \; p_L = \frac{1.0 + Y_n^{1/3} + l_E}{1.0 + Y_n^{1/3} + 1.0/l_E}; \; l_E = \frac{3L_W}{L_W + M_W + S_W} \tag{2.3.2}$$

$a_M$, $a_S$, $p_M$, $p_S$, $m_E$ and $s_E$ are calculated analogously and D represents the contribution of cognitive chromatic adaptation to the transformation (D=1 for hard copy, D=0 for soft copy and D=0.5 for projected transparency).

*Step 3 Reference XYZ*

$$\begin{bmatrix} X_{ref} \\ Y_{ref} \\ Z_{ref} \end{bmatrix} = \mathbf{RAM} \begin{bmatrix} X \\ Y \\ Z \end{bmatrix}; \; \mathbf{R} = \begin{bmatrix} 1.9569 & -1.1882 & 0.2313 \\ 0.3612 & 0.6388 & 0.0 \\ 0.0 & 0.0 & 1.0000 \end{bmatrix} \tag{2.3.3}$$

$\mathbf{R}=\mathbf{M}^{-1}\mathbf{A}^{-1}$ with **A** being the chromatic adaptation matrix for the reference viewing conditions, but as these do not change, it is more convenient to express it numerically.

*Step 4 RLAB coordinates*

$$\begin{aligned} L^R &= 100(Y_{ref})^\sigma \\ a^R &= 430[(X_{ref})^\sigma - (Y_{ref})^\sigma] \\ b^R &= 170[(Y_{ref})^\sigma - (Z_{ref})^\sigma] \\ C^R &= \sqrt{a^{R^2} + b^{R^2}} \\ h^R &= \tan^{-1}(b^R / a^R) \end{aligned} \tag{2.3.4}$$

The exponent σ depends on the surround (1/2.3 for average surround, 1/2.9 for dim surround and 1/3.5 for dark surround) and is included to model the surround's influence on image contrast. XYZ coordinates for the destination viewing conditions can be obtained by reversing the model in a simple analytical way.

## 2.1.4 LLAB

The above model and LLAB (Luo *et al.*, 1996; Luo and Morovic, 1996) are both similar in nature, with the difference that LLAB incorporates a state–of–the–art colour difference formula. The parameters needed by this colour appearance model are:

- *adopted white under source viewing conditions* $X_W Y_W Z_W$
- *luminance of adopted white under source viewing conditions* $L_S$
- *Y value of background under source adapting field* $Y_b$
- *sample under source viewing conditions* $XYZ$
- *information about the medium and the nature of the surround*

Four parameters need to be predetermined according to the viewing conditions considered, i.e. D (Incomplete adaptation factor), $F_S$ (Surround induction factor), $F_L$ (Lightness induction factor), and $F_C$ (Colourfulness induction factor). These values correspond to each set of viewing conditions and are shown next:

| ***Viewing Conditions*** | ***D*** | ***$F_S$*** | ***$F_l$*** | ***$F_C$*** |
|---|---|---|---|---|
| *Reflection samples and images in average surround* | | | | |
| *Large sample subtending more than 4°* | *1.0* | *3.0* | *0.0* | *1.0* |
| *Small sample subtending less than 4°* | *1.0* | *3.0* | *1.0* | *1.0* |
| *Television and VDU displays in dim surround* | *0.7* | *3.5* | *1.0* | *1.0* |
| *Cut–sheet transparency in dim surround* | *1.0* | *5.0* | *1.0* | *1.1* |
| *35 mm projection transparency in dark surround* | *0.7* | *4.0* | *1.0* | *1.0* |

The following steps are then carried out to obtain the appearance attributes of a given colour:

*Step 1 Compute corresponding tristimulus values under reference illuminant ($S_E$)*

$$\begin{bmatrix} R \\ G \\ B \end{bmatrix} = \mathbf{M} \begin{bmatrix} X/Y \\ Y/Y \\ Z/Y \end{bmatrix} \text{ where } \mathbf{M} = \begin{bmatrix} 0.8951 & 0.2664 & -0.1614 \\ -0.7502 & 1.7135 & 0.0367 \\ 0.0389 & -0.0685 & 1.0296 \end{bmatrix} \qquad (2.3.5)$$

The RGB cone responses for the adopted whites under reference and source illuminants, and test colour under source illuminant are calculated using Equation 2.3.5 and are labelled as $R_{wr}$, $G_{wr}$, $B_{wr}$; $R_{ws}$, $G_{ws}$, $B_{ws}$ and R, G, B respectively.

$$R_r = [D\,(R_{wr} / R_{ws}) + 1 - D]\,R$$
$$G_r = [D\,(G_{wr} / G_{ws}) + 1 - D]\,G \qquad (2.3.6)$$
For $B \geq 0$, $B_r = [D\,(B_{wr} / B_{ws}^{\beta}) + 1 - D]\,B^{\beta}$
Otherwise, $B_r = -[D\,(B_{wr} / B_{ws}^{\beta}) + 1 - D]\,|B|^{\beta}$
where $\beta = (B_{ws} / B_{wr})^{0.0834}$

$$\begin{bmatrix} X_r \\ Y_r \\ Z_r \end{bmatrix} = \mathbf{M}^{-1} \begin{bmatrix} R_r Y_s \\ G_r Y_s \\ B_r Y_s \end{bmatrix} \qquad (2.3.7)$$

*Step 2 Calculate appearance attributes*

In addition to lightness ($L_L$), chroma ($Ch_L$) and hue angle ($h_L$), which will be shown here, the model also has predictors for colourfulness ($C_L$), saturation ($s_L$) and hue composition ($H_L$), which are of less importance for the purposes of this study.

$$L_L = 116\,f(Y/100)^z - 16$$
$$A = 500\,[f(X/100) - f(Y/100)] \qquad (2.3.8)$$
$$B = 200\,[f(Y/100) - f(Z/100)]$$
Where $z = 1 + F_l (Y_b / 100)^{1/2}$
If $I > 0.008856$, $f(I) = (I)^{1/Fs}$
Otherwise, $f(I) = [(0.008856^{1/Fs} - 16/116)/0.008856]\,I + 16/116$
$$Ch_L = 25 \ln(1 + 0.05\,C) \qquad (2.3.9)$$

where $C = (A^2 + B^2)^{1/2}$

$h_L = \tan^{-1}(B/A)$ (2.3.10)

## 2.1.5 CIECAM97s

The CIE 1997 Colour Appearance Model – CIECAM97s is based on the work of many different investigators, including Hunt (Hunt, 1982; 1991; 1994; Hunt and Luo, 1994), Nayatani (Nayatani *et al.,* 1986; 1987; 1990; Nayatani, 1995) and the authors of the RLAB and LLAB models. What follows are instructions for the implementation of this model as given by Luo and Hunt (1998) and as used in this study for Experiment 4. The input parameters of CIECAM97s are:

- *adopted white under test viewing conditions* $X_W Y_W Z_W$
- *background under test viewing conditions* $X_b\ Y_b\ Z_b$
- *sample under test viewing conditions* $XYZ$
- *luminance of the test adapting field (cd/m²)* $L_A$

  $L_A$ *is normally taken to be 1/5 of the luminance of the adopted white under source conditions*
- *information about the medium and the nature of the surround.*

Based on the surround, the following parameters need to be chosen:

| ***Surround*** | ***F*** | ***c*** | $F_{LL}$ | $N_C$ |
|---|---|---|---|---|
| *Average* | | | | |
| *Large sample subtending more than 4°* | *1.0* | *0.69* | *0.0* | *1.0* |
| *Small sample subtending less than 4°* | *1.0* | *0.69* | *1.0* | *1.0* |
| *Dim* | *0.9* | *0.59* | *1.0* | *1.1* |
| *Dark* | *0.9* | *0.525* | *1.0* | *0.8* |
| *Cut–sheet* | *0.9* | *0.41* | *1.0* | *0.8* |

*Step 1 Chromatic Adaptation*

$$\begin{bmatrix} R \\ G \\ B \end{bmatrix} = \mathbf{M}_{\mathbf{BFD}} \begin{bmatrix} X/Y \\ Y/Y \\ Z/Y \end{bmatrix} \text{ where } \mathbf{M}_{\mathbf{BFD}} = \begin{bmatrix} 0.8951 & 0.2664 & -0.1614 \\ -0.7502 & 1.7135 & 0.0367 \\ 0.0389 & -0.0685 & 1.0296 \end{bmatrix} \quad (2.3.11)$$

Calculate RGB values for sample (as shown in Equation 2.3.11), adopted white and background under test conditions, the adopted white under reference conditions $X_{WR}\ Y_{WR}\ Z_{WR} = [100,100,100]$ and the degree of chromatic adaptation D.

$$D = F - F/[1 + 2(L_A^{1/4}) + (L_A^2/300)] \quad (2.3.12)$$

Calculate RGB values after chromatic adaptation whereby the adapted values of RGB are $R_C G_C B_C$ and those of $R_W G_W B_W$ and $R_b G_b B_b$ are $R_{WC} G_{WC} B_{WC}$ and $R_{bC} G_{bC} B_{bC}$.

$$R_C = [D(R_{WR}/R_W) + 1 - D]R$$
$$G_C = [D(G_{WR}/G_W) + 1 - D]G$$
$$B_C = [D(B_{WR}/B_W^p) + 1 - D]|B|^p \quad (2.3.13)$$

whereby $B_C$ must be made negative when B is negative and

$$p = (B_W/B_{WR})^{0.0834}$$

$$F_L = 0.2k^4(5L_A) + 0.1(1 - k^4)^2(5L_A)^{1/3} \text{ where } k = 1/(5L_A + 1)$$

*Step 2 Calculate cone responses and apply dynamic response function*

$$\begin{bmatrix} R' \\ G' \\ B' \end{bmatrix} = \mathbf{M_H}\mathbf{M}_{\mathbf{BFD}}^{-1}\begin{bmatrix} R_C Y \\ G_C Y \\ B_C Y \end{bmatrix} \quad \begin{bmatrix} R_W' \\ G_W' \\ B_W' \end{bmatrix} = \mathbf{M_H}\mathbf{M}_{\mathbf{BFD}}^{-1}\begin{bmatrix} R_{WC} Y_W \\ G_{WC} Y_W \\ B_{WC} Y_W \end{bmatrix}$$

$$\mathbf{M}_{\mathbf{BFD}}^{-1} = \begin{bmatrix} 0.98699 & -0.14705 & 0.15996 \\ 0.43231 & 0.51836 & 0.04929 \\ 0.00853 & 0.04004 & 0.96849 \end{bmatrix} \qquad (2.3.14)$$

$$\mathbf{M_H} = \begin{bmatrix} 0.38971 & 0.68898 & -0.07868 \\ -0.22981 & 1.18340 & 0.04641 \\ 0.00000 & 0.00000 & 1.00000 \end{bmatrix}$$

$$Y_{bC} = (0.43231R_{bC} + 0.51836G_{bC} + 0.04929B_{bC})Y_b$$

$$Y_{WC} = (0.43231R_{WC} + 0.51836G_{WC} + 0.04929B_{WC})Y_W$$

$$n = Y_{bC}/Y_{WC},\ N_{bb} = 0.725(1/n)^{0.2} \text{ and } N_{cb} = 0.725(1/n)^{0.2}$$

Apply the dynamic response function $R'G'B'$ and $R_W'G_W'B_W'$ which then become $R_a'G_a'B_a'$ and $R_{aW}'G_{aW}'B_{aW}'$ respectively.

$$R_a' = 40(F_L R'/100)^{0.73}/[(F_L R'/100)^{0.73} + 2] + 1 \qquad (2.3.15)$$

$$\text{if } R' < 0 \text{ then } R_a' = -40(-F_L R'/100)^{0.73}/[(-F_L R'/100)^{0.73} + 2] + 1$$

$G_a'$, $B_a'$, $R_{aW}'$, $G_{aW}'$ and $B_{aW}'$ are calculated similarly.

*Step 3 Calculate Appearance Attributes*

In addition to brightness (*Q*), lightness (*J*), chroma (*C*), saturation (*s*) and hue angle (*h*), which will be shown here, the model also has predictors for colourfulness (*M*) and hue composition (*H*), which are less relevant for imaging applications.

First, redness–greenness (a) and yellowness–blueness (b) are calculated:

$$a = R_a' - 12G_a'/11 + B_a'/11 \qquad (2.3.16)$$

$$b = (R_a' + G_a' - 2B_a')/9$$

This is followed by a calculation of hue:

$$h = \arctan(b/a) \qquad (2.3.17)$$

The eccentricity factor (e) is then calculated using the following unique hue data:

| | *Red* | *Yellow* | *Green* | *Blue* |
|---|---|---|---|---|
| *h* | *20.14* | *90.00* | *164.25* | *237.53* |
| *e* | *0.8* | *0.7* | *1.0* | *1.2* |

$$e = e_1 + (e_2 - e_1)(h - h_1)/(h_2 - h_1) \qquad (2.3.18)$$

where $e_1$ and $h_1$ are the values of $e$ and $h$ for the unique hue having the nearest lower value of $h$ and $e_2$ and $h_2$ are the values having the nearest higher value of $h$. Next, the value of the achromatic signal is calculated for both the sample and the adopted white:

$$A = [2R_a' + G_a' + (1/20)B_a' - 2.05]N_{bb}$$

$$A_W = [2R_{aW}' + G_{aW}' + (1/20)B_{aW}' - 2.05]N_{bb} \qquad (2.3.19)$$

Finally, lightness, saturation and chroma can be obtained as follows:

$$J = 100(A/A_W)^{cz} \text{ where } z = 1 + F_{LL}n^{1/2} \qquad (2.3.20)$$

$$s = \frac{100e(10/13)N_c N_{cb} 50\sqrt{a^{2+} + b^2}}{R_a' + G_a' + (21/20)B_a'} \quad (2.3.21)$$

$$C = 2.44s^{0.69}(J/100)^{0.67n}(1.64 - 0.29^n) \quad (2.3.22)$$

For instructions on how to calculate the reverse model see Luo and Hunt (1998).

## 2.1.6 Viewing Conditions

Sections 2.3.1 and 2.3.2 already highlighted the importance of the environment in which a colour is seen. Here it is of importance to consider several elements including the chromaticity and intensity of the light source used, the colour of the background against which a colour or colour image is viewed and the viewing geometry, which includes viewing distance and viewing angle. What will be presented next is an overview of recommended viewing conditions for CRT monitors and printed reproduction based on a Working Draft of the ISO 3664 standard (1997).

### *2.1.6.1 CRT*

The draft standard for viewing colour images on CRTs is intended for situations when these are seen in isolation and not when they are compared with prints. For such conditions it is recommended that the white point of the monitor is set to chromaticities similar to CIE standard illuminant D65, that it should have a luminance level of at least 75 cd/m$^2$ and preferably 100 cd/m$^2$ and that the level of ambient illumination should be below 32 lux. The surround should be neutral and there should be no strongly coloured areas in the field of view or in places from where they could be reflected on the monitor. Further, sources of glare should also be avoided – light sources should not be reflected from the CRT or be in the field of view.

### *2.1.6.2 Print*

The above draft standard for viewing prints recommends the use of light sources which approximate CIE standard illuminant D50 with a maximum illuminance at the viewing surface of 500 lux ±125 lux. To determine how well a given light source approximates the standard illuminant, the method suggested by the CIE is to be used (CIE, 1981). Prints should be viewed against a neutral, matt surround which should have a luminous reflectance of less that 20 *per cent* and extend around it by at least one third of their dimensions. Further, the backing of these prints should have a luminous reflectance of two to four *per cent*. Note, that the above are the recommendations for "practical appraisal" of prints, i.e. for conditions which are similar to those under which prints are typically viewed. The standard also makes another set of recommendations for the "critical appraisal" of prints, which differs from the above primarily by the illuminance at the viewing surface being 2000 lux ±500 lux.

## 2.1.7 Summary

The importance of colour appearance issues is undeniable in any colour reproduction study for at least the following reason – to attempt to reduce the effects of phenomena which are not being investigated. Due to this, the viewing conditions for both media dealt with here (CRT and prints) were set so as to prevent any appearance phenomena resulting from differences in luminance level, white point or surround (Chapter 3).

# 2.4 Colour Reproduction Media & Intents

An understanding of the basic characteristics of the colour reproduction media used in this study – CRT monitor and colour prints – is essential for their appropriate use and will be discussed in the

following sections. In addition to this, the question of colour reproduction intents will also be dealt with.

## 2.4.1 CRT Monitors

Cathode–ray tube (CRT) monitors use **additive colour reproduction** to obtain the colours within their gamut. This is done by having three types of phosphors – red green and blue – distributed across the face of the monitor's tube. These phosphors can emit light of varying intensities, depending on the energy of the electrons fired at them (Sluyterman, 1995). Note, that the size of the phosphors is such that it is below the resolving power of the human visual system, when viewed at a distance of at least approximately 70 cm and the light emitted by an individual phosphor is merged with the light coming from its neighbours. Due to the phosphors having high chroma, the gamut of a typical computer monitor is quite large in terms of relative colorimetry (Figure 2.4.1).

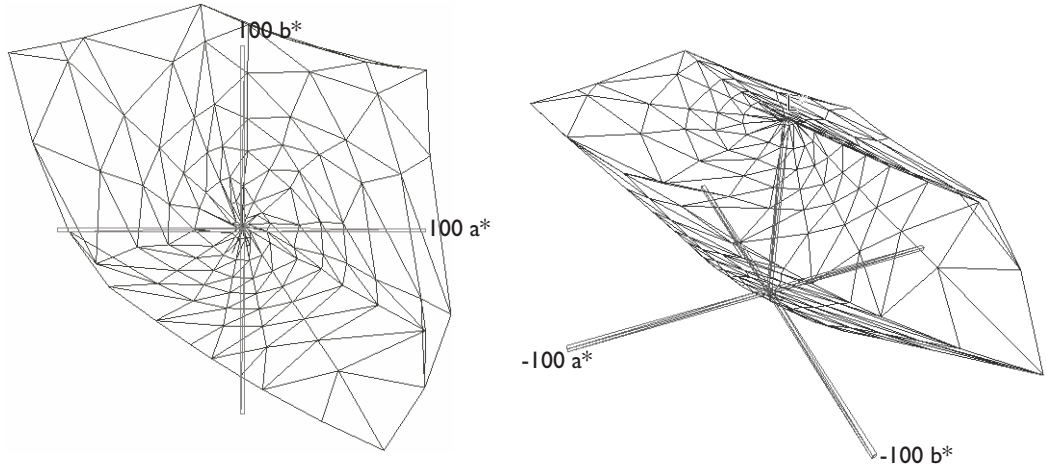


***Figure 2.4.1*** *Barco Calibrator CRT monitor gamut in CIELAB.*

### *2.4.1.1 Chromatic Adaptation to Monitors*

As monitors are light emitting devices themselves, they are not considered as illuminated objects (i.e. the cognitive component of chromatic adaptation is not active), whereby chromatic adaptation does not completely compensate for the illumination in the room where the monitor is viewed (Fairchild, 1992). Incomplete chromatic adaptation also means that users do not adapt to the white on the monitor and will perceive it as having a colour cast even after a long period of time. Some more recent work suggests that the visual system is 60 *per cent* adapted to the monitor's white point and 40 *per cent* to the ambient illumination's white point (Katoh, 1994). This is a further reason for setting the white points of both the monitor and the illuminated print in this study to the same chromaticity.

## 2.4.2 Colour Prints

The printing technologies used currently all employ the **subtractive colour reproduction** principle whereby colorants (e.g. inks, toners, dyes, etc.) with various spectral characteristics absorb different parts of the light illuminating the print (this again shows the importance of the light source used). The intensity of these colorants can in most cases not be varied directly as the majority of printing technologies use a bi–level process for depositing colorants on the printing substrate. Indirect means of producing a change of intensity are therefore used by printing dots of different sizes, which should again be below the resolving power of the human eye when viewed at the intended distance. As individual dots cannot be resolved, the stimuli they produce are mosaiced together with areas of clear substrate and different colours are obtained in this way. This principle – **halftoning** (Figure 2.4.2) – is used in offset lithography, flexography and gravure as well as ink jet, laser,

thermal wax and phase change printers. In dye diffusion printers, however, the optical density of the colorant can be varied directly and halftoning is therefore not needed.

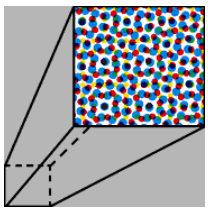

***Figure 2.4.2*** *Halftoning using an amplitude modulated screen.*

The extremes of print gamuts are the colour coordinates of the usually three chromatic colorants used (cyan, magenta and yellow), the overprints of pairs of them, the black colorant (or overprint of all colorants) and the clear substrate. From this it is clear that the size of the gamut for a particular medium depends on the properties of both colorants and substrate in addition to the characteristics of the light source used. However, it is not only the colour of these components, but also their physical properties (including surface and absorption properties of paper; viscosity, trapping and colour fastness of colorants) which influence the gamut of a print (Figure 2.4.3).

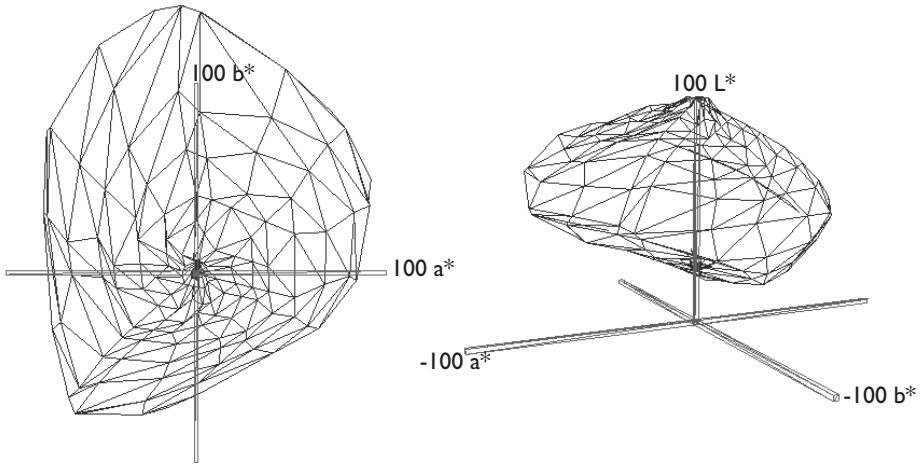


***Figure 2.4.3*** *Gamut of prints made with HP DeskJet 850C inkjet printer on plain paper (CIELAB).*

An additional constraint to the gamut of both colour reproduction media dealt with here (CRT and print) and indeed any digital medium is quantisation, as a consequence of which only colorant amounts of certain values can be addressed, thereby also making the colour gamut discontinuous.

## 2.4.3 Colour Reproduction Intents

The aim of the preceding sections was to illustrate the basic principles and differences of the media used in this study. In addition to the CRT used here, the whole visual gamut can serve as the original gamut when the aim is to reproduce natural scenes (Figure 2.4.4). In spite of this, images on monitors are often assumed to be the originals as the real scene might not be available or exist anymore at the time of reproducing it or because changes were made after the scene was captured and displayed on the monitor.

Due to the differences between original and reproduction gamuts, different kinds of reproduction requirements have been defined previously whereby the following list was given by Hunt (1987, pp. 178) and is in order of decreasing stringency. Note, that reproduction intents in general can be seen as aims for a colour reproduction system and due to the nature of its other elements these intents can be interpreted as aims for gamut mapping:

- *spectral reproduction* – spectral power distributions of original and reproduction are identical
- *exact reproduction* – relative luminances, chromaticities and absolute luminances are identical

- *colorimetric reproduction* – chromaticities and relative luminances match
- *equivalent reproduction* – chromaticities, relative and absolute luminances of original appear as being the same in the reproduction
- *corresponding reproduction* – chromaticities and relative luminances in the reproduction appear to be the same as in the original when both have same luminance levels
- *preferred reproduction* – equality of appearance is sacrificed in order to achieve a more pleasing result

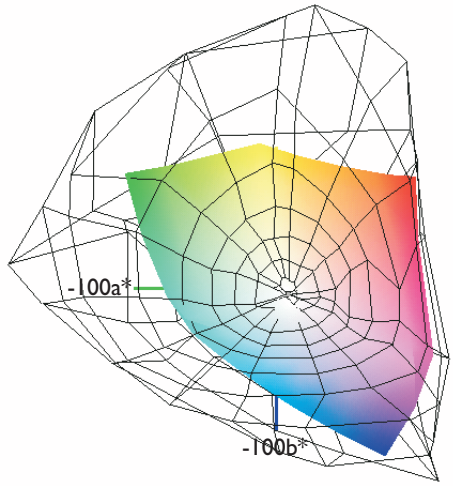


***Figure 2.4.4*** *CRT gamut (solid) and gamut of block dyes representing the gamut of theoretically possible surface colours (mesh), which was obtained by independently varying spectral reflectances at 16 wavelengths whereby generating spectral reflectance curves, which were then combined with the spectral power distribution of CIE Standard Illuminant D50.*

When reproducing images between different gamuts none but the last of these colour reproduction intents are possible by definition. In the case of individual colours, which are from the intersection of original and reproduction gamuts, equivalent and corresponding reproduction are possible in addition to preferred reproduction. The *International Color Consortium* (ICC), which was formed by leading companies and institutions involved in colour management and which is working towards a standard colour management framework, also defined four reproduction intents (ICC, 1998). Two of these could also be reformulated in Hunt's terms:

- *absolute colorimetric reproduction* – chromaticities, relative and absolute luminances of original appear as being the same for the reproduction of colours from the intersection of original and reproduction gamuts and out–of–gamut colours are clipped onto reproduction gamut surface
- *relative colorimetric reproduction* – chromaticities and relative luminances of original appear as being the same for the reproduction of colours from the intersection of original and reproduction gamuts and out–of–gamut colours are clipped onto reproduction gamut surface

Further it is possible to define the following reproduction intents, which are used in the present study:

- *accurate reproduction* – reproduced image is as close to the original image as is possible with respect to gamut differences
- *pleasant reproduction* – reproduced image is considered pleasant in isolation

Note, that the last four intents are explicitly aimed at **complex images** rather than individual colours and that the last two are targets rather than labels which could apply to a given reproduction (at least in the context of the present understanding of image appearance).

As far as pleasant reproduction is concerned, it is of interest to note the work of Yendrikhovskij (1998) who proposed an algorithm for optimising the **colour quality of natural images**. The

method is based on the naturalness and colourfulness indices which were developed in the same work and which are computed on the basis of image statistics. Naturalness is calculated by identifying the locations of prototypical memory colours for 'skin', 'grass' and 'sky' in colour space (which represent a wider range of naturally occurring colours) and then analysing image colours in relation to these. Colourfulness on the other hand is calculated from the average and standard deviation of image chroma. Finally, colour quality is expressed as a weighted combination of naturalness and colourfulness and images can then be optimised in terms of this metric. The above colour quality index was experimentally tested on 20 images from television and the processed images have been judged to be of higher quality than the original images in 16 cases. This algorithm clearly has a wide range of possible applications and could be used as a preliminary step to gamut mapping in a system, which aims to give good quality reproductions independently of the original's quality. In such a case, however, the algorithm would have to be extended by support for synthetic images as well.

## 2.5 Characterisation and Calibration

Now that the colour reproduction media used in this study were briefly introduced and the question of colour appearance was addressed as well, a further element of colour reproduction will be dealt with here. This element is usually called **device characterisation** and, as has already been pointed out in Section 1.3, will also be referred to as such in the following sections even though it should more appropriately be called **medium characterisation**. Before individual methods are discussed, it is important to be aware of the definition of two basic concepts as used in this study and as defined by Johnson (1996):

(1) *Calibration* – the setting up of a device or process so that it gives repeatable data.

(2) *Characterisation* – defines the relationship between the device colour space and the CIE system of colorimetry.

The need for these two techniques is intrinsic in matching colours between different media. As each medium or device uses different colorants, its way of describing colours is device dependent. Therefore, to obtain a match between two device–dependent descriptions of colour, it is best to transform both into a system which is device independent – like the system of CIE colorimetry described in Section 2.1. One could argue that it is possible to transform colour information directly between device dependent colour spaces (which is true), but such a characterisation would have to be done for each pair of devices, rather than just once for each device. Furthermore, such a transformation would make the inclusion of gamut mapping difficult, as this is usually intended to be carried out in a perceptually uniform colour space. The need for calibration should also be clear, as characterisation will only hold true when the device is in the state for which it was characterised.

Even though characterisation methods usually depend to a significant degree on the device for which they are intended, the following three approaches: neural networks, full characterisation and masking equations can be used for any device. The later two will be discussed here as they were used in this study and for an example of the use of neural networks in characterisation see Kang and Anderson (1992). This section on characterisation and calibration is based primarily on a pair of papers by Johnson, Luo, Lo, Xin and Rhodes (1998a; 1998b).

### 2.5.1 Generic Characterisation Methods

#### *2.5.1.1 Cube Interpolation*

Any device's colour reproduction characteristics can be determined by first producing all (or a sufficiently large subset) of the colours it can reproduce and measuring their colorimetric coordinates.

A look–up table (LUT) can then be constructed, which will give the tristimulus values for a given set of device dependent coordinates. Note, that even when all possible colorant combinations are included in the LUT, it will have some errors in predicting the device's characteristics due to the device's variation. The following cube interpolation procedure, which is generally used when prints are made with three inks – cyan (C), magenta (M) and yellow (Y), is based on (Johnson *et al.*, 1998b):

(1) Produce a series of steps with increasing concentration for each colorant (at equal quantisation intervals).

(2) Measure the samples and calculate the lightness of each step.

(3) Plot lightness *versus* colorant quantisation level and if relationship is highly non–linear, define a LUT between quantisation level and lightness.

(4) Select nine quantisation levels for each colorant (including minimum and maximum and seven steps in–between with equal lightness intervals).

(5) Print test images containing all combinations of the above determined nine steps for each colorant (resulting in 729 patches).

(6) Measure each colour patch in terms of XYZ tristimulus values and generate a three dimensional LUT. From this, tristimulus values can be obtained for each of the 729 colorant combinations and intermediate colours can be obtained using tri–linear interpolation (Kasson *et al.*, 1995):

$$\begin{aligned} N = \; & (1 - D_C)(1 - D_M)(1 - D_Y)N_1 + D_C(1 - D_M)(1 - D_Y)N_2 + \\ & (1 - D_C)D_M(1 - D_Y)N_3 + D_C D_M(1 - D_Y)N_4 + \\ & (1 - D_C)(1 - D_M)D_Y N_5 + D_C(1 - D_M)D_Y N_6 + \\ & (1 - D_C)D_M D_Y N_7 + D_C D_M D_Y N_8 \end{aligned}$$

$$N \in \{X,Y,Z\} \qquad (2.5.1)$$

Here $D_C$, $D_M$ and $D_Y$ are a given colorant combination's distances from the origin of the selected sub–cube and $N_i$ are the tristimulus values of the vertices of that sub–cube (Figure 2.5.1).

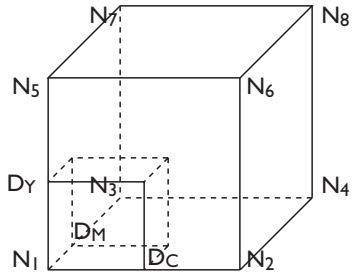


***Figure 2.5.1*** *Tri–linear interpolation within a sub–cube of the 9x9x9 LUT.*

In many cases this method provides the best accuracy, however, it also involves a large number of measurements and is therefore considerably time consuming, which is especially disadvantageous if the variables of the device change often (e.g. as is the case with many digital printing devices). This method is very widely used and a number of different variations of it have been published (Bell and Cowan, 1994; Balasubramanian, 1994; Marcu and Abe, 1994).

### *2.1.1.2 Polynomial Fitting*

Polynomial fitting is conventionally used in printing (where this model is sometimes referred to as *Masking Equations*), but can equally well be applied to other media. This method was first suggested by Yule (1938) by saying that the relationship between colorimetric densities of the colorants and XYZ is of the following nature:

$$\begin{bmatrix} D_r \\ D_g \\ D_b \end{bmatrix} = \mathbf{A} \begin{bmatrix} D_{r(c)} \\ D_{g(m)} \\ D_{b(y)} \end{bmatrix} \quad (2.5.2)$$

Here $D_n$ with $n \in \{r,g,b\}$ are the **colorimetric densities** of the colour resulting from a given CMY colorant combination and are calculated as:

$$D_r = \log(X_0/X),\ D_g = \log(Y_0/Y),\ D_b = \log(Z_0/Z) \quad (2.5.3)$$

$(X_0,Y_0,Z_0)$ is the white point, **A** is a 3x3 matrix determined using the least squares method (Milton and Arnold, 1990, pp. 352) and $(D_{r(c)},D_{g(m)},D_{b(y)})$ are the colorimetric densities of the device's colorants for the combination of which the XYZ coordinates are to be calculated. This simple linear method does not give good results for many devices, as the assumption of additivity and proportionality of colorant densities does not hold for them. However, if higher order and cross–product terms are introduced, as was later suggested by Clapper (1961) and Yule (1967), the precision of this method becomes comparable to full characterisation. The following equation shows a third order polynomial model with cross products used for printer characterisation:

$$\begin{bmatrix} D_r \\ D_g \\ D_b \end{bmatrix} = \mathbf{BC}$$

$$\mathbf{C} = \begin{bmatrix} c & m & y & c^2 & m^2 & y^2 & cm & cy & my & c^3 & m^3 & y^3 & c^2m & c^2y & m^2c & m^2y & y^2c & y^2m \end{bmatrix}^T \quad (2.5.4)$$

Here **B** is a 3x18 matrix again obtained using the least squares method and $(c,m,y)=(D_{r(c)},D_{g(m)},D_{b(y)})$. The precision of this method depends on the number of colours used for obtaining the coefficients of **B** and it was found that for many printing devices there is little benefit in using more than 64 colours for characterising them (Johnson *et al.*, 1998b). However, this number will depend on the device and on how well the colours are chosen (same considerations apply as for full characterisation). A potential problem with using higher order masking equations is the possibility, that local minima and maxima present in the equations do not correspond with the modelled relationship and will create artefacts in some parts of colour space. Before any transformations are carried out, it is useful to normalise and scale the data in both colour spaces (the device dependent and the device independent) using the coordinates of black and white achievable by the device which is being characterised.

Other device specific techniques for characterising and calibrating the devices used in this study will be described in the following sections.

## 2.1.2 CRT Monitor Characterisation & Calibration

As the majority of electronic displays used currently are CRTs (Figure 2.5.2) and as this is the technology used by the medium for displaying original images in this study, only CRT calibration and characterisation will be described here. An overview of alternative display technologies can be found in (Jackson *et al.*, 1994; Budin, 1995) of which the most important are probably liquid crystal displays (LCDs) – for their characterisation see (Selhuber and Parker, 1995). The characteristics of CRTs which determine their colour reproduction capabilities include:

- *chromaticities and maximum luminances of phosphors*
- *gain and offset settings of electron guns' voltage (this is done via the contrast and brightness settings and via adjusting white balance)*
- *gamma of electron guns relating voltage to light output*

- *relationship between digital values sent to display and resulting voltages*
- *amount of ambient flare off CRT*
- *inter–reflections from neighbouring pixels within the CRT*

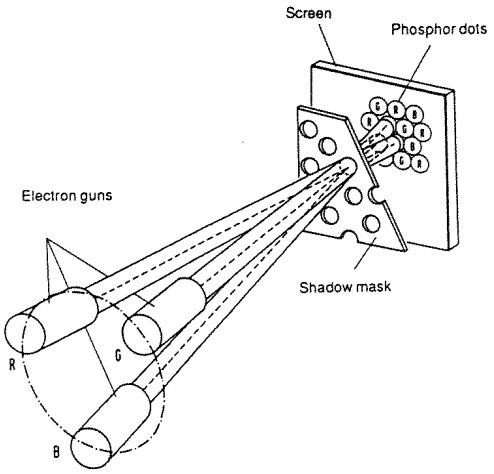


***Figure 2.5.2*** *Schematic view of a cathode ray tube (reproduced from (Schläpfer, 1990)).*

Even if cross–media matching was not an issue, characterisation and calibration of CRTs would still be of importance as the variation in colour between different monitors can be as high as 18 $\Delta E^*_{ab}$ (for the same white point, but using different phosphor sets) (Engeldrum and Ingraham, 1990). For CRT characterisation to be feasible, the following assumptions are usually made (Brill, 1992):

- *spatial independence* Output at a particular location depends only on that location's input (i.e. neighbouring pixels do not affect each other).
- *gun independence* Output of a phosphor is independent from the input to the other guns.
- *approximate homogeneity* Spatial variation is negligible (i.e. whole CRT can be calibrated from average of a few pixels).
- *phosphor constancy* Relative SPD is independent of digital–to–analog converter (DAC) value applied to electron gun (this implies constant chromaticity of phosphors).

Given these assumptions, the tristimulus values for a given pixel can be computed from the following equation, if the luminances and chromaticities of the three phosphors are known (Johnson *et al.*, 1998a):

$$\begin{bmatrix} X \\ Y \\ Z \end{bmatrix} = \begin{bmatrix} \frac{x_r}{y_r} & \frac{x_g}{y_g} & \frac{x_b}{y_b} \\ 1 & 1 & 1 \\ \frac{z_r}{y_r} & \frac{z_g}{y_g} & \frac{z_b}{y_b} \end{bmatrix} \begin{bmatrix} T_r \\ T_g \\ T_b \end{bmatrix} \tag{2.5.5}$$

Here $T_i$ ($i \in \{r,g,b\}$) are the luminances of the phosphors, $x_i$, $y_i$ and $z_i$ are their chromaticities and XYZ are the resulting tristimulus values. Note, that it is important to use the actual chromaticities measured for the CRT being characterised, rather than values published by the manufacturer as these are for a whole range of monitors and can be considerably different from an individual one. This part of CRT characterisation is the same for all methods, which make the assumption of phosphor constancy. However, before this transformation can be carried out, the luminances of the three phosphors need to be established and there are at least seven methods for doing this:

### 2.1.1.1 GOG Model

The GOG model, devised by Berns (1996), takes as its variables the gain, offset and gamma of the monitor to relate digital input to phosphor luminance. This model is based on a previous comprehensive study by the author and his co–workers (Berns *et al.*, 1993a; 1993b). The following equation shows the calculation of spectral radiance from digital values:

$$L_{\lambda,r} = L_{\lambda,r(\max)}\left(k_{g,r}\left(\frac{LUT_r d_r}{2^n - 1}\right) + k_{o,r}\right)^{\gamma_r} \text{ if } \left(k_{g,r}\left(\frac{LUT_r d_r}{2^n - 1}\right) + k_{o,r}\right)^{\gamma_r} \geq 0 \quad (2.5.6)$$

$$\text{otherwise } L_{\lambda,r} = 0$$

Here $L_{\lambda,r}$ is the spectral radiance of the red channel, $L_{\lambda,r(max)}$ is the maximum spectral radiance of the red phosphor, $k_{g,r}$ is the red channel's gain, $k_{o,r}$ is its offset, $LUT_r$ is the video LUT relating digital values to voltage, $d_r$ is the red digital value, $n$ is the number of bits per channel used by the DAC and $\gamma_r$ is the gamma of the red gun. Analogous equations can be set up for the other two channels. Note, that this is already a simplified relationship, as the gain and offset used here relate to the whole system rather than only to the electronics of the CRT. The whole equation can also be re-written as:

$$L_{\lambda,r} = RL_{\lambda,r(\max)}$$

$$\text{where } R = \left(k_{g,r}\left(\frac{LUT_r d_r}{2^n - 1}\right) + k_{o,r}\right)^{\gamma_r} \text{ if } \geq 0, \text{ otherwise } R = 0 \quad (2.5.7)$$

Here $R$ is a scalar representing a percentage of maximum luminance and therefore the luminance $T_r = RL_{r(max)}$ ($L_{r(max)}$ is the maximum luminance of the red channel). Ambient flare and inter–reflection flare (due to failure of spatial independence) can also be allowed for:

$$\begin{bmatrix} X \\ Y \\ Z \end{bmatrix} = \begin{bmatrix} X \\ Y \\ Z \end{bmatrix}_{\substack{ambient \\ flare}} + \begin{bmatrix} X \\ Y \\ Z \end{bmatrix}_{\substack{inter- \\ reflection \\ flare}} + \mathbf{A}\begin{bmatrix} T_r \\ T_g \\ T_b \end{bmatrix} \quad (2.5.8)$$

Here **A** is the (3x3) matrix from equation 2.5.5.

Apart from describing the above model, the author also provided a useful characterisation procedure:

(1) Set–up display visually. Turn brightness and contrast controls to minimum, turn off ambient light and display black image ($d_r$=$d_g$=$d_b$=0). Adjust offset to just above the setting where light is perceptible. Display text image and adjust gain to maximum luminance without loss of sharpness.

(2) Measure peak output from R, G, B, the white point and the darkest neutral, which can be measured with good precision and accuracy and an intermediate neutral between it and the white.

(3) Calculate tristimulus matrix (matrix **A** in Equation 2.5.8) and its inverse. Estimate scalars for the neutrals, calculate gain, offset and gamma for each channel (from the three neutrals).

(4) Change background to neutral with 20 *per cent* luminance of peak white (use the model to calculate the neutral's digital values). Remeasure darkest neutral to determine inter–reflection flare.

(5) Measure a series of neutrals (approximately 5–10) to build the LUTs, then subtract inter–reflection flare and normalise the scalars.

### 2.1.1.2 Meyer 1990 Model

The model proposed by Meyer (1990) is expressed by the following equation:

$$T = k(o + gV^{\gamma})$$
$$k \approx \int_{\lambda} K_{\lambda}\bar{y}_{\lambda}d\lambda \qquad (2.5.9)$$

Here $T$ is the luminance, $o$ and $g$ are the offset and gain of the electron gun (not the whole system as in GOG), $K_{\lambda}$ is the relative SPD of the CRT and $k$ is a constant which corresponds to the luminance (Y) of the monitor. To extend this relationship to the one between DAC values and luminance, it is necessary to include a transformation between DAC values and voltage. This was found to be of the nature of $V = O + Gd$ (Berns *et al.*, 1993a), where $O$ and $G$ are the offset and gain of the video circuitry and $d$ is the digital value sent to it (this is represented by a video LUT in the GOG model).

### 2.1.1.3 PLCC Model

The following six models, including this one, are based on work of Post and Calhoun (1989), which was later evaluated by Johnson *et al.* (1998a). This particular model uses piecewise linear interpolation assuming constant chromaticity coordinates (hence PLCC), i.e. it uses separate LUTs for each channel and assumes that the relationship of $T$ and DAC values is linear between the points in the LUT. The choice of values in the LUT is critical, and more data should be available for the low luminance end of the range.

### 2.1.1.4 LIN–LIN2 Model

Assumes the following relationship, where $c_i$ ($i \in \{1,2,3\}$) are obtained using the least squares method and $D$ represents normalised DAC values:

$$T = c_{1+} + c_2 D + c_3 D^2 \qquad (2.5.10)$$

### 2.1.1.5 LOG–LOG Model

This is the original gamma correction, which disregards the influence of gain and offset:

$$\log T = c \log D \qquad (2.5.11)$$

### 2.1.1.6 LOG–LOG2 Model

An attempt to correct the problems of the LOG–LOG model at low luminances:

$$\log T = c_1 + c_2 \log D + c_3 (\log D)^2 \qquad (2.5.12)$$

### 2.1.1.7 LOG–LIN2 Model

The last of the models which assume constant chromaticity coordinates:

$$\log T = c_1 + c_2 D + c_3 D^2 \qquad (2.5.13)$$

### 2.1.1.8 PLVC Model

As can be seen from the name, this model is related to PLCC, with the difference being, that it does not assume constant chromaticity with changes in luminance. Therefore instead of three 1D LUTs, a 3D LUT is used, just like in the case of cube interpolation described in Section 2.5.1.1.

The analysis carried out by Johnson *et al.* (1998a) has shown that the PLCC model gave the best results, with the GOG and LOG–LOG2 models being slightly less accurate (however, all three models had average $\Delta E_{CMC(1:1)}$ errors of only around 0.40).

### 2.1.1.9 CRT Calibration

The techniques discussed so far were all concerned with the characterisation of CRTs. However, for characterisation to be valid, the device also needs to be calibrated, which is done by setting the variables of the system to the state in which they were when the device was characterised.

Calibration can also be used to make a given CRT behave like a reference CRT or to make it fit given specifications of system gamma and white point. A technique for altering digital values to fulfil these criteria was described by Berns (1996) and has as its inputs the data from the characterisation of the CRT and the target values to be emulated. Digital values are then transformed using the following equation:

$$d_{r(target)} = \mathrm{int}\left[(2^n - 1)R_{white}\left(\frac{\left(\frac{d_{r(original)}}{2^n - 1}\right)^{\frac{1}{\gamma_{r(original)}}} - k_{o,r}}{k_{g,r}}\right)^{\gamma_{r(target)}}\right] \quad (2.5.14)$$

Here the variables use the same notation as in the GOG model and $R_{white}$ is the scalar which would give the target white point under original conditions (analogous equations apply for green and blue). Note, that the software simulation of a white point will inevitably result in a lower maximum luminance, which thereby reduces the available tonal range (e.g. when D50 was simulated on a particular monitor with a 9300K CCT white point, the resulting luminance range reduced to 58.6 *per cent* of the original range) (Jennings and Thompson Pearce, 1993). To preserve as much as possible of the monitors luminance, one of the scalars is usually set to 100 *per cent*.

## 2.1.3 Printer Characterisation & Calibration

Unfortunately there is no simple linear relationship between colorants and tristimulus values, as there is for phosphor luminances. Neither is there a simple additive relationship between the stimulations caused by the individual colorants, which makes the whole process of characterising a printing device more problematic. As the colour in most prints is achieved by partially superimposing halftone dots, there arise some problems (Johnson, 1998b) including **trapping** (the second colorant's density will differ from that of the first colorant as they are printed onto different substrates – the first one is printed onto paper, whereas the second one onto a colorant), **back transfer** and the partial **opacity** of colorant. Further problems are caused by **multiple internal reflections**, **first surface reflections** and the **sideways scattering** of light. Other factors, which also influence the relationship between colorant amounts and tristimulus values are the **halftone structure** of the printed dots (i.e. screen ruling and frequency of amplitude modulated halftone screens or the pixel size and nature of frequency modulated screens) and the **spectral absorption characteristics** of the colorants.

When colour printers use more than three colorants (e.g. cyan, magenta yellow and black), there is no longer only a single possible solution for obtaining a given colour (except for colours, which would be reproduced by only up to two colorants in a three chromatic–colorant system (e.g. CMY)) and this necessitates an algorithm for determining what colorant combination is to be used for a particular colour (e.g. see (Lo, 1995) for an example of CMYK determination). However, as the printer used in this study can only be controlled in terms of three colorants, only models for obtaining CMY values for a given set of XYZ values (and *vice versa*) will be discussed next.

The majority of models for performing this task can be divided into four groups: cube interpolation, polynomial equations, neural networks and Neugebauer equations. The first three have already been dealt with in Section 2.5.1, which leaves only the Neugebauer equations to be discussed here. For other printer characterisation models and their evaluation see (Herzog, 1997; Herzog and Roger, 1998)

### *2.1.3.1 Classical Neugebauer Equations*

This model was originally proposed by Neugebauer (1937) and many modifications to it have been devised since. It is based on the assumption that the colour of a unit area is determined by the addition of the tristimulus values of the different combinations of colorants present in that area. For a three colour system, there are eight possible combinations, whose **fractional dot areas** can be expressed as:

$$\begin{aligned}
f_1 &= (1-p)(1-q)(1-r) && \text{(clear substrate)} \\
f_2 &= p(1-q)(1-r) && \text{(colorant } p\text{)} \\
f_3 &= q(1-p)(1-r) && \text{(colorant } q\text{)} \\
f_4 &= r(1-p)(1-q) && \text{(colorant } r\text{)} \\
f_5 &= qr(1-p) && \text{(overprint of } q \text{ \& } r\text{)} \\
f_6 &= pr(1-q) && \text{(overprint of } p \text{ \& } r\text{)} \\
f_7 &= pq(1-r) && \text{(overprint of } p \text{ \& } q\text{)} \\
f_8 &= pqr && \text{(overprint of } p, q \text{ \& } r\text{)}
\end{aligned} \qquad (2.5.15)$$

Here $p$, $q$ and $r$ are the **percentage dot areas** of the three colorants ($p$, $q$ & $r$ have been used on purpose, as the model can be applied to any set of colorants and using CMY could be confusing). The dot area ($m$) can be calculated from density using the Murray–Davies equation (Murray, 1936), where the subscripts $t$ and $s$ represent a tint (for which the dot area is calculated) and the solid respectively:

$$m = \frac{\left(1 - 10^{-D_t}\right)}{\left(1 - 10^{-D_s}\right)} \qquad (2.5.16)$$

Each of these fractional dot areas has got a set of tristimulus values associated with it, which is obtained by measuring the colorant combination it represents (e.g. $X_4Y_4Z_4$ are the tristimulus values of a solid patch printed with colorant $r$ – see Equation 2.5.15). The Neugebauer equations can now be expressed as:

$$\begin{bmatrix} X \\ Y \\ Z \end{bmatrix} = \sum_{i=1}^{8} \left( f_i \begin{bmatrix} X_i \\ Y_i \\ Z_i \end{bmatrix} \right) \qquad (2.5.17)$$

Note, that the above equation is identical with the tri–linear interpolation equation used for full characterisation (Equation 2.5.1), which makes the Neugebauer equations a 2x2x2 LUT with tri–linear interpolation.

### 2.1.3.2 N–Modified Neugebauer Equations

Some of the inaccuracies in the Neugebauer Equations' predictions can be attributed to the Murray–Davies equation not giving an accurate prediction of the percentage dot area (mainly due to light scatter within the substrate). This was remedied by Yule and Nielsen (1951), who proposed the following modified version, where $n$ is a medium–dependent parameter determined heuristically (Note, that this problem can also be corrected by using a LUT between the digital values and measured density, in which case the classical Neugebauer equations can be used with better accuracy):

$$m = \frac{\left(1 - 10^{\frac{-D_t}{n}}\right)}{\left(1 - 10^{\frac{-D_s}{n}}\right)} \tag{2.5.18}$$

An analogous modification was also incorporated into the Neugebauer equations by Yule and Colt (1951), which are now of the following form:

$$\begin{bmatrix} X^{\frac{1}{n_x}} \\ Y^{\frac{1}{n_y}} \\ Z^{\frac{1}{n_z}} \end{bmatrix} = \sum_{i=1}^{8} \left( f_i \begin{bmatrix} X_i^{\frac{1}{n_x}} \\ Y_i^{\frac{1}{n_y}} \\ Z_i^{\frac{1}{n_z}} \end{bmatrix} \right) \tag{2.5.19}$$

### 2.1.3.3 Modern Neugebauer Equations

This model was devised by Laihanen (1987) and tries to take into account the shape of the halftone dot. Rather than being based on a unit area containing one halftone dot, this model takes as its inputs three binary pixmaps – one for each colorant. The XYZ coordinates for a given pixel with the spatial coordinates *(u,v)* are then calculated in the following way:

$$\begin{aligned} X(u,v) = \quad & X_1 \text{ if } p(u,v) = q(u,v) = r(u,v) = 0 \\ & X_2 \text{ if } p(u,v) = 1,\ q(u,v) = r(u,v) = 0 \\ & X_3 \text{ if } q(u,v) = 1,\ p(u,v) = r(u,v) = 0 \\ & X_4 \text{ if } r(u,v) = 1,\ p(u,v) = q(u,v) = 0 \\ & X_5 \text{ if } q(u,v) = r(u,v) = 1,\ p(u,v) = 0 \\ & X_6 \text{ if } p(u,v) = r(u,v) = 1,\ q(u,v) = 0 \\ & X_7 \text{ if } p(u,v) = q(u,v) = 1,\ r(u,v) = 0 \\ & X_8 \text{ if } p(u,v) = q(u,v) = r(u,v) = 1 \end{aligned} \tag{2.5.20}$$

Similar equations apply to $Y(u,v)$ and $Z(u,v)$. The three resulting arrays containing XYZ values for every halftone pixel can then be integrated over a suitable area (depending on the nature of the digital halftone screen) so as to give XYZ coordinates for individual image pixels. This can be achieved in two ways, either by a three stage process involving empirically optimised filters before and after integration (Laihanen, 1987, pp. 22–23) or by direct integration over a chosen area ($A$):

$$X = \frac{1}{A}\iint_A X(u,v)\, du\, dv \qquad (2.5.21)$$

Analogous relationships apply for $Y$ and $Z$.

### 2.1.3.4 Vector–Corrected Neugebauer Equations

Again this model was devised by Laihanen (1987) and is based on first generating a LUT with L*a*b* values calculated for each combination of percentage dot area of the colorants (65 quantisation levels were assumed by the author). The L*a*b* values were obtained using the Neugebauer or N–Modified Neugebauer equations. Once the LUT is set up, additional colours with known percentage dot areas are measured and their L*a*b* coordinates are calculated. These measured colours are then directly inserted into the LUT and all the other entries are modified in the following way:

$$\begin{bmatrix} L^* \\ a^* \\ b^* \end{bmatrix}_{new} = \begin{bmatrix} L^* \\ a^* \\ b^* \end{bmatrix}_{old} + \frac{1}{\sum_{i=1}^{k} \frac{1}{d_i}} \sum_{i=1}^{k} \frac{1}{d_i} \left( \begin{bmatrix} L^* \\ a^* \\ b^* \end{bmatrix}_{m_i} - \begin{bmatrix} L^* \\ a^* \\ b^* \end{bmatrix}_{n_i} \right) \qquad (2.5.22)$$

Here $k$ is the number of nearest measured L*a*b* vectors taken into account, $d_i$ is the distance between the *old* vector and vector $i$, $m$ denotes one of the $k$ closest measured vectors and $n$ denotes the calculated vector having the same percentage dot area as the measured vector $m$. This method can be used for improving the Neugebauer model's accuracy in critical regions of colour space (e.g. the achromatic axis).

### 2.1.3.5 Cellular Neugebauer Equations

A further modification of the Neugebauer model was proposed by Heuberger *et al.* (1992; 1993) and is based on a similar concept as the Vector–Corrected Neugebauer equations. The main idea is to split the cube formed by the 8 colours of the classical equations into 8 cells and then measure the XYZ coordinates of the 19 new cell vertices (i.e. these are colours formed by 50 *per cent* halftone dots of the colorants and all their combinations). The Neugebauer equations are then applied within these cells (i.e. taking the vertices of a given sub–cell as the 8 colours in the classical Neugebauer equations), whereby the accuracy of the model is improved.

The Neugebauer model was most recently again studied by Mahy (Mahy and Delabastita, 1996; Mahy, 1997; 1998) whereby the analytical calculation of gamut boundaries, the calculation of the model's inverse and a method similar to the Cellular Neugebauer model were proposed.

So far the models have only dealt with obtaining XYZ coordinates from colorant amounts, however, in practice there is a need also for the reverse of this transformation. The reverse of the above printer characterisation models can be obtained either analytically, by reversing the terms of the model (e.g. for masking equations) or by using iterative numerical methods.

### 2.1.3.6 Printer Calibration

For the vast majority of digital printers, calibration is not applicable as it is not possible to alter the variables influencing colour reproduction. Therefore, characterisation needs to be carried out when any of these variables change (e.g. colorant, substrate or software), which makes it particularly important for this characterisation to require a small number of measurements. Related to printer calibration are also techniques for updating characterisation models when printer parameters change. A good example for this is the method described in a paper by Balasubramanian and Maltz (1996) which allows the modification of the characterisation model on the basis of measuring a

small number of colours for which correction vectors are calculated. All predicted colours are then corrected by these vectors in a distance–weighted way. Note, that this paper is not only intended for the purpose given here but can also be used for improving the performance of characterisation models in critical areas (just like the Vector–Corrected Neugebauer equations).

True printer calibration is primarily applicable to conventional printing – e.g. offset lithography where the user has control over parameters like printing speed, viscosity of inks and pressure between blanket and impression cylinders and where it is possible to set target values for solid density and dot gain to which the system needs to be calibrated.

### 2.1.4 Summary

The aim of this section was to give an overview of the characteristics of CRT monitors and printing devices in general and to describe a number of various characterisation models and calibration techniques for them. In the case of CRT characterisation the PLCC was chosen for this study due to its good performance and ease of implementation. For characterising the inkjet printer used in this study, some experimental and developmental work was done before arriving at a suitable characterisation model which is described in Chapter 3.

## 2.6 Gamut Mapping

Now that all other parts of a colour reproduction system – colour appearance and device characterisation – were covered, the actual focus of this study – gamut mapping – can be looked at. To this end, the aims of gamut mapping, methods for finding gamut boundaries and parameters influencing the performance of gamut mapping algorithms will be discussed first. This will be followed by brief reviews of individual gamut mapping papers and finally by a summary of gamut mapping as carried out before the beginning of this study and by other workers in the course of its duration.

### 2.6.1 Gamut Mapping Aims

First of all, it is useful to reconsider the aims of gamut mapping, which have already been touched on in Section 2.4.3. On the highest level, the aim of gamut mapping is to ensure a good **correspondence of overall colour appearance** between the original and the reproduction by compensating for the mismatch in the size, shape and location between the original and reproduction gamuts. As a number of colours are physically not reproducible, it is more advisable to aim for a reproduction of the image's appearance rather than the appearance of individual colours in the image, since the latter can be impossible for some original colours.

One of the difficulties with implementing this aim is that there is as yet no model for quantifying the appearance of complex images and neither is there one for quantifying the difference between them (though S–CIELAB (Zhang and Wandell, 1996) is a step in this direction). In the absence of such a model, a number of objectives were heuristically arrived at in the past and the following aims were identified by MacDonald (1993) to be common to the majority of gamut mapping studies:

- *preserve grey axis of the image & aim for maximum luminance contrast* This means a mapping of the original image's white and black points onto the reproduction's white and black points respectively.
- *reduce the number of out–of–gamut colours* Ideally all the image's colours should be brought within the reproduction's gamut, however, the exclusion of some extremes is sometimes though to improve the overall appearance match.
- *minimise hue shifts* It is often thought that when colours are reproduced the hue of colours needs to be left unmodified.

- *increase in saturation is preferred* As the reproduction gamut is already limited in terms of saturation, at least the available potential should be used to enable the preservation of chroma differences present in the original.

Note, that the above list represents assumptions made by some gamut mapping studies whereby the reasons for making these assumptions are in most cases based on experience from traditional colour reproduction. Even though experience from traditional colour reproduction is of great value, its maxims need to be looked at carefully when used in an environment which enables far more control over colour attributes than was previously possible.

A further commonly found aim of gamut mapping was expressed by Stone *et al.* (1988) in saying that "the relationship between the colours present was felt to be more important than their precise value." This suggests a move of the what–you–see–is–what–you–get (**WYSIWYG**) concept onto another level – i.e. it is applied to images rather than individual colours and could therefore be called **MetaWYSIWYG**. In spite of playing down the importance of a match in the traditional sense, it is still crucial for a colour reproduction system to be able to reproduce individual colours accurately – even though some original colours cannot reproduced accurately, their modifications need to be reproduced as such.

## 2.6.2 Calculating Gamut Boundaries

To fulfil the aim gamut mapping has in a particular colour reproduction system, it is first necessary to know the gamut boundaries of the original and reproduction gamuts. An understanding of colour reproduction media gamuts was considered to be of some importance for some time and was investigated by many researchers (Oittinen *et al.*, 1992; Schläpfer and Widmer, 1993; Bristow et al., 1994; Marcu and Abe, 1995a; 1995b; Meyer and Robertson, 1997). Knowing the boundaries of the gamuts between which mapping is to be carried out is essential for the majority of GMAs developed to date and can be divided into two separate problems.

Firstly, it is necessary to compute a **gamut boundary descriptor (GBD)** – i.e. some overall way of approximately describing a gamut. For media gamuts this can be done either directly from specific characterisation models – e.g. Kubelka–Munk equations (Engeldrum, 1986) or Neugebauer equations (Mahy, 1997) – or using methods which can be applied to any characterisation model (Inui, 1993). Further there are also some methods which can be used for computing the gamuts of images as well as media (Kress and Stevens, 1994).

Secondly, it is also important to be able to find the intersections between the gamut boundary (as computed using the above methods) and a given line along which mapping is to be carried out – these points will be referred to as the **line gamut boundary (LGB)**. The papers published by Herzog (1996; 1998) and Braun and Fairchild (1997) describe methods for doing this as well as obtaining the initial gamut boundary descriptor. Note, that these methods are aimed at obtaining the LGB for lines of constant hue and lightness, which are most often used by present GMAs.

As the GMAs dealt with in this study map colours in a variety of directions, new methods were developed for calculating GBDs and LGBs (Chapter 4).

## 2.6.3 Gamut Mapping Parameters

### *2.6.3.1 Colour Space*

As can be seen from the definitions of a colour gamut and of gamut mapping given in Section 1.3, they are both closely associated with colour spaces. Most gamut mapping algorithms intend to work with **perceptual attributes**, i.e. colourfulness, chroma, saturation, brightness, lightness, hue (Section 2.1.2.1) or colour names (e.g. red, dark green, orange, etc. whereby each of these would

represent a subset of colours represented by a volume in colour space) and to make this possible, they are implemented in colour spaces which predict them. More specifically, they usually intend to maintain some of a colour's perceptual attributes while changing others. If under these circumstances the **predictors** are imperfect, changes in the predictor of one attribute can also result in changes of another perceptual attribute (e.g. in some cases, if the L* – the predictor of lightness in CIELAB – of a colour is changed, its perceived hue or chroma might also change).

In the colour spaces which are most often used for gamut mapping – CIELAB and CIELUV (CIE, 1986) and in some cases LLAB (Luo and Morovic, 1996) or RLAB (Fairchild, 1998) – there are problems especially with the predictors of hue. In particular there are deficiencies in the uniformity of hue angles in the blue region of CIELAB (e.g. hue angles of around 290°) which can result in changes of perceived hue when only the L* or C* of a colour is changed. The performance of the hue predictor in CIECAM97s (Luo and Hunt, 1998) is somewhat better for this region. More detail on the performance of hue predictors of various colour spaces can be found in papers by Hung and Berns (1995) and Ebner and Fairchild (1998).

When implementing or evaluating GMAs, it is important to understand the deficiencies of the colour space used for the mapping and not to confuse the colour space's predictor with the predicted perceptual attribute (e.g. in CIELAB $h_{ab}$ is not hue and L* is not lightness – they are only their predictors).

In this study CIELAB was used in the first two experiments and in both experiments one of the GMAs was also implemented in LLAB so as to see, which of these spaces is more suitable for gamut mapping. The reason for using CIELAB was to make the results of the experiment more easily comparable with previous studies as well as due to there not being a space which has significantly better predictors. By the time the third experiment was conducted, CIECAM97s was available and was used since its hue predictor is better in the blue region and due to it being proposed as a standard colour appearance model.

### *2.6.3.2 Type of Mapping*

Once the necessary gamuts are known in the chosen colour space, it is possible to implement a GMA. One way of grouping these algorithms is by distinguishing between gamut clipping and gamut compression.

#### 2.6.3.2.1 Gamut Clipping

Gamut clipping algorithms only change colours which are outside the reproduction gamut either from the very beginning or after lightness compression. For colours outside the reproduction gamut, these algorithms specify a mapping criterion, which is used for finding the point on the reproduction gamut to which a given original colour is mapped.

#### 2.6.3.2.2 Gamut Compression

Gamut compression algorithms make changes to all colours from the original gamut so as to distribute the differences caused by gamut mismatch across the entire range. Compression is needed when larger differences are to be overcome, as gamut clipping could result in unacceptable loss of variation in out–of–gamut regions under such circumstances.

A review of studies looking at both gamut clipping and gamut compression will be given in Section 2.6.4.

### *2.6.3.3 Image v. Media Gamuts*

When gamut compression is used, there arises a question as to which gamuts to map between. This is the case as the original gamut can be seen as either the gamut of the original medium or the gamut of the original image (i.e. a subset of the original medium's gamut (Figure 2.6.1)). For current gamut clipping methods this is not an issue as it is sufficient to know the reproduction gamut to which any unreproducible colours from the original are mapped.

To make as few changes to the original image as possible, it is more reasonable to use the image gamut as the original gamut since this means that colours are only modified when necessary. Indeed there are a number of experimental studies which support the idea that the use of image gamuts gives preferred reproductions (Gentile *et al.*, 1990; Pariser, 1991; Montag and Fairchild, 1997; Wei *et al.*, 1997).

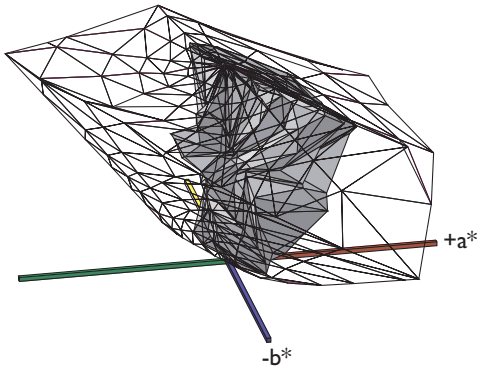


***Figure 2.6.1*** *Gamut of CRT (mesh) and MUS image (solid) in CIELAB.*

If, on the other hand, media gamuts are used, a given image could be modified to allow for colours which are not present in it (e.g. when the medium gamut is used an image's colours are changed even if all of them are in the reproduction gamut to begin with). However, there is a practical advantage to mapping between media gamuts as lookup tables (LUTs) can be calculated from them and then used for transforming an image without knowing its individual gamut.

## 2.6.4 Overview of Individual Gamut Mapping Algorithms

The reviews of gamut mapping papers given here will be presented in chronological order by year, within which they will be listed alphabetically as it would be difficult to group them according to more meaningful criteria (of which there is an overabundance and according to any one of which it would be difficult to categorise many individual papers). Note, that the following reviews focus on GMAs and their evaluation and are not intended as reviews of entire papers. Further, note that the following includes reviews not only of papers thought to be particularly important but of all gamut mapping papers which were available to the author and that (unless stated otherwise) the gamut mapping space used in these papers is CIELAB. A summary of the following papers is given in Section 2.6.5.

### *2.6.4.1 Johnson (1979)*

The method proposed by Johnson is based on the 'relativity' proposal made by Evans (1943) who said that "the rendition of some colours must not be better than that of others." Therefore the following rules were suggested as a gamut mapping algorithm (Figure 2.6.2):

- maintain hue
- compress perceived lightness linearly (using Bartleson–Breneman Lightness (Bartleson and Breneman, 1967))
- compress perceived colourfulness (chroma) linearly

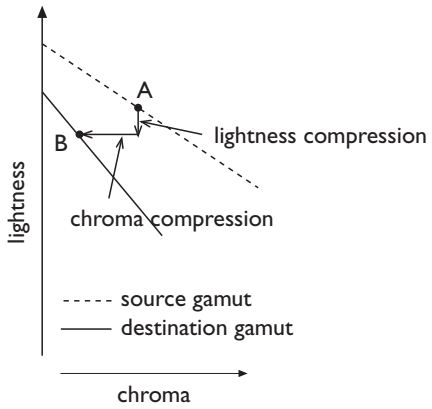


***Figure 2.6.2*** *Gamut mapping in plane of constant hue (A – original colour, B – gamut mapped colour).*

Note, that the description of this algorithm was taken from a CARISMA Project Report (1992) as the original paper was not available.

### *2.6.4.2 Sara (1984)*

In his thesis, Sara describes the following six gamut mapping methods:

(a) Clipping to the colour on the reproduction gamut boundary, which has the smallest distance in XYZ.

(b) Clipping along lines towards the centre of the lightness axis.

(c) Clipping along lines of constant lightness and hue.

(d) Clipping, whereby gamut mapping is subjectively defined for 26 points. For each of these points a centre–of–gravity is defined as the intersection of the lightness axis and the line connecting the original and gamut–mapped colours. The centre–of–gravity towards which a given colour is clipped is then calculated as a weighted average of the centres–of–gravity for the 26 points.

(e) Compression towards the centres–of–gravity as suggested in method (d).

(f) Compression as suggested by Johnson (1979).

For the compression methods the author suggests the use of piece–wise linear functions whereby there is no compression for the first segment, some compression for the second segment and clipping for the third segment.

Reproductions made with these six GMAs were subjectively evaluated by the author alone who judged the clipping to the closest colour (method (a)) to give the best results, but noted objectionable hue shifts with this method. Clipping towards the centre was judged to darken highlights and lighten shadows too much and clipping along lines of constant lightness and hue angle was judged as giving too light reproductions.

### *2.6.4.3 Gordon, Holub & Poe (1987)*

This paper sets out to achieve a faithful reproduction between two media, which it defines as being the case when:

- *neutrals of original and reproduction media are mapped onto each other and*
- *colour differences in the reproduction are equal to colour differences in the original scaled by a constant scale factor.*

The CIELUV colour space was used and as the range of colours increases in L*u*v* with lightness, the colours were stored in a tetrahedral LUT (made up of unit tetrahedra), rather than a cubic one (Figure 2.6.3).

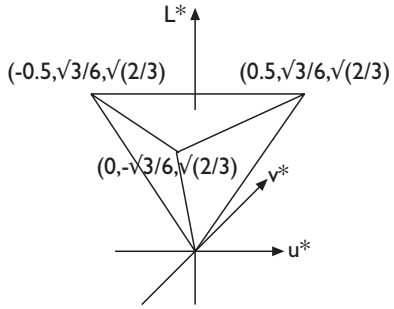


***Figure 2.6.3*** *Unit tetrahedron used for coding colours in L*u*v*.*

The importance of the above coding is not only in being a more appropriate way of storing the L*u*v* data, but also that the whole gamut compression algorithm is based on it. The method proposed by the authors is to find the colour in the original device's gamut which is furthest out of the reproduction gamut and then scaling the original gamut's unit tetrahedra so that this colour gets onto the boundary of the reproduction gamut. The authors have recognised the naiveté of this approach and have also suggested that the image gamut should be used rather than the device gamut. Non–uniform compression is also considered, however it is suggested that this would "no longer preserve similar perceptual relationships among the colours in the input image".

The method described above will inevitably result in excessive compression, as the gamut is being compressed uniformly and linearly. All but one region of the colour space will be compressed too much and this will be most noticeable if the shapes of the original and reproduction gamuts are dissimilar. The argument of loss of perceptual relationship when gamut compression is carried out in a non–linear manner would be valid if the gamut mapping colour space would be uniform. However, in CIELAB or CIELUV colour differences around the neutral axis (for example) are more perceptible than those between highly chromatic colours in which case a non–linear mapping could better preserve perceptual relationships.

### *2.6.4.4 Laihanen (1987)*

The aim of this paper is "to maintain the general colour appearance of an image as unchanged as possible" when it is transferred between monitor and print. The colour space used for the gamut mapping was LABHNU, which is similar to CIELAB and was probably chosen due to the author's familiarity with it rather than due to any advantage over CIELAB.

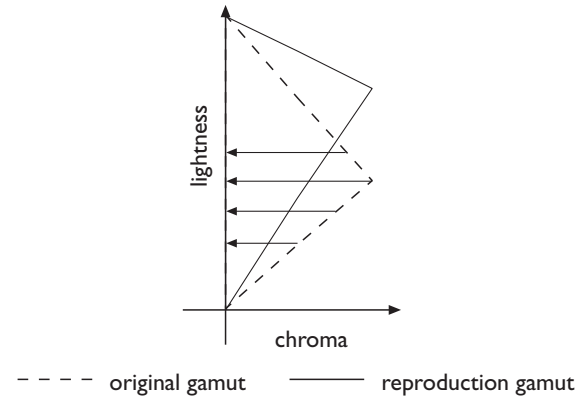


***Figure 2.6.4*** *Gamut compression with constant hue and lightness.*

Two approaches of gamut mapping are presented in this paper. They both start with normalising the lightness ranges of both gamuts to be in the range between 0 and 100 range, which in effect is uniform, linear lightness compression. The first GMA then compresses colours towards the lightness axis along lines of constant lightness and hue angle (Figure 2.6.4). Note, that the rate of compression is determined independently along each individual line, which ensures that the amount of compression used for fitting the original gamut into the reproduction gamut in a given region of

colour space is as small as possible. However, this approach was abandoned by the author as it results in potentially large variations of the rate of compression between lightness levels.

The second compression method is defined in terms of **spherical coordinates**, which are calculated as follows (Figure 2.6.5):

$$r = \sqrt{L^{*2} + A^{*2} + B^{*2}}$$
$$\psi = \arctan\left(\frac{B^*}{A^*}\right) \qquad (2.6.1)$$
$$\varphi = \arctan\left(\frac{L^*}{\sqrt{A^{*2} + B^{*2}}}\right)$$

The formulæ shown above are the ones given in the paper, however, they would not give the desired data, as they take L*=0 to be the centre. To give the correct angles and distance, L* should be changed to (L*-50) in the above equations.

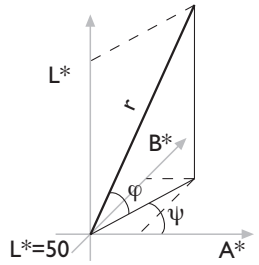


***Figure 2.6.5*** *Spherical coordinates in LABHNU.*

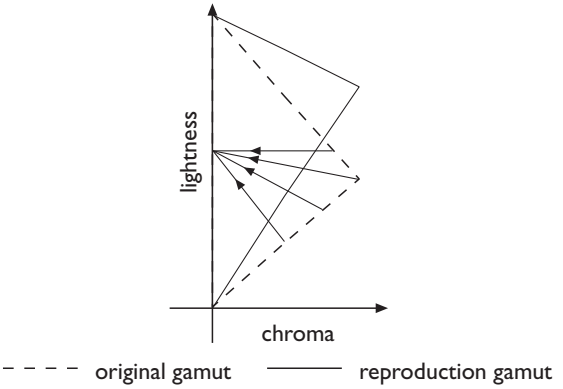


***Figure 2.6.6*** *Gamut compression towards centre of lightness axis.*

Compression is then carried out towards the centre of the lightness axis (L*=50), whereby the rate of compression is again determined independently along each individual line (Figure 2.6.6). This compression, which is carried out only on the distance from the centre (*r*) uses the following formula:

$$r_{compressed} = r_{original} k(\psi, \varphi)$$
$$k(\psi, \varphi) = \frac{r_{pr(\max)}(\psi, \varphi)}{r_{or(\max)}(\psi, \varphi)} \text{ if } r_{pr(\max)}(\psi, \varphi) < r_{or(\max)}(\psi, \varphi), \qquad (2.6.2)$$
$$\text{otherwise } k(\psi, \varphi) = 1$$

Here the indices *pr* and *or* represent proof and original respectively. Note, that the gamut of the original image is used instead of the gamut of the original medium, which, as has already been mentioned, has the advantage of compressing colours only where this is actually needed.

### 2.6.4.5 Stone, Cowan & Beatty (1988)

The gamut mapping algorithm proposed here uses the XYZ colour space, whose choice was seemingly made by default and not after considering other colour spaces. Image and reproduction gamuts are used and compression is carried out in a linear and uniform way. To illustrate the starting point of the gamut mapping algorithm, the XYZ gamuts of a CRT monitor and a Cromalin proof (both illuminated at 500 lux) are shown in Figure 2.6.7.

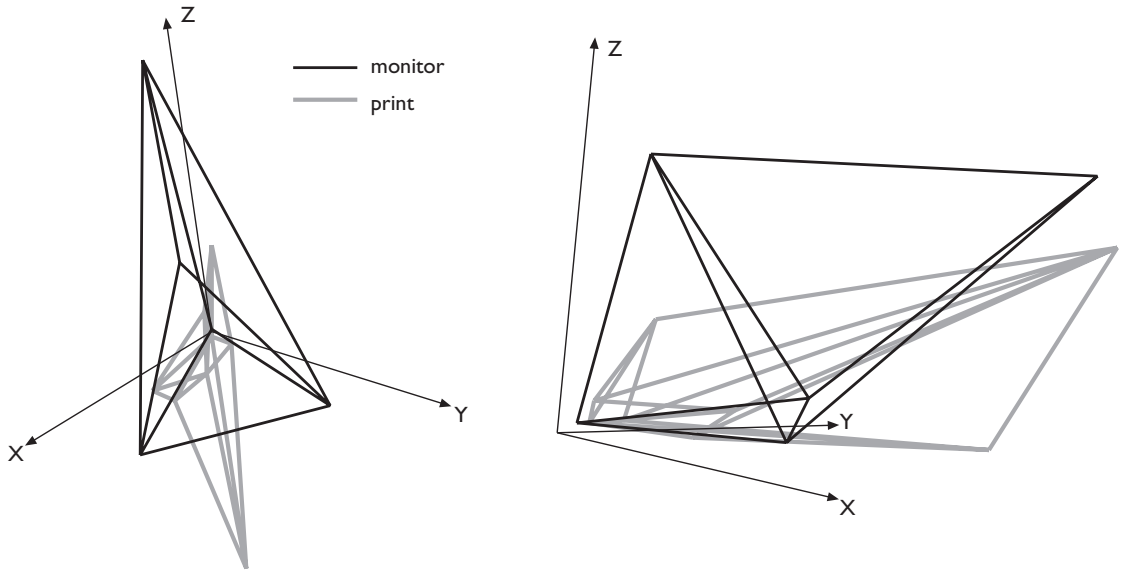


***Figure 2.6.7*** *Cromalin & monitor gamuts based on data from (Morovic, 1995).*

What follows are the individual steps of this gamut mapping technique:

*(a) Scaling*

Scaling of the image gamut so as to fit the destination device gamut is done using the following formula:

$$N_d = N_{Bd} + bs*(N_{Wd} - N_{Bd}) + csf*N_i \text{ where } N \in \{X,Y,Z\} \qquad (2.6.3)$$

$N_d$ are the tristimulus values of the reproduction device, $N_i$ are the image's tristimulus values, $N_{Bd}$ are the tristimulus values of the reproduction's black point, $N_{Wd}$ are those of the white point, *bs* is the distance by which the black point is moved along the grey axis and *csf* is the contrast scale factor. The effect of this transformation is to move the image black to the reproduction black and to re–scale the image's range to fit into the reproduction's range. As this paper focused on gamut mapping between monitor and printer, the $bs*(N_{Wd} - N_{Bd})$ term was added to move the black point further up the grey axis, as the monitor gamut is much wider near the black, than the printer gamut. A heuristic technique for selecting *csf* and *bs* values is described in the paper.

*(b) Grey Axis Rotation*

As the faithful reproduction of neutral colours is one of the prerequisites of a good gamut mapping algorithm, it is thought necessary to map the grey axes of the two gamuts onto each other. This is done by rotating the image gamut and even though the chromaticities of all colours are changed by this step their relative locations are maintained.

*(c) Umbrella Transformation*

As the original image is displayed on a monitor, all its colours are specified relative to the monitor's phosphor chromaticities. Original image colours can therefore be expressed as [R*$R_s$, G*$G_s$, B*$B_s$], where RGB are the DAC values for each phosphor and $R_sG_sB_s$ are the chromaticities of the original monitor. To reduce the saturation of the image (so as to fit into the reproduction gamut) the real phosphor chromaticities are replaced by ones closer to the white point which results in the follow-

ing colours – [$R^*R_d$, $G^*G_d$, $B^*B_d$], where $R_dG_dB_d$ are the chromaticities of virtual desaturated phosphors. The effect of this is the same as if the image was displayed on a less saturated monitor. To maintain the grey axis, the following condition needs to be satisfied, whereby $k$ is a scaling constant:

$$R_d + G_d + B_d = k^*(R_s + G_s + B_s) \qquad (2.6.4)$$

Note, that this transformation may also alter the perceived hue of the colours.

*(d) Projective Clipping*

Some extreme colours could be left out when compressing the gamut, so that the colour differences around the neutral axis are preserved better. These colours can then be projected back onto the nearest point of the reproduction gamut. However, if the surface of the gamut is concave, smoothly varying colours in the original image will have discontinuities when clipped.

A problem with the approach outlined above is the environment in which it is implemented as the mapping in a perceptually non–uniform colour space (XYZ) will lead to excessive compression around the neutral axis – exactly the area in which colour changes are most perceptible. Furthermore the effects of chromatic adaptation also need to be taken into account as they will reduce the apparent difference between the two media and will therefore result in a reduction of the extent of compression needed. Some of these points were later recognised and implemented by the authors themselves (Stone and Wallace, 1991).

### 2.1.1.6 Meyer & Barth (1989)

The gamut mapping proposed here consists of three stages: L* compression, C* compression and clipping. The lightness compression in this paper is different from all the other methods as it uses homomorphic image processing techniques. For this purpose the lightness at a given point [x,y] in the image can be expressed as follows:

$$F(x,y) = I(x,y)^*R(x,y) \qquad (2.6.5)$$

where $I$ is the spatially slowly varying contents in an image (depending on the illuminant) and $R$ is a spatially rapidly varying function containing the image detail itself. The $I$ component is the one controlling the dynamic range, which needs to be scaled to obtain a match in the lightness ranges of the two gamuts (a technique for extracting the two components is given in the paper). Chroma compression is carried out using a piecewise linear function along lines of constant L* and hue angle. Finally any colours which are still out of gamut after the first two stages are clipped onto the gamut boundary along lines of constant lightness and hue angle.

The technique proposed here is similar to the technique proposed by Johnson (1979) with the only difference being lightness compression. The idea of gamut compression using image processing techniques is an interesting one and could be further investigated to include chroma compression as well.

### 2.1.1.7 Taylor, Murch & McManus (1989)

The method used in the *Tektronix HVC* system described in this paper results in an XYZ match for colours in the overlap of the original and reproduction gamuts. Out–of–gamut colours are clipped onto the nearest colour on the reproduction gamut boundary, which has the same hue as the original colour. This method is similar to method (a) from the paper by Sara (1984) and presumably reduces the extent of hue changes noted there. Note, that the description of this GMA is based on a paper by Murch and Taylor (1989).

### 2.1.1.8 Gentile, Walowit & Allebach (1990)

Both clipping and compression techniques are described in this paper and for both kinds the gamut mapping environment is either RGB or CIELUV. In terms of clipping algorithms two possibilities are looked at: clipping to the closest colour in terms of $\Delta E$ and clipping to such a colour, which is closest when one or more attributes are kept constant (i.e. lightness, chroma, saturation or hue angle). Two compression algorithms were also investigated: compression along lines of constant lightness and hue angle and compression along lines of constant saturation. In addition to looking at linear compression along a given line, piecewise linear compression, which varied the slope of two segments joined at the point having the value of the reproduction range was also investigated (Figure 2.6.8). These piecewise linear functions were labelled with a λ value which represented the normalised distance of the connection point from the linear compression function.

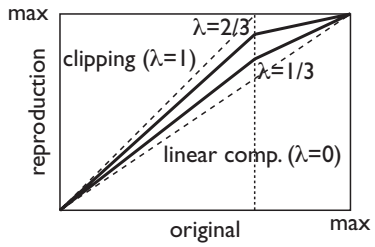


***Figure 2.6.8*** *Piecewise linear compression functions.*

A psychophysical experiment looking at the preference of gamut mapped images was conducted to test a number of algorithms. To this end, three images were used and gamuts of different sizes were simulated on screen. The results suggested that clipping is preferred to compression and that lightness and hue angle are more important than chroma and saturation.

However, it needs to be seen how well the results of an experiment which uses synthetic gamuts and simulates a reproduction medium on the original medium correlate with the performance of GMAs on real reproduction media. Further it needs to be noted that the compression of lightness is not addressed in this paper and different methods for this could also have an effect on the results of the discussed mappings. Nonetheless, the range of chroma and saturation compressions suggested here is a very good one and well worth investigating in future.

### 2.1.1.9 Lamming & Rhodes (1990)

The approach used in this paper is strictly intended for matching a monitor and a printed medium and uses iterative empirical methods to obtain LUTs for transforming RGB to CMYK. Its lightness mapping relies on two LUTs – one between RGB and L* and the other between CMY and L* (all the patches for obtaining the LUT are achromatic, as the lightness mapping is thought to be similar for chromatic and achromatic colours). Out–of–gamut colours are modified by transforming all colours using the following matrix:

$$\begin{bmatrix} D_C \\ D_M \\ D_Y \end{bmatrix} = \mathbf{A} \begin{bmatrix} D_R \\ D_G \\ D_B \end{bmatrix} \qquad (2.6.6)$$

$$D = -\log_{10}\left(\frac{L^* + 16}{116}\right)^3$$

Here **A** is a 3x3 matrix, which starts off as being an identity matrix and is then iteratively modified by the user so as to improve the appearance of the reproduction. To maintain the grey balance, the sum of the terms in each row needs to be equal to one. Note, that the matrix can be used for adjusting both saturation and hue.

For the majority of applications where accuracy is of importance, this method is not particularly useful as its performance depends heavily on the skills of the person setting up the transformation matrix by trial and error.

### 2.1.1.10 Hoshino (1991)

A method for gamut compression and **expansion** is described here which is intended for the mapping between images defined in terms of CMYK values and the colour gamut of high definition television (HDTV) on which they are to be displayed. Lightness mapping is carried out using a non–linear tone reproduction curve, which, however, is not described in more detail. After this, the chroma of original colours in general is either compressed or expanded along lines of constant lightness and hue angle, depending on the gamut boundaries of the two media along a given line. In the case of gamut expansion, a hue shift was also employed for some colour regions (i.e. cyan and blue) so as to make the degree of expansion more similar between neighbouring areas.

### 2.1.1.11 Pariser (1991)

Various combinations of clipping and compression techniques either along lines of constant L* and hue angle or towards the centre of the lightness range were tested in this paper. Synthetic gamut boundaries were used as in the case of Gentile *et al.* (1990) and the experimental evaluation suggested that both kinds of clipping techniques gave better reproductions than algorithms using compression. When interpreting these results it needs to be taken into account again, that the lightness and chroma ranges of the two gamuts as well as their gamut shapes were similar.

### 2.1.1.12 Stone & Wallace (1991)

Like many other papers, this one too starts with an outline of general principles which in this case were the following:

- *adjust lightness to make detail visible throughout tonal range,*
- *maintain hue (not hue angle, as planes of constant $h_{ab}$ do not have constant perceived hues) and*
- *maintain or enhance overall chroma relative to output gamut.*

To achieve these aims, the following technique is proposed. Lightness is calculated using relative colorimetry (hence the white points of the two media are the same in terms of CIELAB) and the lightness ranges of the two gamuts are first mapped linearly onto each other so that the black of the original's gamut is mapped slightly below the black of the reproduction gamut. Chroma is then non–linearly mapped along lines of constant hue and lightness (Figure 2.6.9).

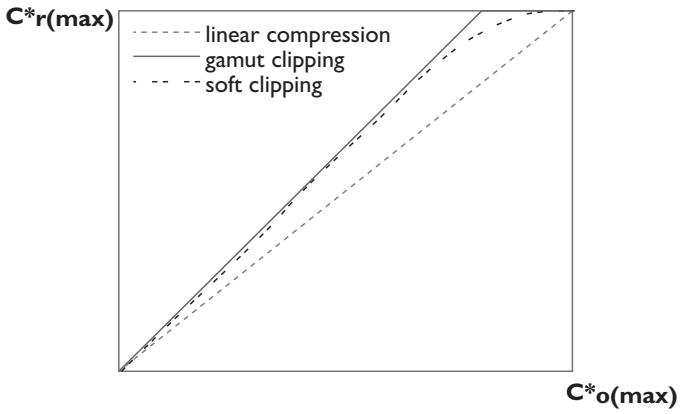


***Figure 2.6.9*** *Chroma mapping functions.*

What is later described as a soft clipping function (Hoshino and Berns, 1993) is introduced in this paper and is a non–linear compromise between a linear mapping and gamut clipping. This is done

with a higher order function which is tangent to the y=x function near the grey axis and then diverges from it near the maximum reproduction chroma. The authors also point out that the soft clipping function could be made to be tangent to a function whose slope is greater than 1, so as to increase overall chroma, which can help to obtain more pleasing results in some cases.

A problem, which was identified by the authors is that the lines along which the compression is carried out are not lines of constant hue, which reduces the effectiveness of this approach.

### 2.1.1.13 CARISMA (1992)

This report describes the gamut mapping work carried out by Johnson, Luo, Rhodes and their co–workers as part of a project entitled *Colour Appearance Research for Interactive System Management and Application* (CARISMA). Their approach to investigating gamut mapping was to "get experienced [scanner] operators to reproduce images and see what they do to them". To do this, a Kodak Q60 Ektachrome transparency – on which the IT8.7/1 chart (ANSI, 1993) is based – was given to five colour reproduction companies in the UK and the USA. Scanner operators were then asked to scan the transparency both with their "standard" setup and also to edit the setup to give a better reproduction if they felt it was necessary and a gamut mapping algorithm (which will be described in detail in Section 7.5) was then developed on the basis of the resulting reproductions.

The interesting characteristics of this algorithm are that it suggests changes to hue and that it uses different mapping methods for different hues depending on the relative shapes of the original and reproduction gamuts. Apart from the main gamut mapping algorithm, the report also shows that there was substantial agreement between the different scanner operators (using different equipment and being in different countries).

### 2.1.1.14 Viggiano & Wang (1992)

The aim set out in this paper was to compare various lightness mapping techniques both in XYZ and in CIELAB, which was done by looking at the following methods:

*(a) Compress Y and keep X and Z constant*
This was rejected as it resulted in a shift towards yellowish green.

*(b) Compress Y and keep x and y constant*
Even though hue and grey balance were maintained, chroma was increased and this was found to be particularly unacceptable for dark colours – therefore this method was also rejected.

*(c) Compress L* and keep C* and $h_{ab}$ constant*
The compression suggested for L* is a linear compression in Bartleson and Breneman's Darkness (*V*) (Bartleson and Breneman, 1967). The compression is carried out using the following formulæ:

$$V_r = TCR * V_o \qquad (2.6.7)$$

$$V = 1.16 - 0.175*[100*(Y/Y_n) + 0.6]^{0.41} \text{ (dim surround)} \qquad (2.6.8)$$

$V_r$ and $V_o$ are the darkness values for the reproduction and original respectively and *TCR* is the tone compression ratio (which should be the ratio of the darkness range of the reproduction and the original). Formulæ for calculating darkness values for other backgrounds are also given in the paper.

Even though this approach results in a reduction of saturation, it yields good results, as the constancy of chroma has already been identified by some earlier work (Pobboravsky *et al.*, 1971) as an important condition for good colour reproduction.

*(d) Compress L* and C* equally and keep $h_{ab}$ unaltered*

Here the same compression ratio is applied to chroma and darkness, i.e.

$$C_r = CCR * C_o \tag{2.6.9}$$

$$CCR = TCR \tag{2.6.10}$$

Here *CCR* is the chroma compression ratio, $C_r$ and $C_o$ are the C* coordinates of the reproduction and original respectively. Note, that this technique is based on earlier work (Gordon *et al.*, 1987).

*(e) Compress L* and C* independently and keep $h_{ab}$ unaltered*

What *CCR* and *TCR* values give best results was experimentally tested and the best results were achieved by the following relationship between the two ratios (i.e. a chroma compression half way between the tone compression ratio and unity):

$$\mathrm{CCR} = 0.5*(1 + \mathrm{TCR}) \tag{2.6.11}$$

The experimental evaluation of the above methods found that the independent compression of lightness and chroma with an unchanged hue angle (method (e)) gave the best results. However, the experimental results need to be treated with caution, as the effects of the different compression methods were simulated on the monitor, rather than comparing the two media for which the gamut mapping was intended. Furthermore it is not clear from the description of the experiment what images were used, especially what their characteristics were in terms of chroma range, which might also influence the results. Nonetheless, the paper gives a good overview of a range of possible mapping techniques with some useful suggestions as to compression ratios.

### 2.1.1.15 Haneishi, Miyata, Yaguchi & Miyake (1993)

As in many other papers, the method described here is aimed at obtaining a match between a monitor and a printer, whereby the match is attempted by transforming RGB values from the monitor to RGB values sent to the printer. The technique uses the RGB colour space to classify colours into five classes: skin colours, neutrals (grey), red, green & blue and then determines separate transformations for each class. The classification is done by projecting all colours onto a unit triangle and analysing the coordinates within that triangle (Figure 2.6.10).

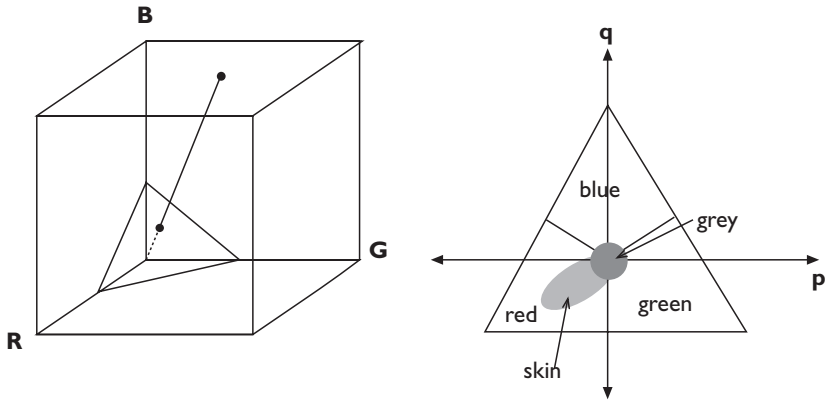


***Figure 2.6.10*** *Colour classification of RGB colours.*

The transformation into the *pq* plane is achieved with the following matrix:

$$\begin{bmatrix} p \\ q \end{bmatrix} = \begin{bmatrix} -\frac{1}{\sqrt{2}} & \frac{1}{\sqrt{2}} & 0 \\ -\frac{1}{\sqrt{6}} & -\frac{1}{\sqrt{6}} & \frac{2}{\sqrt{6}} \end{bmatrix} \begin{bmatrix} r \\ g \\ b \end{bmatrix} \tag{2.6.12}$$

To decide into which class a colour belongs, the following equations are analysed:

**skin colour**, where $p = -0.102, \bar{q} = -0.099$, $\lambda = 1$, $a = 0.601$, $\sigma_p = 0.00769$ and $\sigma_q = 0.0035$:

$$2(1-a^2)\lambda \geq \frac{(p-\bar{p})^2}{\sigma_p^2} - 2a\frac{(p-\bar{p})(q-\bar{q})}{N\sigma_p\sigma_q} + \frac{(q-\bar{q})^2}{\sigma_q^2} \qquad (2.6.13)$$

**neutral colour**:

$$p^2 + q^2 = 0.15^2 \qquad (2.6.14)$$

Whether a colour is **red**, **green** or **blue** is determined by the largest of the three coordinates (RGB). As the classes overlap, the following scale of priorities is used: skin > grey > red, green, blue.

Once the colours are classified, a separate transformation matrix is calculated for each class in the following way. A 17x17x17 $R_cG_cB_c$ colour cube is output on the printer and the XYZ coordinates of each patch are measured. These are then converted to L*a*b* and a lightness compression is carried out, so as to accommodate for the different lightness ranges of the two media.

$$L^{*\prime} = k(L^* - L^*_{p(min)}) + L^*_{c(min)} \qquad (2.6.15)$$

$$k = (L^*_{c(max)} - L^*_{c(min)})/(L^*_{p(max)} - L^*_{p(min)}) \qquad (2.6.16)$$

Here the index *c* refers to the CRT and *p* to the printer. The CIELAB coordinates are then converted back to XYZ and finally to $R_pG_pB_p$, then the (3x11) transformation matrix ($\mathbf{M}_i$) used for a particular class is obtained using linear regression. Finally, the transformation for a particular class is the following:

$$f_{(x,y)} = \boldsymbol{M}_i f'_{(x,y)} \qquad (2.6.17)$$

$$f_{(x,y)} = [R_p, G_p, B_p]^T \qquad (2.6.18)$$

$$f'_{(x,y)} = [R_c, G_c, B_c, R_c^2, G_c^2, B_c^2, R_cG_c, R_cB_c, G_cB_c, R_cG_cB_c, 1]^T \qquad (2.6.19)$$

To avoid unnatural colour edges between areas of pixels of different colour classes, the transformation matrices for colours on the edge of a region having a particular colour class are convoluted with the matrices of the neighbouring pixels' transformation matrices in the following way:

$$f_{(x,y)} = \sum\{w_{i(x,y)} M_i f'_{(x,y)}\} \qquad (2.6.20)$$

$$w_{i(x,y)} = \frac{k_{i(x,y)}}{n^2} \qquad (2.6.21)$$

Here *i* is the label of a colour class (1 = skin, 2 = grey, …), $n^2$ is the number of pixels in the neighbouring area taken into account and $k_i$ is the number of pixels in the neighbouring area belonging to class *i*.

Even though some details of the implementation could be improved, the idea of classifying colours is probably worth considering, as the need for different kinds of transformation for different colours is commonly suggested and was also implemented by other authors (e.g. Spaulding *et al.* (1995)). Also the technique for colour classification proposed here is a simple and generic one, which makes it easy to incorporate it into other gamut mapping algorithms.

### *2.1.1.16 Hoshino & Berns (1993)*

An overview of different gamut mapping techniques (all of which are described in the preceding sections) is given in the beginning of this paper after which the following four lightness mapping techniques are evaluated using a paired comparison method:

- *linear lightness mapping* (compression to 95 *per cent* (minimum necessary to fit into reproduction gamut) and 90 *per cent* of the original scale were used)

- *soft clipping* (a technique similar to the one used by Stone and Wallace (1991) was used, whereby the first 75 *per cent* or 95 *per cent* of the reproduction lightness scale from white were left unaltered and the remaining 25 *per cent* or 5 *per cent* respectively were linearly mapped onto the darkest black of the reproduction's gamut (Figure 2.6.11). Again clipping to 95 *per cent* and 90 *per cent* of the original scale were used)

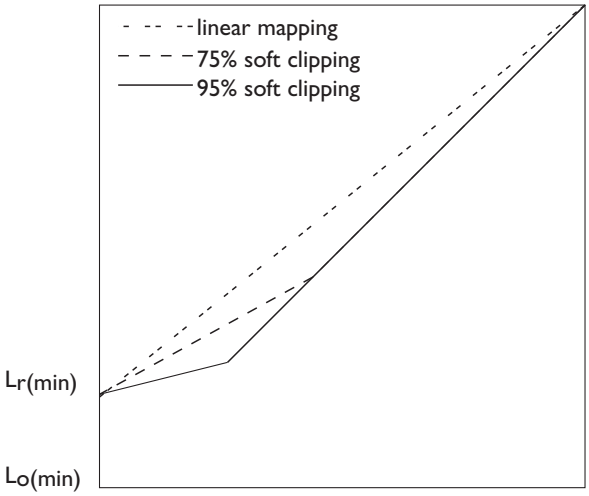


***Figure 2.6.11*** *Lightness mapping techniques.*

Colourfulness mapping was not evaluated in this experiment and chroma clipping with constant hue and colourfulness was used. Note, that the gamut mapping space was based on Hunt's colour appearance model (Hunt, 1991).

The results from the paired comparison experiment in which printed reproductions and original images on transparencies were compared, suggested that the successfulness of the compression depends on the amount of compression. Where only small amounts of compression were needed, 95 *per cent* soft clipping resulted in the best reproduction, whereas for large amounts of compression the results were image dependent. For large amounts of compression, the soft–clipping approach was better for images of high to medium lightness, but was found to be worse for dark images as it introduced an artefact referred to as fluorence. **Fluorence** was defined as the instance "when the brilliance of the stimulus exceeds that of its surrounding or comparison stimuli" (Evans, 1974), i.e. when it appears to be fluorescent.

In terms of interpreting the results of this paper, it would have been useful to know the colourfulness ranges of the test images used and it is of use to keep in mind that the differences between original and reproduction gamuts were relatively small (compared to gamut differences in the experiments of this thesis). Nonetheless, the evaluation of lightness mapping techniques described here provides useful data for setting up a gamut mapping algorithm and should be taken into account.

### *2.1.1.17 MacDonald (1993)*

The aim of this paper is to outline the advantages of implementing gamut mapping in a colour appearance model's colour space. It highlights the importance of the illuminant, surround and medium on which a given image is shown and points out that these crucial factors are not taken into account when other environments, like XYZ or uniform colour spaces, are used. A five stage transform (as mentioned in Chapter 1) is proposed, where gamut mapping is performed between the appearance attributes (lightness, hue, colourfulness) of the two gamuts and the recommended colour appearance model is the one developed by Hunt (1991). Overall this paper gives a good overview of the issues involved in gamut mapping and can be seen as a good general introduction to the topic.

### 2.1.1.18 Appel, Durbin & Lehman (1994)

This patent of the Xerox Corporation uses a set of two look up tables (RGB → XYZ and XYZ → CMYK) and maps a given RGB colour onto the CMYK colour with the closest XYZ coordinates.

### 2.1.1.19 Harrington (1994)

As the aim of this Xerox patent is to provide a gamut mapping for real–time applications, it suggests a computationally fast transformation scheme. The environment, in which this gamut mapping algorithm is implemented is the YES colour space as specified by the Xerox Corporation (1989). Its axes are linear transformations of XYZ (or RGB) and are similar in nature to ATD, by being modelled on opponent colour signals. The following are equations for obtaining YES coordinates from RGB (where RGB are cone responses similar to those in CIECAM97s):

$$\begin{aligned} Y &= 0.253R + 0.684G + 0.063B \\ E &= \frac{R-G}{2} \\ S &= \frac{R+G}{4} + \frac{B}{2} \end{aligned} \tag{2.6.22}$$

YES can also be obtained from XYZ by:

$$\begin{aligned} Y &= Y \\ E &= 2.019X - 1.743Y - 0.2467Z \\ S &= 0.423X + 0.277Y - 0.831Z \end{aligned} \tag{2.6.23}$$

The gamut mapping is then carried out on the logarithms of these coordinates:

$$\begin{aligned} l_e &= \text{sign}(E)(A\log(\max(|E|, N) + B) \\ l_s &= \text{sign}(S)(A\log(\max(|S|, N) + B) \end{aligned} \tag{2.6.24}$$

The sign function returns either plus or minus depending on the value of $E$ or $S$. $A$, $B$ and $N$ are used to determine the range and domain of $E$ & $S$, whereby $A$ results in scaling, $B$ in offset and $N$ prevents determination errors by providing a non–zero cut off value. A similar transformation can also be applied to $Y$, but this is considered by the author to be optional. After the colours are divided into four quadrants, they are arranged according to hue and lightness using the following correlation of hue:

$$H = |l_e| - |l_s| \tag{2.6.25}$$

To obtain the gamut boundary, four tables (one for each quadrant) are set up, whereby the maximum values for $|l_e|$ are stored for each combination of $H$ and $Y$ and this is done for both source and destination gamuts. From these, another set of four tables ($F[H,Y]$) can be determined, which contains the factors by which the two gamuts differ:

$$F[H,Y] = \max(0, Table[H,Y] - PrinterTable[H,Y]) \tag{2.6.26}$$

Here $Table[H,Y]$ represents the input and $PrinterTable[H,Y]$ the output. As all the values involved are logarithms, their difference represents the factor by which the original values ($E$ & $S$) differ. The gamut compression can therefore be carried out as follows:

$$|l_e'| = \max(0, |l_e| - F[H,Y]) \tag{2.6.27}$$

$$|l_s'| = \max(0, |l_s| - F[H,Y]) \tag{2.6.28}$$

Alternatively, the compression factor can be forced to be below a chosen value ($M$):

$$|l_e'| = \max(0, |l_e| - \min(F[H,Y], M)) \tag{2.6.29}$$

$$|l_s'| = \max(0, |l_s| - \min(F[H,Y], M)) \tag{2.6.30}$$

As can be seen, a non–uniform compression technique is used, since the compression factors are determined depending on the hue angle and lightness. After the compression, the $|l_e'|$ & $|l_s'|$ values are converted back to $l_e$ & $l_s$ (their sign will be determined by their source quadrant) and then to $E$ & $S$. The method described above uses a cylindrical method of compression i.e. hue and lightness are constant and compression is only applied to chroma. The patent also discusses a spherical implementation of the linear compression described above, which is analogous.

This is certainly one of the more useful patents as it describes a computationally effective way of implementing linear chroma compression, or linear compression towards the centre. However, in terms of actual gamut mapping approaches it does not propose any new solutions.

### 2.1.1.20 Hoshino (1994)

This patent deals with gamut expansion so as to extend the gamut of a printed image to be displayed on a CRT. The algorithm described here can be either implemented in CIELAB or CIELUV and is based on first extending L*, depending on the ratio of lightness ranges of the two gamuts, and then C*, again depending on the ratio of maximum chromas along a given line of constant lightness and hue angle. After this, further compensation is carried out to maintain the appearance of the image, e.g. the lightness of colours is also increased when their chroma was increased (i.e. to maintain their saturation).

### 2.1.1.21 Liang (1994)

The aim of this DuPont patent is to match the responses of two different printers to RGB data. To achieve this, a number of patches with known RGB values are first printed on both printers. These are then measured using a colorimeter and LUTs are generated to relate input values to measured values. Colours from the overlap of the two gamuts are mapped by finding the RGB value from the second printer's LUT, which has the CIELAB coordinates of the RGB value chosen from the first printer's LUT. The technique chosen for mapping colours from the first gamut, which are outside of the second gamut is the following:

- find the two (or more) colours closest to the out of gamut colour, which have a corresponding colour in the output gamut. Find a colour in the output gamut for the out–of–gamut colour by extrapolating using the two (or more) colours inside the gamut. The extrapolation is carried out in the target printer's device gamut (it is carried out for R, G and B separately) and it can be linear or of a higher order if necessary. The linear extrapolation is shown graphically in Figure 2.6.12.

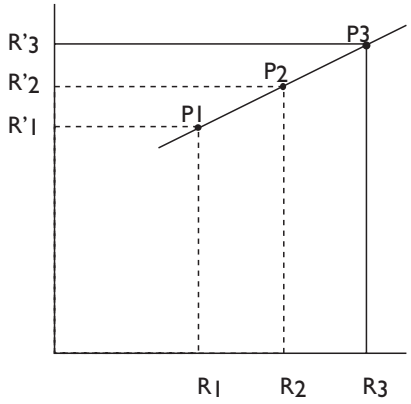


***Figure 2.6.12*** *Linear extrapolation to calculate red coordinate ($R'_3$) for out–of–gamut colour $P_3$ using the coordinates of two of the closest colours $P_1$ and $P_2$.*

- if the extrapolated value exceeds 255, it is set to 255

- if the slope of the extrapolating line is too small (the out of gamut colours are greatly compressed), a point which is further from the out–of–gamut point is selected and the colours in between are remapped

Mapping the out–of–gamut colours as proposed in this patent would probably have unpredictable effects on its perceptual attributes, as the three device dependent coordinates are altered independently.

### 2.1.1.22 Ruetz (1994)

This patent, held by an employee of Canon Information Systems, describes a gamut mapping strategy, where lightness is mapped so that the central part of the lightness scale (e.g. from L*=38 to L*=90) is kept unmodified and only the extremes are compressed in a way which is not disclosed (most probably a function similar to the soft clipping function used by Stone and Wallace (1991)).

As in the majority of algorithms, here too the hue angle is kept unchanged. Finally, chroma is clipped onto the surface of the reproduction gamut boundary along lines, which are at an angle ($\alpha$) to the horizontal axis (Figure 2.6.13). Note, that all the colours within $2\alpha$ of the destination gamut's cusp are mapped onto the cusp and that the angle of 15 degrees was identified to give the best results in most cases.

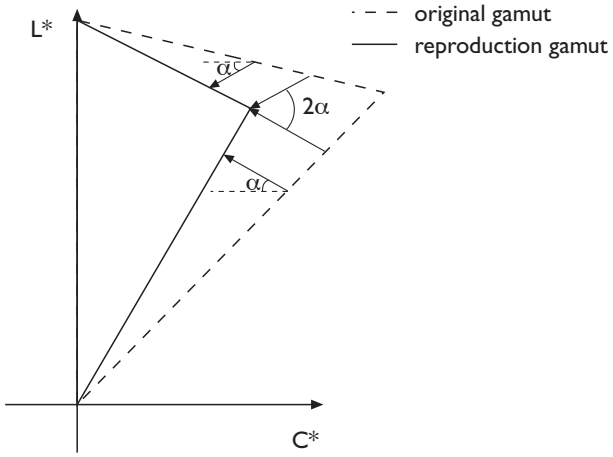


***Figure 2.6.13*** *Chroma clipping proposed by Ruetz (1994).*

The problems, which were identified in the patent are the changes in the perceived hue of colours with high chroma, which are due to the non–uniformity of the lines of constant $h_{ab}$.

### 2.1.1.23 Schläpfer (1994)

This document of the *Swiss Federal Laboratories for Materials Testing and Research* (EMPA) gives data describing the "correlation between calculated and measured values" for two gamut mapping algorithms for transforming colours from transparencies to newsprint (i.e. a medium having a very limited L* range – from approximately 35 to 80 [using absolute colorimetry] and a maximum chroma of approximately 50). The following is the description of the two algorithms reproduced here *verbatim*:

**Model 1**

- *Lightness:* Linear compression based on the values of the substrate and of $D_{max}$.
- *Hue:* Individual correction for each hue angle based on the values of primary and secondary colours.
- *Chroma:* Hue–dependent non–linear compression based on a lookup–table.

**Model 2**

- *Lightness:* Identical with Model 1.
- *Hue:* No correction.
- *Chroma:* Non–linear compression based on a hue–independent empirical formula.

Unfortunately the document reviewed here does not give more detail on the above algorithms. Nonetheless, Model 1 in particular bears some resemblance to the model described in CARISMA (1992). This is an interesting fact, as the former model is intended for going between transparency and newsprint whereas the latter was developed on the basis of reproducing transparencies on Cromalin proofs and as these two reproduction media have very different gamut sizes.

### 2.1.1.24 Spence, Granger & Rinehart (1994)

This patent of the Eastman Kodak Co. describes a technique which uses an iterative process for determining a set of transformations between two colour reproduction systems, whereby the device–independent colour space is that of the ATD colour appearance model (Guth, 1989). As focus of the work seems to be the matching of two printers, the problem of gamut mapping is not fully addressed. The solution which is suggested is to map the out–of–gamut colours onto the closest colour on the gamut boundary. The technique claims to obtain a good colour reproduction by achieving the following objectives, which in effect are the matching of six colours:

- *match lightness of three–colour (CMY) black solid overprint*
- *match hue angle of CY (green) & MY (red) solid overprints*
- *match colour of 50 per cent grey CMY tint overprint*
- *match solid and 50 per cent black (K)*

The problem being addressed here is one of mapping between two very similar gamuts using only densitometry – i.e. it is directed at setting up a match between different individual presses and proofing systems in a printing environment. It might be a good solution for this particular task, but it is unlikely that this method will work when other media are involved.

### 2.1.1.25 Spence (1994)

This is a variation of the patent discussed in the previous section and differs from it by using the CIELAB colour space, other than that the same comments apply.

### 2.1.1.26 Wolski, Allebach & Bouman (1994)

Here a system is proposed which combines some of the techniques suggested by previous authors – i.e. soft clipping (Stone and Wallace, 1991) and separate mapping algorithms for different parts of colour space (CARISMA, 1992; Haneishi *et al.*, 1993). The algorithm, which is implemented in the CIELUV colour space and maps between the original image and reproduction medium gamuts, consists of the following steps (Figure 2.6.14):

(1) map source colours into smallest rectangle containing the target gamut in a given plane of constant hue by soft clipping saturation (chroma), shifting and then soft clipping lightness (i.e. use 75 *per cent* between L*=50 and maximum L* as cut off point in soft compression and clip colours with too low L*, after the whole range was shifted in an unspecified manner by between -5 and 2 L* units depending on the target gamut)

(2) divide input gamut into three regions: cylinder around neutral axis (radius between 0.3 and 1 saturation units), upper chromatic region (L*>50) and lower chromatic region (L*<50)

(3) compress saturation and maintain lightness for the neutral cylinder (how it is done is not specified…)

(4) maintain saturation and compress lightness for upper chromatic region

(5) map lightness and saturation simultaneously in a ratio of two lightness units to one saturation unit (however, this ratio can be different for some images)

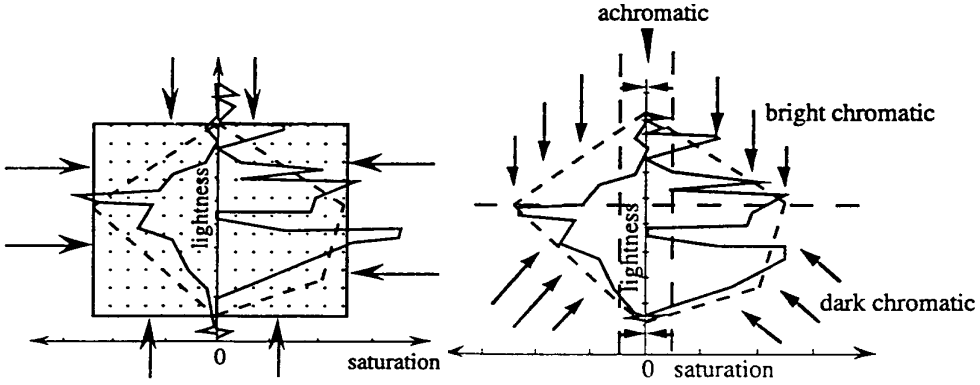


***Figure 2.6.14*** *Visualisation of the gamut mapping algorithm (reproduced from (Wolski et al., 1994)).*

The method proposed in this paper recognises the need for different kinds of mapping for different regions. However, the techniques suggested for the actual mapping are in some cases not particularly well–defined.

### 2.1.1.27 Berns & Choh (1995)

This paper primarily focused on colour appearance modelling and the gamut mapping it used was in effect gamut clipping, which minimises $\Delta E_{ab}$.

### 2.1.1.28 Granger (1995)

In this paper the ATD colour appearance model (Guth, 1989). Its properties are exploited by the gamut compression method as it makes the largest changes in regions which would be compressed by the visual system anyway. In the words of the author, "pixel values should be distorted in regions where the eye compresses the response to the input stimulus". As the colour differences are relatively much smaller away from the neutral axis, it is possible to make heavier compression in these regions, which is implemented in the following way:

First it is necessary to transform all colours into the ATD colour space. To do this, "Meta RGB" is calculated from XYZ (inverse transformation is also shown):

$$\begin{bmatrix} X \\ Y \\ Z \end{bmatrix} = \begin{bmatrix} 0.257 & 0.066 & 0.049 \\ 0.115 & 0.286 & -0.009 \\ -0.026 & 0.015 & 0.438 \end{bmatrix} \begin{bmatrix} R \\ G \\ B \end{bmatrix}; \quad \begin{bmatrix} R \\ G \\ B \end{bmatrix} = \begin{bmatrix} 4.271 & -0.963 & -0.5 \\ -1.709 & 3.878 & 0.271 \\ 0.314 & -0.189 & 2.243 \end{bmatrix} \begin{bmatrix} X \\ Y \\ Z \end{bmatrix} \quad (2.6.31)$$

The RGB values are then transformed into ATD itself:

$$A = \frac{R + 3G}{4};\ T = R - G;\ D = \frac{R + G - 2B}{2} \quad (2.6.32)$$

There is also a chromaticity diagram associated with the space:

$$t = \frac{R - G}{R + 1.5G + B}; d = \frac{R + G - 2B}{2R + 3G + 2B} \quad (2.6.33)$$

Finally, saturation is defined as $C = (d^2 + t^2)^{1/2}$.

*Saturation Compression*

It was suggested by Guth (1989) that the adaptation for ATD channels is of the following nature ($V$ is visual sensation, $S$ is the stimulus and $K1$, $K2$ are the model's parameters):

$$V \approx \frac{K_1 S}{K_2 + S} \tag{2.6.34}$$

Based on the same work, a Taylor series expanded to third order was proposed as the compression function to be used (see following formula):

$$V \approx \frac{K_1 S}{K_2} - \frac{K_1 S^2}{K_2^2} + \ldots \tag{2.6.35}$$

Here the second order term is the "compression cost factor", which determines how much a given region of the colour space can be compressed.

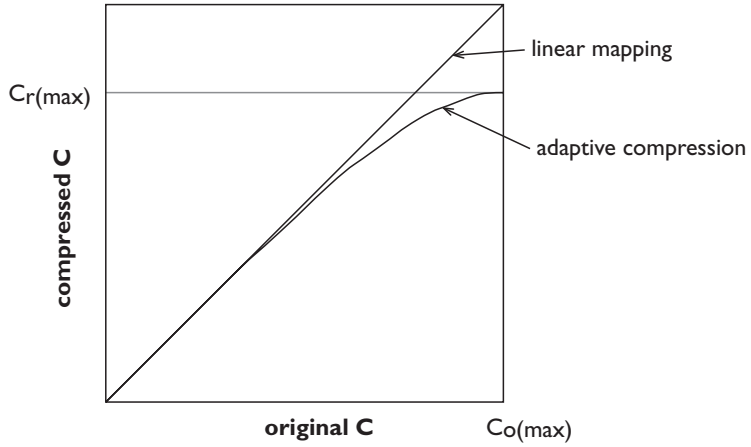


***Figure 2.6.15*** *Adaptive compression of chroma for a particular hue angle (The indices o and r signify original and reproduction respectively).*

Note, that the compression depends on the hue angle and Figure 2.6.15 shows the type of compression obtained with the above formula.

*Lightness Compression*

The same strategy is adopted for lightness ($A$) as was used for saturation. However, as the visual system is less sensitive to dark colours, the mapping is carried out on darkness, which is defined as:

$$D = 1 - A \tag{2.6.36}$$

Even after darkness and chroma are compressed, there could be some out–of–gamut colours, which will be mapped in the following way.

*Out–of–Gamut Colour Mapping*

Out–of–gamut colours are treated depending on which extreme of the lightness scale they are at. For light colours $A$ and hue are maintained and chroma is clipped to the boundary of the gamut. The chroma of dark colours is reduced to a percentage of the maximum chroma (for a given hue angle), depending on the darkness of the colour (Figure 2.6.16).

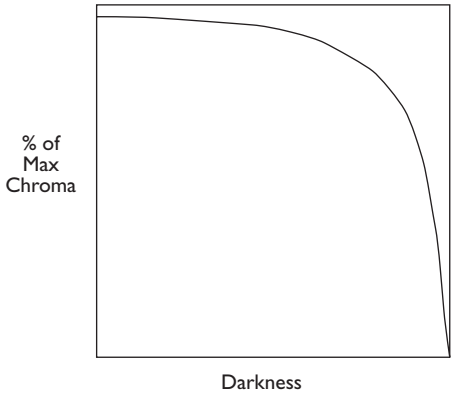


***Figure 2.6.16*** *Mapping of dark out–of–gamut colours.*

### 2.1.1.29 Hung (1995)

A new way of dealing with gamut mismatch is presented in this paper. It aims at reducing the limitations of printer gamuts in terms of chroma by using an artificially darker reference white, as a consequence of which the chroma of printed colours increases. The following formula is used for the white point shift:

$$L^* = 116(Y/(aYn))^{1/3} - 16 \text{ where } a \in (0.1] \qquad (2.6.37)$$

The author suggests to use $a = 0.95$ for soft–proofing and $a = 0.7$ or less for prints. While this method might sound promising, it also reduces the dynamic range of the output medium and will only work if the 'real' reference white is not present in the observer's field of view.

### 2.1.1.30 Ito and Katoh (1995)

This is the only paper published before this study which did not assume that an overall uniform lightness compression needs to be applied as the first step of gamut mapping. Instead, a method is suggested here whereby (in a plane of constant hue angle) colours are mapped towards three different centres of gravity depending on where they are relative to the colour *K* which has the lightness of the reproduction's cusp and can have different chroma values (Figure 2.6.17).

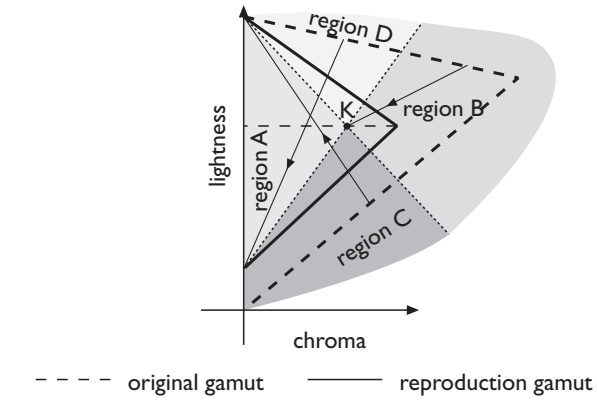


***Figure 2.6.17*** *Gamut compression proposed by Ito and Katoh (1995).*

*K* divides the input gamut into three regions: A – the *colorimetric* region where colours are reproduced exactly in terms of CIELAB, B – the region where colours are compressed towards *K*, C – the shadow region where colours are compressed towards the white point and D – the highlight region where colours are compressed towards the minimum lightness point of the reproduction medium on the L* axis.

This is only one of the methods described in the paper, which also deals with their evaluation. Unfortunately, the paper was only published in Japanese and the present review is based on private communication with one of the authors (Katoh, 1998).

### 2.1.1.31 MacDonald & Morovic (1995)

Rather than proposing new gamut mapping algorithms, this paper is aimed at evaluating some previously suggested approaches by comparing the reproductions of some fine–art paintings with the actual originals. Combinations of the following techniques were used in the paired comparison experiment described in this paper:

- *paper cast removal* – a*b* of substrate are subtracted from all colours.
- *lightness mapping* – using a linear technique.
- *gamut clipping* – two approaches were tried: *orthogonal* (Figure 2.6.18a) and *cusp* clipping (referred to as *chord* clipping in the paper) (Figure 2.6.18b).

- *gamut compression* – towards L*=50 on lightness axis (i.e. similar to Laihanen's second method (1987)), whereby the compression was the same across the whole space (in this case 20 *per cent*) rather than being determined along individual lines of compression.

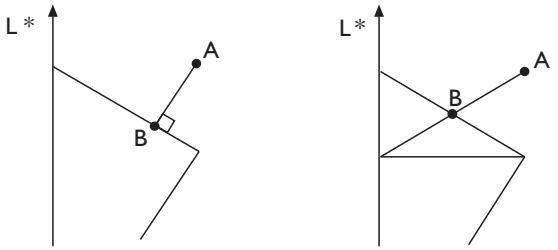


(a) orthogonal clipping (a) chord clipping

***Figure 2.6.18*** *Gamut clipping techniques.*

Psychophysical evaluation of reproductions of three paintings from the National Gallery in London was carried out in the same way as is described in Chapter 5. The results suggested that a different kind of GMA was preferred for each painting whereby the preference seemed to have depended on the **percentage of out–of–gamut pixels** in a particular painting. The painting which had 68 *per cent* of its pixels out–of–gamut was best reproduced by the reproductions having gamut compression, paper cast removal and lightness mapping applied to them whereas the painting with virtually all pixels in the gamut of the reproduction device was best reproduced without alteration of the original data, or with only paper cast removal. The third painting, having 30 *per cent* out of gamut pixels, was best reproduced by the images having lightness mapping and paper cast removal. The results also suggest that there is no statistically significant difference between the two gamut clipping techniques used. For a more detailed description of the experiment see MacDonald *et al.* (1995).

### *2.1.1.32 Spaulding, Ellson & Sullivan (1995)*

This algorithm is the one implemented in the *Kodak ColorEase PS* and *Kodak XLS 8600 PS* printers and the main idea is to use different kinds of mappings in different parts of colour space (as was suggested by previous authors as well). It is claimed, that the core around the neutral axis of the colour space (which includes skin tones and some other memory colours) needs to be mapped colorimetrically whereas highly saturated colours benefit from a transformation which preserves as much of their chroma as possible. Two different mapping approaches are described first:

- *colorimetric mapping* This is very similar to one of Sara's methods (1984) (i.e. chroma is clipped along lines of constant hue and lightness)
- *non–colorimetric mapping* This method uses 1D LUTs which map R to C, G to M and R to Y whereby the result is that the two colour gamuts are mapped exactly onto each other so that maximum possible C* is preserved. However, all colours (most notably memory colours) are distorted.

What is new in this paper is an approach called **colour gamut morphing**, which consists in combining different mappings for different regions of colour space with smooth transitions between them. The algorithm is made up of two stages:

(1) explicit definition of colour gamut mapping functions for subsets of the original gamut (e.g. neutrals, memory colours, saturated colours) in the form of:

$$\begin{aligned} D &= f_D(A,B,C) \\ E &= f_E(A,B,C) \\ F &= f_F(A,B,C) \end{aligned} \qquad (2.6.38)$$

(2) colour mapping for remaining colours, which uses interpolation between the existing mapped colours and should be smooth and continuous relative to them. Extrapolation may also be needed for colours which are outside the convex hull of explicitly mapped colours.

A particular embodiment of this technique is *UltraColor*, which uses the colorimetric algorithm for mapping the core of the colour gamut and the non–colorimetric algorithm for mapping highly saturated colours. It was implemented in the printers mentioned above in the form of a Postscript ColorRenderingDictionary (i.e. a 3D LUT).

The framework for gamut mapping outlined in this paper emphasises the need for different mappings in different parts of colour space and suggests a way for achieving smooth transitions between the individual mappings.

### 2.1.1.33 UGRA (1995)

The GMA suggested here is a combination of Methods A and B, briefly described by Schläpfer (1994) and is in fact a continuation of the same author's work. Hue angle is not altered by this method and the first step is a uniform linear lightness compression. Chroma compression is then carried out by first calculating the hue angle dependent ratio $k$:

$$k = \frac{C^*_{r(\max)}}{C^*_{o(\max)}} \tag{2.6.39}$$

Here $r$ and $o$ signify the reproduction and original respectively. The gamut mapped chroma is the calculated using the following quadratic equation:

$$C^*_r = kC^*_o\left(\frac{C^*_o}{C^*_{o(\max)}}(k-1)+2-k\right) \tag{2.6.40}$$

This equation changes chroma in a non–linear way when $k < 1$ and leaves original values unchanged when $k = 1$.

### 2.1.1.34 Chau & Cowan (1996)

This paper presents a new method of gamut mapping in terms of reflectance coordinates, which have the advantage of being illuminant independent. However, the paper only deals with the mapping of colours from the intersection of the original and reproduction gamuts and the mapping of out–of–gamut colours is not addressed.

### 2.1.1.35 Katoh & Ito (1996)

The approach taken in this paper consists in first defining a functional model whose parameters are then chosen on the basis of experimental data. It suggests that out–of–gamut colours should be clipped to colours on the reproduction gamut boundary, which have the smallest ΔE value calculated using a weighted colour difference formula in CIELAB:

$$\Delta E = \sqrt{\left(\frac{\Delta L^*}{Kl}\right)^2 + \left(\frac{\Delta C^*}{Kc}\right)^2 + \left(\frac{\Delta H^*}{Kh}\right)^2} \tag{2.6.41}$$

where ΔL*, ΔC* and ΔH* are differences in lightness, chroma and hue predictors respectively and $Kl$, $Kc$ and $Kh$ are the corresponding weighting coefficients. Based on a psychophysical experiment, the authors found that the most accurate reproductions were obtained when the ($Kl$:$Kc$:$Kh$) coefficients were set to (1:2:1) or (1:2:2). This indicates that larger changes are acceptable in chroma than in hue and that the smallest change is tolerated in lightness.

### 2.1.1.36 Marcu & Abe (1996)

In addition to overviewing a number of previously published techniques, this paper also proposes a new algorithm, where colours are clipped towards a centre on the lightness axis. This centre is determined for each colour individually depending on its lightness relative to the gamut's extremes (Figure 2.6.19).

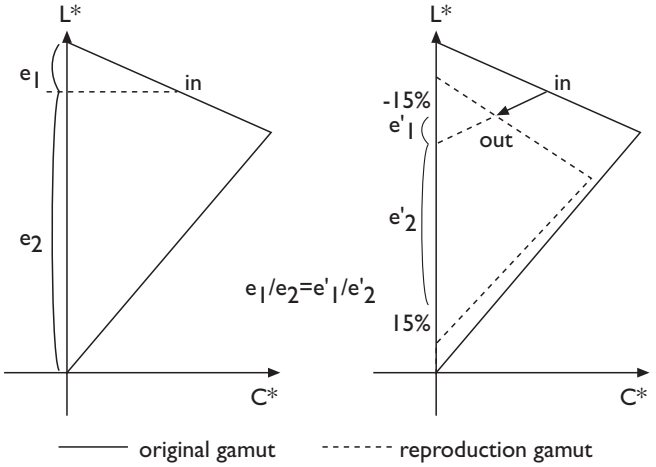


***Figure 2.6.19*** *Gamut clipping algorithm proposed by Marcu and Abe (1996).*

In addition to clipping, a white shift technique like the one described in Hung (1995) is used. This paper also contains a description of some very useful gamut visualisation techniques developed by its authors.

### 2.1.1.37 Nakauchi, Imamura & Usui (1996)

The solution proposed in this paper is quite novel as it defines gamut mapping as an optimisation problem of finding an image such that:

*(a) it is perceptually closest to the original and*

*(b) all it's pixels are within the reproduction gamut*

The perceptual difference between reproduction and original – *PD(r,o)* – is then defined by applying band–pass filters to the images and then obtaining their difference using the following formula, which takes into account human contrast sensitivity:

$$PD(r,o) = \left\| h * [o(x,y) - r(x,y)] \right\|^2 \qquad (2.6.42)$$

Here $h$ is the impulse response of an observation filter, $r(x,y)$ and $o(x,y)$ are the CIELAB coordinates of the reproduction and original at the point $(x,y)$ in the image and $*$ represents convolution.

A method for calculating an image which satisfies the two criteria stated above is given in the paper and this method has the advantage of taking into account image detail rather than being pixel–based like almost all the other algorithms reviewed here. However, the accuracy of the difference metric being minimised is a potential problem with this method, which is otherwise a very good one.

### 2.1.1.38 Ebner & Fairchild (1997)

The study described in this paper is of particular importance, as it results in experimental data on which gamut clipping can be based. It consisted of a psychophysical experiment designed to "find the perceptually smallest distance from a point in color space to a closed surface of color (gamut boundary)". This was done by having as the originals three kinds of images (abstract [a uniformly

coloured square with or without a border], data [a uniformly coloured chart] and figurative [a uniformly coloured cartoon car]) which were coloured with 25 colours from the surface of the original CRT gamut. Observers were then asked to "adjust the color of the image on the left–hand side of the screen to make it look as close as possible to the image on the right–hand side of the screen", whereby the original image was on the right and the left–hand image could only have colours from the simulated reproduction gamut. The reproduction gamut was the gamut obtained by intersecting the gamut of a colour laser printer with that of the CRT. Even though this meant that the gamut shapes of the two media were different, it seems from the figures in this paper that the lightness ranges were made to be equal. As there was no significant difference between the results for the different image types, they were all pooled together for further analysis.

For a given out–of–gamut colour, the experimental results were then modelled by a weighted combination of the following three vectors: (a) constant L* vector, (b) centroid vector (towards L*=50 on the lightness axis) and (c) minimum distance to gamut surface vector at the original colour's hue angle. The experimental results were also compared with the work of Katoh and Ito (1996) and a very good agreement with the (1:2:2) coefficient model was shown. These results indicate some maturity in the understanding of gamut clipping and the above model seems to be a good choice for situations where it is sufficient to overcome gamut differences by clipping.

### 2.1.1.39 Herzog & Müller (1997)

The gamut mapping algorithms proposed here were evaluated by mapping between media with the same lightness ranges. No lightness compression was therefore necessary, the hue angle of colours was kept unchanged and the following chroma mapping methods were evaluated:

(a) Piecewise linear compression along lines of constant lightness and hue angle as proposed by Gentile et al. (1990).

(b) Piecewise linear compression along the same lines, which leaves part of the range (between zero and a chosen chroma) unchanged and compresses the rest of the range more heavily.

(c) Non–linear compression along the lines of soft–clipping proposed by Stone and Wallace (1991) using the following formula:

$$C_r^* = \frac{1}{2}\left(C_{\max}^* - 1\right) + \frac{1}{2}\left(\frac{1}{\lambda} + C_o^*\right) - \frac{1}{2}\sqrt{4C_{\max}^*\left(1 - C_o^*\right)\left(\frac{1}{\lambda} - 1\right) + \left(1 + C_{\max}^* - C_o^* - \frac{1}{\lambda}\right)^2} \tag{2.6.43}$$

Here $r$ and $o$ represent the reproduction and original respectively, $\lambda$ is a parameter, whereby the function results in clipping when $\lambda = 1$ and linear compression when $\lambda = 0$ and $C^*_{max} = C^*_{r(max)}/C^*_{o(max)}$.

(d) Compression towards L*=50 on lightness axis.

(e) Mapping whereby colours with a lightness larger than $L^*_0$ were compressed towards $L^*_0$ on the lightness axis and colours with a smaller lightness were compressed along lines of constant lightness or *vice versa*, whereby $L^*_0$ was either 50 or the lightness of the reproduction cusp.

(f) Two–step mapping where a colour's chroma is first compressed to a certain value after which the colour is mapped towards L*=50 on the lightness axis.

These methods were experimentally studied using the pair comparison technique by evaluating reproductions made by mapping between two printed media. It was found that clipping along lines of constant lightness and hue angle gave the best results. Indeed this is in line with a number of previous studies carried out under similar circumstances (e.g. Gentile et al., 1990; Pariser, 1991)

### 2.1.1.40 Montag & Fairchild (1997)

Four mapping techniques applicable either to lightness or to chroma are presented in this paper. The approach adopted here is to evaluate the effects of the proposed techniques on lightness and chroma separately, whereby CIELAB hue angle is kept constant. Figure 2.6.20 shows the principles of the following four proposed techniques.

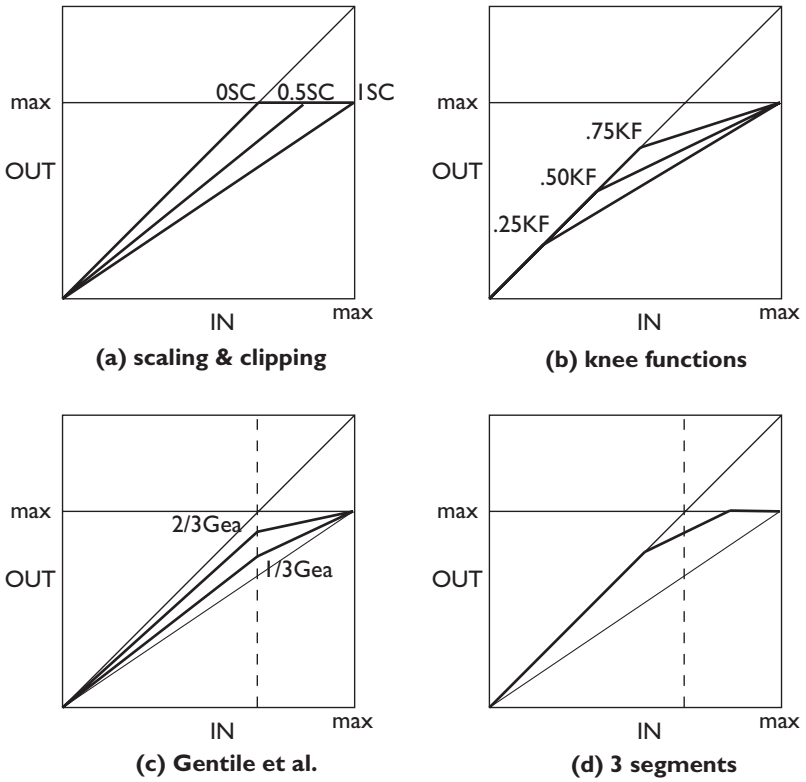


***Figure 2.6.20*** *Mapping techniques evaluated by Montag and Fairchild (1997).*

*Scaling & clipping (SC)*

As can be seen, this technique is a combination of linear scaling and clipping, whereby the individual implementations lie between the two extremes of clipping all out–of–gamut colours onto the boundary and of compressing all colours so as to fit into the reproduction's gamut. Several combinations of scaling and clipping were used and are denoted by the distance between the two extremes.

*Knee function (KF)*

This technique, as well as the following two, is a piecewise linear mapping technique. It consists of two linear mappings, the first of which has a slope of one and the second compresses the remaining range to the maximum of either the image or the device gamut (this is similar to method (b) by Herzog and Müller (1997)).

*Gentile et al technique (Gea)*

This method was proposed by (Gentile *et al.*, 1990) and also consists of two linear mappings: the first has a slope between one and that of the complete linear compression and the second slope is determined by the first lines intersection with the cut–off line determined by the function x = max (output).

*3 Segments (3S)*

As the name suggests, three linear mappings are used here, the first segment being the same as in the KF technique, the last being a clipping and the middle segment connects the other two (this is similar to the piecewise linear method proposed by Sara (1984)).

Paired comparison was used to evaluate the various implementations of the above techniques. This was done by gamut mapping simple rendered images to artificial gamuts simulated on the CRT on which the original image was displayed as well.

The evaluation suggested that the best results were obtained when image gamuts rather than the medium gamut were used as the original gamut. For chroma mapping on its own, the best reproductions were made with the SC algorithm, whereby all out–of gamut colours were clipped onto the boundary. Lightness mapping was tested for two cases: one where the top end of the lightness range was limited (here the 1/3Gea technique and the maintaining of saturation worked best) and another where the bottom end was limited (here the maintaining of chroma and the clipping of all out–of–gamut colours was preferred). The authors have also noted that the use of a colour appearance model space would be beneficial, as it could prevent hue shifts caused by the mapping when CIELAB was used. Further it was suggested that combined chroma and lightness mappings should be investigated.

### *2.1.1.41 Motomura, Yamada & Fumoto (1997)*

A novel method for gamut mapping called **categorical color mapping** is suggested in this paper. This method starts with a *categorical segmentation* of the original and reproduction gamuts (in terms of chroma and hue) whereby the categories are determined on the basis of **colour naming** and are the following nine: grey, red, green, yellow, blue, purple, pink, orange and brown. This is then followed by *likeness comparison*, which "extracts a pair of points which gives the highest likeness from [the] same categorical segment". The reproduced colour is then found by minimising a metric which relates an original colour's position relative to the centres of categories in the original gamut and the position of the reproduced colour relative to the centres of categories in the reproduction gamut. A detailed discussion of how this is done is given in the paper.

The idea of maintaining colour names in the process of gamut mapping is certainly of importance. However, whether this criterion alone suffices for obtaining accurate (or pleasant) reproductions needs to be seen – it would be particularly interesting to compare this method with algorithms proposed by other authors.

### *2.1.1.42 Voicu, Myler & Weeks (1997)*

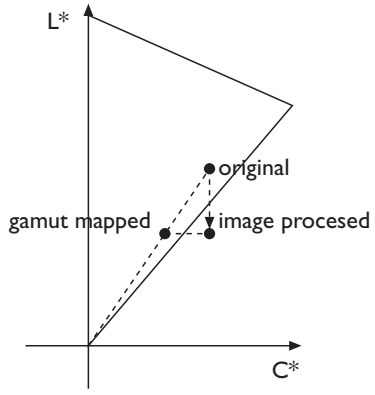


***Figure 2.6.21*** *Gamut mapping of image processed colours.*

This paper about homomorphic image filtering suggests a simple method for gamut mapping colours which become out–of–gamut as a result of image processing. If an image processed colour moves out–of–gamut, it is mapped in a way which maintains its lightness and the saturation of the original colour (Figure 2.6.21). However, this algorithm is not directly applicable to cross–media reproduction as it determines the reproduction colour on the basis of original and image–processed colours.

### 2.1.1.43 Wei, Shyu & Sun (1997)

A method altering all three perceptual attributes (like the method in CARISMA (1992)) is proposed in this paper. Both the use of image and medium gamuts is considered. Lightness compression, which is the first step of this model, is carried out using a function which is the combination of a soft–clipping and an S–shaped tone reproduction curve traditionally used in the Graphic Arts for increasing the contrast of images. This seems to suggest that one of the aims of this gamut mapping algorithm is to enhance the appearance of reproductions. The second step of the algorithm is compression towards $P$ – the colour having the lightness of the reproduction medium's cusp on the lightness axis (at a given hue angle), whereby compression along a given line is carried out using the following non–linear function:

$$R = \frac{G_r\left(a\frac{O}{G_o} - \left(\frac{O}{G_o}\right)^a\right)}{a-1} \text{ where } a = \frac{G_o}{G_o - G_r} \qquad (2.6.44)$$

Here the capital letters represent distances from $P$ whereby $O$ and $R$ stand for original and reproduction colour and $G_o$ and $G_r$ are the gamut boundaries for the original and reproduction respectively. Gamut mapped colours are calculated in the above way for a number of hue angles around the original's hue angle and that colour is chosen as the final reproduction colour, which has the smallest ΔD colour difference calculated as follows:

$$\Delta D = \sqrt{(l\Delta L)^{2+} + (c\Delta C)^2 + (h\Delta H)^2} \qquad (2.6.45)$$

Note, that ($l$:$c$:$h$) = (3:1:2) is suggested to be the best choice by a previous study of the same authors and this is indeed in–line with the findings of Katoh and Ito (1996). In addition to this method, a second algorithm was also proposed where lightness was compressed via a soft–clipping function and chroma was compressed overall in the way suggested by Viggiano and Wang (1992). This was again followed by finding the gamut mapped colour with the minimum ΔD which again had the same parameters as above.

These two models were used for mapping between a dye sublimation and an inkjet printer and the resulting reproductions were evaluated using the pair comparison method. The experimental results suggested that the first model using image gamuts performed better than both the first and second models using media gamuts.

### 2.1.1.44 Kim, Lee, Kim, Lee & Ha (1998)

Here a gamut mapping algorithm is proposed which is based on the misinterpreted CARISMA (1992) method published by Morovic and Luo (1997a). A different method for finding the centre–of–gravity towards which colours are mapped is suggested and clipping along lines of constant lightness below L*=50 and compression towards the centre–of–gravity above it are used. Reproductions made using this technique are only subjectively assessed by the authors who consider the new method to perform better than the algorithm described by Luo and Morovic (1997a).

## 2.1.5 Summary of Gamut Mapping Techniques

It could be seen from the above reviews that a wide variety of gamut mapping strategies have been proposed and in some cases also evaluated in the past. What will be attempted here is an identification of the more prevalent approaches and those which seem to be particularly promising or inductive of future work.

Firstly, one of the most noticeable trends in the reviewed gamut mapping work is the agreement among different studies that **image–dependent methods** are preferred over medium–dependent methods, which is in some sense supported by all of the following sources (Gentile *et al.*, 1990; Pariser, 1991; Hoshino and Berns, 1993; MacDonald and Morovic, 1995; Nakauchi *et al.*, 1996; Montag and Fairchild, 1997; Wei *et al.*, 1997).

Secondly, there is significant number of studies where **clipping** is given preference over compression whereby this is done implicitly in some cases. This is the case in (Sara, 1984; Meyer and Barth, 1989; Taylor *et al.*, 1989; Gentile, 1990; Pariser, 1991; Berns and Choh, 1995; Katoh and Ito, 1996; Marcu and Abe, 1996; Ebner and Fairchild, 1997; Herzog and Müller, 1997; Montag and Fairchild, 1997). In some of these papers minimum ΔE clipping is used by default and in others clipping algorithms are proposed without reference to compression. In addition, there is a also good number of papers among the above which have arrived at the preference of clipping by means of well–designed psychophysical experiments (e.g. Gentile, 1990; Pariser, 1991; Ebner and Fairchild, 1997; Herzog and Müller, 1997; Montag and Fairchild, 1997). However, in all these cases the relationship between original and reproduction gamuts was either artificial, relatively small (when compared with gamut differences between the media used in this study) or there was no lightness difference between them. It was therefore decided to include both clipping and compression algorithms in Experiment 1 of this study (Chapter 6) to see whether clipping is still preferred when gamut differences are large and when there is a significant lightness–range difference between the gamuts used.

Thirdly, the vast majority of algorithms (with the exception of Ito and Katoh (1995)) **start with lightness compression**. Whether this is the best thing to do in the context of this study will also be looked at in Experiment 1.

Fourthly, the **preservation of hue** (or hue angle) is also a point which occurs in all but the following papers (CARISMA, 1992; Schläpfer, 1994; Wei *et al.*, 1997) and the papers where minimum ΔE clipping is used.

Fifthly, there are a good number of papers which suggest the use of **different mapping methods for different parts of colour space** (CARISMA, 1992; Haneishi *et al.*, 1993; Schläpfer, 1994; Wolski *et al.*, 1994; Granger, 1995; Ito and Katoh, 1995; Spaulding *et al.*, 1995; Herzog and Müller, 1997; Wei *et al.*, 1997; Kim *et al.*, 1998) and this is an idea which will also be looked at in this study.

In terms of gamut clipping, the method proposed by Katoh and Ito (1996) seems to be a good solution, not least because of its simplicity and good correlation with the results of the experimental study of Ebner and Fairchild (1997). In addition the relative importance of $L > h > C$ used in this model is also confirmed by Wei *et al.* (1997).

In terms of compression algorithms, there is a degree of inhomogeneity between the various proposals, whereby the CARISMA (1992) paper seems to be a good reference in this area due to it containing experimental data about gamut compression used by experienced scanner operators.

Finally, there are some papers describing interesting approaches, which have either not been tested in comparison to other methods (e.g. (Motomura *et al.*, 1997)) or which rely on a more satisfactory solution of other problems before they can become effective (e.g. (Nakauchi, 1996)).

Most of the techniques reviewed here were closely related to CRT and printed media. In this context, other methods were also tried to reduce the gamut mismatch problem by using more than four inks, in which case the gamut of the printed medium is increased. However, it was suggested that some of these systems do not actually provide significant improvements (MacDonald *et al.*, 1994) and therefore do not diminish the need for gamut mapping. Attempts have also been made to obtain exact colour matches (i.e. relative luminances, CIE chromaticities and absolute lumi-

nances are identical) between CRT and print (Laihanen, 1994), however, this means that only colours from the overlap of the two gamuts can be used.

Gamut mapping is also of importance in other fields and, as an example, proprietary solutions have been devised for the ray tracing of prisms and rainbows (Musgrave, 1989) and for the joining together of several images (e.g. for panoramic pictures) (Pham and Pringle, 1995).

# Chapter 3

# Implementation of Colour Reproduction System

*To be uncertain is to be uncomfortable,*
*but to be certain is to be ridiculous.*

*Chinese Proverb*

# 3.1 Apparatus

The colour reproduction system chosen for evaluating gamut mapping algorithms comprised of an inkjet printer, a CRT monitor and a viewing booth, which will be described in this chapter. These two media were chosen for the evaluation of gamut mapping algorithms as they are the most widely used ones both in the professional pre–press sector and primarily the home and business market.

## 3.1.1 Preliminaries

Note, that unless otherwise specified, colour differences were calculated using the **CMC(1:1)** colour difference formula described in section 2.1.3 (Clarke *et al.*, 1984).

As the quantitative characteristics of the colour reproduction system described here are estimates of true characteristics based on samples taken from their populations, it is necessary to know their accuracy. To calculate 95 *per cent* **confidence intervals** for an estimate $\overline{X}$ of the mean $\mu$ of a normal distribution whose standard deviation is $\sigma$, the following formula is used (Milton and Arnold, 1990):

$$\overline{X} \pm 1.96 \frac{\sigma}{\sqrt{N}} \qquad (3.1.1)$$

where $N$ is the size of the sample from which $\overline{X}$ was calculated. This means that if there are two estimates $\overline{X}_1$ and $\overline{X}_2$ and one is within the confidence interval of the other, then they are not significantly different from each other at the 95 *per cent* level and conversely that they are different if that is not the case.

## 3.1.2 Viewing Booth

A *VeriVide* viewing booth, whose walls were achromatic and had a lightness of approximately L*=50, was used for viewing printed reproductions. These were illuminated with fluorescent tubes simulating *CIE Standard Illuminant D50*. A diffuser was placed in front of the light source and its density was chosen so that the luminance of printed substrates viewed in the booth was similar to the luminance of the CRT's white point, which was approximately 85 cd/m$^2$. The variation of luminance across the back panel of the viewing booth had a standard deviation which was 19 *per cent* of the maximum whereby the mean standard deviation in the vertical direction was five times as large as that in the horizontal direction (Figure 3.1.1).

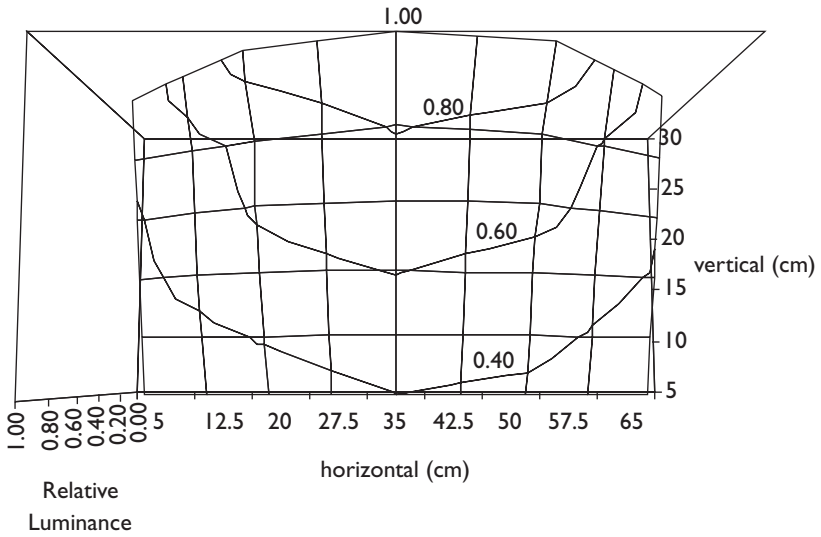


***Figure 3.1.1*** *Variation of luminance across pack panel of viewing booth.*

### 3.1.3 CRT Monitor

To display the images, which were taken to be the originals in the colour image reproduction system used here, a *Barco Reference Calibrator* CRT monitor was used. It's CRT was 20" in diameter, had a 0.31 mm pitch and had 1280 x 1024 addressable pixels. The chromaticity of the monitor's white point was set so as to be close to the chromaticity of the illuminant used in the viewing booth. In terms of spatial uniformity the CRT had a variation in L* of approximately 25 *per cent* from the brightest area (centre) and no visual hue variation. The CRT was driven by a 24–bit display card in a *Sun SPARCstation* workstation running *X–Windows 11* under *Unix* (*SunOS*™ Release 4.1.3_U1).

The choice of this CRT was influenced in particular by its closed–loop calibration feature, which facilitates long–term stability and repeatability. Most importantly, it was also easy to calibrate this CRT before each experimental session.

Measurements of the CRT were made with a *Bentham* telespectroradiometer (TSR), which was calibrated against a *CIE Standard Illuminant A* lamp traceable to the *National Physical Laboratory* (NPL) standard. 81 measurements were taken at 5 nm intervals between 380 nm and 780 nm whereby the integration and delay times were 0.5 and 0.05 seconds respectively.

Colours for characterising the CRT were measured in a dark room whereby an approximately 12 cm × 12 cm square of a given colour was displayed on its own in the centre of the monitor against a mid–grey background. A measurement was then taken of a circular area with a diameter of approximately 3 cm in the centre of the square. Both the monitor and the TSR were used and described in studies previously carried out at the Colour & Imaging Institute (Rhodes and Luo, 1996; Lo *et al.*, 1996).

### 3.1.4 Inkjet Printer

Reproductions of images displayed on the original CRT were made on an *Hewlett Packard* (HP) *DeskJet 850C* inkjet printer having a resolution of 600×600 *dots per inch* (dpi) for black and 300×300 dpi for cyan, magenta and yellow. The substrates used with this printer were *HP Glossy Paper* (a plastic substrate), which was used in all experiments and in Experiment 3 *HP Premium Inkjet Paper* (an uncoated paper substrate) was used in addition to it. To obtain printed reproductions, data was sent to the printer via HP's software driver from an *Apple Macintosh*™ computer running *Adobe Photoshop*™ (versions 3.0.5 – 4.0) under *MacOS*™ (versions 7.5.5 – 8.1).

This printer was chosen as it gave the best results from the range of HP printers available at the beginning of the project. It also represented the performance of printing devices most widely used in the consumer and business markets, which would be the primary users of universal GMAs.

Measurements of prints were made with an *X–Rite 938* spectrophotometer, which used a 0°/45° measuring geometry. The mean short–term repeatability of this instrument was calculated on the basis of four measurements of the set of 12 *BCRA–NPL Series II Ceramic Colour Standards* and was found to be 0.19 ΔE with a standard deviation of 0.11 ΔE (hence the standard error of this instrument's measurements at the 95 *per cent* confidence level is $0.19+1.96*0.11/\sqrt{4}$, which is 0.30). Its accuracy (as traced to measurements made at the NPL) was calculated in the same way and was 0.42 ΔE with a standard deviation of 0.25 ΔE. For calculating accuracy, the D65 illuminant was used as the reference white since reference XYZ values from the NPL were available for this illuminant. For repeatability, the D50 illuminant was used and XYZ values were obtained using the *CIE 1931 Standard Colorimetric Observer*.

### 3.1.1.1 Temporal Stability

To characterise a printer effectively, its characteristics need to be known first. Temporal stability in particular is a factor, which determines when characterisation data ought to be measured after colour patches are printed so that the characterisation model then corresponds to what the prints look like when they are evaluated.

To obtain information about this characteristic, cyan, magenta, yellow, red (M+Y), green (C+Y), blue (M+C) and black colour patches were printed on the two substrates. These were then measured at different times and the whole process was repeated twice. Colour differences were subsequently calculated between measurements made at different times and the initial measurement (Figure 3.1.2). According to Equation 3.1.1 the 95 *per cent* confidence interval of these measurements was $\pm 1.96*0.30/\sqrt{16}$ (as 0.3 is the standard error of the X–Rite spectrophotometer's measurements and 16 was the sample size from which they were obtained). The confidence interval for the difference of a pair of measurements is then twice the confidence interval of an individual measurement.

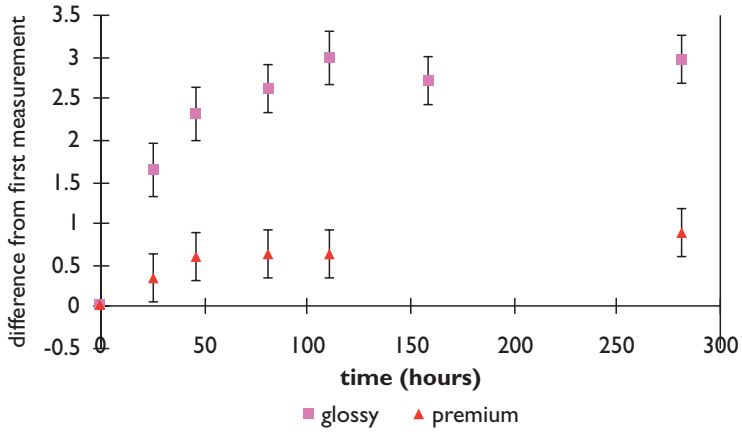


***Figure 3.1.2*** *Colour difference as a function of time.*

In addition to these overall results, the direction of colour change is of some interest as well. For the premium inkjet paper the lightness of the colours decreased with time and their hue shifted towards magenta (by approximately 0.3 ΔE in 300 hours), whereas the lightness of colours on glossy paper increased and their hue shifted towards blue (by approximately 3 ΔE in 300 hours). Furthermore, the biggest change for both substrates was for the blue colour patch, which changed by 1.5 ΔE on the premium inkjet paper and by 5.0 ΔE on the glossy paper.

The larger changes for glossy paper could be caused by changes in gloss as well as the drying of the inks. The stabilising times for both substrates (approximately 48 hours) are as expected, as they correspond to drying times typical for oxidation drying (which presumably is the mechanism used by the 850C's inks).

### 3.1.1.2 Spatial Uniformity

The colour measurements for this and the next characteristic were made 72 hours after the test charts were printed, so as to allow for them to stabilise. Spatial uniformity of a single print was investigated by printing two sets of cyan, magenta yellow and black scales – one at the top of the page and the other at the bottom – and calculating their colour difference (Table 3.1.1). These scales had 14 steps each (being 100, 90, 80, 70, 60, 50, 40, 30, 25, 20, 15, 10, 7 and 2 *per cent* in terms of colorant amounts), which were taken from the ANSI IT8.7/3 chart (ANSI, 1993) and they were printed in opposite sequences at the two ends of the page (see Appendix A). The colour differences between these two sets of 56 patches (i.e. the four times 14 patches as described above) were as follows:

| | glossy | premium |
|---|---|---|
| **mean** | 1.5 ΔE | 1.0 ΔE |
| **standard deviation** | 1.9 ΔE | 0.6 ΔE |
| **maximum** | 9.0 ΔE | 2.9 ΔE |

***Table 3.1.1*** *Spatial Uniformity of prints made with HP DeskJet 850C.*

### *3.1.1.3 Repeatability*

Here the colour differences between successive pages were measured in the same way as for spatial uniformity, with the difference that the corresponding patches from successive prints were compared rather than different parts of a single print.

| | glossy | premium |
|---|---|---|
| **mean** | 1.4 ΔE | 1.9 ΔE |
| **standard deviation** | 1.5 ΔE | 0.9 ΔE |
| **maximum** | 7.5 ΔE | 6.8 ΔE |

***Table 3.1.2*** *Repeatability of HP DeskJet 850C.*

As was to be expected, these colour differences were fairly similar to those for spatial uniformity (especially for the glossy substrate). This is because the 850C prints in terms of horizontal bands rather than whole pages, which makes it less important whether the next band is on the same or on a successive page.

### *3.1.1.4 Difference Between Ink Cartridges*

The final parameter of the 850C printer, whose variability was examined is the colour difference between colours printed using different ink cartridges from the same batch. The results shown in Table 3.1.3 are colour differences between 2 sets of 125 colours printed with different cartridges, which were from a 5×5×5 training colour cube with 0, 10, 30, 60 and 100 *per cent* steps in terms of colorant amounts (see Appendix A).

| | glossy | premium |
|---|---|---|
| **mean** | 4.8 ΔE | 3.6 ΔE |
| **standard deviation** | 2.3 ΔE | 1.9 ΔE |
| **maximum** | 10.8 ΔE | 9.8 ΔE |

***Table 3.1.3*** *Repeatability of HP DeskJet 850C.*

These large colour differences suggest that the characterisation of the printer needs to be carried out for each individual cartridge separately.

## 3.1.5 Media Gamuts

Among the most important factors affecting the performance of GMAs are the characteristics of the gamuts between which colours are mapped. To this end the gamuts of the media used in this study were calculated using the SMGBD method and the gamut boundaries for individual hue angles were obtained with the FSLGB method, both of which are described in Chapter 4.

The projection of gamuts onto the *a*b** (Figure 3.1.3) or *a'b' (*for whose definitions see Equations 9.1.1 and 9.1.2 on pp. 184) (Figure 3.1.4) plane and *L** v. *C** (Figure 3.1.5) or *J* v. *C* (Figure 3.1.6) plots at the CRT's primary and secondary hue angles are shown in the figures of this section. There are two figures for each kind of plot as gamut mapping was carried out in CIELAB or CIECAM97s respectively. In these figures E*n* denotes that the gamut is that of a medium from experiment *n*.

Note, that the same physical medium can have different gamuts depending on the characterisation used. This was the case with the inkjet printer used here, which when characterised in terms of CMY had the gamut labelled *E1* and when characterised in terms of RGB it had the gamut labelled *E2&4* in Figures 3.1.3 and 3.1.5. It can be seen from there that the characterisation model can have an impact on the available chroma as well as lightness ranges and in some cases even on gamut shape (e.g. see the green hue angle in Figure 3.1.5).

The impact of the difference between CIELAB and CIECAM97s as colour spaces on the relative sizes of the gamuts dealt with here can be seen by comparing the plots for the CRT from the two sets of figures and by comparing the inkjet gamut for glossy paper from Experiment 3 (being in CIECAM97s) and the inkjet gamut from Experiment 2 (being in CIELAB). In both cases these media as well as their characterisation models were the same and the only difference was that of colour space. Of particular importance is also that the difference in terms of lightness ranges between the CRT and the printed medium is smaller under CIECAM97s. Indeed this was the reason for using HP Premium Inkjet paper as well in the third experiment, the relationship of which to the CRT gamut was closer to relative gamut sizes in the first two experiments (for more detail see Chapter 10).

It can further be seen from these figures that overall the differences between original and reproduction gamuts were largest in Experiment 1 and that they were smallest in Experiment 3 and that in each case the gamut differences were larger for some hue angles (e.g. blue) than for others (e.g. red). An understanding of these and other gamut characteristics will be of importance when interpreting experimental results.

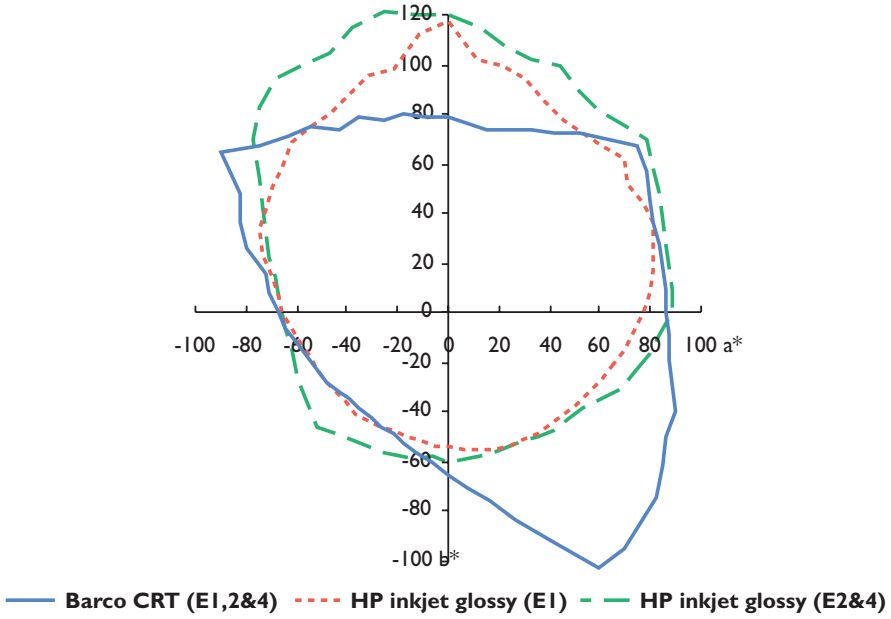


***Figure 3.1.3*** *Gamuts projected onto a*b* plane in CIELAB.*

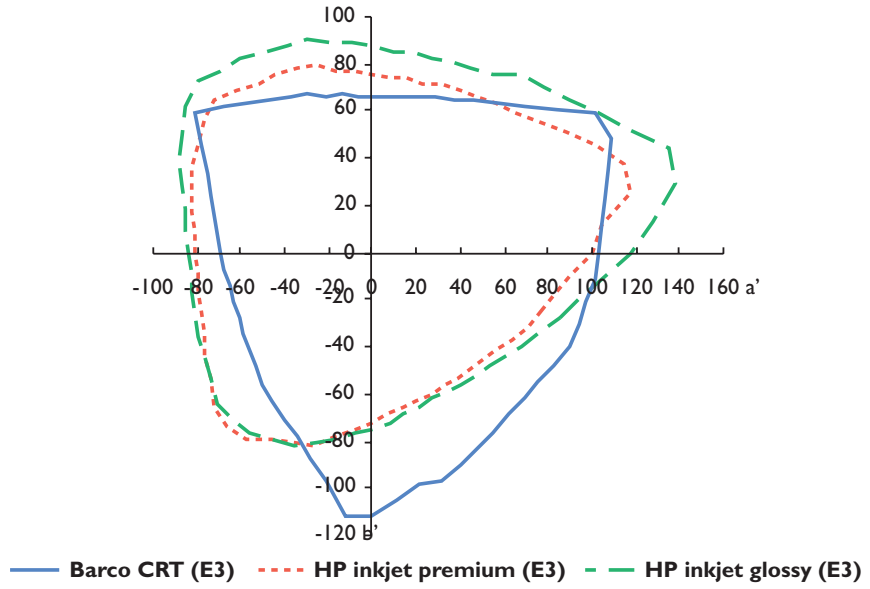


***Figure 3.1.4*** *CRT gamut projected onto a'b' plane in CIECAM97s.*

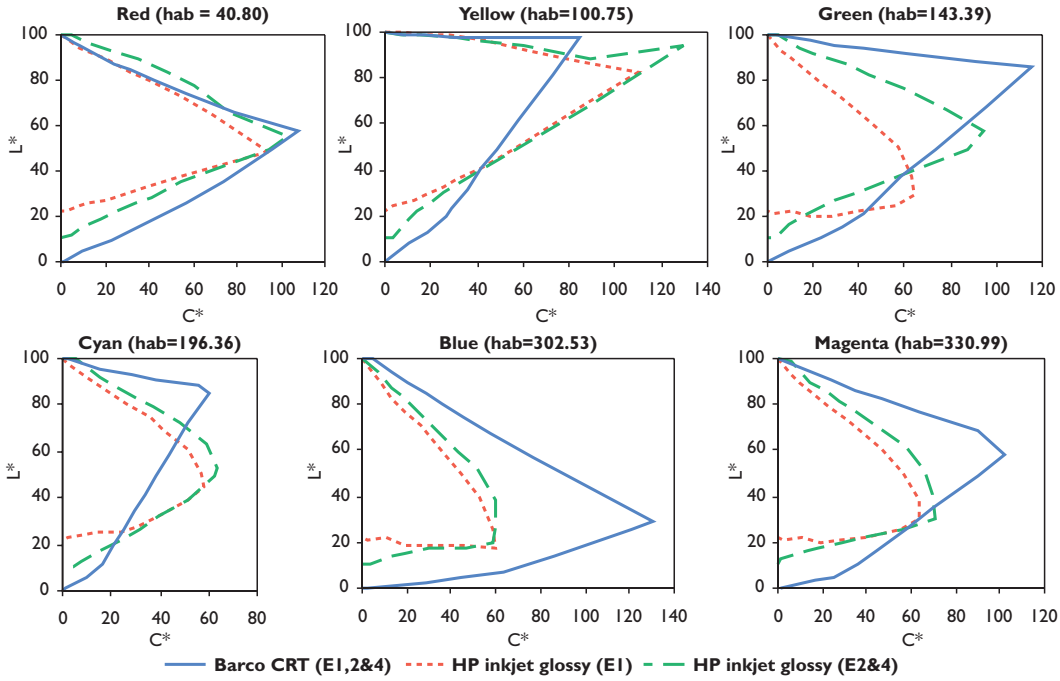


***Figure 3.1.5*** *Gamuts at primary and secondary hue angles in CIELAB.*

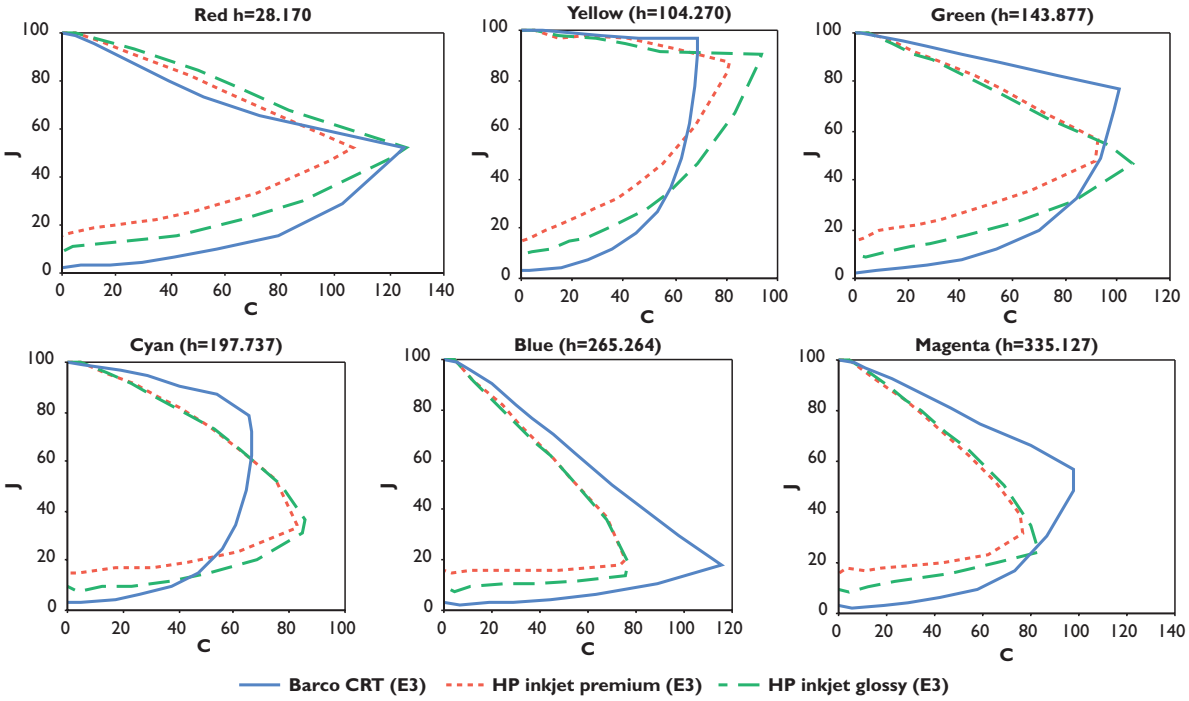


*Figure 3.1.6 Gamuts at primary and secondary hue angles in CIECAM97s.*

## 3.2 Development of Characterisation Models and Investigation of Their Accuracy

The following sections will discuss the CRT monitor and printer characterisation work carried out for the colour reproduction system in which GMAs were implemented and evaluated.

### 3.2.1 CRT Characterisation Model

The **PLCC model** (Post and Calhoun, 1989), which was described in Section 2.5.2.3 was used to characterise the CRT. For each channel look–up tables (LUTs) between digital values and luminances had 18 equally spaced entries in terms of digital values. As all experiments were carried out in a dark room and XYZ values were calculated from digital values by first obtaining their luminances from the LUTs using piece–wise linear interpolation and then transforming them via a 3x3 matrix based on the tristimulus values of the three channel maxima. The mean prediction error of this model was 0.4 ΔE units and it was therefore considered to be satisfactory.

Note, that there was no need for using flare correction under the circumstances used for measuring the CRT (Section 3.1.3) and due to the negligible amount of inter–reflections within the CRT. If measurements were taken in a lit room, flare correction would have been of great importance and not using it would have resulted in larger characterisation errors in particular for low–lightness colours.

### 3.1.2 Printer Characterisation Model Development and Evaluation

Due to the characteristics of the printer used here, its characterisation was a more elaborate process. Therefore a range of characterisation models was implemented first so as to find the model, which best described it. An overview of this investigation, which was already published (Morovic and Luo, 1996), will be given next.

One of the most serious obstacles to successfully characterising the DeskJet 850C is that it is not possible to control its colorant amounts directly. Hence black generation is carried out by the printer automatically and unalterably and the characterisation can be regarded as being a transfor-

mation between the cyan, magenta and yellow (CMY) values sent to the printer and the tristimulus values of the resulting printed colour. Even though the **virtual CMY values** considered here are not those directly output by the printer, they still are the most practical correlates available for them.

The characteristics of the 850C force its treatment as a **black box**, which makes it paramount to adjust it carefully, as certain settings make its colorimetric characterisation virtually impossible. The settings of the 850C's driver software used here are shown in Table 3.2.1.

| Intensity | Halftoning | Color Matching | Media | Quality |
|---|---|---|---|---|
| Automatic | Scatter | Text/Graphics | HP Glossy | Best |

***Table 3.2.1*** *HP driver settings.*

Setting *HP Premium Inkjet Paper* as the medium in the driver gave very unsatisfactory results when characterising the printer for that substrate. *HP Glossy* was therefore chosen as the medium setting regardless of the actual substrate used.

The four kinds of characterisation models investigated were distance weighted interpolation, third and fourth order masking equations and a new so–called four–sector model.

### *3.1.2.1 Distance Weighted Interpolation Model*

This interpolation technique (Shepard, 1968) is potentially less accurate than other interpolation methods used previously for characterisation purposes – e.g. tetrahedral or tri–linear interpolation (Kasson *et al.*, 1995), which was mentioned in Section 2.5.1.1. However, its advantages are that it works well even with non–monotonic data, which is often the case with desktop printers and that it also works for values, which are outside the range of the interpolation data, which again is of importance in a system, which includes quantisation. To obtain the virtual CMY values for a given set of CIELAB co–ordinates, the following procedure is used by this model:

1. A colour cube of arbitrary size is loaded.
2. Eight colours forming the smallest sub–cube around the target LAB co–ordinates are found (whereby for near–boundary colours only a smaller number can be located).
3. The distances between these eight colours and the target colour are used for computing weights ($w_i$):

$$w_i = \frac{\sigma_i}{\sum_{j=1}^{8} \sigma_j}, \text{ where } \sigma_i = \frac{1}{d_i^{\mu}}. \qquad (3.2.1)$$

   In Equation 3.2.1 $d_i$ is the distance of the $i$th colour from the target and the exponent $\mu$ determines the smoothness of the interpolation, whereby if $\mu>1$ then the first derivative is continuous. In this case $\mu$ was set to 1.5 so as to achieve a smooth interpolation (an optimisation of this exponent could possibly have given better results).
4. To obtain the colorant amounts of the given LAB colour, the virtual colorant amounts of the eight colours are combined as follows:

$$C = \sum_{i=1}^{8} w_i C_i, \; M = \sum_{i=1}^{8} w_i M_i, \; Y = \sum_{i=1}^{8} w_i Y_i \qquad (3.2.2)$$

### *3.1.2.2 Third Order Masking Equations*

As mentioned in Section 2.5.1.2, the third order masking equations are a well established characterisation model dating back to Clapper (1961). Their aim is to describe the relationship between

tristimulus values and colorant amounts using a set of three third order equations, whereby the following polynomial was used in this investigation:

$$\begin{aligned} C = \quad & a_{11}D_r + a_{12}D_g + a_{13}D_b + \\ & a_{14}D_r^2 + a_{15}D_g^2 + a_{16}D_b^2 + \\ & a_{17}D_rD_g + a_{18}D_rD_b + a_{19}D_gD_b + \\ & a_{110}D_r^3 + a_{111}D_g^3 + a_{112}D_b^3 + \\ & a_{113}D_r^2D_g + a_{114}D_r^2D_b + a_{115}D_g^2D_r + \\ & a_{116}D_g^2D_b + a_{117}D_b^2D_r + a_{118}D_b^2D_g \end{aligned} \qquad (3.2.3)$$

Here $C$ is the virtual amount of cyan and $D_r$, $D_g$ and $D_b$ are the corresponding *colorimetric densities*, which can be obtained from measured tristimulus values using Equation 2.5.3 from Section 2.5.1.2, which is again given here:

$$D_r = log(X_0/X),\ D_g = log(Y_0/Y) \text{ and } D_b = log(Z_0/Z) \qquad (3.2.4)$$

Here $X_0Y_0Z_0$ is the reference white (i.e. in this case the printing substrate). Analogous equations apply for the two other virtual colorants – magenta and yellow.

The 3×18 coefficients in these equations are calculated using the least–squares method, whereby the error is minimised for colours from a colour cube of arbitrary size.

### 3.1.2.3 Fourth Order Masking Equations

These are an extension of the previous model where nine new terms were added to the 18 from the third–order model (again using the same notation):

$$\begin{aligned} C = \quad & a_{11}D_r + a_{12}D_g + a_{13}D_b + \\ & a_{14}D_r^2 + a_{15}D_g^2 + a_{16}D_b^2 + \\ & a_{17}D_rD_g + a_{18}D_rD_b + a_{19}D_gD_b + \\ & a_{110}D_r^3 + a_{111}D_g^3 + a_{112}D_b^3 + \\ & a_{113}D_r^2D_g + a_{114}D_r^2D_b + a_{115}D_g^2D_r + \\ & a_{116}D_g^2D_b + a_{117}D_b^2D_r + a_{118}D_b^2D_g + \\ & a_{119}D_r^2D_g^2 + a_{120}D_r^2D_b^2 + a_{121}D_g^2D_b^2 + \\ & a_{122}D_r^3D_g + a_{123}D_r^3D_b + a_{124}D_g^3D_r + \\ & a_{125}D_g^3D_b + a_{126}D_b^3D_r + a_{127}D_b^3D_r \end{aligned} \qquad (3.2.5)$$

### 3.1.2.4 Four–Sector Model

The four–sector model is an extension of the third order masking equations, which tries to resemble the actual workings of the printer more closely. As the 850C seems to use black generation similar to 100 *per cent* grey component replacement (GCR), only three different colorant combinations are possible: CMK, CYK and MYK. This model therefore consists of three separate transformation matrices for each of these three sectors.

When transformation matrices are calculated from colour cube data, the smallest of the CMY colorant amounts determines into which sector a particular colour belongs. When the actual XYZ to CMY transformation is carried out, the CIE LAB hue angle calculated from the XYZ tristimulus values determines, which sector's transformation matrix to use. Even though the boundary is defined using a piece–wise linear function (Figure 3.2.1), there are some problems as the boundaries between the sectors are not lightness–independent.

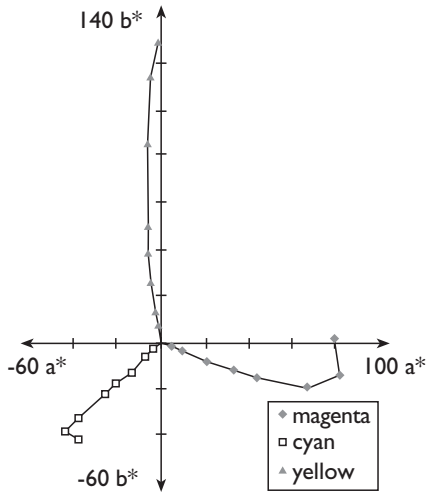


***Figure 3.2.1*** *Boundaries of chromatic sectors in the four–sector model.*

So far only three sectors were described, however, an additional sector was used for neutral colours as these would have had a colour cast if reproduced using a three sector model. Colours, which have a C* smaller than 3.0 were thus transformed separately.

Even though this model resembles the printer more closely, its problem is that it has inaccuracies in the border regions between individual sectors and colours from one sector are sometimes transformed using another sector's matrix.

### *3.1.2.5 Evaluation of Initial Characterisation Models*

In addition to testing the performance of the four models, the effect of the number of colours used for calculating their parameters was also examined. Four colour cubes were used with three, four, five and nine levels per colorant. The steps in these colour cubes were chosen so as to be visually equal rather than to have equal differences in terms of colorant values (Table 3.2.2) as this was found to give better results in an earlier study (Johnson *et al.*, 1998a&b).

| **Size** | **Steps (*per cent*)** |
|---|---|
| **3×3×3** | 0, 40 and 100 |
| **4×4×4** | 0, 20, 60 and 100 |
| **5×5×5** | 0, 10, 30, 60 and 100 |
| **9×9×9** | 0, 5, 10, 20, 30, 40, 60, 80 and 100 |

***Table 3.2.2*** *Colorant levels used in colour cubes.*

An additional 5×5×5 colour cube was generated and measured for testing purposes. The steps in this cube were of equal colorant value (i.e. 0, 25, 50, 75 and 100 *per cent*), whereby only the eight cube vertices were common to both the training and the testing sets. The use of a separate training set is quite important, as it gives a more realistic idea of the models' performance. Using training colours for testing would have resulted in unrealistic errors for the distance–weighted interpolation model (equal to the variation of the printer) and would not have shown whether there are problems with local extremes in the case of the masking equation models.

To test the XYZ to CMY transformation, the 125 test colours were transformed using the four models and the resulting CMY values were printed and measured. The resulting colour differences therefore represent the differences between original XYZ co–ordinates and XYZ measurements of calculated CMY values. This, however, means that they include not only modelling errors but errors due to printer variation as well.

The assumption is often made that characterisation errors are normally distributed and therefore the mean is used as a measure of central tendency and the standard deviation as a measure of dis-

persion. However, when the error distribution is skewed, as was the case with the results of this investigation (Figure 3.2.2), other descriptive statistics are needed. To describe this data more meaningfully, the median and the 95$^{th}$ percentile were used.

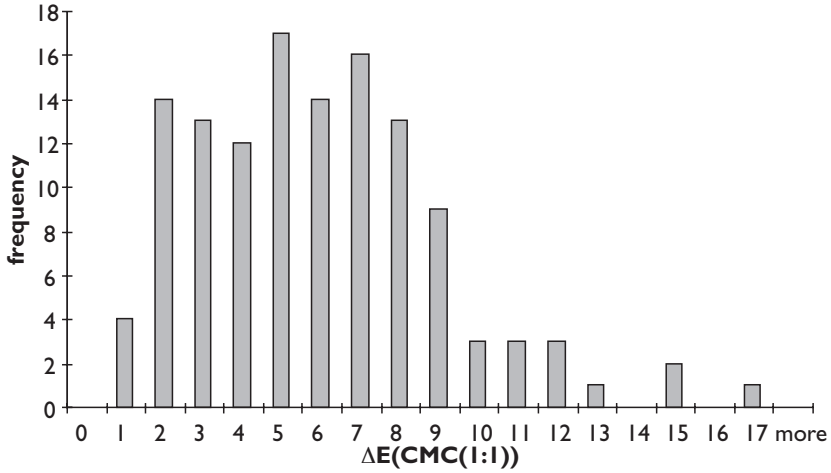


***Figure 3.2.2*** *Histogram of errors from 4th order masking equations using 9×9×9 training cube.*

Figure 3.2.3 shows the results of the XYZ to CMY transformation in terms of median, 95th percentile and maximum error. To give the possibility of comparing these results with other experiments the mean and standard deviation are also given in Appendix A. From these results it can be seen that the four–sector model is clearly inferior to the other three models. This is most probably due to the inadequate definition of the sector boundaries as well as due to the insufficient number of colours available to the least squares method for setting up four third–order polynomials.

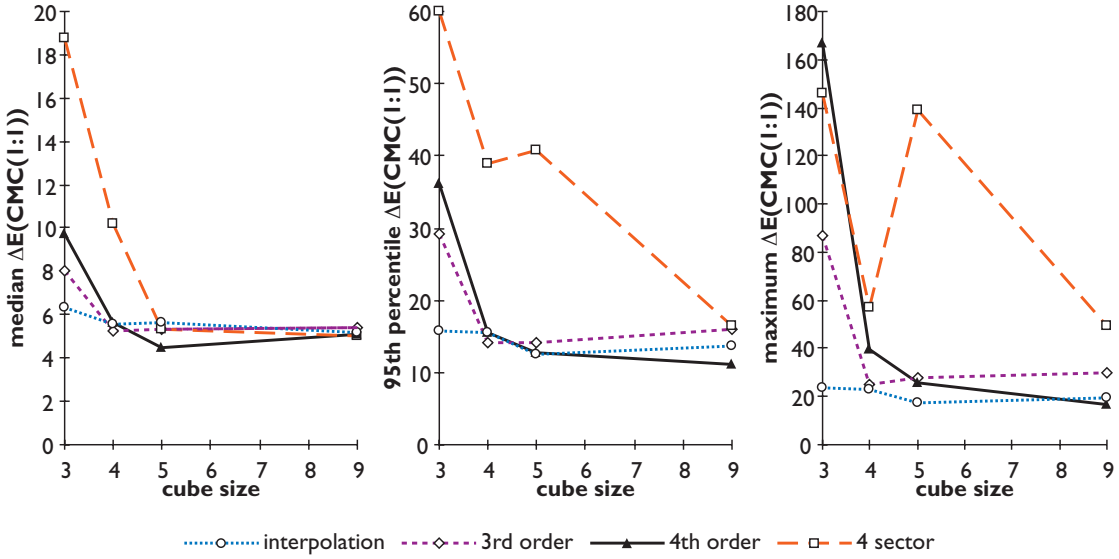


***Figure 3.2.3*** *Descriptive statistics of characterisation model errors as a function of training–cube size.*

Comparing the third and fourth order masking equation models derived from the 9×9×9 cube, there is only a 0.3 ΔE improvement in terms of median, however the 95th percentile is reduced by 4 and the maximum error by 13 ΔE units when the higher order equations are used. Considering the size of the training colour cube, it is sufficient to use five steps per colorant if these are chosen appropriately. As can be seen from Figure 3.2.3, the increase in colour cube size mainly influences the dispersion of the colour differences while the mean is not affected significantly.

Finally, the distance–weighted interpolation gave the best or second best results (depending on cube size) and was least affected by training cube size. Nonetheless, this method is not particularly suited for reproducing complex images as gradual transitions in input data are not reproduced monotonically and smoothly. This is caused by the distance–weighting method shifting colours

towards the centre of the sub–cube within which it interpolates whereby causing problems for colours, which are close to sub–cube boundaries. However, this method gives the best results, when only a small number of colours are available for setting up the characterisation model.

The above models (with the exception of the four–sector model) can also be used for transforming CMY values to XYZ, which is done simply by reversing the terms in Equations 3.2.1–3 and 3.2.5. As this cannot be done in a straight–forward way for the four–sector model and as this model did not perform well for the XYZ to CMY transformation, its inverse was not derived for the CMY to XYZ direction.

Evaluating this transformation is a more straightforward task as it can be done by simply calculating XYZ values from the CMY values of the test cube and then obtaining colour differences between the results and the original XYZ data. Overall the performance of the three models used for this transformation was worse than their performance for the XYZ to CMY direction (see Appendix A), which can also be seen from Table 3.2.3 and is even more marked for other models and training cube sizes.

As a result of this investigation, the fourth–order masking equations and the 5×5×5 training cube were chosen for the colour reproduction system used in Experiment 1 and its prediction error statistics are summarised in Table 3.2.3. In terms of the quality of resulting reproductions made with this model, there was a particular problem with the achromatic axis, which was reproduced with a brownish colour cast. The 5×5×5 training set was chosen instead of the larger 9×9×9 as calculating the model on the basis of the larger set did not produce qualitatively better results (including the colour cast for neutrals) and as the printer needed to be characterised every time the print cartridge was changed.

| | Median | 95$^{th}$ perc. | Max. | Mean | Std. dev. |
|---|---|---|---|---|---|
| **XYZ to CMY** | 4.51 | 12.67 | 25.88 | 6.03 | 4.63 |
| **CMY to XYZ** | 5.86 | 12.35 | 21.10 | 6.40 | 3.80 |

***Table 3.2.3*** *Performance of fourth–order masking equations used in Experiment 1 (in terms of ΔE).*

### *3.1.2.6 Grey–Scale–Corrected RGB Printer Characterisation*

As it was felt that improvements were needed to the performance of the printer characterisation model used in Experiment 1 further work was carried out after the first experiment's completion. In particular the reduction of maximum errors and the correction of the colour cast with which the neutral scale was reproduced were priorities at this stage. The first step towards improving the characterisation was the use of RGB instead of CMY for driving the printer as this was suggested by Jay Gondek of HP Vancouver (Gondek, 1996). To have visually equally spaced training data, the steps in the 5×5×5 colour cube were the 0, 25, 43, 59 and 100 *per cent* colorant amounts.

This change alone resulted in a larger gamut as can be seen from Figures 3.1.2 and 3.1.4 where the main difference between the printed medium gamut boundaries from Experiments 1 and 2 is in the kind of device dependent data used. An additional effect of using RGB was that third order masking equations gave better results than before and were therefore used from Experiment 2 onwards.

It is always advantageous to use lower–order equations in least–squares based characterisation models as the higher the order of an equation the more local extremes it can have, which might not correspond to the relationship being modelled.

As even the use of RGB for controlling the printer did not sufficiently improve the performance of the characterisation model for the achromatic axis, a new method was developed for correcting this shortcoming. It was briefly introduced in a previous paper (Morovic and Luo, 1997b) and consists of the following steps:

1. Print a series of $n$ grey patches with known colorant amounts. In this case $n = 14$ and patches with equal RGB values were used (these were 100, 90, 80, 70. 60, 50, 40, 30, 25, 20, 15, 10, 7 and 3 *per cent*).
2. Measure the patches and predict colorant amounts using the original characterisation model from these measured values.

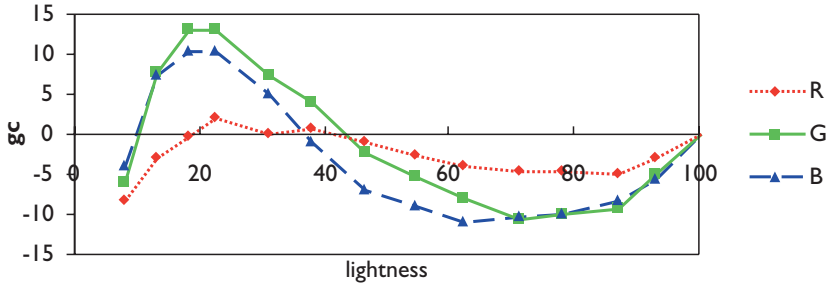


***Figure 3.2.4*** *Components of* gc *in terms of R, G & B colorant amount percentages used in Experiment 2.*

3. For each of the $n$ grey patches calculate an RGB grey–scale–correction vector ($\mathbf{gc}_i$) between the predicted colorant amounts and the colorant amounts defined for the grey patch (Figure 3.2.4).
4. To calculate grey–scale–corrected RGB values (R'G'B') for a given XYZ value, first calculate RGB using the original model and then calculate the grey–scale–correction vector. This is done by linearly interpolating between the $n$ **gc** vectors obtained in step 3 based on the lightnesses of the $n$ patches and the lightness of the given colour. So as not to reduce the precision of the model for more chromatic colours only apply full correction to neutrals using the following equation:

$$R'G'B' = RGB + w\mathbf{gc} \qquad (3.2.6)$$

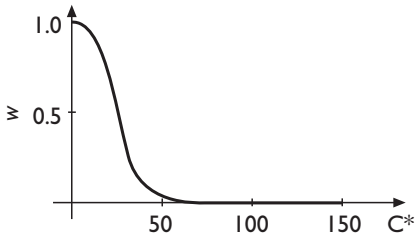


***Figure 3.2.5*** *Grey–scale correction chroma–dependent weight function.*

In this equation $w$ is calculated using the following formula (Figure 3.2.5) where C* is the chroma of the colour for which R'G'B' is to be predicted:

$$w = 1 - \sqrt{\frac{C^{*6}}{C^{*6} + 10^9}} \qquad (3.2.7)$$

Note, that this equation is very similar to the one used in the GCUSP algorithm (Section 7.2) with the difference that a larger additive constant and exponent are used here to limit the influence of correction more strongly.

Even though using third order masking equations (Equation 3.2.3) on the basis of a 5×5×5 colour cube with grey–scale correction made little improvement to the median prediction error, which was 5 ΔE, the maximum error was approximately halved to 13 ΔE. In addition to this the colour cast on the neutral axis was significantly reduced so that it became acceptable and reproductions made using this model were notably improved in qualitative terms. In view of the typical repeatability error of 1.5 ΔE with a maximum of 7.5 ΔE, the current model's accuracy is considered to be quite acceptable.

Finally, it needs to be kept in mind that the results of all the experimental work in this study have an element of uncertainty caused by the accuracy of the characterisation models and variation of the media used.

## 3.2 Overall Workflow

Understanding the properties of colour imaging devices and establishing their characterisation models is only a preliminary step necessary for including them in a colour reproduction system. The system used here follows the principles of a **five–stage transform** (MacDonald, 1993) whereby colours from the original medium are first transformed to tristimulus values via a characterisation model, their perceptual attributes are calculated using a colour appearance model (CAM), they are gamut mapped and colorant amounts for the reproduction medium are calculated via an inverse CAM and characterisation model.

As the aim of this study is to investigate the problem of gamut mapping, an attempt was made to reduce the influence of other factors. The luminances of the two media white points and the viewing conditions (in particular viewing geometry and viewing field) were therefore chosen to be as similar as possible (Section 3.1.2 & 3.1.3).

One of the important decisions to be made in a colour image reproduction system is the choice of adopted whites for the original and reproduction media. As the reproductions made in this system were intended to be viewed on their own, adaptation to their media white points was assumed and relative colorimetry was used throughout the system (i.e. media white points were assumed to be the adopted whites). Even thought both the CRT and printed reproductions were viewed side–by–side in the psychophysical experiments, the use of relative–colorimetry was justified, as both the chromaticities and luminances of the media white points were similar.

To obtain individual reproductions, the appearance of a particular image on the CRT was then taken to be the original. Hence an image's RGB values were first transformed into XYZ tristimulus values using the CRT's characterisation model from which colour space coordinates were calculated using R=G=B=100 *per cent* as the adopted white. Gamut mapping was then carried out in CIELAB for Experiments 1,2&4 and in CIECAM97s for Experiment 3. The resulting $L^*C^*h_{ab}$ or *JCh* coordinates respectively were transformed back to XYZ using the printer's substrate as the adopted white. Finally, the resulting tristimulus values were transformed into colorant amounts using the printer characterisation model (Figure 3.3.1).

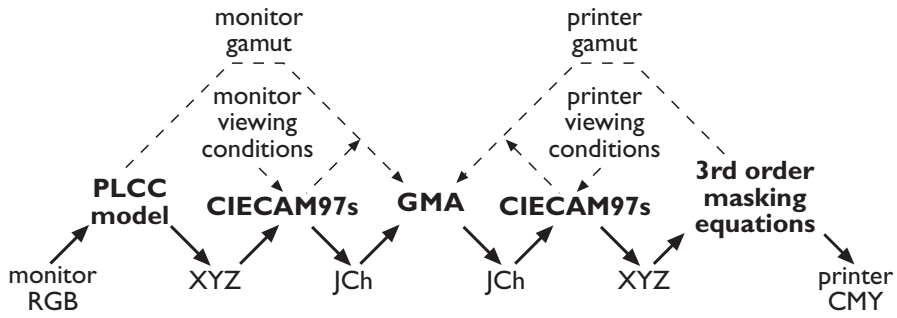


***Figure 3.3.1*** *Data flow of colour reproduction system in Experiment 3.*

## 3.3 Summary

The colour reproduction system used here comprised of a CRT monitor and various printed media viewed in a booth using a D50 simulator. Details of the characteristics of these media, their gamuts, the characterisation models used and the overall colour image reproduction system were given in

this section. An understanding of these parameters will be necessary for a meaningful interpretation of experimental results described in chapters to come.

# Chapter 4

# Development of Methods for Calculating Colour Gamuts

*The changing of bodies into light, and light into bodies,*
*is very comfortable to the course of Nature,*
*which seems delighted with transmutations.*

*Sir Isaac Newton (Opticks)*

# 4.1 Calculating Gamut Boundaries

Knowing the boundaries of the gamuts between which mapping is to be carried out is essential for the GMAs used in this project and, as is pointed out in Section 2.6.2, it can be divided into two separate problems.

Firstly, it is necessary to compute a **gamut boundary descriptor (GBD)** – i.e. some overall way of approximately describing a gamut. To do this, the *Segment Maxima GBD* method was developed and then used throughout this study. It was first published in a paper (Morovic and Luo, 1997b) and then discussed in more detail in a book chapter (Morovic and Luo, 1998d).

Secondly, it is also important to be able to find the intersections between the gamut boundary (as characterised by the GBD) and a given line along which mapping is to be carried out whereby points in which these intersections occur will be referred to as the **line gamut boundary (LGB)**. Two methods have been developed to this end whereby the *Constrained LGB* method is limited to finding the gamut boundary along lines of constant spherical angles or constant $L^*$ and $h_{ab}$ (Morovic and Luo, 1997b). The *Flexible Sequential LGB* method (Morovic and Luo, 1998d), on the other hand, was designed so as to efficiently calculate the intersections between the gamut boundary and any line having a constant hue angle.

Note, that even though these models will be described in terms of CIELAB, they can easily be used in any other uniform colour space or colour space associated with a colour appearance model.

## 4.1.1 Basic Geometry

The basics of 2D and 3D geometry, which are most important for the calculation of gamut boundaries will be briefly introduced in this section. They are by no means comprehensive and are only intended as a sample of the techniques used for dealing with the present problem.

### *Lines*

For each point ($P$) of a given line, the following equation describes the coordinates of its points in n–dimensions:

$$P = A + t^*\mathbf{u} \tag{4.1.1}$$

whereby each point on the line has a different value of $t$ and fixed values of $A$ and $\mathbf{u}$. If a line is determined by two different points $J = [j_1,j_2,\ldots,j_n]$ and $K = [k_1,k_2,\ldots,k_n]$ then $A = J$ and the vector $\mathbf{u} = [k_1 - j_1, k_2 - j_2, \ldots, k_n - j_n]$.

### *Planes*

For each point ($Q$) of a given plane, the following equation describes the coordinates of its points in n–dimensions:

$$Q = B + r^*\mathbf{v} + s^*\mathbf{w} \tag{4.1.2}$$

whereby each point on the line has a different set of $r$ and $s$ values and fixed $Q$, $\mathbf{v}$ and $\mathbf{w}$ values. If a plane is determined by three points $J = [j_1,j_2,\ldots,j_n]$, $K = [k_1,k_2,\ldots,k_n]$ and $L = [l_1,l_2,\ldots,l_n]$ (which must not be collinear) then $B = J$ and the vectors $\mathbf{v} = [k_1 - j_1, k_2 - j_2, \ldots, k_n - j_n]$ and $\mathbf{w} = [l_1 - j_1, l_2 - j_2, \ldots, l_n - j_n]$.

### *Intersecting a Line with a Plane in 3D*

Using the above notation this can be done on the basis of equations 4.1.1 and 4.1.2, which when combined result in the following system of three linear equations from which $t$ can be calculated. The value of $t$ then gives the position of the intersection point on the line:

$$A + t^*\mathbf{u} = B + r^*\mathbf{v} + s^*\mathbf{w} \qquad (4.1.3)$$

### *Determining Whether Point is in Triangle*

To establish whether point $P$ is in the triangle determined by points $A$, $B$ and $C$ (whereby all four points are co–planar), it is necessary to calculate the area of triangle ABC and the see whether the areas of triangles PBC, APC and ABP add–up to the same value. The area of triangle ABC is half the length of the vector obtained by multiplying any two of its vectors, e.g. **AB** and **AC**:

$$\frac{\|\mathbf{AB} \times \mathbf{AC}\|}{2} \qquad (4.1.4)$$

## 4.2 Segment Maxima GBD (SMGBD) Method

Using this method, the gamut boundary of a colour reproduction medium (or an image from it) is described by a matrix containing the most extreme colours for a given **segment** of colour space. In this study colour space was segmented either in terms of $L^*$, $C^*$ and $h_{ab}$ or spherical coordinates whereby spherical coordinates were calculated from CIELAB using the following formulæ:

$$r = [(L^*\text{-}L^*_E)^2 + (a^*\text{-}a^*_E)^2 + (b^*\text{-}b^*_E)^2]^{1/2} \qquad (4.2.1)$$

$$\alpha = \tan^{-1}((b^*\text{-}b^*_E)/(a^*\text{-}a^*_E)) \qquad (4.2.2)$$

$$\theta = \tan^{-1}[(L^*\text{-}L^*_E)/((a^*\text{-}a^*_E)^2 + (b^*\text{-}b^*_E)^2)^{1/2}] \qquad (4.2.3)$$

where the centre ($E$) is defined as the point having L*a*b* coordinates of [50,0,0], $r$ is the distance of a colour from the centre, $\alpha$ is the hue angle having a range of 360° and $\theta$ is the angle in a plane of constant $\alpha$ having a range of 180° (Figure 4.2.1a).

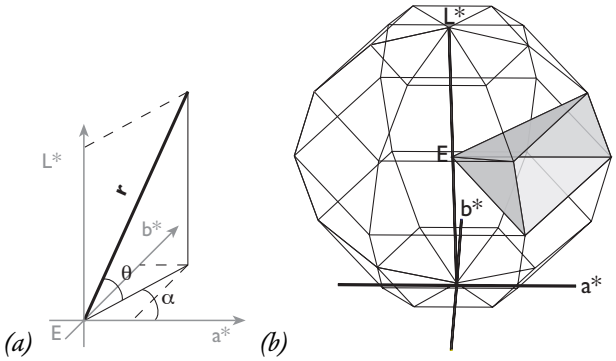


***Figure 4.2.1*** *Overview of Segment Maxima GBD in CIELAB: (a) spherical coordinates, (b) sphere segmented in terms of $\alpha$ and $\theta$ (only 6×6 segments – of which one is highlighted – are shown for the sake of clarity).*

The GBD matrix is calculated by first dividing colour space into $n \times n$ segments (whereby $n$=16 for this study) according to either $\alpha$ and $\theta$ (Figure 4.2.1b) or $L^*$ and $h_{ab}$. Hence, the data is stored in each segment either in terms of $\alpha$, $\theta$ and $r$ or $h_{ab}$, $L^*$ and $C^*$ respectively.

The following procedure assumes spherical angle segmentation and to calculate the matrix for $L^*$ and $h_{ab}$ segmentation, $\theta$ is replaced by $L^*$, $\alpha$ by $h_{ab}$ and $r$ by $C^*$ in the following description.

For colour reproduction media, colours are generated on the surface of the device coordinate gamut. This is done by setting one of the device coordinates to 0 or 100 *per cent* for each coordinate

in turn and varying the other two coordinates. For the media in this study coordinates were changed in 2 or 4 *per cent* steps resulting in 15,000 or 3,750 colours respectively.

When calculating the GBD of an image, its colours are used instead of colours from the surface of the medium gamut (as described above) whereby the rest of the procedure is the same for both media and images.

Each of the device–dependent colour descriptions is then transformed into XYZ tristimulus values using the appropriate characterisation model (Chapter 3). L*a*b* values are subsequently calculated and transformed into spherical coordinates using Equations 4.2.1–3. From these, the colour with the largest $r$ is stored for each of the $n \times n$ segments. Note, that it is not only $r$, which is stored for a given segment but spherical angles as well. If in the end there are segments in which there are no colours, values for them are linearly interpolated on the basis of the nearest GBD matrix entries (this is very rare for colour reproduction media but can often be the case when image gamuts are calculated).

GBD points obtained using the above method (Figure 4.2.2) are actual colours from the medium's gamut boundary and inaccuracies in the descriptor are only due to the number of segments chosen. The advantage of using unevenly distributed points in colour space is that the extremes of the gamut (including the colours of its colorants) will always be stored accurately, which would be a problem with an evenly spaced set.

For each medium used in this study, generating colours from within the entire gamut in device coordinate space gave the same results as generating them only from the surface. The boundaries obtained using these two approaches are called *natural* and *physical* respectively (Mahy, 1997) and for some media they can give different results.

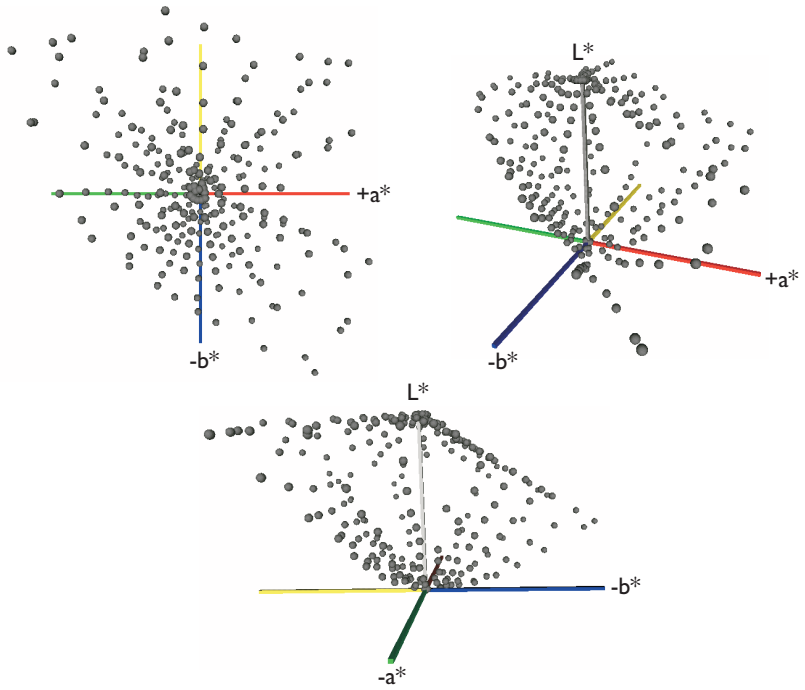


***Figure 4.2.2*** *GBD points calculated for Barco Reference CRT.*

## 4.3 Constrained LGB (CLGB) Method

Once a gamut boundary descriptor is calculated using the *Segment Maxima* method, there still remains the problem of finding the gamut boundary along a given line. The first solution to this problem developed for this study was one, which enabled the calculation of LGBs along lines hav-

ing constant spherical angles ($\alpha$ and $\theta$) or constant $L^*$ and $h_{ab}$. What will be described here is the former of these cases whereby the latter is analogous to it.

The first step in CLGB is to calculate the equation of the line ($l$) from the centre (L*a*b* = [50,0,0]) along which the gamut boundary is to be found. The next task is to find those three colours *a, b* and *c* from the gamut boundary matrix, which comply with the following conditions:

1. the plane (φ) determined by *a, b* and *c* intersects *l* within the triangle formed by *a, b* and *c* and
2. *a, b* and *c* are from neighbouring segments as defined by the GBD (this condition is necessary for the resulting intersection point to be on the gamut boundary).

For a given colour ($C$) these three points can be found by going through all the triangles formed by neighbouring points in the GBD and finding that triangle for which *Condition 1* holds. As the GBD points are from an evenly spaced set of segments (though the points are not evenly spaced themselves), it is possible to speed up this process by only checking the triangles from the 5×5 sub–matrix centred around the segment into which $C$ belongs.

Due to the finite precision of computation, it is possible that no intersection is found, which satisfies *Condition 1* even when all triangles from the GBD made up of neighbouring points are checked. In this case the triangle to which the intersection point between φ and *l* is closest is found and the gamut boundary point is the point on *l*, which is closest to this triangle.

## 4.4 Flexible Sequential LGB (FSLGB) Method

A new method for calculating LGBs was needed for the more complex models used in this study as existing methods were similar to CLGB in terms of being restricted to finding boundary points along very specific lines, e.g. ones having constant $L^*$ and $h_{ab}$ or constant spherical angles. This meant that a new, flexible method had to be developed so as to make gamut boundary calculations faster and more accurate.

As all the algorithms studied here map colours in planes of constant hue angle, the FSLGB algorithm first finds the 2D gamut boundary at the hue angle in which the mapping is to be carried out (Figure 4.4.1). For a given colour ($C$) this is done in the following way:

1. Calculate equation of constant hue angle plane ($\varphi$) having hue angle of $C$ ($\alpha_C$).
2. For each θ level find the pair of neighbouring points from the GBD matrix of which one has a larger and one a smaller hue angle than $\alpha_C$.
3. For each pair calculate the intersection of the line connecting the two GBD points with φ.
4. In addition to these $n$ points calculate the points on the L* axis where the surface defined by the GBD matrix intersects it.

   For the top of the lightness axis this can be done by considering only the $n$ GBD points from segments having the largest θ values. Triangles are then formed between the point with the largest L* and neighbouring pairs of the other points. The intersection of each of these triangles and the lightness axis is calculated and if it is within the triangle then it is the LGB point. An analogous procedure is used for finding the intersection of the gamut boundary with the bottom of the lightness axis.

The resulting set of $n+2$ points form a polygon (Figure 4.4.1c) describing the gamut boundary for a given hue angle. The intersection of a given line ($l$) and this polygon can then be found using the following procedure:

1. For each pair of neighbouring points in the polygon calculate the equation of the line determined by them.

2. For each of these lines calculate their intersection with *l* and if it lies between the two points from the polygon then it is an LGB point.

Depending on the shape of the gamut boundary, this procedure can result in varying numbers of LGB points for a given line. For the gamuts and gamut mapping lines dealt with in this study the algorithm always calculated at most two points, giving the maximum and minimum along a given line (e.g. points $b_1$ and $b_2$ from Figure 4.4.1c).

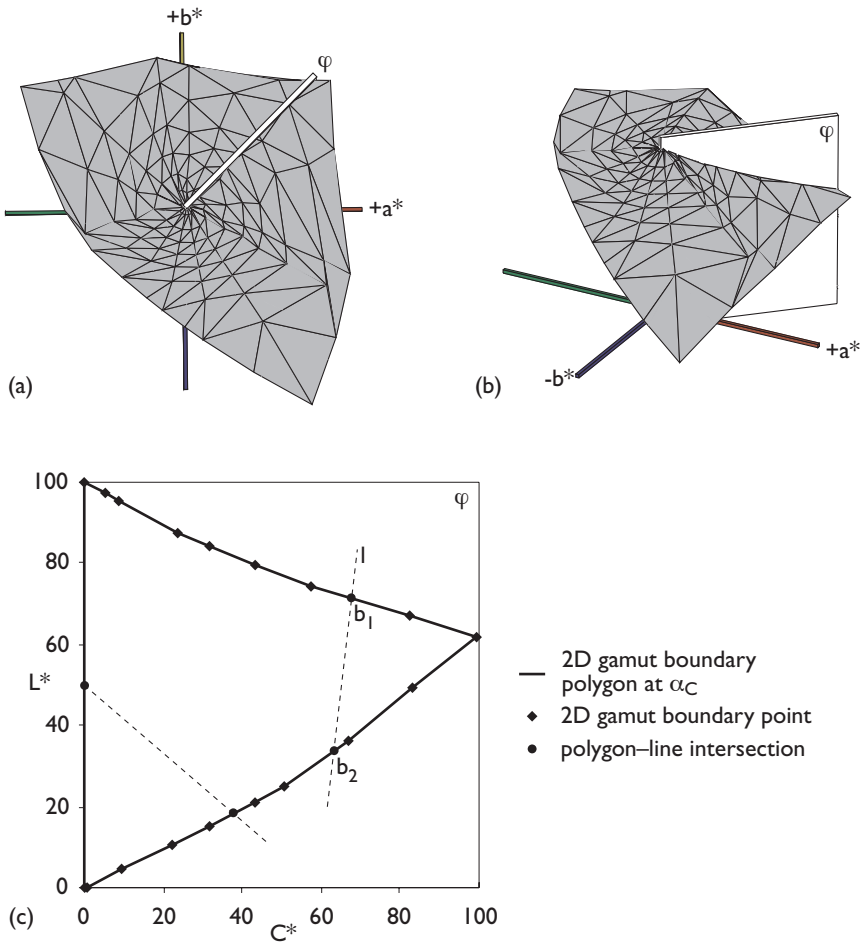


***Figure 4.4.1*** *Overview of Sequential LGB algorithm in CIELAB: (a & b) gamut boundary of Barco Reference Calibrator CRT obtained using Segment Maxima method and φ (a plane of constant hue angle), (c) their intersection and the intersection of the resulting 2D boundary polygon with lines for which boundary points are to be determined.*

## 4.5 Summary

The methods described in this chapter were used in this study for calculating overall gamut boundary descriptors (*Segment Maxima GBD* method), for obtaining the gamut boundary along a given line of constant $L^*$ and $h_{ab}$ or constant spherical angles (*Constrained LGB* method) or for doing this along any line of constant $h_{ab}$ (*Flexible Sequential LGB* method).

# Chapter 5

# Experimental Methods

*All the mighty world*
*Of eye and ear, both what they half–create,*
*And what perceive.*

*William Wordsworth (Lines composed … above Tintern Abbey)*

## 5.1 Overview

Inasmuch as there is as yet no satisfactory model for quantifying the appearance of complex pictorial images and neither is there a good model for the quantification of their differences, the paradigm chosen for the evaluation of the performance of GMAs is psychophysics (Section 2.2). As is stated in the introduction (Section 1.3), the aim of this study is to find a universal GMA. This will be done by finding the method, which for a variety of original images displayed on a CRT gives the most **accurate** reproduction on a range or printed media (using the inkjet printer described in Chapter 3). Hence, the experimental part of this study will be geared towards ascertaining whether the proposed models fulfil this aim.

As GMAs cannot be directly judged in terms of how accurate they are, judgements are made on reproductions made with various GMAs and as everything else was the same for these reproductions, their accuracy is considered to be that of the corresponding GMA. It is in this sense that the accuracy or pleasantness of GMAs is understood in this study.

This chapter will describe the psychophysical methods (briefly introduced in Sections 2.2.1 and 2.2.2) used for evaluating reproductions made with different GMAs. A description of the test images and viewing techniques used in this study will be followed by an overview of the two psychophysical methods used – pair comparison and category judgement – and the data analysis techniques with which results were obtained from raw observer data.

## 5.2 Test Images

As one of the requirements of a universal GMA is to give good results over a wide range of originals, it is necessary to use a representative set of test images. To this end five images were chosen, which covered a range of image content types and which had various image gamut characteristics useful for the evaluation of GMAs. For their reproductions as well as information on their gamuts see Appendix B.

In terms of **image contents** four of the images were scanned photographs where three images (SKI, DOL and MUS) had colours from the majority of hues and one image (NAT) was predominantly green and blue. The fifth image (BUS) was a computer generated business graphic whose colours were the most chromatic primary and secondary colours obtainable on the original medium.

A useful statistic for the description of image gamuts is **chroma range**, which is defined as the area in the $a^*b^*$ plane delimited by the cusps at each hue angle (whereby for a given hue angle the **cusp** is the colour with maximum chroma). In this study, chroma range was calculated by finding the largest chromas at 60 equally spaced hue angles and calculating the area of the 2D polygon formed by them (for these polygons see Figures B.1&2 in Appendix B). The relative chroma ranges (i.e. in this case image chroma range divided by medium (CRT) chroma range) of the five test images are shown in Table 5.2.1, as they had a very good correlation with the performance of GMAs in Experiment 2.

| Image | BUS | DOL | SKI | MUS | NAT |
|---|---|---|---|---|---|
| Relative chroma range | 82% | 78% | 71% | 28% | 10% |
| Out–of–gamut pixels | 67% | 49% | 61% | 45% | 28% |

***Table 5.2.1*** *Sample test image statistics in CIELAB.*

The percentages of **out–of–gamut pixels** (in this case relative to the gamut of prints from Experiment 2) can in some cases have an impact on the performance of GMAs and are shown in Table 5.2.1 (for more details on the values of these two statistics for all experiments see Appendix B). When investigating differences between individual test images in terms of the accuracy of reproduc-

tions obtained using various GMAs, the values of the above parameters (i.e. image contents, relative chroma range and the percentage of out of gamut pixels) can often be of use.

## 5.3 Viewing Technique

As viewing conditions are one of the defining elements of colour appearance, the viewing technique used for the psychophysical experiments in this study will be described here. For the pair comparison experiments the **simultaneous binocular** viewing technique (Braun *et al.*, 1996) was used. Using this technique, observers sat at approximately 100 cm from the CRT and prints, which when shown in a viewing booth had similar chromaticities and luminances for the media white points (Chapter 3). To reduce differences in adaptation further, a white border was displayed around the images, which had a chromaticity similar to the white border of printing substrate left around the printed reproductions. The pair of printed reproductions and the original image on the CRT were approximately co–planar (Figure 5.3.1) and equal in size (Table 5.3.1), the viewing geometry was such that the diffused illuminant was not directly visible to observers and the whole scene was viewed in a dark room.

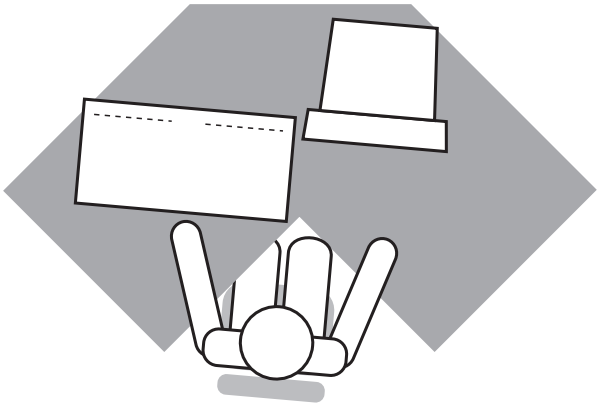

***Figure 5.3.1*** *Viewing technique for pair comparison experiment.*

| Image | Dimensions (cm) | | Angular subtense (°) | |
|---|---|---|---|---|
| | Width | Height | Horizontal | Vertical |
| **BUS** | 27.0 | 17.2 | 30.8 | 19.7 |
| **DOL** | 22.2 | 18.0 | 25.3 | 20.6 |
| **MUS** | 18.0 | 18.0 | 20.6 | 20.6 |
| **NAT** | 18.0 | 18.3 | 20.6 | 20.9 |
| **SKI** | 18.0 | 23.4 | 20.6 | 26.7 |

***Table 5.3.1*** *Sizes of test images & corresponding angular subtense under viewing conditions in this study.*

The viewing conditions for the category judgement method differed from the above only inasmuch as only printed reproductions were shown to observers without them the being able to see the original CRT images.

## 5.4 Pair Comparison

In all experiments where the accuracy of gamut mapping algorithms was evaluated, the pair comparison method derived from Thurstone's **law of comparative judgement** (Thurstone, 1927) was used. This law is 'based on the notion that the proportion of times stimulus A will be judged greater than stimulus B is determined by the degree to which sensation A and sensation B differ' (Gescheider, 1976). Furthermore, Thurstone suggests that an organism's response to a given stimulus will result in a range of responses forming a normal distribution on the psychological contin-

uum. Therefore, to determine the difference between two stimuli, it is necessary to determine the distance between the means of their response distributions, which can be expressed as follows:

$$\overline{\psi}_B - \overline{\psi}_A = z_{BA}\sqrt{\sigma^2_{\psi_A} + \sigma^2_{\psi_B} - 2r_{\psi_A\psi_B}\sigma_{\psi_B}\sigma_{\psi_A}} \qquad (5.4.1)$$

Here $\overline{\psi}_A$ and $\overline{\psi}_B$ are the means of response distributions to stimuli A and B respectively, $r$ is the correlation coefficient between the two distributions, $\sigma$ is the standard deviation and $z$ is the z–score of B compared to A. As the populations dealt with in this experiment can be assumed to have the same standard deviations and no correlation, the z–score represents the difference between the two stimuli on a scale where the unit is $\sigma\sqrt{2}$ and 0 represents the mean (in Thurstone's paper this set of assumptions is referred to as case 5).

A disadvantage of this method is that it gives results, which are relative to the set of GMAs being evaluated in a given experiment, which is a problem particularly when the results of different experiments are compared. Further the time it takes to conduct a pair comparison experiment is significantly longer than for the category judgement method and this technique is not practicable in its basic form for the comparison of large numbers of stimuli. However, its advantage, which makes it one of the most trustworthy techniques, is that it requires the least amount of subjective input from observers and is therefore a simple task.

## 5.1.1 Experimental Procedure

To obtain the differences between $n$ chosen GMAs, observers were shown all pair combinations of reproductions made with them under the viewing conditions described above. Note, that to each observer pairs of reproductions were shown in a different and random order. Given the number of GMAs to be compared, the number of pairs in an experiment can be calculated using the following formula:

$$Number\ of\ pairs = n(n\text{-}1)/2 \qquad (5.4.2)$$

For each pair, observers were then asked to make a judgement as to which reproduction was closer to the original shown on the CRT in terms of appearance. In addition to making judgements about overall accuracy, observers were asked to make that judgement for individual regions within the images whereby each region had a characteristic colour (see Appendix B). The evaluation of such regions in colour images was previously used by MacDonald and Morovic (1995) and provides a solid, quantitative basis for understanding the performance of GMAs in different parts of colour space.

Note, that observers were not forced to make a choice in these experiments and therefore had the option to say that both reproductions were equally close to the original.

## 5.1.2 Data Analysis

For a given pair, the reproduction chosen by an observer was given a score of 1, the other of a pair of reproductions a score of 0 and when both were judged to be equally accurate they both received a score of 0.5. For each observer this data was stored in an $n \times n$ **raw data matrix** where the value in column $i$ and row $j$ was the score given to GMA $i$ as compared with GMA $j$.

The following procedure was then used to obtain accuracy scores from the raw data obtained from observer judgements (for a worked example see Appendix C):

1. An $n \times n$ **frequency matrix** was calculated from the responses recorded for each observer followed by the calculation of a corresponding **percentage matrix**. For each pair combination of GMAs these matrices showed how often one GMA was preferred over another.

2. An *n*×*n* **z–score matrix** was then calculated from the percentage matrix as a percentage is the area under the normal distribution curve on the interval (–∞,z] where 0 is the mean and σ is the unit. As discussed above, these values represent the difference between pairs of GMAs. For extreme values (i.e. 0 *per cent* and 100 *per cent*) in the percentage matrix, z–scores – the limit of which approaches -∞ and ∞ respectively – were obtained by first calculating their **logistic function** values using the following formula (Bartleson, 1984, pp. 463):

$$LG = \ln\left(\frac{f + c}{N - f + c}\right) \qquad (5.4.3)$$

where *f* is the value from the frequency matrix, *N* is the number of observations and *c* is an arbitrary additive constant (0.5 was suggested by Bartleson (1984) and has also been used in this study). These LG values were then transformed to z–scores by using a simple scaling in the form of z = LG*0.64 where the scaling coefficient was calculated using linear regression between z–scores and corresponding LG values (as LG values depend on the number of observations this scaling coefficient varied between experiments since their sample sizes were similar but not identical).

3. To obtain the final **accuracy score** (*A*) for each GMA, the values in its corresponding column of the z–scores matrix were averaged. The resulting scores are on an interval scale where 0 represents the mean accuracy of the *n* GMAs being evaluated.

4. *A* is an estimate of μ – the true accuracy score of a GMA (which is the mean of a normally distributed population), therefore it is also necessary to calculate its precision. As *A* is based on a random sample of size *N* from a normal distribution with mean μ and variance $\sigma^2$, its 95 *per cent* **confidence interval** is calculated using the following formula, which has already been introduced in Chapter 3 (Equation 3.1.1):

$$A \pm 1.96\frac{\sigma}{\sqrt{N}} \qquad (5.4.4)$$

The mean of the population (μ) of which A is an estimate will then lie in this interval at the 95 *per cent* confidence level (i.e. at this level a GMA is significantly different from another only if its score is outside the confidence interval of the other GMA). As the scale of *A* has units which equal $\sigma\sqrt{2}$, $\sigma = 1/\sqrt{2}$. Hence, if the sample size is 13 (as was the case for individual images in Experiment 2) then the confidence interval is $\pm$ 1.96*(1/$\sqrt{2}$)/$\sqrt{13}$, which is approximately ±0.38.

Finally, inter–observer variance will be quantified by first calculating the mean values of all columns for each individual raw data matrix. Next, for each of these columns the standard deviations between the column means for each observer will be calculated. Overall, inter–observer variance will be reported in terms of the mean and maximum standard deviations for each individual test image. When interpreting these values, it is important to understand that they represent the standard deviation of the means for the columns in the *percentage matrix* and not directly the standard deviations of accuracy scores.

## 5.5 Category Judgement

The category judgement technique was used to evaluate the pleasantness of reproductions made with different GMAs in Experiment 4. It is based on the **law of categorical judgement** (Torgerson, 1954), which is an extension of Thurstone's law of comparative judgement. The difference between the two is that the law of categorical judgement relates to the relative position of stimuli with respect to category boundaries on the psychological continuum rather than with respect to one an-

other (Bartleson, 1984). Using this technique observers are asked to locate an attribute on a predetermined equi–interval scale.

Compared with the pair comparison method this approach has the advantage that results are on an absolute scale. On the other hand, its disadvantages include the fact that observers are asked to make a judgement requiring more subjective input than pair comparison. This makes the results more dependent on training as well as on the characteristics of individual observers themselves.

### 5.5.1 Experimental Procedure

In the case of this experiment, each observer was shown reproductions made with a number of GMAs one at a time. Note, that this was done in a different and random order for each observer who was then asked to make a judgement for each reproduction in terms of how pleasant it was on an integer scale of 1 – 7. To aid consistency, they were read the following instructions:

> For each of the images you will be shown we would like you to tell us how pleasant you think it is. Please give your opinion on a scale of numbers from one to seven where one represents the most pleasant image and seven represents the least pleasant image you can think of. Use numbers between one and seven to represent equal intervals of pleasantness so that the difference between any neighbouring categories be the same.

Furthermore, before carrying out the actual experiment, observers were shown two images whereby each of these two images was considered to be in the highest and lowest categories respectively by the majority of observers. Note, that observers were not told how to categorise these images – they only served the purpose of helping observers with imagining images close to the extremes of the category scale.

### 5.5.2 Data Analysis

To obtain the ranking of $n$ reproductions made for each image, the following steps were carried out (Bartleson, 1984; Lo, 1995):

1. An $n \times n$ **frequency matrix** was calculated from raw experimental data where each column contained the frequency of each GMA being judged as being in the corresponding category.
2. As the law of categorical judgement is concerned with the percentages of times that a given stimulus (in this case image) is assigned to a position below a given category, an $n \times (n-1)$ **cumulative percentage matrix** was calculated.
3. The matrix from step 2 was transformed into a **z–score matrix** where the same method was used to deal with extreme percentages as in the pair comparison method.
4. An $n \times (n-2)$ **difference matrix** between adjacent columns was then calculated followed by obtaining the mean for each column.
5. Next, **boundary estimates** between the seven categories were determined by setting the origin (which is between category 7 and 6) to zero and adding adjacent mean values from the difference matrix (from step 4).
6. **Scale values** in an a $n \times (n-1)$ matrix indicating image pleasantness were calculated by subtracting z–scores (step 3) from boundary estimates (step 5). This was done as the z–scores represent the distance from each of the category boundaries. For each reproduction the mean scale value was then computed, the ranking of which corresponds to the ranking of the GMAs being evaluated. Note, that the most pleasant reproduction will have a rank of one and the least pleasant reproduction will rank seventh and that confidence intervals of these pleasantness scores are calculated in the same way as for the pair comparison method (Equation 5.4.4).

Inter–observer variance will be quantified by calculating the mean category value ($c$) for each row in the *raw data matrices* of each observer using the following equation:

$$c = \frac{\sum_{i=1}^{7} r_i i}{\sum_{i=1}^{7} r_i} \tag{5.5.1}$$

where $r_i$ are the frequencies in the row of the *raw data matrix* for which $c$ is to be calculated. Mean category values are also calculated for each row of the *frequency matrix* and differences are calculated between individual $c$ values and the corresponding $c$ values from the *frequency matrix*. Finally, these differences are expressed as percentages of the original $c$ values and their mean is calculated for each of the test images.

## 5.6 Summary

The pair comparison and category judgement techniques presented in this chapter were used for evaluating the accuracy or pleasantness of reproductions made with a variety of GMAs. The experimental results then served as a basis for the improvement of these or the development of new algorithms, which will be described in the following chapters.

Chapter 6

# Experiment 1: Initial Psychophysical Evaluation of Existing Gamut Mapping Algorithms

*The last thing one knows*
*in constructing a work*
*is what to put first.*

*Blaise Pascal (Pensées)*

# 6.1 Choice of Initial Algorithms

Now that the preliminary work – colour reproduction (Chapter 3), gamut boundary calculation (Chapter 4) and experimental methods (Chapter 5) – was introduced, the first stage of the development of gamut mapping algorithms can be dealt with. Note, that the work covered here was partly published before (Morovic and Luo, 1997a).

As indicated in the introduction (Section 1.4), the first stage of the approach taken here consists of a literature survey of gamut mapping algorithms (Section 2.6) on the basis of which some are chosen, implemented and psychophysically evaluated. The majority of the surveyed GMAs have stages, which can be categorised as being either **sequential** or **simultaneous** in their compression of lightness and chroma. Sequential mappings treat these two attributes separately, whereas simultaneous methods map them together.

A number of algorithms using both kinds of mappings were chosen to represent previously proposed solutions to the gamut mapping problem. All the algorithms discussed here kept hue unchanged and only made changes to lightness and chroma. Note, that the descriptions of GMAs often refer to changing perceptual attributes, however, this is always implemented in terms of their predictors in a colour space (for the implications of this see Section 2.6.3.1).

In addition to the six algorithms described in sections 6.1.1 and 6.1.2, another GMA was evaluated in this experiment. It was meant to be an implementation of the gamut mapping algorithm proposed by Johnson *et al.* (CARISMA, 1992; Johnson *et al.*, 1998b), however, it will not be discussed here, as it turned out to be an incorrect interpretation and as it did not perform well. Its details can be found in Morovic and Luo (1997a) where it was labelled JOHNSON.

Throughout the following descriptions of gamut mapping algorithms it is useful to keep in mind the key characteristics of gamut boundaries in planes of constant hue angle (Figure 6.1.1). These are the **maximum** and **minimum lightness** and the **cusp**, whereby the cusp is the colour with maximum chroma in a plane of constant hue (as has already been said in Section 5.2). It is primarily these values, which determine the effect of individual GMAs on the colours of a given hue.

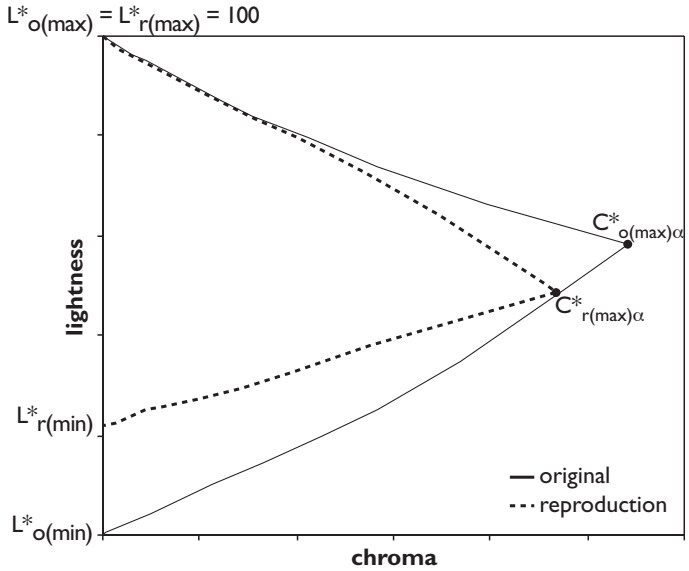


***Figure 6.1.1*** *Key characteristics of original and reproduction gamut boundaries in a plane of constant hue.*

The following algorithms will be described in terms of CIELAB as that is the colour space in which they were originally proposed and also in which they were implemented in this study.

### 6.1.1 Sequential GMAs – LLIN, LNLIN, LCLIP & LSLIN

The sequential algorithms implemented here intend to map perceptual attributes separately and consist of two stages: (a) **lightness mapping** and (b) **chroma mapping**.

In the first stage they map lightness linearly so that the minima and maxima of the two gamuts are transformed onto each other and that the lightness of a given colour relative to these extremes is maintained. This is done using the following formula:

$$L^*_r = L^*_{r(\max)} - (L^*_{o(\max)} - L^*_o) * \frac{(L^*_{r(\max)} - L^*_{r(\min)})}{(L^*_{o(\max)} - L^*_{o(\min)})} \qquad (6.1.1)$$

Here the subscripts *o* and *r* denote the original and reproduction gamuts respectively and *max* and *min* are the maximum and minimum lightnesses available in a given gamut.

In the second stage each of the four algorithms perform a different mapping.

**LCLIP** (Sara, 1984) clips out–of–gamut colours onto the gamut boundary and leaves the chroma of in–gamut colours unchanged. To do this, the following formula is used:

$$C^*_{s_r} = \begin{cases} C^*_{g_{r\alpha L}}; C^*_{s_o} \geq C^*_{g_{r\alpha L}} \\ C^*_{s_o}; C^*_{s_o} < C^*_{g_{r\alpha L}} \end{cases} \qquad (6.1.2)$$

where *s* a given colour, *g* is the LGB point calculated for hue angle $\alpha$ and lightness *L* and *r* refers to the reproduction (Figure 6.1.2).

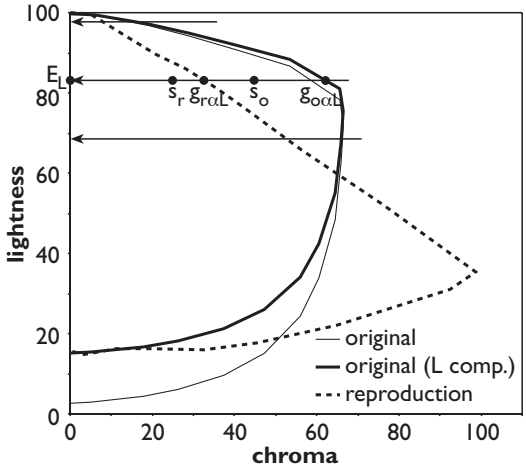


***Figure 6.1.2*** *Overview of LCLIP, LLIN and LNLIN algorithms ($s_o$ is the original colour after L* compression).*

**LLIN** (Johnson, 1979) linearly compresses chroma along lines of constant lightness using the following formula:

$$C^*_{s_r} = \begin{cases} C^*_{s_o} \dfrac{C^*_{g_{r\alpha L}}}{C^*_{g_{o\alpha L}}}; C^*_{g_{o\alpha L}} > C^*_{g_{r\alpha L}} \\ C^*_{s_o}; C^*_{g_{o\alpha L}} \leq C^*_{g_{r\alpha L}} \end{cases} \qquad (6.1.3)$$

Again the same notation is used as for the previous algorithm with the addition of the *o* subscript which refers to the original (Figure 6.1.2). As can be seen from Formula 6.1.3, compression is only carried out when the original gamut boundary has a larger chroma than the reproduction gamut boundary. Note, that this will not result in discontinuity, as the rate of compression is constant for a given lightness and hue angle combination and varies smoothly with both (for well–behaved gamuts – i.e. gamuts, which in a plane of constant hue angle are approximately uni–modal).

**LNLIN** (Stone and Wallace, 1991) performs the compression along lines of constant lightness in a non–linear way whereby it leaves chroma unaltered for the majority of the range and then makes a smooth transition to clipping. In this study a third–order function of the following form was used:

$$C^*_{s_r} = \begin{cases} a_1 C^*_{s_o} + a_2 C^{*2}_{s_o} + a_3 C^{*3}_{s_o}; C^*_{g_{ocL}} > C^*_{g_{rcL}} \\ C^*_{s_o}; C^*_{g_{ocL}} \le C^*_{g_{rcL}} \end{cases} \qquad (6.1.4)$$

whereby the coefficients $a_1$, $a_2$ and $a_3$ were calculated by solving the following system of linear equations:

$$\begin{pmatrix} C^*_{g_r} \\ C^*_{g_r}/4 \\ C^*_{g_r} \end{pmatrix} = \mathbf{M} \begin{pmatrix} a_1 \\ a_2 \\ a_3 \end{pmatrix}$$

$$\text{where } \mathbf{M} = \begin{pmatrix} C^*_{g_o} & C^{*2}_{g_o} & C^{*3}_{g_o} \\ C^*_{g_r}/4 & \left(C^*_{g_r}/4\right)^2 & \left(C^*_{g_r}/4\right)^3 \\ C^*_{g_r} + 2\left(C^*_{g_o} - C^*_{g_r}\right)/3 & \left(C^*_{g_r} + 2\left(C^*_{g_o} - C^*_{g_r}\right)/3\right)^2 & \left(C^*_{g_r} + 2\left(C^*_{g_o} - C^*_{g_r}\right)/3\right)^3 \end{pmatrix} \qquad (6.1.5)$$

Note, that all the values in Equation 6.1.5 with a *g* subscript are again hue angle and lightness dependent and that clipping (Equation 6.1.2) is applied after this function, so as to ensure that output colours are inside the reproduction gamut.

Calculating the parameters of Equation 6.1.4 in the above way results in the function going through the four fixed points shown in Figure 6.1.3. The first and last of these points are obvious choices, as the extremes are always mapped onto each other so as to maintain as much variation as possible. How the other two points are chosen then determines the degree to which the non–linear function is similar to clipping or linear compression. Note, that for a given chroma level these functions delimit the range of values, which the non–linear function can have.

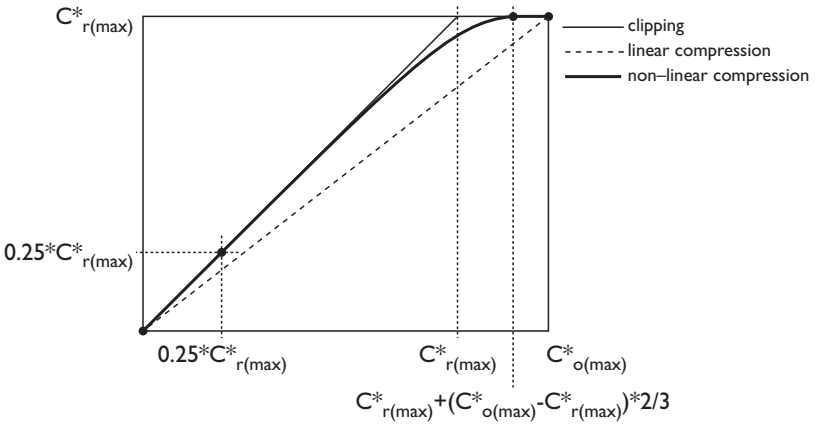


***Figure 6.1.3*** *Clipping, linear and non–linear chroma compression functions. Bullets represent fixed points for LNLIN algorithm.*

Lastly, the **LSLIN** algorithm (Laihanen, 1987) can be seen as a hybrid between the two kinds of algorithms. Even though it has a separate, initial lightness compression stage, this is followed by a simultaneous mapping of both lightness and chroma using the SLIN algorithm, which will be described next.

## 6.1.2 Simultaneous GMAs – CUSP & SLIN

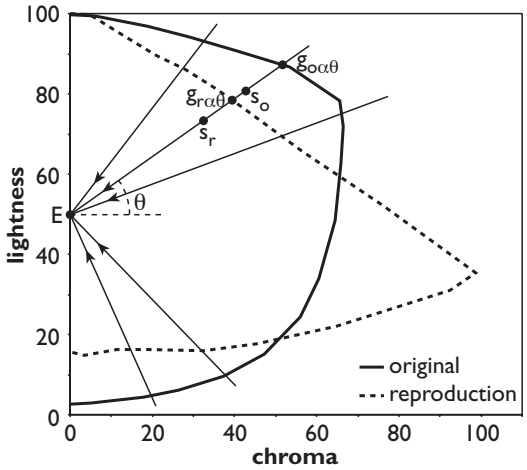


***Figure 6.1.4*** *Overview of SLIN algorithm.*

Algorithms in this group transform colours so that their lightness and chroma are changed simultaneously. This is achieved by mapping colours towards a particular point in colour space (i.e. a "centre–of–gravity").

For **SLIN** this centre is the point on the lightness axis for which L*=50 (labelled *E* in Figure 6.1.4) and for the **CUSP** algorithm the centre–of–gravity is the point on the lightness axis which has the same lightness as the gamut's cusp ($E_\alpha$ in Figure 6.1.5). The compression along a given line is then done linearly using Equation 6.1.3 with the difference that instead of using chroma, distances from *E* (or $E_\alpha$) are used. Note, that an algorithm similar to CUSP has previously been proposed by Ito and Katoh (1995).

The SLIN algorithm was also implemented in the colour space of the LLAB colour appearance model as described by Luo *et al.* (1996) – reproductions made with this algorithm were labelled **SLINLLAB**.

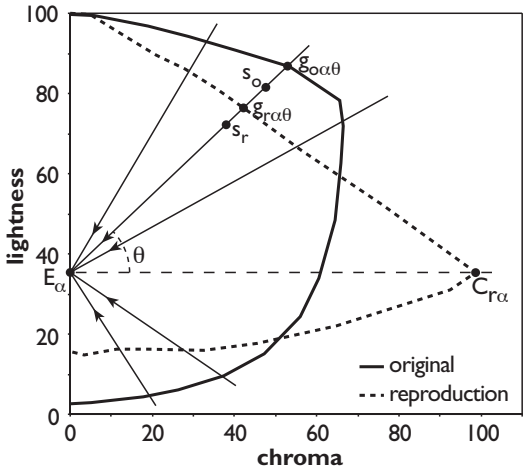


***Figure 6.1.5*** *Overview of CUSP algorithm.*

As can be seen, the algorithms in this group do not have an initial lightness compression. This was done to test the correctness of the (sometimes implicit) assumption, made by all previous studies – except for Ito and Katoh (1995) – that an overall lightness mapping needs to be the first step of a GMA. This assumption arises from the results of investigations where colour reproduction could only be controlled via tone–reproduction curves. Under such conditions, it is indeed linear compression of lightness, which gives the best results, as has also been shown in a study carried out by Johnson and Birkenshaw (1978). Whether this still holds when individual attributes of a colour can

be controlled independently of each other and of the attributes of other colours is a hypothesis which can by no means be declared *a priori* correct.

## 6.2 Experimental Evaluation

Reproductions of the five test images (Section 5.2) were made using the above seven algorithms in the colour reproduction system described in Chapter 3. These reproductions were evaluated by 12 observers with normal colour vision of which five were female and seven male. The observers, who were all either staff or students at the Colour & Imaging Institute, were aged between 22 and 38 years. The pair comparison technique was then used in the way described in Chapter 5 with the outcome being the following results.

### 6.2.1 Overall Results

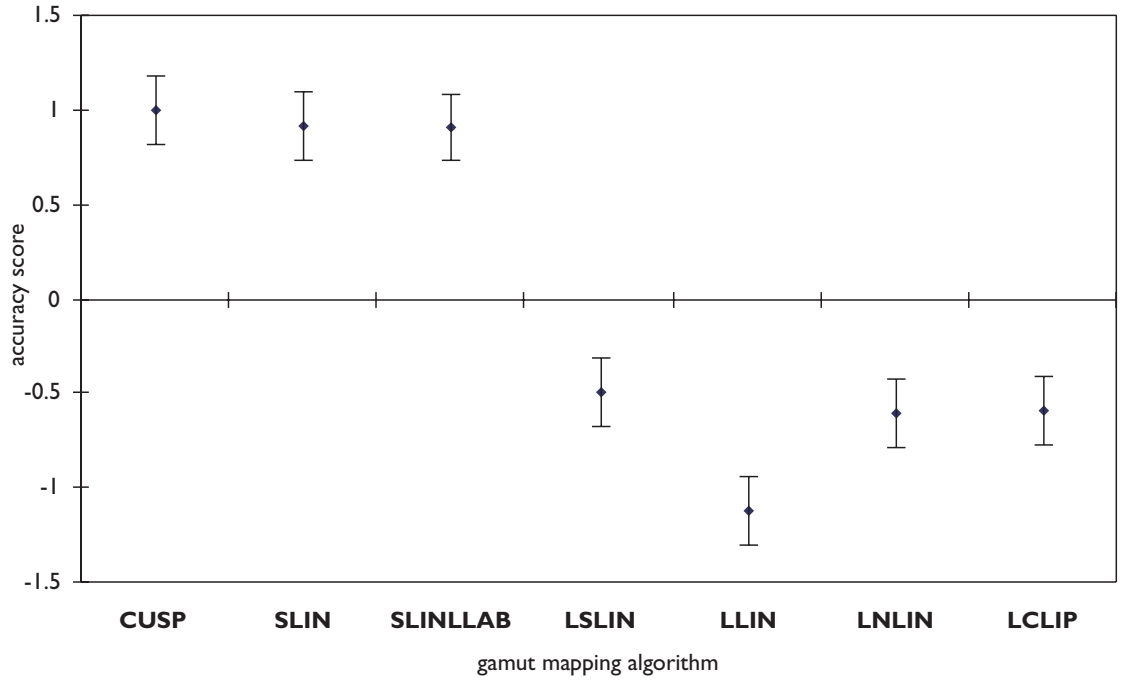


***Figure 6.2.1*** *Results of initial experiment based on the judgements made for the overall accuracy of five test images (including 95 per cent confidence intervals).*

The results shown in this section were obtained by averaging the percentage matrices obtained for the overall judgements made for the five test images. The remainder of the data analysis follows the procedure from Section 5.4.2 whereby the LG to z–score scaling coefficient and the 95 per cent confidence interval were those for sample–size 60 (i.e. 12 observers for five images) and can be found in Appendix D.

The results shown in Figure 6.2.1 represent the overall results of this experiment. However, the following analysis and interpretation of experimental results will exclude the reproductions made with SLINLLAB. This is done, as SLIN and SLINLLAB both represent the same algorithm (their difference being only the colour space in which they are implemented) and as the inclusion of both would in effect give SLIN a larger weighting. This would be contrary to the aim of this study, which is the investigation of GMAs and not that of colour spaces. Nonetheless, Figure 6.2.1 is included so as to show the very similar performance of the two SLIN variations.

Excluding SLINLLAB results in the accuracy scores shown in Figure 6.2.2 which will serve as the basis for drawing conclusions from Experiment 1. These accuracy scores were obtained in the same way as for Figure 6.2.1 with the difference that the values from SLINLLAB's row in the z–score matrix were excluded.

From the overall results we can clearly see that the simultaneous algorithms (CUSP and SLIN) performed significantly better than the sequential algorithms. This suggests that the use of an overall lightness compression as the first step does not give optimal results and it indicates that maintaining chroma is of greater importance than was previously thought. Hence, the lightness–compression hypothesis discussed at the end of Section 6.1.2 does not hold for the present set of algorithms.

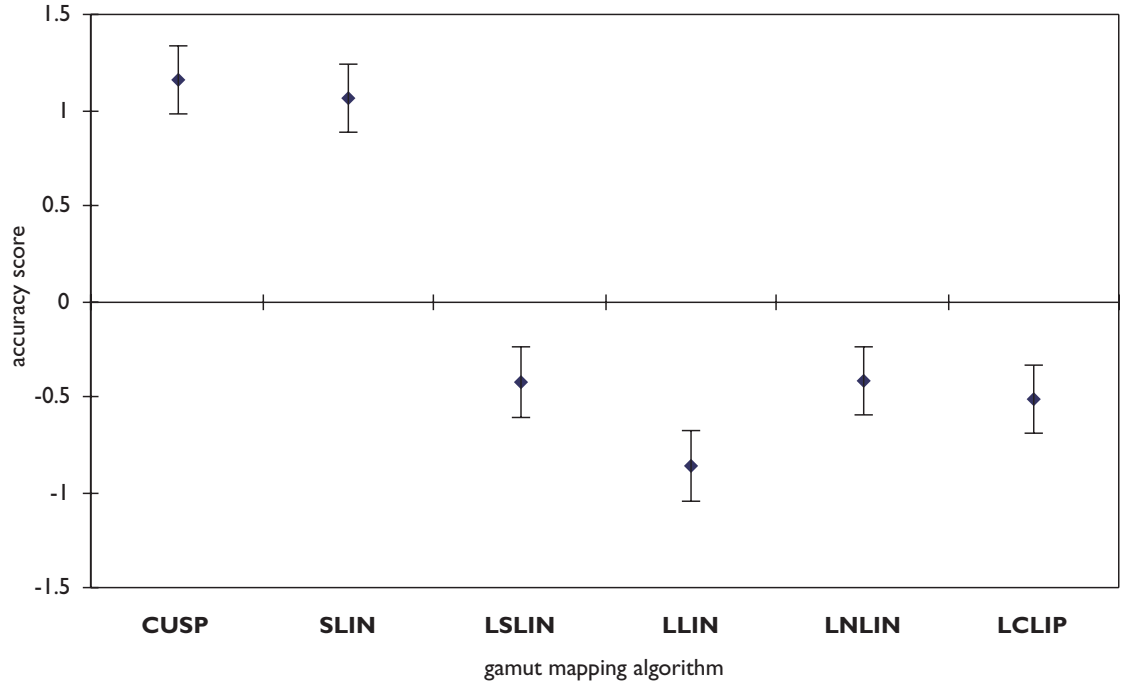


***Figure 6.2.2*** *Results of initial experiment based on the judgements made for the overall accuracy of five test images reproduced by algorithms implemented in CIELAB (including 95 per cent confidence intervals).*

The reason for the failure of overall lightness compression can be found in the shapes of the original and reproduction gamuts which, in planes of constant hue angle, usually resemble triangles (the vertices being $L^*_{min}$, $L^*_{max}$ and the cusp – see Figure 6.1.1) and in the lightnesses of the original gamut's cusps being higher than those of the reproduction. Therefore, compressing lightness linearly (i.e. increasing the lightness of all colours) moves many – especially highly chromatic – colours into a region where the maximum achievable chroma is significantly lower than at the original colour's lightness (Figure 6.2.3a). This had a particularly marked effect on the reproduction of highly chromatic yellow colours which were reproduced as virtually achromatic using the LLIN, LCLIP and LNLIN algorithms – resulting in obvious artefacts.

Having established that simultaneous algorithms (which give more importance to chroma) perform better, it is important to note their main shortcoming, which is that they give worse results for the reproduction of dark colours and the achromatic axis than algorithms which have overall lightness compression. This was also confirmed by the results obtained for individual colour regions (i.e. the "shadow" region in MUS and the "grey" region in NAT – see Appendix D) . The reason for the worse performance of SLIN and CUSP in these regions is that they in effect use a piece–wise linear lightness compression, which more heavily compresses colours below the centre–of–gravity and does not compress those above it at all (Figure 6.2.3b). Clearly this results in a loss of detail for dark colours.

The following two sections look at the results obtained for individual test images and colour regions.

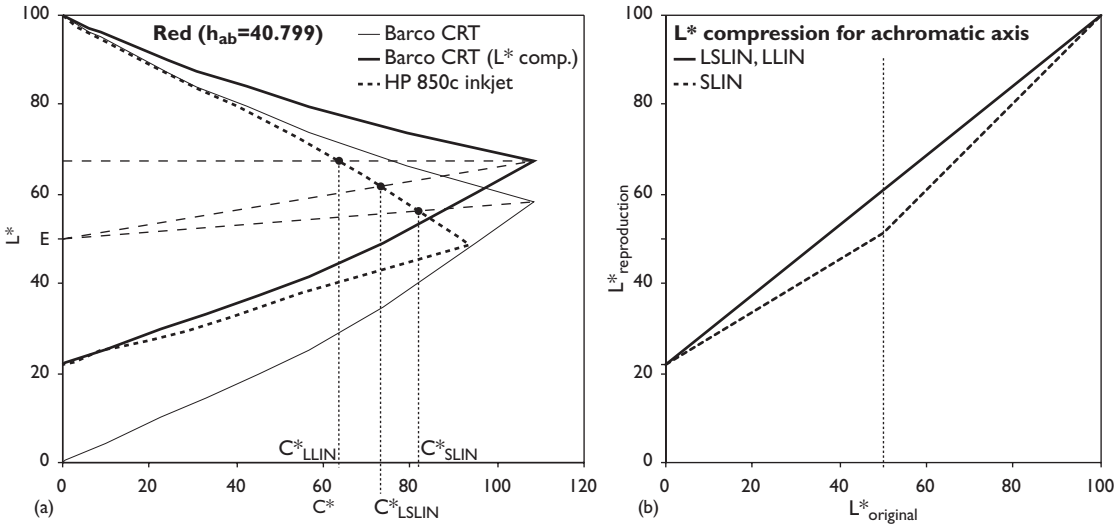


*Figure 6.2.3 Effect of using initial lightness compression demonstrated by comparing SLIN, LSLIN and LLIN: (a) chroma of gamut mapped colours, (b) effective lightness compression for achromatic axis.*

## 6.2.2 Results for Colour Regions

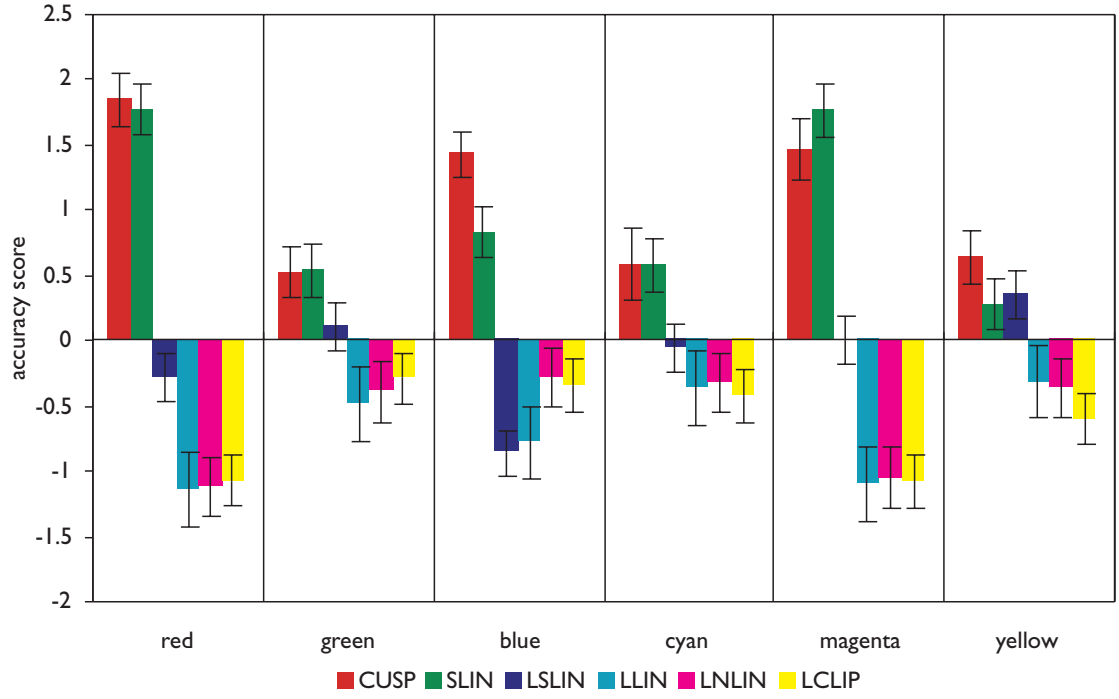


*Figure 6.2.4 Results for colour regions by colour region.*

The results presented here for the primary and secondary colours were obtained by combining the percentage matrices for regions from different test images having the same characteristic colour. As the number of images from which a colour region's overall score was obtained varied, the 95 *per cent* confidence intervals were also different. The blue region's results were obtained on the basis of all five images (N=60), those for red, green and yellow on the basis of four (N=48), those for magenta on the basis of three (N=36) and those of cyan on the basis of two images (N=24). Their sample–size dependent parameters can be found in Appendix D.

As can be seen from Figure 6.2.4, the results for individual algorithms are not significantly influenced by the colour region of colours transformed with them. However, it can be seen that the range of accuracy scores does depend on colour region, whereby the ranges for red, blue and magenta are significantly larger than those for green, cyan and yellow. This means that there are larger differences between the algorithms in the first set of regions than in the second and that the choice

of algorithm is therefore more critical for the former rather than the later set. One of the differences between these two sets is that the lightnesses of the original cusps in the first set are lower than those in the second set (see Figure 3.1.4) and are therefore more influenced by lightness compression (or its absence). In other words, the criterion which divides these two sets of colour regions is **relative gamut shape**.

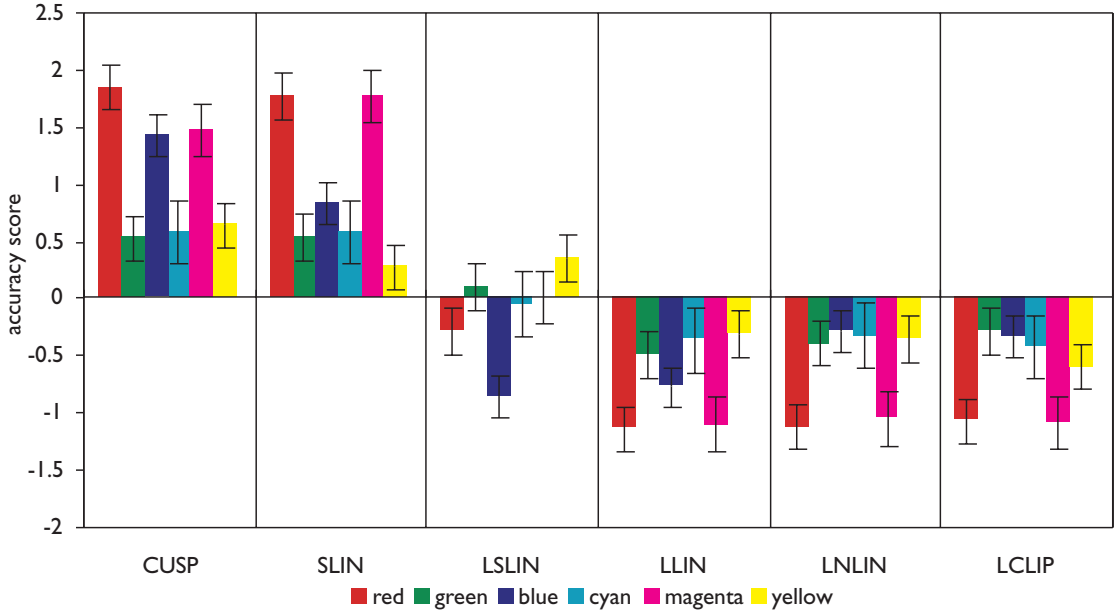


***Figure 6.2.5*** *Results for colour regions by GMA.*

Further, it is also useful to see the data from Figure 6.2.4 grouped by GMA, as this shows how variable a given algorithm is (Figure 6.2.5). It can again be seen that the performance of algorithms evaluated here is not influenced by colour region. Further, this view more clearly shows that the hybrid algorithm LSLIN is an exception to this whereby it performs well in some regions where sequential algorithms perform badly (e.g. yellow) and badly where simultaneous algorithms perform well (e.g. blue). For the results for individual colour regions for each test image see Appendix D.

### 6.2.3 Results for Individual Images

The results obtained for the performance of GMAs for individual images can be viewed in the same way as the pooled results for colour regions shown in the previous section. Note, that these are the results of judgements made for the overall accuracy of reproductions and that each of the accuracy scores dealt with here is based on a sample of 12 (for corresponding parameter values see Appendix D).

Overall, the results in Figure 6.2.6 show a strong correlation between the accuracy scores of GMAs for SKI, DOL and BUS, whereas the other two images have different overall patterns. This grouping is very similar to that of the images' **chroma ranges** (i.e. the areas of polygons determined by gamuts' cusps at a number of hue angles – for details see Section 5.2), which are in the region of 15,000 to 18,000 units for SKI, DOL and BUS and 6,000 and 2,000 for MUS and NAT respectively (for details see Appendix B). This indicates a link between the size of an image's gamut and the performance of GMAs in terms of its reproduction. However, it is of importance to note that some algorithms (in particular CUSP and SLIN) perform well for all of the five test images and also for the colour regions discussed in the previous section. The above data can also be grouped by GMA (Figure 6.2.7) and the resulting overall pattern is again similar to that for colour regions (with the exception of the NAT image).

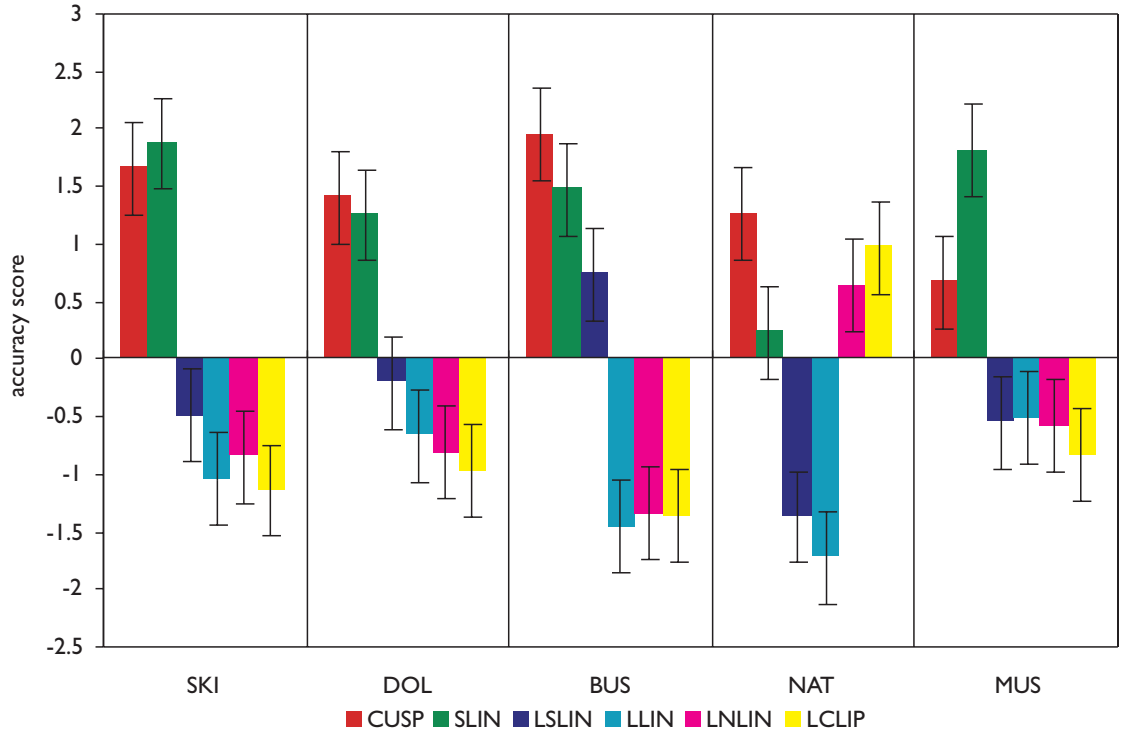


***Figure 6.2.6*** *Results for test images by image.*

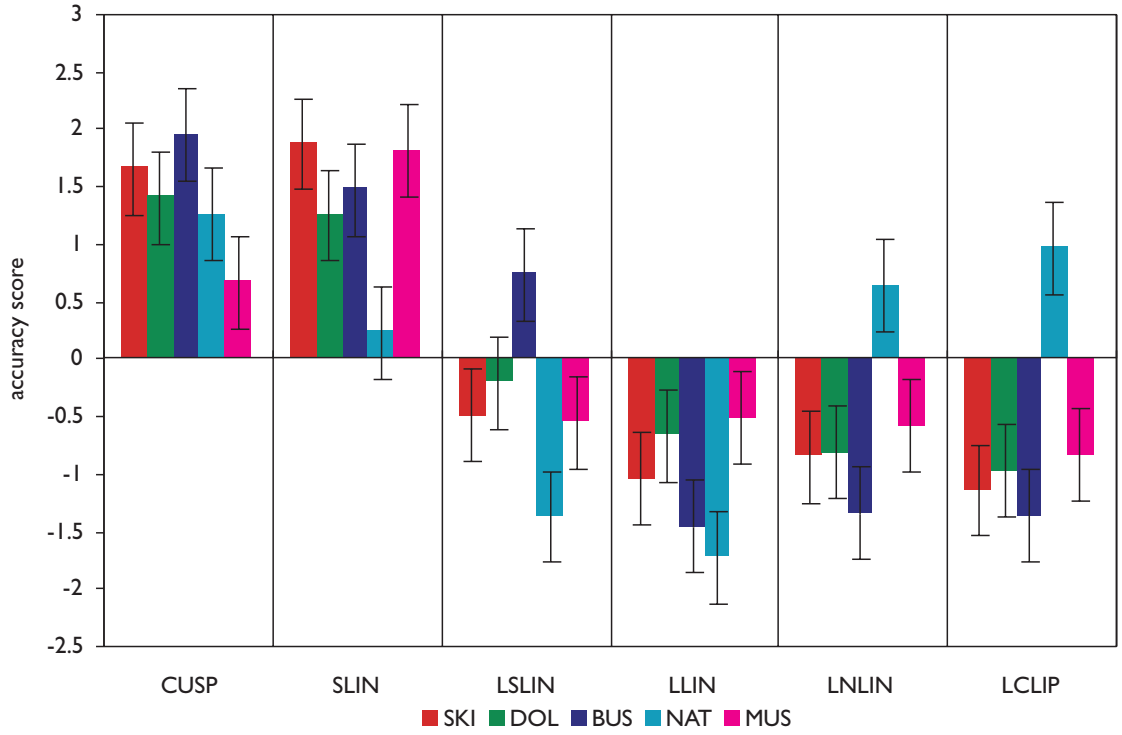


***Figure 6.2.7*** *Results for test images by GMA.*

## 6.3 Summary

Seven GMAs were evaluated in this experiment, whereby their characteristics are briefly summarised in Table 6.3.1.

| Mnemonic | Type | Description |
|---|---|---|
| **LCLIP** | sequential | L* compression + C* clipping |
| **LLIN** | sequential | L* compression + linear C* compression |
| **LNLIN** | sequential | L* compression + non-linear C* compression |
| **LSLIN** | hybrid | L* compression + SLIN |
| **SLIN** | simultaneous | Compression to L*=50 |
| **SLINLLAB** | simultaneous | SLIN in LLAB |
| **CUSP** | simultaneous | Compression to L* of cusp |

***Table 6.3.1*** *Overview of GMAs evaluated in Experiment 1.*

Of these, the group of simultaneous algorithms performed significantly better overall as well as for most colour regions and individual test images. An exception to this is their performance for the neutral axis and for dark colours, where sequential algorithms performed better. Hence, the aim for the development of new algorithms is to combine the behaviour of sequential and simultaneous methods on the basis of this experiment.

# Chapter 7

# Development of Second Generation Gamut Mapping Algorithms

*We operate with nothing but things which do not exist,*
*with lines, planes, bodies, atoms, divisible time, divisible space –*
*how should explanation even be possible when we first*
*make everything into an image, into our own image!*

*Friedrich Nietzsche*

## 6.1 Overview

The results of evaluating the initial GMAs in Experiment 1 showed that algorithms like SLIN and CUSP performed well for all but the dark and achromatic regions of colour space. Hence, the aim of the algorithms described in this chapter is to combine the behaviour of sequential algorithms for the neutral axis with the behaviour of simultaneous algorithms for the remainder of colour space. In other words:

> *the lightness of achromatic colours ought to be mapped linearly while the chroma of highly chromatic colours ought to be maintained to a greater extent than was the case with sequential algorithms.*

Three new algorithms (GCUSP, CLLIN and TRIA) were developed to this end. Further, a fourth GMA will also be described here (CARISMA), which is the second attempt of implementing the GMA proposed by Johnson *et al.* (CARISMA, 1992; Johnson *et al.*, 1998b). CARISMA, as described here, is in line with the original authors' intentions as well as being in line with the findings of Experiment 1.

Note, that all algorithms (except for CLLINLLAB) were again implemented in CIELAB and that their descriptions were previously published (Morovic and Luo, 1997b; Morovic and Luo, 1998a). Note also that all the following algorithms (except for CARISMA) keep hue unchanged.

## 6.2 GCUSP

The first algorithm developed on the basis of Experiment 1 (GCUSP) is intended as a direct implementation of its results – i.e. it gives more importance to chroma and compresses lightness linearly for achromatic colours.

GCUSP does this by first compressing the lightness of a colour in a chroma–dependent way using the following equation:

$$L^*_r = (1 - p_C)L^*_o + p_C\left(L^*_{r(\max)} - (L^*_{o(\max)} - L^*_o)\frac{(L^*_{r(\max)} - L^*_{r(\min)})}{(L^*_{o(\max)} - L^*_{o(\min)})}\right) \qquad (7.2.1)$$

where the subscripts *o* and *r* denote the original and reproduction gamuts respectively, *max* and *min* are the maximum and minimum lightnesses available in a given gamut and $p_C$ is the chroma–dependent weighting coefficient. This coefficient is calculated using the following formula, which resembles the Gaussian distribution (Figure 7.2.1):

$$p_C = 1 - \sqrt{\frac{C^{*3}}{C^{*3} + 5 \times 10^5}} \qquad (7.2.2)$$

where C* is the chroma of the colour for which lightness is to be compressed.

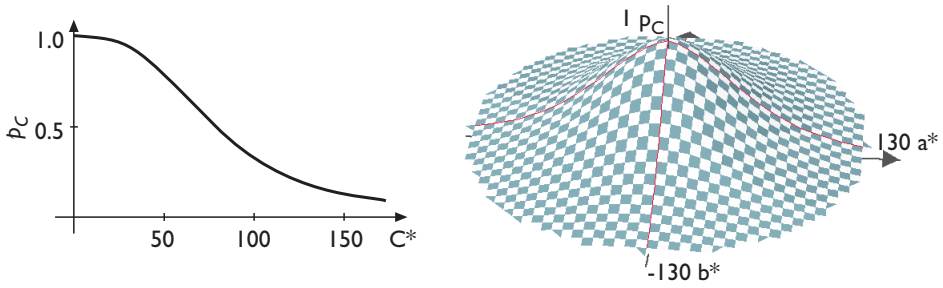


***Figure 7.2.1*** *Chroma–dependent Gaussian lightness compression.*

The use of Equation 7.2.1 for lightness compression means that full linear compression (as in Equation 6.1.1) is applied only to achromatic colours and that the lightness of high–chroma colours is

altered only to a lesser extent. Note that the choices of exponent (3) and constant term ($5\times10^5$) were made on the basis of trial–and–error with the aim of finding such a combination which gives full compression for a sufficiently large region around the achromatic axis, doesn't change highly chromatic colours too significantly and has a smooth gradual transition between these two regions. It was felt that other combinations of exponent and constant term gave too quick a transition between these two regions, that they did not apply full compression for a large enough region or that they compressed chromatic colours too heavily. Ideally, one would set up an experiment solely for determining a more optimal combination of these two parameters, which should indeed be done if this algorithm is found to perform well for a wide range of conditions. However, at this stage, such an experiment was not considered to be justified.

Lightness compression is then followed by simultaneous lightness and chroma mapping using the CUSP algorithm (Section 6.1.2). The chroma–dependent nature of lightness compression ensures that highly chromatic colours are altered only slightly by the initial lightness compression and are in effect reproduced as with the CUSP algorithm.

## 6.3 CLLIN

In essence this algorithm is the conceptual inverse of LLIN, as it first compresses chroma and then maps the lightness ranges (at a particular chroma) onto each other. This results in a linear lightness compression of the achromatic axis (as in LLIN) and the mapping of the original cusp onto the reproduction cusp, which in fact maintains as much of the original cusp's chroma as is possible (while maintaining hue).

If the original cusp has a larger chroma than the reproduction cusp, this algorithm first linearly compresses the chroma ranges depending on the two cusps at a particular hue angle. Chroma compression is then carried out using the following equation:

$$C_r^* = \begin{cases} C_o^* \dfrac{C_{cusp_r}^*}{C_{cusp_o}^*}; C_{cusp_o}^* \geq C_{cusp_r}^* \\ C_o^*; C_{cusp_o}^* < C_{cusp_r}^* \end{cases} \qquad (7.3.1)$$

This is followed by a linear mapping of lightness ranges along lines of constant chroma using the following formula:

$$L_r^* = L_{r2}^* + (L_o^* - L_{o2}^*) * \frac{(L_{r1}^* - L_{r2}^*)}{(L_{o1}^* - L_{o2}^*)} \qquad (7.3.2)$$

where the subscripts *o1* and *o2* denote the maxima and minima respectively of the original gamut and *r1* and *r2* denote those or the reproduction as shown in Figure 7.3.1.

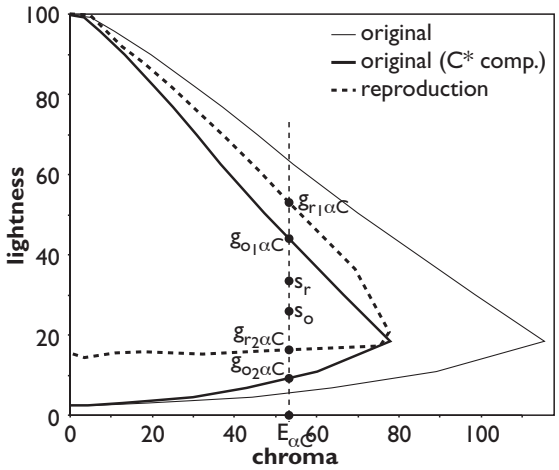

***Figure 7.3.1*** *Overview of CLLIN ($s_o$ is original colour after C* compression).*

Note, that the CLLIN algorithm was also implemented in the LLAB colour space, as described in the paper by Luo and Morovic (1996) and reproductions made with this algorithm will be referred to as **CLLINLLAB**.

## 6.4 TRIA

In addition to complying with the findings of the initial experiment, this algorithm also maintains a monotonic relationship between original and resulting reproduction colours and maps the original cusp onto the reproduction cusp. A monotonic relationship between original and reproduction is in fact not ensured by any other existing GMA.

To do this, both gamuts are defined using only three points for each hue angle – the minimum (A) and maximum (B) on the L* axis and the cusp (C). Hence, for a particular hue angle, each gamut can be expressed using the two vectors (**BA** and **BC**) and any point in the gamut can be described as a linear combination of these (i.e. $u$.**BA** + $v$.**BC**). The gamut mapping is carried out by first calculating the scalars $u$ and $v$ of a colour from the original gamut (i.e. from $\mathbf{B_oA_o}$ and $\mathbf{B_oC_o}$) and then calculating the corresponding L* and C* coordinates in the reproduction gamut using the vectors $\mathbf{B_rA_r}$ and $\mathbf{B_rC_r}$ (Figure 7.4.1). To do this, the vectors **b**, **c**, **d** and **e** and the point $o$ are defined as follows:

$$\mathbf{b} = \mathbf{B}_o\mathbf{A}_o; \mathbf{c} = \mathbf{B}_o\mathbf{C}_o$$
$$\mathbf{d} = \mathbf{B}_r\mathbf{A}_r; \mathbf{e} = \mathbf{B}_r\mathbf{C}_r$$

$\mathbf{b} = (b_1, b_2)$ where $b_1 = A_{oC^*} - B_{oC^*}$ and $b_2 = A_{oL^*} - B_{oL^*}$
(**c**, **d** and **e** analogously)
$s_o = [s_{o_{C^*}}, s_{o_{L^*}}]$

As $o = u \cdot \mathbf{b} + v \cdot \mathbf{c}$, $u$ and $v$ can be calculated as follows:

$$u = \frac{s_{o_{L^*}} \cdot c_1 - s_{o_{C^*}} \cdot c_2}{c_1 \cdot b_2 - c_2 \cdot b_1}$$
$$v = \frac{s_{o_{C^*}} \cdot b_2 - s_{o_{L^*}} \cdot b_1}{c_1 \cdot b_2 - c_2 \cdot b_1}$$

The reproduced colour can then be calculated as follows:

$$s_r = u \cdot \mathbf{d} + v \cdot \mathbf{e}$$

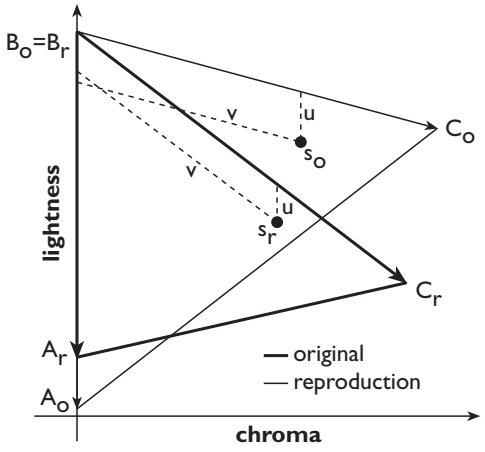

***Figure 7.4.1*** *Overview of triangular mapping.*

## 6.5 CARISMA

This algorithm is based on the work by Johnson *et al.* (CARISMA, 1992; Johnson *et al.*, 1998b) modelling the gamut mapping implicitly used by some scanner operators and it also satisfies the requirements established on the basis of the initial experiment. The algorithm described here differs somewhat from the original in the specification of the criteria used for deciding between individual mappings, the details of the third mapping method and the hue dependent interpolation. CARISMA, as implemented here, consists of the following steps:

(1) Map the white and black points of the two media onto each other and then scale lightness between them linearly (Equation 6.1.1).

(2) Determine the hue shift of the six primary and secondary colours between the two gamuts and translate the original medium's hues half–way towards the reproduction medium's hues (Figure 7.5.1). The purpose of this hue shift is to move colours into parts of colour space where there is more chroma available. Note, that the impact of this hue shift in terms of colour difference is chroma–dependent – colours of low chroma are affected only slightly and the effect is larger for more chromatic colours.

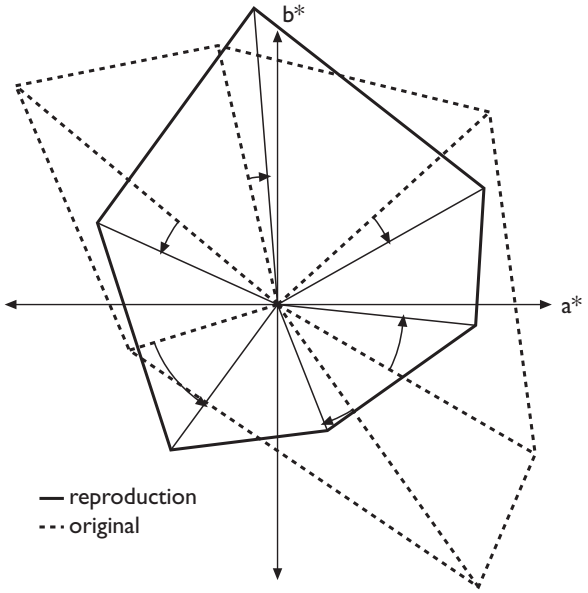


***Figure 7.5.1*** *Full hue–shifts at primary and secondary hues of the original medium.*

(3) Perform additional compression of L* and C* depending on the characteristics of the gamut boundaries of the two media at the hue angles of the primary and secondary colours of the original medium and their corresponding hue angles obtained after the hue shift on the reproduction medium:

(a) Define the cusp at each of these hue angles. After this there are three possible cases for which different mappings are used:

(b) **Case 1:** If the original gamut completely encloses the reproduction gamut and the intersection of the line going through the two cusps with the lightness axis is within the lightness range of the reproduction gamut then map towards $E_\alpha$ (Figure 7.5.2a). **Case 2:** If it is not within that range then map towards the point ($E_\alpha$) on the lightness axis, which has the same lightness as the reproduction gamut's cusp (Figure 7.5.2b). In both these cases compression along a given line is determined using Equation 6.1.3 whereby distances from $E_\alpha$ are used instead of chroma.

**Case 3:** Otherwise, if the reproduction gamut is not enclosed by the original gamut, map towards $E_\alpha$ on the C* axis, which has half the chroma of the reproduction cusp. Compression along a given line is determined using Equation 7.3.2 whereby distances from $E_\alpha$ are used instead of lightness (Figure 7.5.2c).

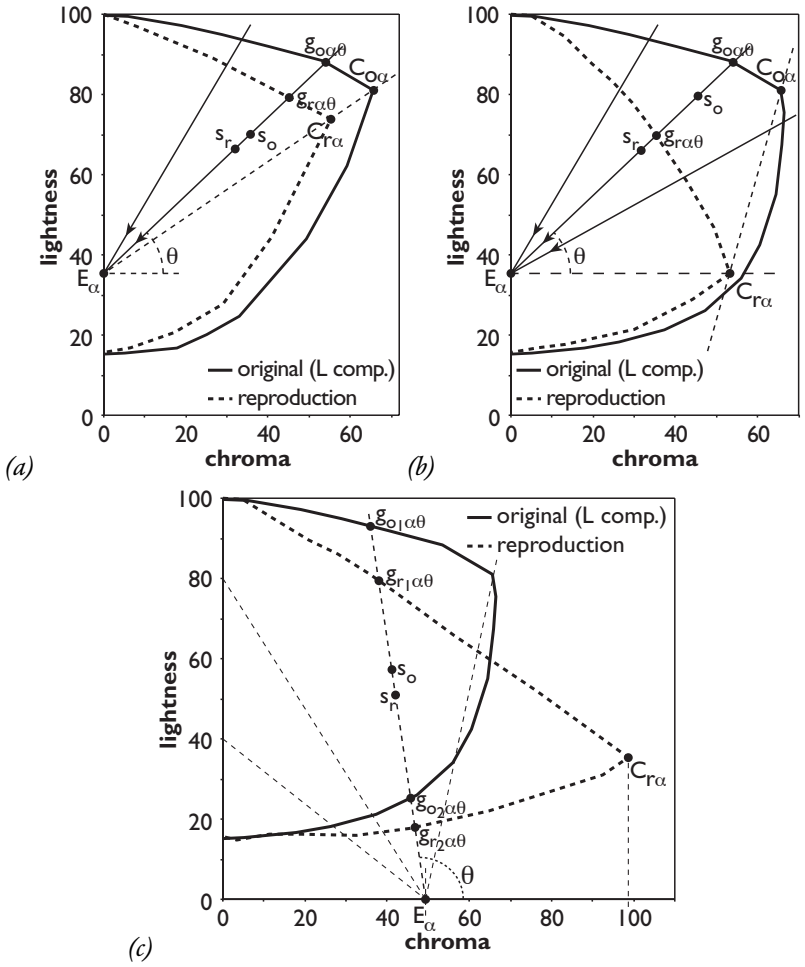


***Figure 7.5.2*** *Visual overview of the CARISMA algorithm.*

Then, for a given colour, calculate the gamut–mapped reproduction with the methods used for its neighbouring primary and secondary colours and interpolate between them using the angular differences between the given colour and the closest primary and secondary colour as weights. That is, if the two angular differences are $\Delta\alpha_1$ and $\Delta\alpha_2$ and the two corresponding gamut mapped lightnesses are $L^*_1$ and $L^*_2$ then the resulting L* is calculated using the following formula:

$$L^* = L^*_1 \frac{\Delta\alpha_2}{\Delta\alpha_1 + \Delta\alpha_2} + L^*_2 \frac{\Delta\alpha_1}{\Delta\alpha_1 + \Delta\alpha_2} \qquad (7.5.1)$$

whereby a* and b* are interpolated analogously.

## 6.6 Summary

The GMAs presented in this chapter were developed (or re–interpreted) on the basis of Experiment 1 whereby each of these methods uses a linear lightness mapping for the achromatic axis and maintains more of the chroma of highly chromatic colours. The performance of these GMAs was evaluated in Experiment 2, which is described in the following chapter.

Chapter 8

# Experiment 2: Evaluation of Second Generation Gamut Mapping Algorithms

*Statistics are no substitute for judgement.*
*Henry Clay*

## 8.1 Overview of Experiment

The accuracy of algorithms developed on the basis of Experiment 1 (Chapter 7) was again evaluated using the pair comparison method (Chapter 5). The reproductions made with the second generation algorithms (GCUSP, CLLIN, CLLINLLAB, TRIA and CARISMA) were compared with reproductions made using some of the initial GMAs (SLIN and LLIN) and the default reproductions obtained by sending the original monitor RGB values directly to the printer via its driver software (these are referred to by the mnemonic **DEF**).

The experiment was carried out by 13 observers with normal colour vision of which five were female and eight male whereby their ages were between 23 and 39 years and all but one of the observers were either staff or students at the Colour & Imaging Institute. Note, that the contents of this chapter was partly published before (Morovic and Luo, 1997b).

## 8.2 Overall Results

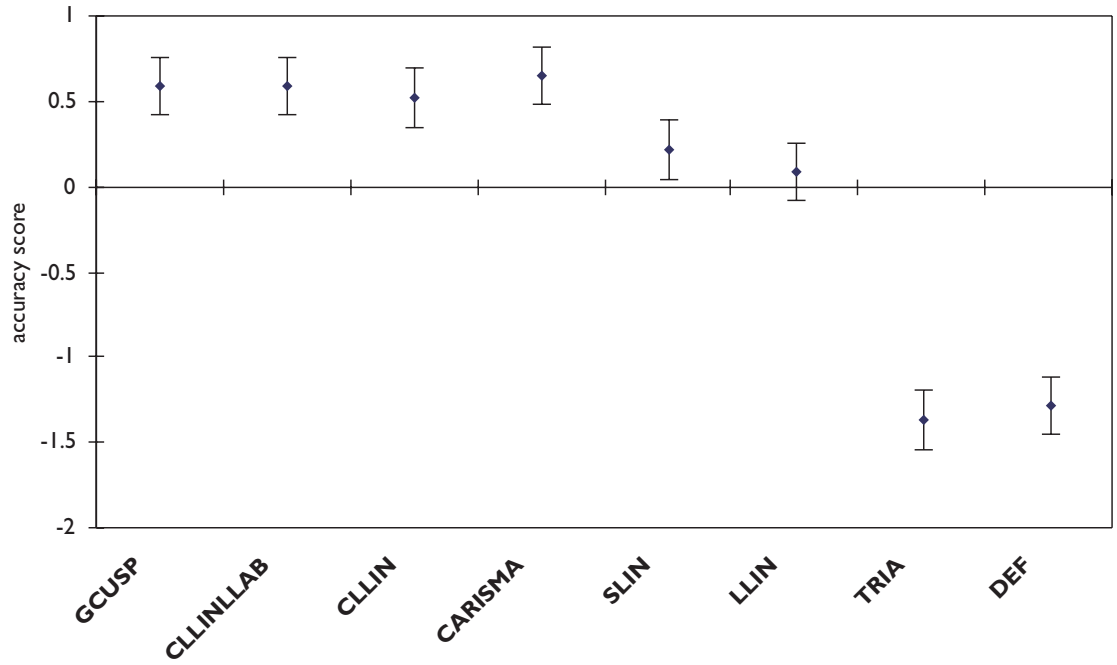


***Figure 8.2.1*** *Overall results of Experiment 2.*

The accuracy scores shown in Figure 8.2.1 are the average scores of the overall judgements made for the five test images and were obtained from the results for individual images in the same way as in Experiment 1 (Section 6.2.1). For sample–size dependent parameters in the calculation of accuracy scores in this experiment see Appendix E.

Again the reproductions made with the algorithm implemented in two colour spaces (CLLIN in CIELAB and CLLINLLAB in LLAB) were not different from each other at the 95 *per cent* significance level. Hence, the reproductions made with CLLINLLAB will be excluded from further analysis, as this would have meant that more weight would have been given to the CLLIN algorithm (this is the same reason as was used for excluding SLINLLAB from the analysis of Experiment 1). Excluding CLLINLLAB from accuracy score calculation results in the following results (Figure 8.2.2).

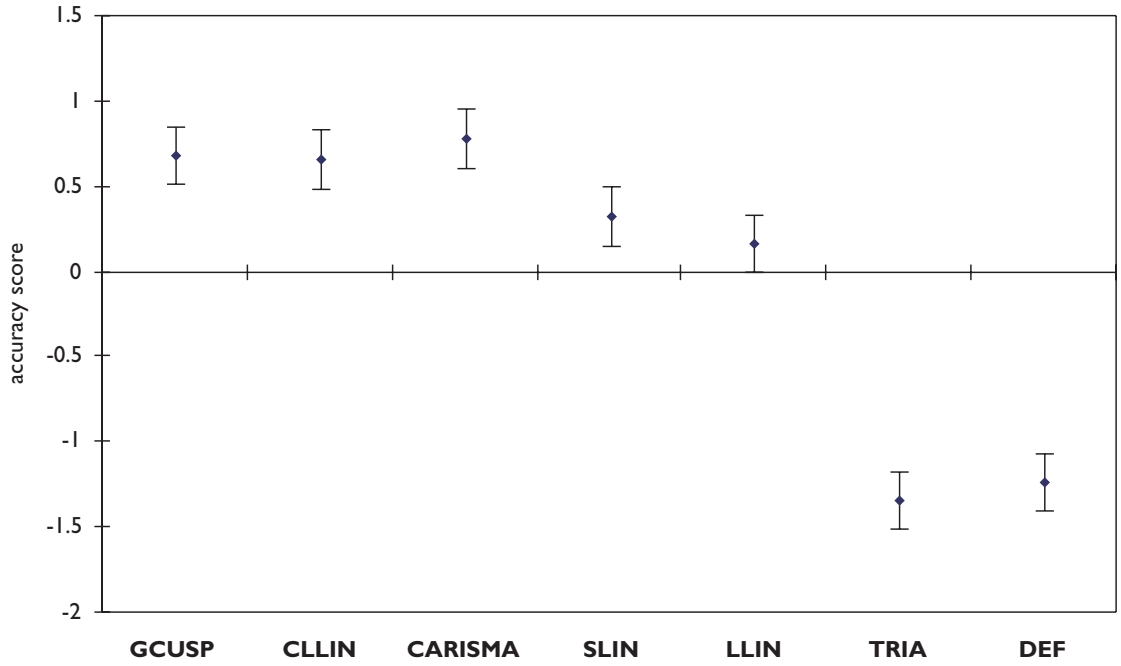


***Figure 8.2.2*** *Overall results of algorithms implemented in CIELAB and evaluated in Experiment 2.*

From these results it can be seen that three of the four new algorithms (GCUSP, CARISMA and CLLIN) performed significantly better than the algorithms tested in the previous experiment. Further, the algorithms form three distinctive groups, which are significantly different from each other and within which the difference between algorithms is not significant. The top group contains the three successful new algorithms, this is followed by the SLIN and LLIN algorithms from Experiment 1 and lastly by TRIA and DEF. As SLIN was in the top group of algorithms in Experiment 1, the algorithms which performed better than SLIN would also very likely have performed better that the other initial algorithms. The inclusion of LLIN was done so as to represent the worst results from Experiment 1 and any algorithm which has a lower score that LLIN would probably have performed worse than the algorithms from Experiment 1.

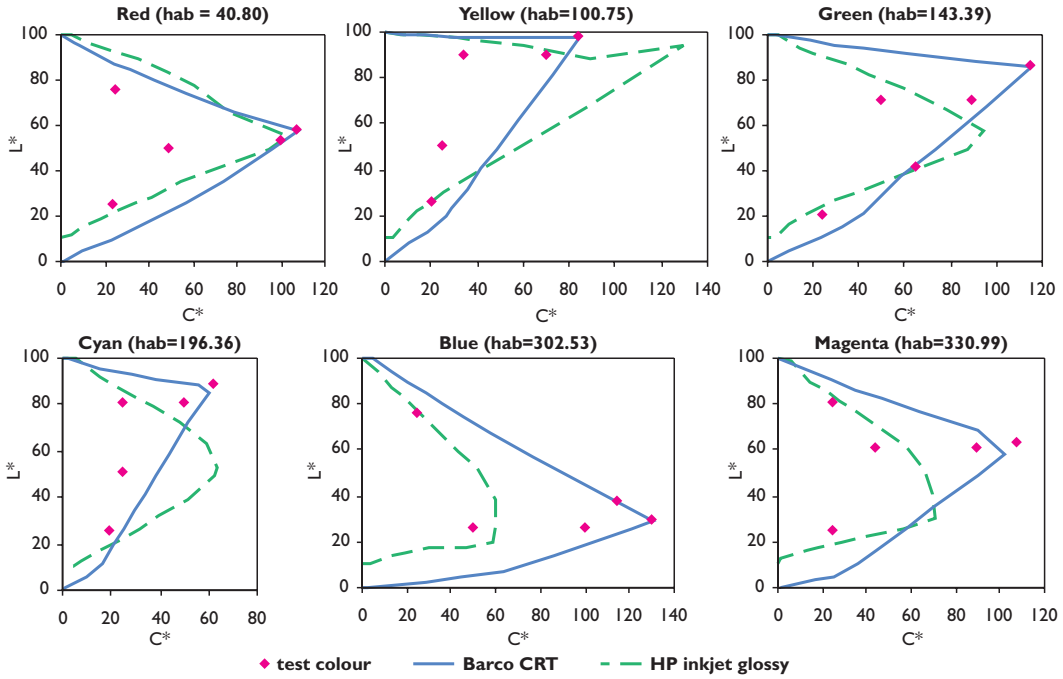


***Figure 8.2.3*** *LC coordinates of 30 test colours at CRT's primary and secondary hues.*

The nature of changes made by the individual algorithms was investigated so as to better understand the reasons for the above results. To do this, 30 colours were chosen (Figure 8.2.3),

gamut–mapped and their original and gamut–mapped *LCh* values were compared. Note, that the gamut–mapped values are not the *LCh* values of the reproduced colours, but are the values which would be transformed via the printing medium's characterisation model and then printed. That is, they do not include characterisation and printer variation errors. As gamut–mapped values were not available for the reproductions made with DEF, that method is not considered here.

The above set of 30 colours was chosen so that there were five colours for each of the primary and secondary hues of the CRT whereby each of these sets of five colours included the cusp at the corresponding hue angle. Differences between original and gamut–mapped colours were expressed in terms of median $\Delta E_{ab}$, median $|\Delta L^*|$, median $|\Delta C^*|$, the median $\Delta(C/L)$ which represents changes in saturation and the median $|\Delta C^*|/|\Delta L^*|$ ratio (Table 8.2.1 – for complete data see Appendix E). The last of these attributes was chosen, as it expresses the weight given to lightness *versus* chroma in a given GMA and the median was used as a measure of central tendency instead of the mean as the distributions of these values were skewed.

| GMA | median $\Delta E_{ab}$ | median $\|\Delta L^*\|$ | median $\|\Delta C^*\|$ | $\Delta(C/L)$ | $\|\Delta C^*\|/\|\Delta L^*\|$ |
|---|---|---|---|---|---|
| **GCUSP** | 12.22 | 4.79 | 8.10 | -0.18 | 1.69 |
| **CLLIN** | 15.59 | 7.37 | 9.66 | -0.23 | 1.31 |
| **CARISMA** | 12.45 | 6.59 | 3.77 | -0.05 | 0.57 |
| **SLIN** | 11.02 | 5.24 | 7.60 | -0.14 | 1.45 |
| **LLIN** | 11.97 | 5.30 | 11.69 | -0.29 | 2.20 |
| **TRIA** | 20.05 | 6.63 | 14.84 | -0.10 | 2.24 |

***Table 8.2.1*** *Median changes made by GMAs in Experiment 2.*

First of all it needs to be noted that the data in Table 8.2.1 does not follow the grouping of algorithms in terms of accuracy scores – in particular, there is a difference in the attributes of SLIN and LLIN, which is not paralleled in the accuracy scores. The differences between the above data and the overall experimental results might well be due to the small sample–size of the former. Nonetheless, the above data is useful for understanding the performance of the algorithms it describes.

It is of interest to note that the median $|\Delta C^*|/|\Delta L^*|$ ratio seems to correlate well with the ranking of the algorithms – the Pearson correlation coefficient being 0.85. This suggests that, within the set of algorithms considered here, those algorithms which in relative terms maintain more chroma (at the expense of lightness) are judged to be more accurate. Of interest is also the correlation between median $\Delta E_{ab}$ and the accuracy score, which is -0.78 and suggests that the algorithms which make the smallest change (within the set of algorithms considered here) also give the most accurate reproductions.

It is also of interest to note that the algorithm (CARISMA) which made the smallest $\Delta(C/L)$ saturation change is also the most accurate algorithm and that this indeed agrees with what was found in other studies (e.g. Montag and Fairchild, 1997). However, it can also be seen that maintaining saturation is not a sufficient criterion on its own to ensure accuracy as the TRIA algorithm makes the second–smallest change but performs worst. Overall, the correlation between saturation changes and accuracy scores (or their ranks), which is –0.18 and –0.30 respectively, can be considered to be fairly weak.

Further, the data from Table 8.2.1 also gives a possible explanation of the TRIA algorithm's failure, which could be due to it making changes which on average are about twice as large as those made by most other algorithms. Note, however, that it is not the algorithm with the smallest overall change (SLIN) which performs best – for if that were the case then the best gamut mapping algorithm would be gamut clipping which maps out–of–gamut colours onto the nearest colour on the reproduction gamut's boundary. Instead of this minimisation approach, TRIA tries to maintain relative characteristics of colours within corresponding gamuts and have a monotonic relationship

between original and reproduced colours. However, this doesn't work either, as it is done at the expense of unacceptably large absolute changes to the gamut–mapped colours. This would suggest that the solution is somewhere in–between minimisation and the maintenance of relative characteristics, which is indeed what happens in the case of GCUSP, CARISMA and CLLIN.

To put the values in Table 8.2.1, which show differences between original and gamut mapped colours, into context, it is useful also to know the differences between the individual GMAs (Table 8.2.2). Further, it is also useful to compare these values with the accuracy of the characterisation model used, which had a median error of prediction of 5 ΔE and a maximum error of 13 ΔE. It can be seen that some GMAs, which had differences smaller than the characterisation model's accuracy (e.g. GCUSP and SLIN) were judged to be significantly different from each other. This is probably due to characterisation errors being randomly distributed, whereas differences between GMAs being systematic and due to systematic differences being noticeable even after random errors in their reproduction.

| | GCUSP | CLLIN | CARISMA | SLIN | LLIN | TRIA |
|---|---|---|---|---|---|---|
| **TRIA** | 8.57 | 9.64 | 9.52 | 9.58 | 12.51 | |
| **LLIN** | 6.74 | 7.19 | 8.57 | 6.54 | | |
| **SLIN** | 3.04 | 5.55 | 5.47 | | | |
| **CARISMA** | 6.23 | 6.25 | | | | |
| **CLLIN** | 5.09 | | | | | |
| **GCUSP** | | | | | | |

***Table 8.2.2*** *Median ΔE differences between individual GMAs.*

Another important characteristic of GMAs is the variance of their performance for different image contents, which should be as small as possible for universal gamut mapping algorithms. The variance of the accuracy scores of the seven algorithms considered here was therefore calculated on the basis of all judgements made for them (i.e. the images overall and all the colour regions within each image).

| | GCUSP | CLLIN | CARISMA | SLIN | LLIN | TRIA | DEF |
|---|---|---|---|---|---|---|---|
| **variance** | 0.359 | 0.623 | 0.405 | 0.537 | 0.749 | 0.365 | 0.877 |

***Table 8.2.3*** *Variances of accuracy scores.*

It can be seen from Table 8.2.3 that the GCUSP, TRIA and CARISMA algorithms perform more stably than the other algorithms. In the case of TRIA, this means a consistently low accuracy, whereas the accuracy of GCUSP and CARISMA is consistently high.

The following sections will now look at the results obtained for individual colour regions and test images.

## 8.3 Results for Colour Regions

Figure 8.3.1 shows the overall results for the primary and secondary colours obtained in the same way as in Experiment 1 (Section 6.2.2). For the sample–sizes and 95 *per cent* confidence intervals see Appendix E.

It can be seen from Figures 8.3.1 and 8.3.2 that the results of this experiment are less homogeneous than the results of Experiment 1. Nonetheless, it can be seen that GCUSP and CARISMA perform well for all colour regions (with the exception of CARISMA for green) whereas TRIA and DEF perform consistently badly and the performance of CLLIN and LLIN (and to a lesser extent SLIN) is strongly influenced by colour region.

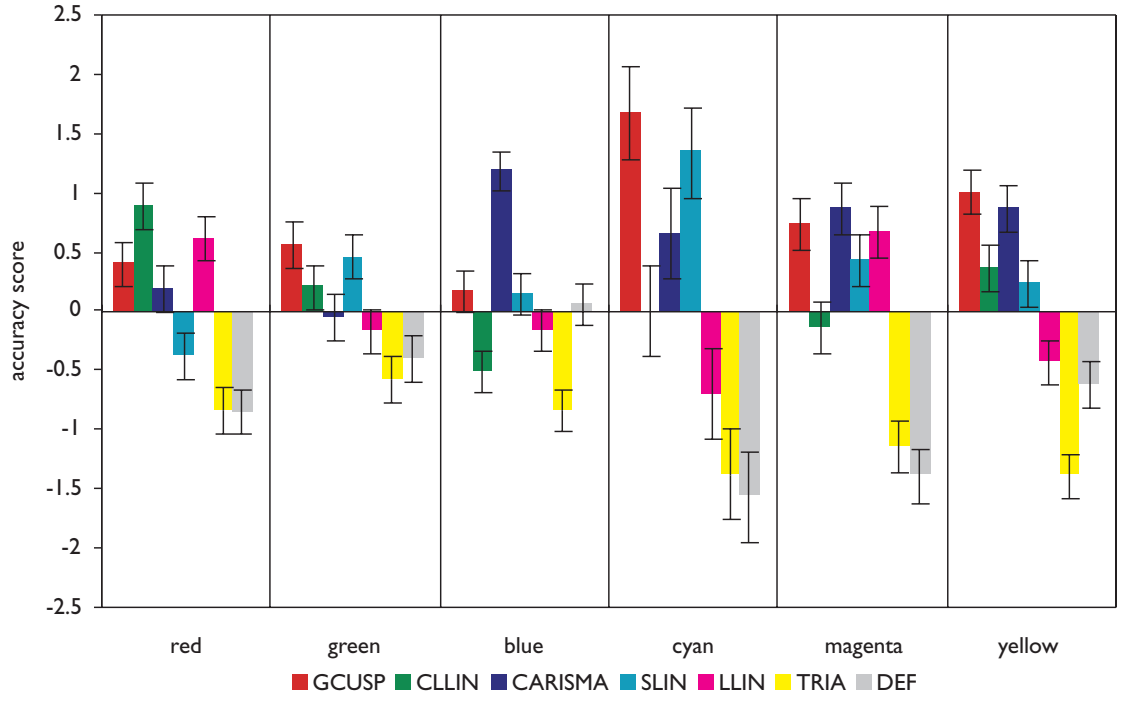


***Figure 8.3.1*** *Results for colour regions by colour region.*

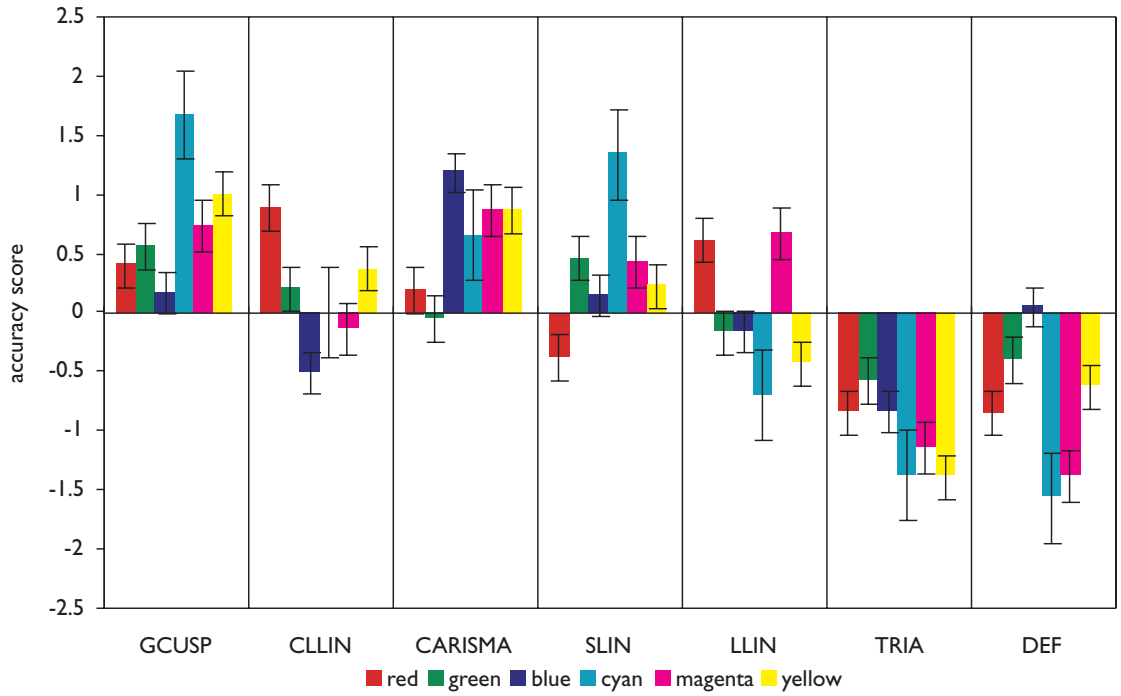


***Figure 8.3.2*** *Results for colour regions by GMA.*

This indicates that, out of the algorithms dealt with here, GCUSP and CARISMA are closest to the aim of universal applicability. Even though CLLIN has good overall accuracy scores, it was shown in the previous section that its performance varies significantly with respect to colour region and this would make it an unreliable choice.

As far as comparisons with Experiment 1 are concerned, it also needs to be noted that they can only be made in terms of relative differences between pairs of algorithms which were evaluated in both experiments (i.e. only SLIN and LLIN). Comparing the absolute scores of algorithms evaluated in both Experiment 1 and Experiment 2 is not meaningful as the score for a given GMA is its distance from the mean of the set of GMAs with which it was compared and as the distance between the means of the two experiments is not known. However, as already mentioned, it is valid

to compare the performance of SLIN and LLIN in the different experiments. Here it can be noted that the results are similar (in relative terms) except for the red colour region, which is probably due to the difference between the two experimental conditions in terms of relative gamut boundaries at this hue angle. In Experiment 2 the red gamut boundaries for the original and reproduction are significantly more similar than they were for Experiment 1 and as LLIN seems to be better suited for overcoming small gamut differences, it now performs better for colours in this region.

## 8.4 Results for Individual Images

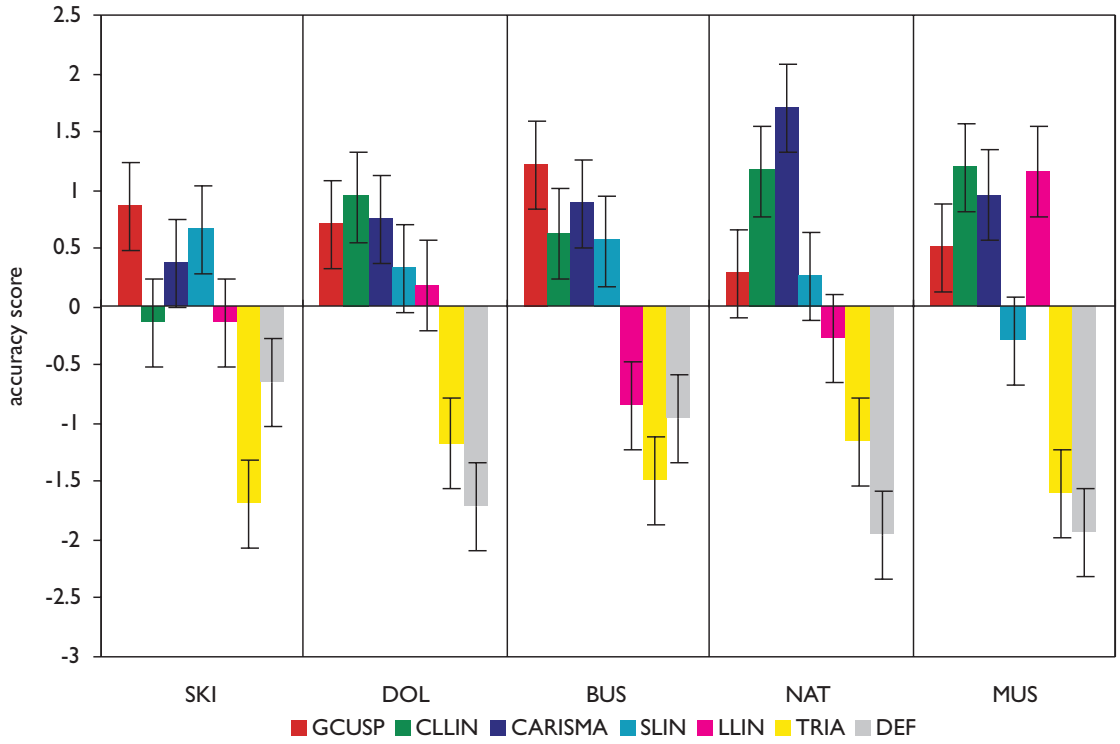


***Figure 8.4.1*** *Results for test images by image.*

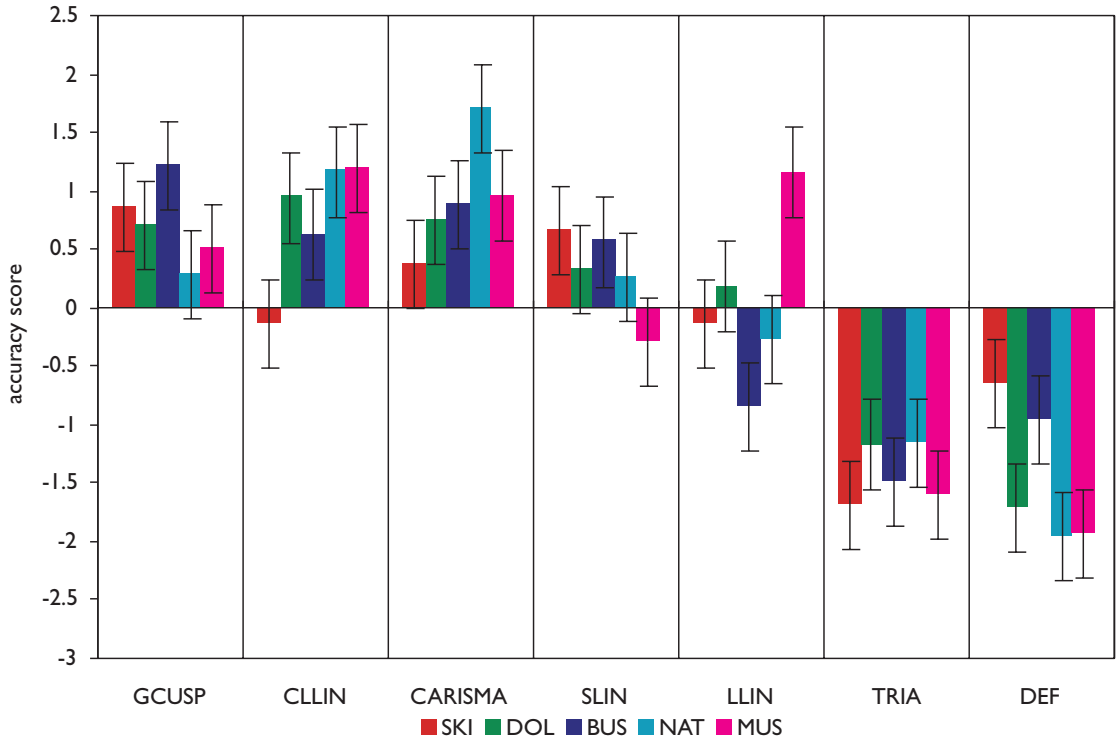


***Figure 8.4.2*** *Results for test images by GMA.*

The results obtained for individual images again show a similar trend to the results from the colour regions, which is not surprising as the colour regions looked at in the previous section can be considered to be images themselves. The good performance of GCUSP and CARISMA, the worse performance of TRIA and DEF and the variable nature of the performance of the other algorithms can be seen again (though CLLIN is less influenced by the test images than it was by colour regions).

Comparing these results with results from Experiment 1, it can be seen that LLIN performs better for the DOL and MUS images than it did in the previous experiment. This could again be due to the same reason, which makes LLIN perform better for red colours, as it is these which are dominant both in the DOL and MUS images.

The data shown in Figures 8.4.1 and 8.4.2 can also be looked at in terms of the ranking of significantly different groups. As the algorithms cannot always be divided into groups for which each member of one group is significantly different from the members of all other groups, the grouping is done by first selecting the top algorithm and including in its group all algorithms which are not different from it. The second group is then formed by that remaining algorithm which has the highest score and the algorithms, which are not significantly different from it and which are not in group one (the other groups are then formed analogously).

The ranking of algorithm groups formed in the above way is shown in Table 8.4.2. It is particularly encouraging to see that the CARISMA algorithm is always in the top two groups (whereby for the SKI image it is not significantly different from the CLLIN algorithm, which is in the top group). Further, it can be seen that the GCUSP algorithm is in the top group for images which have large chroma ranges (see Appendix B for the chroma ranges of test images).

| | BUS | DOL | MUS | NAT | SKI | mean |
|---|---|---|---|---|---|---|
| **GCUSP** | 1 | 1 | 2 | 3 | 1 | **1.6** |
| **CLLIN** | 2 | 1 | 1 | 2 | 3 | **1.8** |
| **CARISMA** | 1 | 1 | 1 | 1 | 2 | **1.2** |
| **SLIN** | 2 | 2 | 3 | 3 | 1 | **2.2** |
| **LLIN** | 3 | 2 | 1 | 4 | 3 | **2.6** |
| **TRIA** | 4 | 3 | 4 | 5 | 5 | **4.2** |
| **DEF** | 3 | 3 | 4 | 6 | 4 | **4.0** |

***Table 8.4.1*** *Ranking of GMA groups for five test images.*

## 8.5 Summary

Eight GMAs, which were described in Chapter 7 and whose characteristics are summarised in Table 8.5.1, were evaluated in this experiment. The overall results of the experiment were presented alongside the results for individual colour regions and test images. An interpretation of the results was then done on the basis of investigating the nature of changes made to colours by individual algorithms, the variance of the algorithms' accuracy scores, the chroma ranges of the test images and the ranking of significantly–different GMA groups.

| Mnemonic | Description |
|---|---|
| **GCUSP** | C* dependent L* compression + CUSP |
| **CLLIN** | C* range compression + L* compression at fixed C* |
| **CARISMA** | L* compression + hue shift +<br>relative, gamut shape dependent mapping |
| **SLIN** | Compression to L*=50 |
| **LLIN** | L* compression + linear C* compression |
| **TRIA** | Triangular monotonic cusp–to–cusp mapping |
| **DEF** | Monitor RGB values sent to printer using its own driver software |

***Table 8.5.1*** *Overview of GMAs evaluated in Experiment 2.*

The results discussed in this chapter clearly show that the performance of CARISMA and GCUSP makes them good candidates for being accepted as universal gamut mapping algorithms, as their accuracy scores are consistently high for the images and colour regions looked at in this experiment.

Chapter 9

# Development of Third Generation Gamut Mapping Algorithms

*"Would you tell me, please, which way I ought to go from here?"*
*"That depends a good deal on where you want to get to," said the Cat.*
*Lewis Carroll (Alice in Wonderland)*

# 9.1 GMA Development on the Basis of Colour Region Performance

To develop a new algorithm, which would give good results in all regions of colour space, the results of Experiment 2 were looked at in terms of the ranking of significantly–different GMA groups for individual colour regions. This was done to see what the smallest number of simple mapping methods would be, which (when combined) would give the best results in each colour region. The colour–region accuracy scores of GMAs from Experiment 2 were again grouped in the same way as was done for the overall accuracy scores for individual images in Section 8.4.

For each test image, Table 9.1.1 lists the algorithms in the top or top two groups for a particular colour region whereby the algorithms in the rightmost column of the table (labelled 'best') are those which had the highest score for a particular colour region. This score was obtained by giving each GMA one point for being in the top group and half a point for being in the second group.

| Colour | SKI | BUS | DOL | MUS | NAT | Best |
|---|---|---|---|---|---|---|
| **red** | llin, cllin | gcusp, cllin, carisma | llin, cllin, gcusp | cllin, llin | n/a | **CLLIN** |
| **skin** | n/a | n/a | n/a | llin, cllin | n/a | **LLIN, CLLIN** |
| **brown** | n/a | n/a | n/a | llin, cllin | n/a | **LLIN, CLLIN** |
| **yellow** | gcusp, carisma | gcusp | gcusp, carisma | carisma, cllin | n/a | **GCUSP, CARISMA** |
| **green** | slin, gcusp | gcusp, cllin | slin, cllin, gcusp | n/a | carisma, tria | **GCUSP** |
| **cyan** | n/a | 1 gcusp<br>2 slin | n/a | n/a | n/a | **GCUSP** |
| **blue** | carisma | carisma | carisma | slin, carisma | carisma | **CARISMA** |
| **magenta** | 1 llin<br>2 gcusp, carisma, slin | carisma, gcusp | carisma, gcusp, llin | n/a | n/a | **CARISMA, GCUSP** |

***Table 9.1.1*** *Algorithms in top groups for individual colour regions in the SKI, BUS, DOL, MUS and NAT images of the second experiment.*

The above data suggests that it is possible to achieve the top result for each colour region by using only the following three algorithms: GCUSP, CARISMA and CLLIN – i.e. the algorithms which had the best overall performance in Experiment 2. In addition, the same CARISMA mapping method (Case 2) – compression to cusp after linear lightness mapping (**LCUSP**) – was used for both the blue and magenta regions and Case 3 was used for the yellow region. It can be seen that the three colour regions which have similar hue angles: red, skin and brown are best reproduced by the same algorithm – CLLIN.

Further, it is interesting to note that the hues for which the same algorithms performed best have similar relationships between the gamut shapes of the original and reproduction gamuts – CLLIN performed well when the difference between the two gamuts was small, LCUSP when the reproduction gamut was enclosed in the original gamut and GCUSP when there was only a partial overlap between the gamuts. Hence, an algorithm similar in structure to CARISMA could provide the most consistently accurate results for the five test images used here. This could be done by using the methods shown in Figure 9.1.1 for the primary and secondary hues.

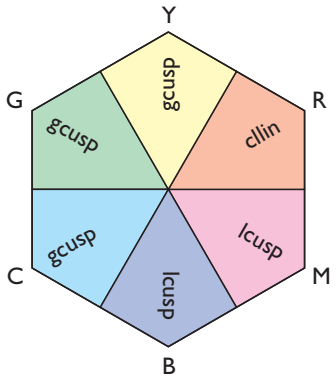


***Figure 9.1.1*** *Combination of most accurate algorithms for primary and secondary hues.*

Clearly, this is not the only possible combination, as CARISMA could have been used for the yellow region and GCUSP for magenta. However, the advantage of the above choice is that a particular method is always applied to a contiguous region which means that the areas in which mapping methods are interpolated between is minimised. In general, it is of importance to have as few transitional regions as possible as the influence of the neighbouring algorithm in a CARISMA–like scenario can in some cases be negative (e.g. if one were to use LLIN for the red primary hue angle, it would have a negative impact on yellow even though its effect would be weighted by angular difference)

The above analysis was the basis for the development of two algorithms – the first one (**UniGMA**) is an algorithm which is similar in structure to CARISMA and which combines the three algorithms from the previous set which performed best in different colour regions. The second algorithm (**LCUSPH**) is a simplification of UniGMA (as well as CARISMA), which uses a single mapping method for the entire colour space. The choice of CARISMA Case 2 was influenced by it being the method which performed well in a region of colour space (blue) where all other algorithms gave significantly worse results.

Note, that these algorithms were implemented in CIECAM97s (Luo and Hunt, 1998) whereby both media were assumed to have the same viewing conditions (which is indeed what was attempted in the experimental setup). The predictors for lightness ($J$), chroma ($C$) and hue ($h$) were then used as the cylindrical coordinates of the colour space in which gamut mapping was carried out.

For computational convenience, wherever $a^*$ and $b^*$ were used in the CIELAB implementation of GMAs, $a'$ and $b'$ were used and were calculated as follows:

$$a' = C^*\cos(h) \tag{9.1.1}$$

$$b' = C^*\sin(h) \tag{9.1.2}$$

This means that the orthogonal coordinates ($a'$ and $b'$) had the same relationship to $C$ and $h$ as $a^*$ and $b^*$ had to $C^*$ and $h_{ab}$ in CIELAB. Note, that these coordinates are not the redness–greenness and yellowness–blueness coordinates of CIECAM97s and that they are not meant to be interpreted in any other way than as the orthogonal equivalents of the cylindrical $C$ and $h$ coordinates.

The reason for using CIECAM97s for the implementation of GMAs for Experiment 3 was to test whether the mapping methods which performed well under CIELAB will also perform well in the recently recommended CIE colour appearance model. Further, the change of colour space is of use for understanding whether it is the relative shape of gamuts, which is the decisive factor in gamut mapping since this is assumed by one of the most successful algorithms so far – CARISMA and by one of the new third–generation algorithms – UniGMA.

## 9.2 UniGMA

This algorithm is a direct implementation of the analysis described in the previous section and as its structure is similar to that of CARISMA, only the differences will be described here. First of all, there is no overall lightness compression. Secondly, the mappings for the primary and secondary hues are different and are decided using the following rules:

1 If the cusps of the two gamuts are similar (e.g. if their difference is less than 12 ΔE), use the CLLIN algorithm (Section 7.3). Note, that the value of 12 ΔE was chosen heuristically and that a better way of deciding whether the two gamuts are similar for the purposes of this algorithm might need to be devised.

   Further note, that as there is no colour difference formula defined for CIECAM97s, the Euclidean distance of two colours was used as their colour difference (just as is the case for $\Delta E_{ab}$ in CIELAB). Hence, colour difference in CIECAM97s ($\Delta E_{97s}$) was calculated as follows:

$$\Delta E_{97s} = \sqrt{\Delta J^2 + \Delta a'^2 + \Delta b'^2} \qquad (9.2.1)$$

   Note again, that there is no experimental justification for this colour difference formula and that it was defined only for want of any colour difference formula being available in CIECAM97s.

2 Else if the original gamut completely encloses the reproduction gamut, then use uniform linear lightness compression followed by compression towards the lightness of the cusp on the lightness axis.

3 Otherwise use the GCUSP algorithm.

The mapping for a given colour is then determined in the same way as in CARISMA and the same hue shift is used as well.

## 9.3 LCUSPH

As already mentioned, this is a simplified version of both UniGMA and CARISMA which uses the same mapping throughout colour space. It first compresses lightness linearly and then maps colours towards the lightness of the cusp on the lightness axis. Finally, this algorithm also has the same hue shift as CARISMA. LCUSPH was chosen for evaluation in Experiment 3, as it performed particularly well where other algorithms failed and as it is significantly simpler than the two complex algorithms which use it as one of their mapping methods.

## 9.4 Summary

The results for individual colour regions in Experiment 2 were used for specifying an algorithm, which for each colour region uses that algorithm which performed best for it. This demonstrates a way of effectively utilising the information obtained from the experimental method used in this study. How successful these methods are in comparison to previous algorithms will be investigated in Experiment 3, which will be described in the following chapter.

Chapter 10

# Experiment 3: Evaluation of Third Generation Gamut Mapping Algorithms

*'Where shall I begin, please your Majesty?' he asked.*
*'Begin at the beginning,' the King said, gravely*
*'and go on till you come to the end: then stop.'*

*Lewis Carroll (Alice in Wonderland)*

# 10.1 Overview of Experiment 3

In Experiment 3 the CARISMA, GCUSP, UniGMA, LCUSPH and LLIN algorithms were evaluated by ten observers with normal colour vision. Of these observers, who were all staff or students at the Colour and Imaging Institute, four were female, six were male and they were all aged between 23 and 40 years. The following four aims were set for this experiment:

1 to evaluate the new, third–generation **UniGMA** and **LCUSPH** algorithms,

2 to investigate the effect of changing the gamut mapping colour space from CIELAB to **CIECAM97s** on CARISMA, GCUSP and LLIN,

3 to obtain additional information about the performance of **CARISMA** and **GCUSP** (which performed best in Experiment 2) and

4 to study the influence of the magnitude of **gamut difference** on the performance of the selected algorithms.

To facilitate aims 3 and 4, the five algorithms evaluated here were used for making reproductions of the test images both on *HP Premium Inkjet Paper* (this will be referred to as **plain paper**) and on *HP Glossy Inkjet Paper* (this will be referred to as **glossy paper**). The reason for using two substrates with the same printing device is, that the resulting pair of gamuts are similar to each other in terms of shape, but have different lightness ranges (Figure 10.2.2). This makes it possible to understand how the reduction of a gamut's lightness range affects the performance of gamut mapping algorithms.

Note, that parts of the contents of this chapter were submitted for publication (Morovic and Luo, 1998c).

## 10.1.1 The influence of CIECAM97s on Gamut Mapping

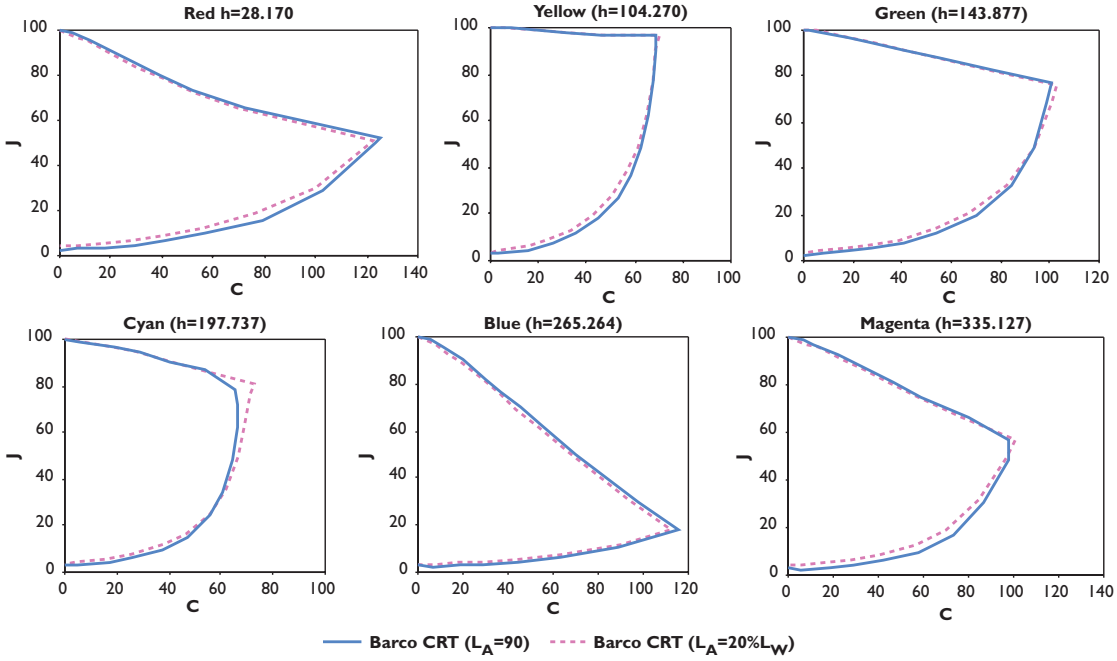


***Figure 10.1.1*** *Gamuts of CRT calculated using different $L_A$ values.*

The choice of CIECAM97s, from which lightness (*J*), chroma (*C*) and hue (*h*) were used as the colour space for gamut mapping, resulted in some changes, which affected all algorithms and the most important of which will be described next. Note, that in the colour reproduction system for this experiment the parameters of CIECAM97s were set to F=1.0, c=0.69, $F_{LL}$=1.0 and $N_c$=1.0, which are the values specified for an average surround and the background ($Y_b$) had the same chromaticity

as the adapting white and 20 *per cent* of its luminance. The luminance of the adapting field ($L_A$) was mistakenly set to 90 cd/m$^2$, instead of being set to 20 *per cent* of the adapting white's luminance (i.e. 17 cd/m$^2$), which would have more closely described the conditions used in the experiment and which is also recommended in the model. Fortunately, the consequences of this result in little change to the evaluated reproductions both in terms of colour gamut (this is illustrated in Figure 10.1.1 by showing the gamut of the CRT as calculated with the different $L_A$ settings) and contrast (Figure 10.1.2), which means that choosing the correct $L_A$ value would have given very similar reproductions.

The first effect of using CIECAM97s is the uniformity of its **hue predictor**, which was shown by Ebner and Fairchild (1998) to be better in the blue region and worse in the red–yellow region than the hue predictor of CIELAB. Both these results could be observed in the reproductions made for this experiment. Red colours tended to be bluer than the original and yellows greener; the hue of blue colours, on the other hand, was maintained after lightness and/or chroma changes.

The second effect of using CIECAM97s *versus* CIELAB was a change in the contrast of images due to a difference in the **lightness predictors** of the two colour spaces. Figure 10.1.1 shows the plot of J *versus* L* values of 86 achromatic colours which were obtained by first calculating the XYZ tristimulus values from the device–dependent coordinates of colours which had equal RGB values and were equally–spaced and then calculating L* and J from these (the parameters for CIECAM97s were the same as for the whole experiment).

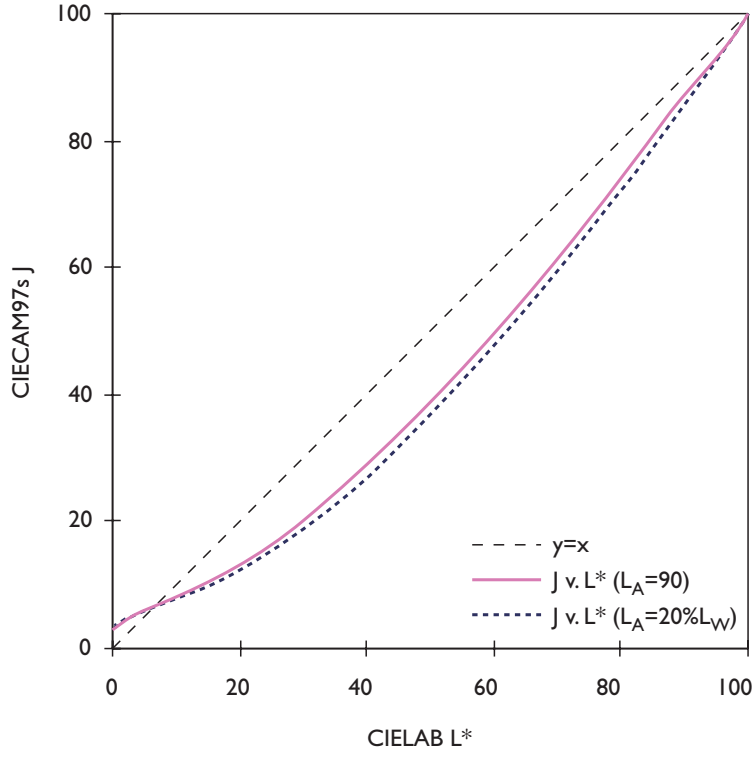


***Figure 10.1.2*** *J versus L* plot for XYZ values of colours with equal RGB values (showing two $L_A$ settings).*

It can be seen from Figure 10.1.2 that the contrast of colours with an L* of above approximately 40 is increased, that of between approximately 20 and 40 is kept the same and that of below this interval is decreased. The change of the lightness predictor also resulted in a change of **lightness range** for a given medium and hence also of the ratio between the lightness ranges of media pairs. The following table shows the lightness ranges of the three media used in this experiment and the lightness–range ratios of the two printed media with the CRT.

| medium | CRT | glossy print | glossy/CRT | plain print | plain/CRT |
|---|---|---|---|---|---|
| L* range | 100.00 | 87.01 | 87.01% | 76.58 | 76.58% |
| J range | 97.25 | 90.88 | 93.45% | 84.88 | 87.28% |

***Table 10.1.1*** *Lightness ranges of Experiment 3 media in CIELAB and CIECAM97s.*

As can be seen, the lightness–range ratios in CIECAM97s are larger than those in CIELAB, which means that the gamut differences are smaller. The extent of this is such that the CIECAM97s ratio of the plain paper medium's lightness range to that of the CRT is almost the same as the CIELAB ratio of the glossy paper medium's lightness range to that of the CRT. This was indeed one of the reasons for adding the plain paper substrate to Experiment 3, as the gamut differences for the glossy substrate were significantly smaller than the differences in Experiment 2.

Summing up the above sections, it can be said that the differences between CIECAM97s and CIELAB are significant, which will be a good basis for seeing whether algorithms implemented in CIELAB can successfully be implemented in another colour space.

## 10.2 Overall Results

The accuracy scores shown in Figure 10.2.1 were obtained by combining the overall judgements made for five test images on two media in the same way as in Experiment 1 (Section 6.2.1). For sample–size dependent parameters in the calculation of accuracy scores in this experiment see Appendix F.

The overall results in Figure 10.2.1 show that CARISMA and GCUSP gave significantly more accurate reproductions than the other three algorithms. Within the group of the bottom three algorithms the UniGMA algorithm performed best, while being on the boundary of the LLIN algorithm's 95 *per cent* confidence interval.

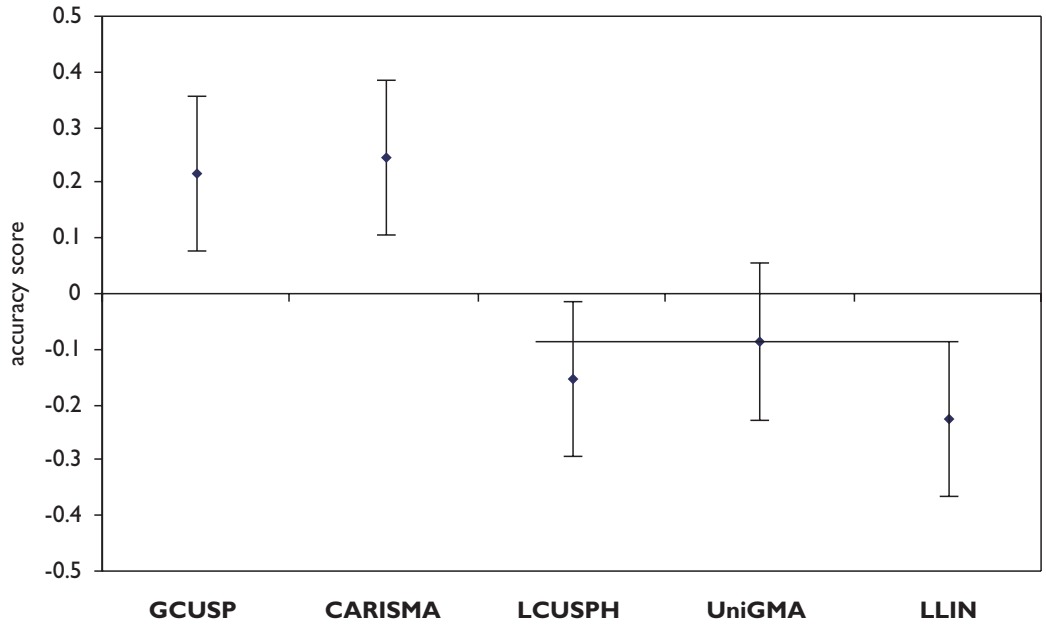


***Figure 10.2.1*** *Overall results of Experiment 3.*

From these results it would seem that the two third–generation algorithms have failed completely, as they are significantly outperformed by CARISMA and GCUSP. However, a look at all the judgements made for the GMAs evaluated here shows that the new algorithms (in particular UniGMA) had lower variances (Table 10.2.1), which means that their performance was less influenced by colour region and test image. In addition to this, it is important to note that the accuracy scores dealt with here are relative within a given group. Hence, average scores on a relative scale do

not have to imply average scores on an absolute scale. Nonetheless, CARISMA and GCUSP perform better overall and one would ideally want an algorithm which combines their good performance with the low variance of UniGMA. The variance scores also suggest a notable advantage of GCUSP over CARISMA, as it has a much lower variance, which means that it is more stable.

| | GCUSP | CARISMA | LCUSPH | UniGMA | LLIN |
|---|---|---|---|---|---|
| **variance** | 0.341 | 0.901 | 0.329 | 0.192 | 1.186 |

***Table 10.2.1*** *Variances of GMAs evaluated in Experiment 3.*

To have a better understanding of the five algorithms looked at here, the 30 colours from Section 8.2 were used again (Figure 10.2.2) and the changes made to them by the GMAs were studied. Note, that these 30 colours had the same monitor RGB values as the colours used in Experiment 2 and that they were also analysed in the same way.

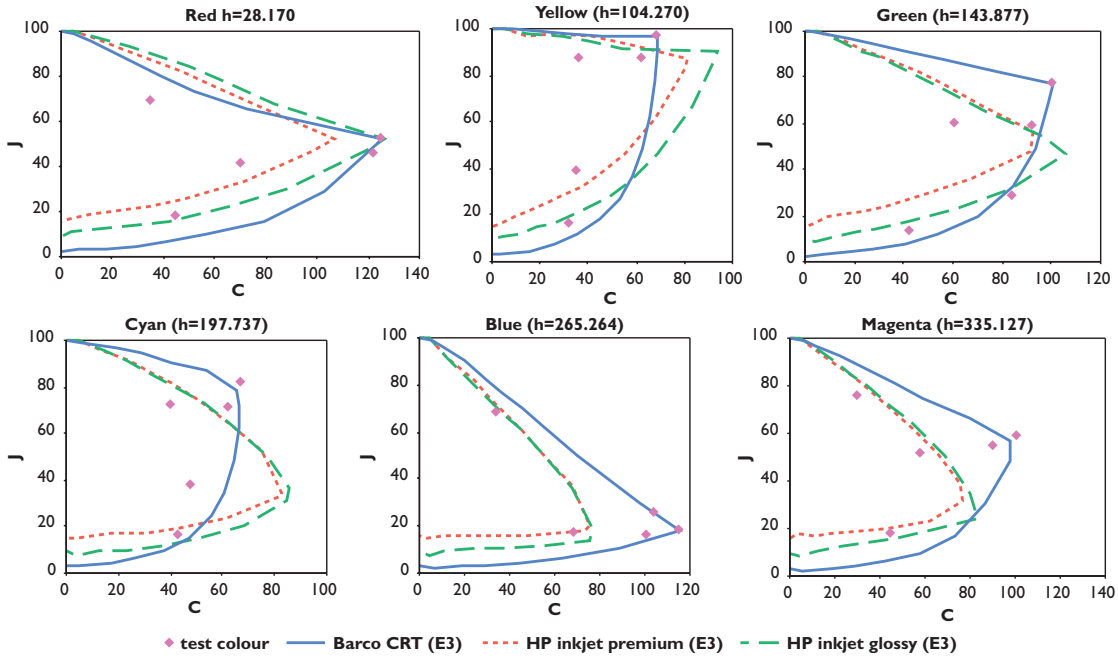


***Figure 10.2.2*** *Test colours used for investigating the changes made by GMAs in Experiment 3.*

The statistics of the differences made to these colours by the five GMAs – combined for both printed media – are shown in Table 10.2.2 (separate results for the two media can be seen in Appendix G). It is encouraging to see that the Pearson correlation coefficient between the median $|\Delta C|/|\Delta J|$ ratio and the GMAs' ranking is 0.94, which suggests the same principle as was found in Experiment 2 and already indicated in Experiment 1; i.e. to maintain more chroma at the expense of lightness (in relative terms). However, it needs to be noted that this correlation is much lower when the two printed media are considered separately (0.60 and 0.39 for the glossy and plain paper media respectively). Another difference compared with Experiment 2 is that for the GMAs looked at here there is as strong correlation between saturation changes and accuracy scores whereby those GMAs which reduce saturation least are judged to be most accurate.

At the same time, it is interesting to note the strong negative correlation between the accuracy score and the median $\Delta E_{97s}$ colour difference, which is –0.82, –0.72 and –0.92 for the combined, glossy and plain media respectively. This suggests that (within the group of five GMAs considered here) the algorithms, which make the smallest change give the most accurate reproduction. It is also encouraging to see that the correlation between these two parameters is strong for the printed media both individually and collectively as well as for the results from Experiment 2.

| GMA | median $\Delta E_{97s}$ | median $\|\Delta J\|$ | median $\|\Delta C\|$ | $\Delta(C/J)$ | $\|\Delta C\|/\|\Delta J\|$ |
|---|---|---|---|---|---|
| **GCUSP** | 11.20 | 4.20 | 9.94 | -0.24 | 1.52 |
| **CARISMA** | 13.51 | 6.19 | 1.81 | -0.03 | 0.32 |
| **LCUSPH** | 15.44 | 4.57 | 6.05 | -0.30 | 1.82 |
| **UniGMA** | 15.27 | 3.27 | 8.32 | -0.22 | 1.67 |
| **LLIN** | 14.93 | 5.57 | 12.78 | -0.48 | 2.68 |

***Table 10.2.2*** *Statistics of changes made by GMAs to 30 test colours.*

To sum up, it can be said that the accuracy of the CARISMA and GCUSP algorithms was significantly higher than that of the other results, whereby the GCUSP algorithm performed more stably and made a smaller overall change to the colours of the five test images used here.

## 10.3 Overall Results for Plain and Glossy Media

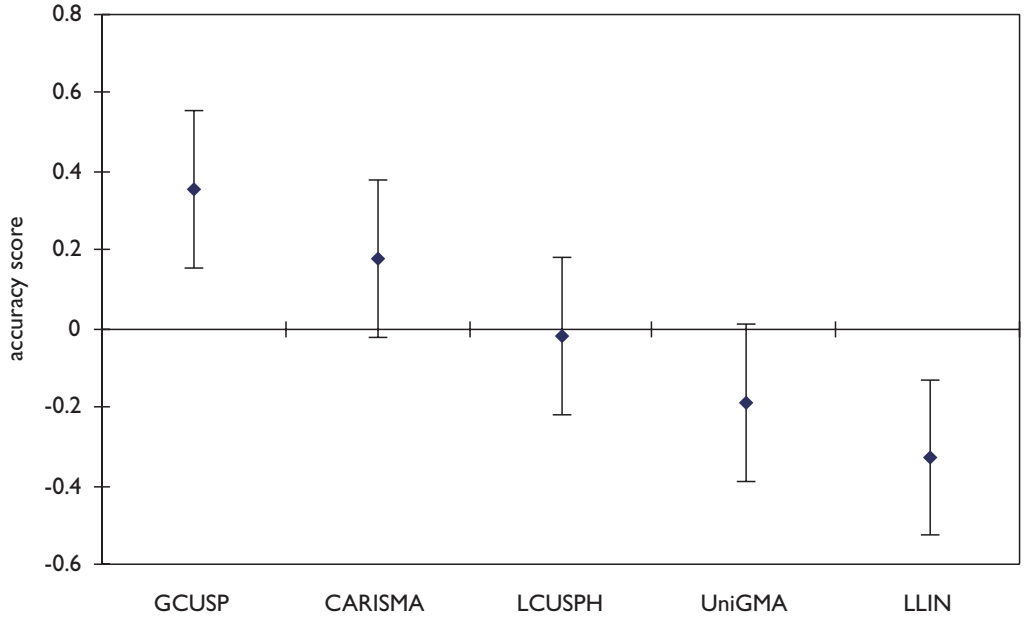


***Figure 10.3.1*** *Overall results for plain paper.*

Even though the overall results for the two media show significant differences, there are some common features in them. For both, the CARISMA and GCUSP algorithms are ranked first and second and the LLIN algorithm is always ranked among the bottom two. It can also be seen that LLIN performs better when the gamut difference is smaller and GCUSP when it is larger, whereby the performance of GCUSP is in–line with its results from Experiment 2 where it performed best for the SKI, BUS and DOL images which had the largest chroma ranges.

When looking at the individual accuracy scores obtained in this experiment (Appendix F), we can see that the range of accuracy scores is larger for plain paper than for glossy paper. This is the case for 80 *per cent* of all judgements made for overall images and colour regions within them and the ratio of plain paper accuracy–score range to glossy paper accuracy–score range is 1.6. This means that there are larger differences between the reproductions made on plain paper than between the reproductions on glossy paper, or, in other words, that the choice of GMA is more critical when the gamut difference is larger.

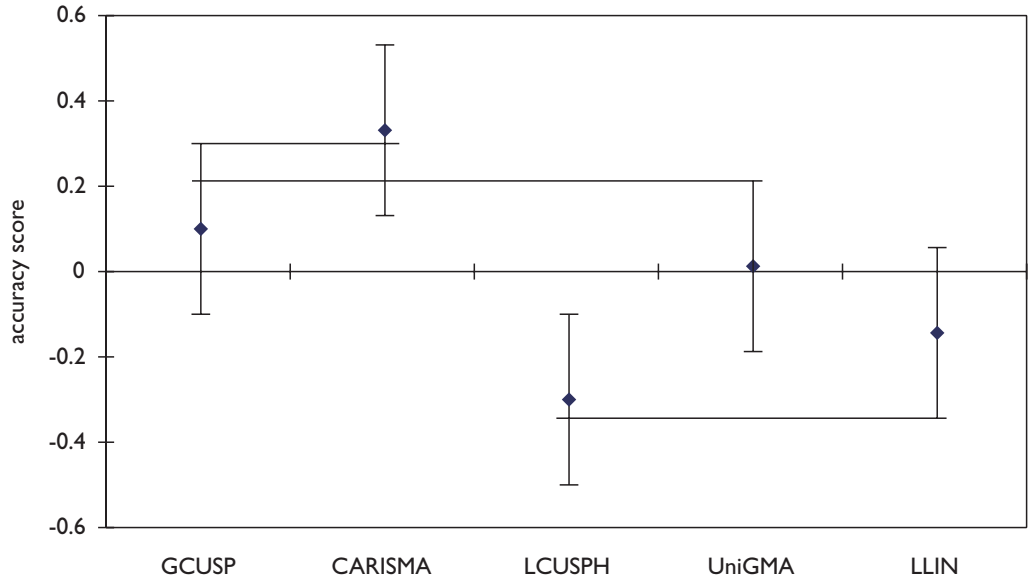


***Figure 10.3.2*** *Overall results for glossy substrate.*

The relationship between the lightness range difference of the two media and the resulting accuracy–score range difference is also of interest. Here it can be seen that the plain printed medium has a lightness range which is seven *per cent* smaller than that of the glossy substrate (Table 10.1.1) and that this difference results in an accuracy–score range which is 60 *per cent* larger. This clearly suggests the importance of gamut difference for the evaluation of gamut mapping algorithms and differences in this parameter might well have been the causes of differences in the results of experimental studies from different sources.

## 10.4 Results for Colour Regions

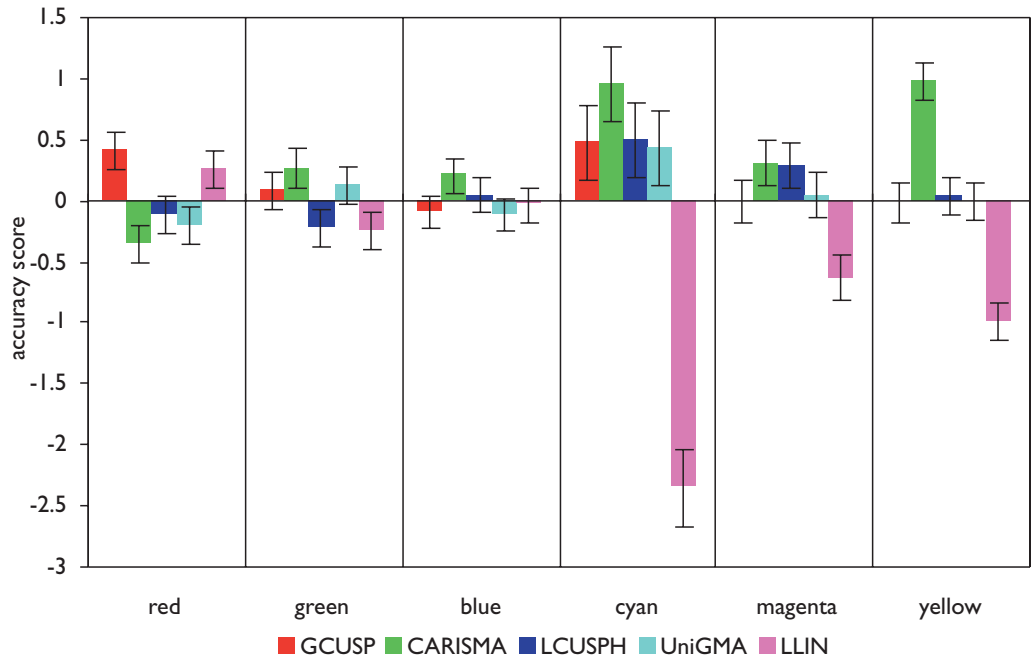


***Figure 10.4.1*** *Results for colour regions by colour region.*

From the results for colour regions, shown in Figures 10.4.1 and 10.4.2, it can be seen that the CARISMA algorithm performs well for all but the red region and that the LLIN algorithm performed badly for all but the red region. It can also be seen that the LLIN algorithms performs best for the regions (red and blue) where the original and reproduction gamuts are most similar in terms of shape (i.e. the lightness or the two cusps is similar – see Figure 10.2.2).

The results for individual colour regions also show an influence of the colour space in which gamut mapping is carried out. It can be seen by considering the results for the red colour region for which the algorithms which had no hue shift (i.e. GCUSP and LLIN) performed better than those which had a hue shift. This could be a consequence of CIECAM97s' hue predictor non–uniformity in that region as a result of which the hue of red colours becomes bluish when their lightness and chroma predictors are changed. Hence the reproductions made with the algorithms which had a hue shift performed worse, as the hue shift specified by the algorithms was towards blue (Appendix G). This meant that it added to the hue shift already inherent in the colour space and caused the combined hue shift to be unacceptable.

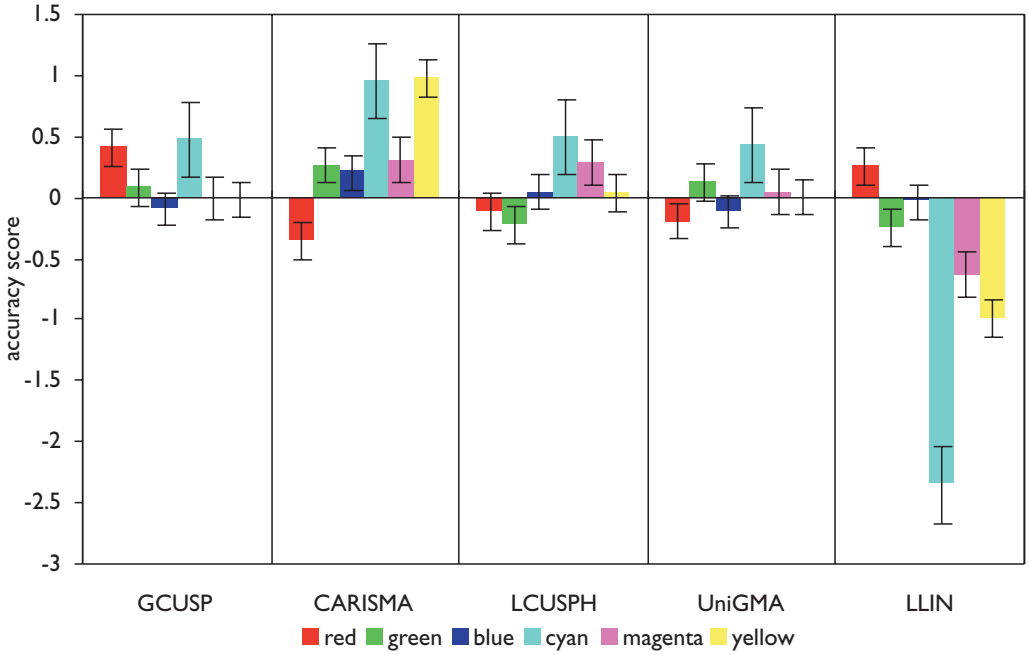


***Figure 10.4.2*** *Results for colour regions by GMA.*

The results shown in this section again confirm the findings presented in the section about overall results (Section 10.2). It can be seen that the CARISMA and GCUSP algorithms perform best and that the GCUSP algorithm has a low variance relative to the colour region from which it maps colours.

## 10.5 Results for Individual Images

In this experiment the results for individual images, which are shown in Figures 10.5.1 and 10.5.2, do not exhibit such homogeneity as was the case with the results from Experiment 1. However, there are some characteristics of GMAs, which can be seen in spite of this. The performance of CARISMA is worse for the images which have a significant red–contents (DOL and MUS) and GCUSP does well for images which have a large chroma range (with the exception of SKI where it is in the second–best group).

Further, it can be seen that the ranges of accuracy values are fairly limited for all but the BUS image (in this experiment the accuracy score range of the other four images was approximately 1 to 1.5 whereas in Experiment 1 the range was 2 to 3 accuracy units). The fact that the differences between algorithms are small in this experiment is a consequence of comparing algorithms which perform similarly – four of the five algorithms looked at here (i.e. except for LLIN) are either the best ones from Experiment 2 or were developed from them.

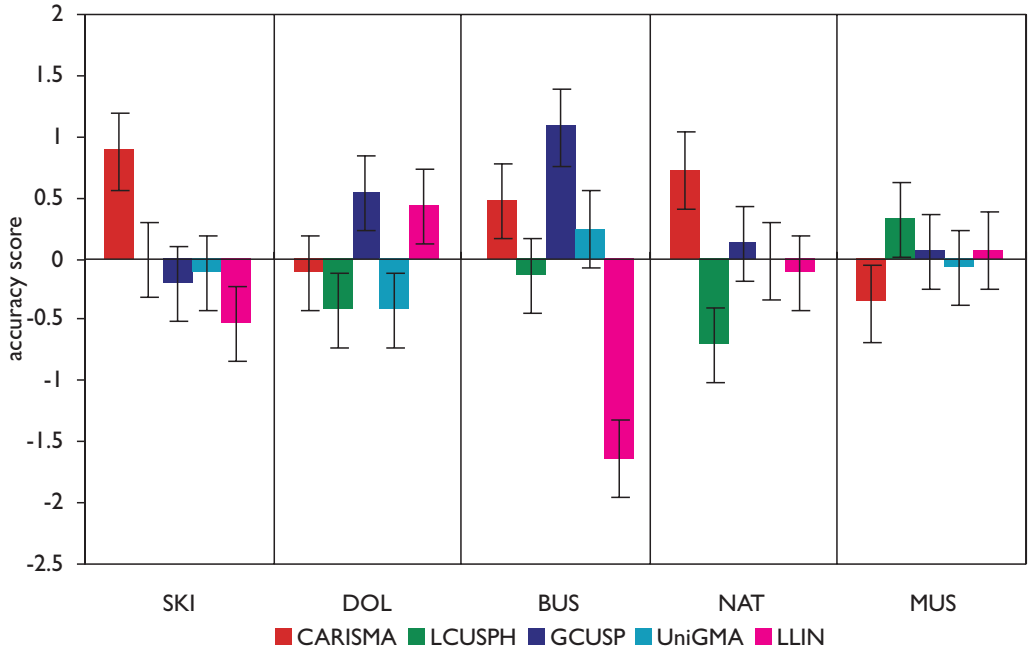


***Figure 10.5.1*** *Results for test images by image.*

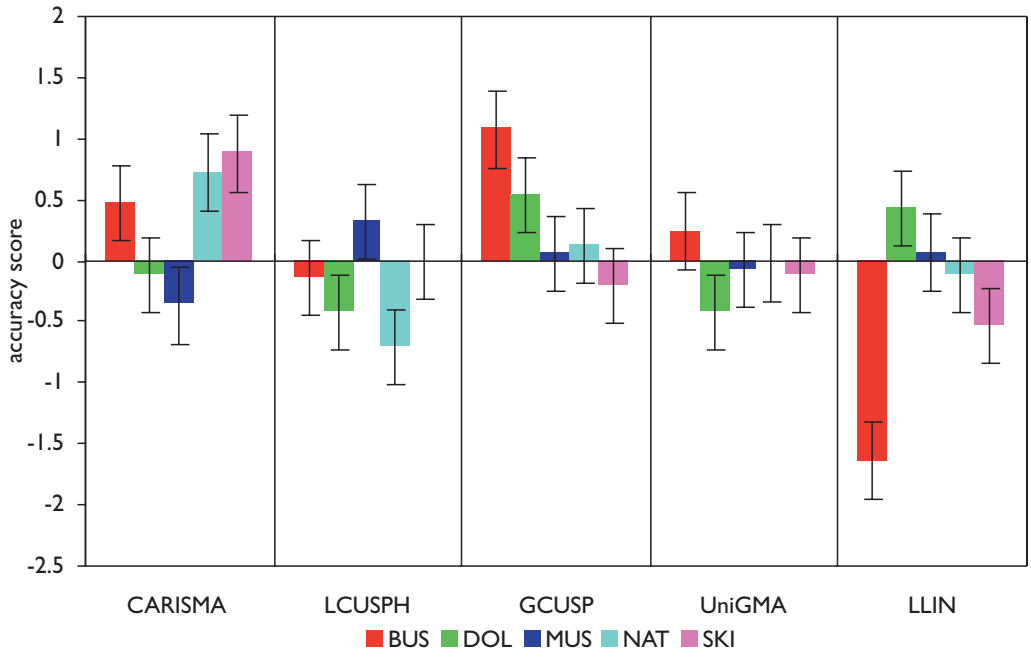


***Figure 10.5.2*** *Results for test images by GMA.*

Finally, it is of interest to consider the grouping of GMAs for the five test images used here (Table 10.5.1), as a good performance in this is of great practical importance for universal gamut mapping algorithms. It can be seen that the GCUSP and CARISMA algorithms are in the top two groups for each of the five test images, which is further evidence for their suitability as universal GMAs.

| | BUS | DOL | MUS | NAT | SKI | mean |
|---|---|---|---|---|---|---|
| **GCUSP** | 1 | 1 | 1 | 2 | 2 | **1.4** |
| **CARISMA** | 2 | 2 | 2 | 1 | 1 | **1.6** |
| **LCUSPH** | 3 | 2 | 1 | 3 | 2 | **2.2** |
| **UniGMA** | 2 | 2 | 2 | 2 | 2 | **2.0** |
| **LLIN** | 4 | 1 | 1 | 2 | 3 | **2.2** |

***Table 10.5.1*** *Ranking of GMA groups for five test images.*

## 10.6 Summary

| Mnemonic | Description |
|---|---|
| **GCUSP** | C dependent J compression + CUSP |
| **CARISMA** | J compression + hue shift +<br>relative, gamut shape dependent mapping |
| **UniGMA** | hue shift + relative, gamut shape dependent J compression and mapping |
| **LCUSPH** | J compression + hue shift + CUSP |
| **LLIN** | J compression + linear C compression |

***Table 10.6.1*** *Overview of GMAs evaluated in Experiment 3.*

Five GMAs (Table 10.6.1) were used in CIECAM97s for obtaining reproductions of five test images on two printed media (plain and glossy substrates). These reproductions were then evaluated in terms of their accuracy using the pair comparison method whereby ten observers took part in the experiment.

Based on this experiment, it can be said that the GCUSP and CARISMA algorithms performed best in terms of overall results as well as the results for individual test images and colour regions in them and that the GCUSP algorithms in particular had a low variance of accuracy scores. It was again shown that those algorithms which maintained relatively more chroma gave more accurate reproductions and that these algorithms also made smaller overall changes to the images' colours.

Further, the results suggested that the magnitude of original and reproduction gamut difference has a significant influence on the range of the GMAs' performances, which means that the choice of GMA for the reproduction of images between two media is more critical when there are larger differences between these.

Chapter 11

# Experiment 4: Investigation of the Relationship Between Accuracy and Pleasantness

*If we do not find anything pleasant,*
*at least we shall find something new.*
*Voltaire (Candide)*

# 11.1 Introduction

Unlike the first three experiments of this study, which were part of an iterative process of developing and evaluating gamut mapping algorithms, Experiment 4 is aimed at investigating the relationship between two of the characteristics of reproductions made with the GMAs dealt with here – pleasantness and accuracy (for their definitions see Section 1.3).

The primary reason for conducting the present study – i.e. that the reproduction of images across different media does not permit the exact matching of all original colours – also necessitates the choice of a criterion or **colour reproduction intent** according to which colours are gamut–mapped (Section 2.4.3). The existence of different criteria could be seen as implying the need for different gamut mapping algorithms to fulfil their requirements. Whether this is the case for the accuracy and pleasantness criteria within the framework of this study was therefore investigated in the present experiment.

As is stated in the introduction (Section 1.3), "the development of algorithms described in this study assumes that the appearance of the original image is what needs to be reproduced [i.e. the aim is accuracy] and that the original image has a pleasant appearance." It is important to be aware of two issues, which arise in conjunction with this statement. Firstly, that the decision of focusing on accuracy was not taken out of disregard for the pleasantness of reproductions obtained using the investigated algorithms, but because the accuracy of a reproduction was considered to be a feature, which is less influenced by individual observers' characteristics and can therefore be assessed more objectively. Secondly, that when interpreting the results of this experiment, it is important to keep in mind that the original images were considered to be pleasant.

Hence, the aim of this experiment is to see whether the accuracy of a reproduction is positively correlated with its pleasantness when the original image is pleasant and not whether there is this correlation also for original images which could themselves be considered unpleasant. The importance of understanding this lies in it determining whether one needs to develop separate GMAs which will give either accurate or pleasant reproductions.

Note, that the results of this experiment were partly published before (Morovic and Luo, 1998b).

# 11.2 Overview of Experiment

Eight observers (four female and four male) with normal colour vision, who were all staff or students at the Colour & Imaging Institute and aged between 22 and 39 years, took part in this experiment. Unlike the previous experiments, only the **overall characteristics** of reproductions were considered here, without looking at individual colour regions. As was already said in Chapter 5, the viewing conditions were also different for this experiment, since observers evaluated reproductions in isolation – i.e. without seeing the original image. The seven algorithms evaluated in the present experiment are the same ones as in Experiment 2 (whereby CLLINLLAB was excluded altogether) and the pleasantness results will be compared with accuracy scores from that experiment. Note, however, that only the MUS, NAT and SKI test images were used here, as the performance of the GMAs in Experiment 2 for BUS and DOL were similar to their performance for SKI.

Another difference between this experiment and the previous ones is that it uses two different psychophysical methods – **category judgement** (*cj*) and **pair comparison** (*pc*) – both of which are described in Chapter 5. Category judgement was used because it gives data on an absolute scale, which is more appropriate for pleasantness as it can be considered to be an absolute attribute (with the qualifications given in Section 1.3). The reason for using pair comparison as well was that it would be difficult to compare the results from the category judgement experiment with the accuracy results from Experiment 2, which were obtained using the pair comparison method.

The relationship between the results obtained using these two methods will also provide useful information about how much the pleasantness scores depend on the technique used for obtaining them and therefore also how trustworthy these techniques are within the context of evaluating complex images.

## 11.3 Pleasantness Results

The overall results (Figure 11.3.1) obtained using the category judgement method were calculated by summing up the frequency matrices from the three individual test images and calculating pleasantness scores from these (for the data analysis procedure see Section 5.5.2). Note, that the sample–size dependent parameters as well as the numerical results for this experiment can be found in Appendix H.

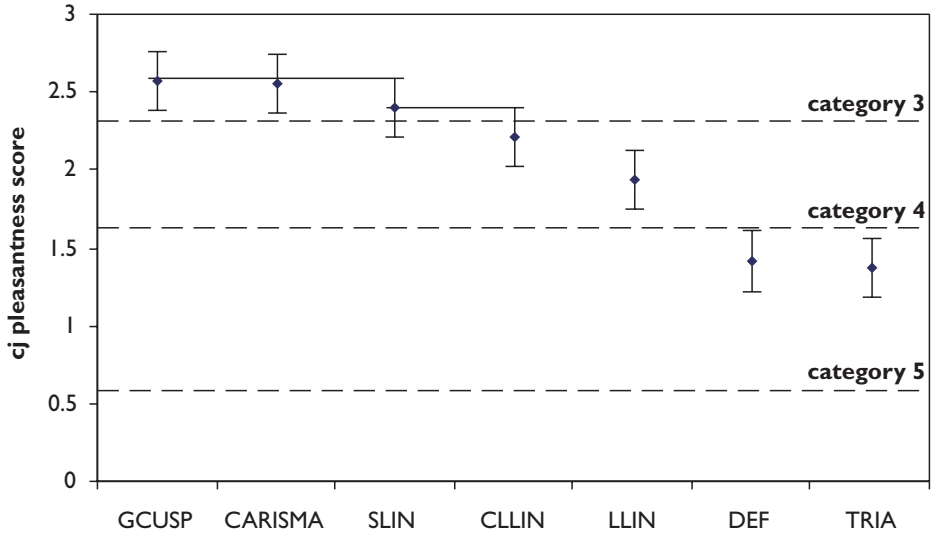


***Figure 11.3.1*** *Overall pleasantness scores obtained using category judgement method.*

The above results clearly show the good performance of CGUSP and CARISMA, which have the top two ranks (while not being significantly different from SLIN) as well as the bad performance of reproductions made with DEF and TRIA. The results of the category judgement experiment also allow an analysis of the absolute pleasantness of the GMAs looked at here. In these terms it can be seen that CLLIN and LLIN are judged to be in category four, which is the category into which images are placed when they are considered to be half–way between the most and the least pleasant image an observer can imagine. Hence this category can be considered to be neutral or indeterminable in terms of pleasantness and any category above it is pleasant and any category below it unpleasant. Looked at the results in this way, the GCUSP and CARISMA algorithms are considered to give pleasant reproductions as they are in category three at the 95 *per cent* confidence level. At this level the SLIN algorithm could be either in category three or four and DEF and TRIA are considered unpleasant, as they fall into category five.

It is encouraging to see the close similarity between the results of Experiment 2 (where GCUSP and CARISMA did best and DEF and TRIA worst) and the above scores. The results for individual images again exhibit some of the features of the results of Experiment 2 – in particular the degree to which GMAs are influenced by individual images (Figure 11.3.2). We can again see the low variance of GCUSP and CARISMA and the high variance of LLIN.

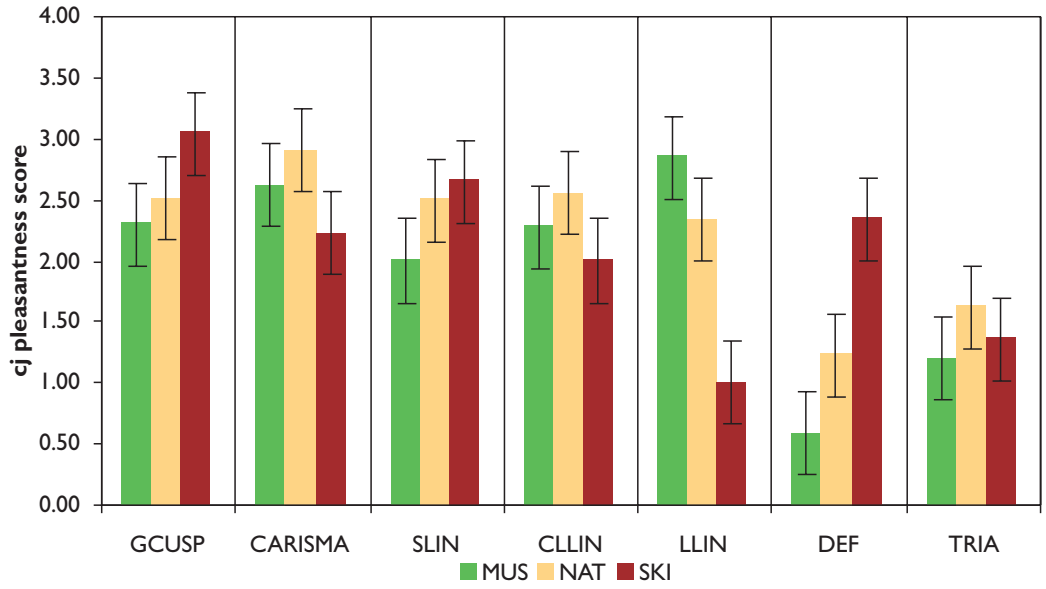


***Figure 11.3.2*** *Pleasantness scores for three test images obtained using the category judgement method.*

As mentioned above, the pleasantness of the reproductions made of these three test images was also evaluated using the pair comparison method. These results for the individual images were combined in the same way as for Experiments 1 to 3 (see Section 6.2.1) and the overall scores are shown next (Figure 11.3.3).

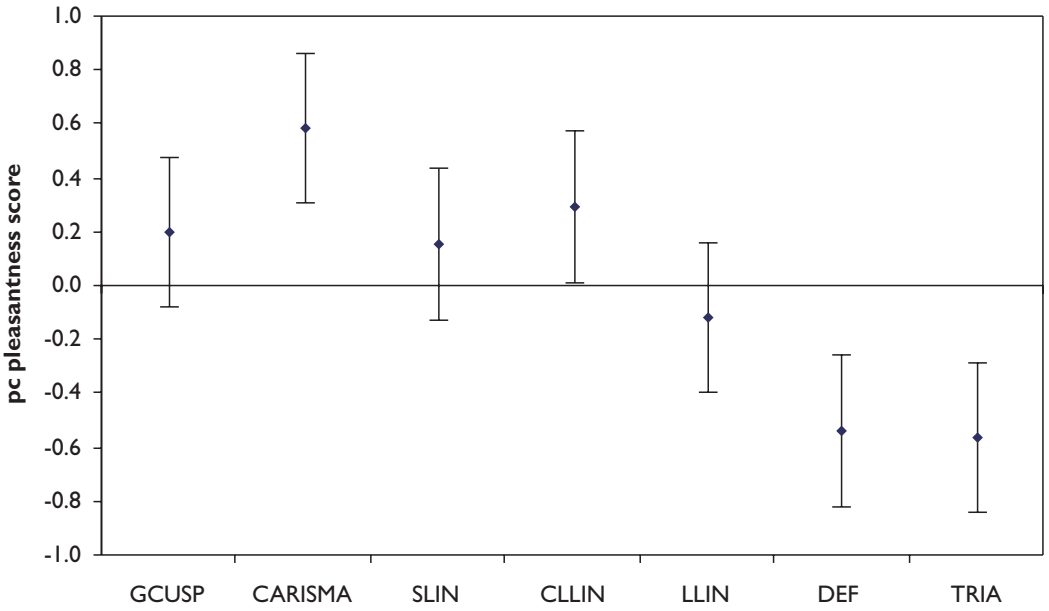


***Figure 11.3.3*** *Overall pleasantness scores obtained using pair comparison method.*

It can be seen that the above results are very similar to the results obtained with the category judgement method and that even though the ranking of the algorithms is not identical, the main features observed before can again be seen here (even though GCUSP is not ranked among the top two algorithms, it is not significantly different from CLLIN, which is ranked second).

## 11.3.1 Pair Comparison v. Category Judgement

To quantify how well the GMA results obtained using these two methods agree with each other, the Pearson correlation coefficients were calculated between the two sets of overall results as well as between the pairs of results for the individual images (Table 11.3.1).

| Image | Overall | MUS | NAT | SKI |
|---|---|---|---|---|
| **Correlation between scores** | 0.94 | 0.96 | 0.76 | 0.89 |
| **Correlation between ranks** | 0.82 | 0.96 | 0.96 | 0.89 |

***Table 11.3.1*** *Relationship between category judgement and pair comparison results.*

The correlation coefficients between the pleasantness scores shown above are very high in particular for the overall results and the results for the MUS and SKI images. It can be seen that the correlation between the two sets for the NAT image is somewhat lower, but obtaining the results for the ranking of GMAs shows consistently high correlations for all images as well as for the overall results. Note, that this is also in–line with the findings of Lo *et al.* (1996) who used the pair comparison and category judgement methods for the evaluation of reproductions made with different colour appearance models and again found a good agreement between the results of the two methods.

Hence, it can be said that the agreement between the results of the two psychophysical methods used here is very good and that the interpretation of the absolute pleasantness results (from the category judgement method) can be combined with the comparison of relative accuracy and pleasantness scores (obtained using the pair comparison method), which will be carried out next.

## 11.4 Accuracy v. Pleasantness

The pleasantness scores obtained with the pair comparison method on the basis of the three test images used here were compared with the accuracy scores from Experiment 2. The correlation coefficients between these overall results as well as the results for each image individually are shown in Table 11.4.1.

| Image | Overall | MUS | NAT | SKI |
|---|---|---|---|---|
| **Correlation** | 0.92 | 0.92 | 0.88 | 0.68 |

***Table 11.4.1*** *Correlation between accuracy and pleasantness results based on pair comparison experiments.*

It can be seen from the above table that there is a strong correlation (0.92) between the two kinds of results and that this is also the case for the individual images. The lower correlation coefficient between accuracy and pleasantness scores for the SKI image is due to the difference in performance of the LLIN algorithm in terms of pleasantness and accuracy (without LLIN the correlation for SKI is 0.94). The reason for this difference is that the reproduction of the SKI image made with LLIN exhibits a discontinuity artefact in some yellow regions of the image which has a smaller impact on the overall accuracy judgement than on the judgement made for pleasantness (for details of why this artefact occurs see Section 6.2.1).

A plot of overall accuracy scores *versus* pleasantness scores (Figure 11.4.1) again confirms the good correlation and also points towards another interesting characteristic of the results, which is the relationship between the ranges of these two kinds of scores. The range of accuracy scores [-1.43,0.81] is larger than the range of pleasantness scores [-0.57, 0.58] by a factor of 1.95, which suggests that the sensitivity to accuracy is larger than the sensitivity to pleasantness (note that the difference is smaller for individual images but that this factor is always larger than one). It is interesting to note that in an experiment carried out by Stokes *et al.* (1992) it was found that differences between pictorial images which are above approximately 3 $\Delta E_{ab}$ are noticeable but that differences of up to 6 $\Delta E_{ab}$ are acceptable (i.e. they differ by a factor of two). These parallels between accuracy and perceptibility and pleasantness and acceptability are an encouraging sign of convergence suggesting some common underlying characteristic.

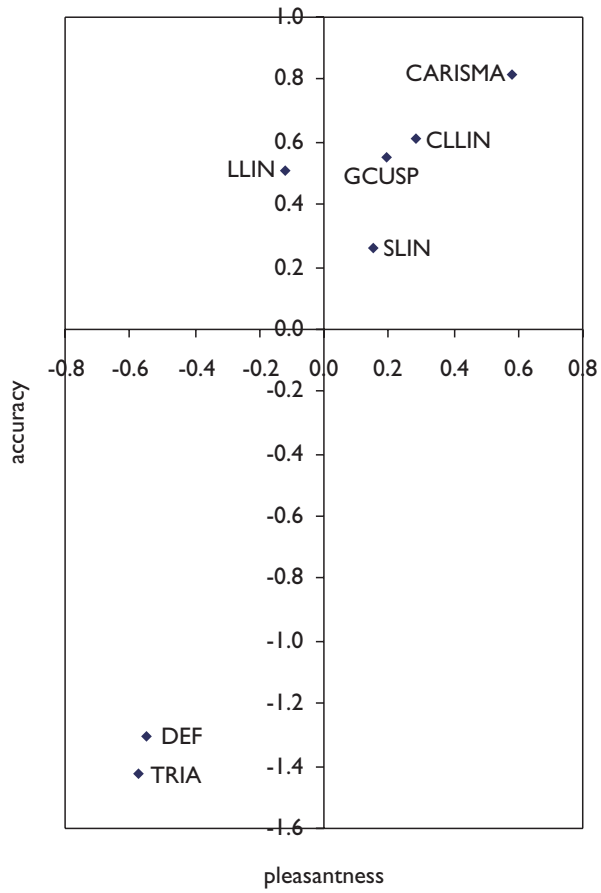


***Figure 11.4.1*** *Overall accuracy scores versus pleasantness scores for the seven GMAs evaluated here.*

## 11.5 Summary

Seeing that there is a strong positive correlation between the accuracy and pleasantness scores of GMAs dealt with in this study is a reassuring fact, which implies a wider applicability for accurate algorithms than would otherwise be the case. Finding a strong and positive correlation between these results also prevents possible contradictions, which could have arisen if the opposite result would have been the case. Contradictions could have occurred inasmuch as (for a pair of reproductions) the more accurate reproduction of a pleasant image could have been less pleasant and, more absurdly, the less pleasant image could have been the more accurate reproduction of a pleasant image.

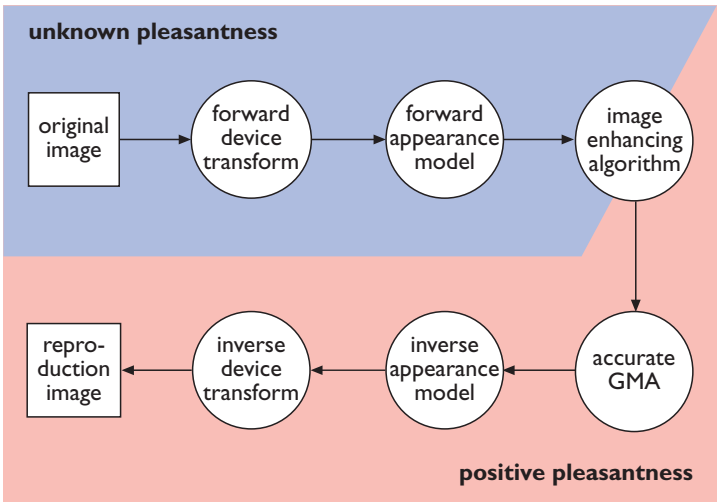


***Figure 11.5.1*** *Six–stage transform including image enhancing stage.*

A positive correlation also means that the algorithms, which perform well in terms of accuracy can be used in a system, which modifies images so that they become more pleasant. A system like that could be implemented as a **six–stage transform** (Figure 11.5.1) along the lines of the five–stage transform by MacDonald (1993) discussed in Chapter 1.

An example of such an image enhancing algorithm could be the "algorithm for optimising color quality of natural images" given by Yendrikhovskij (1998) and briefly discussed in Section 2.4.3.

# Chapter 12

# Conclusions

*It is not knowledge,*
*but the act of learning,*
*not possession,*
*but the act of getting there,*
*which grants the greatest enjoyment.*

*Karl Friedrich Gauss (Letter to Bolyai, 1808)*

# 12.1 Overview of Findings

The aim of this thesis is to give account of work carried out towards the development of universal colour gamut mapping algorithms. This was done by starting with a literature survey (Chapter 2), then implementing a colour reproduction system (Chapter 3), developing methods for determining gamut boundaries (Chapter 4) and designing and conducting a series of psychophysical experiments evaluating accuracy, which alternated with the development of gamut mapping algorithms on their basis (Chapters 5 – 10). In addition to this, the relationship between the accuracy and pleasantness of reproductions made with various algorithms was also investigated (Chapter 11). A more detailed summary of the most important of these points will be given in the following sections.

## 12.1.1 Colour Reproduction System

The colour reproduction system used in this study was described in Chapter 3 and consisted of a CRT monitor and various printed media obtained using an inkjet printer and viewed under a D50 simulator. In this system, special attention was paid to printer characterisation, as this has proven to be particularly problematic. A satisfactory solution was finally found by the use of third–order masking equations combined with a new grey–scale correction method developed for the purposes of this study.

## 12.1.2 Gamut Boundary Determination

Knowing the gamut boundaries of the media used in a colour reproduction system is a prerequisite to mapping colours between them. To this end, new methods were developed for calculating overall gamut boundary descriptors (*Segment Maxima GBD* method), for obtaining the gamut boundary along a given line of constant $L^*$ and $h_{ab}$ or constant spherical angles (*Constrained Line Gamut Boundary (LGB)* method) or for doing this along any line of constant $h_{ab}$ (*Flexible Sequential LGB* method) (Chapter 4). Having a colour reproduction system and knowing the gamut boundaries of its media then enabled the investigation of gamut mapping.

## 12.1.3 Experiment 1 – Initial Evaluation

The first in a series of experiments aimed at the development of universal algorithms was one where a selection of previously proposed algorithms were evaluated (Chapter 6). These initial algorithms belonged into two groups: sequential algorithms, which map individual colour attributes (e.g. lightness and hue) separately and simultaneous algorithms, which map them at the same time. The results showed that the group of simultaneous (CUSP and SLIN) algorithms performed significantly better overall as well as for most colour regions and individual test images. An exception to this was their performance for the neutral axis and for dark colours, where sequential algorithms performed better. Hence, the aim for the development of new, second–generation algorithms was to combine the behaviour of sequential and simultaneous methods on the basis of the experimental results.

## 12.1.4 Experiment 2 – Evaluation of new GMAs

The new algorithms (Chapter 7) developed on the basis of Experiment 1 were again evaluated in comparison with two of the initial GMAs. The results of this experiment (Chapter 8) clearly showed that two of the new algorithms – CARISMA and GCUSP – had consistently high accuracy scores for the images and colour regions considered, which makes them good candidates for being universal gamut mapping algorithms. Further, the results also showed that it is algorithms which

maintain more chroma and make smaller overall changes to the gamut–mapped colours, which perform best. The variance of accuracy scores for all the judgements made for the five test images and colour regions within them was also calculated and found to be smallest for the GCUSP algorithm. Finally, the algorithms were looked at in terms of the ranking of significantly different groups for the overall judgements made for each test image. Here, the CARISMA algorithm gave the best results, followed by GCUSP.

### 12.1.5 Experiment 3 – Verification of GMAs

The aims of Experiment 3 (Chapter 10) included the following: to evaluate the new, third–generation UniGMA and LCUSPH algorithms (Chapter 9) developed on the basis of Experiment 2, to verify the performance of CARISMA and GCUSP and to study the influence of the magnitude of gamut difference on the performance of selected algorithms by evaluating reproductions made on two different printing substrates.

Experiment 3 showed that the GCUSP and CARISMA algorithms performed best in terms of overall results as well as the results for individual test images and colour regions in them and that the GCUSP algorithm's accuracy scores had a particularly low variance. It was again shown that those algorithms which maintained relatively more chroma gave more accurate reproductions and that these algorithms also made smaller overall changes to the images' colours. Further, the results suggested that the magnitude of original and reproduction gamut difference has a significant influence on the range of the GMAs' performances, which means that the choice of GMA is more critical when there are larger differences between the original and reproduction gamuts.

### 12.1.6 Experiment 4 – Accuracy *versus* Pleasantness

The pleasantness of each reproduction made for Experiment 2 was evaluated in isolation using both the pair comparison and category judgement methods and the resulting pleasantness scores were then compared with corresponding accuracy scores from Experiment 2. Firstly, these results showed a very good agreement between the data obtained using the two psychophysical methods. Secondly, a strong positive correlation was found between the accuracy and pleasantness scores, which implies a wider applicability of algorithms which are successful in terms of accuracy than would otherwise be the case. Thirdly, the data from the category judgement method showed that reproductions made with the CARISMA and GCUSP algorithms were pleasant in absolute terms.

## 12.2 Summary

Developing a universal gamut mapping algorithm first lead to the implementation of a colour reproduction system for the printer characterisation of which a new grey–sclae correction method was developed. This was followed by the development of new methods for the determination of gamut boundaries and the choice of an overall developmental philosophy. It was decided to start with the choice of a group of existing algorithms and to develop new ones from them in an evolutionary way. A particularly important decision at this point was to evaluate colour regions within test images in addition to the evaluation of their overall performance, which resulted in more detailed and useful data than would otherwise have been the case.

The evolutionary approach to developing gamut mapping algorithms used in this study has clearly resulted in a new algorithm (GCUSP) which significantly and consistently outperforms the initial methods on which it is based. GCUSP achieved high accuracy scores for the vast majority of judgements made both in Experiment 2 (where it was first evaluated) and Experiment 3 (where it was verified). In addition to the good overall performance, the variance of its accuracy scores was also very small (it was lowest in Experiment 2 and lower than that of CARISMA in Experiment 3),

which indicates a stable performance across the range of images used. Further, it was shown that this method performs well both in CIELAB and CIECAM97s, which is of particular practical interest and in Experiment 4 it was also shown that the reproductions made with this GMA are pleasant. All these features make GCUSP an excellent candidate for being a universal gamut mapping algorithm.

The current study led to nine publications including seven scientific papers (Luo and Morovic, 1996; Morovic and Luo, 1996; 1997a; 1997b; 1998a; 1998b; 1998c) and two book chapters (Morovic, 1998; Morovic and Luo, 1998d). In addition, the author is now the Chairman of a CIE Technical Committee (TC) on Gamut Mapping of the newly–formed Division 8 on Imaging Technology. This also demonstrates the significance of the present study.

## 12.3 Future Work

Even though the field of gamut mapping has made a great advance since the beginning of this project, many of gamut mapping's parameters (e.g. gamut shape & difference, image characteristics, etc.) have been studied only partially and there might still be some which have not even been identified. Clearly, the work described in the present thesis (unlike other studies) has not contributed to this field by the systematic investigation of individual parameters, but has instead aimed at the development of a method which could be universally used. In addition to being of use for this end, it is also of use in the systematic study of gamut mapping, since it can serve as a reference when individual parameters are systematically studied.

As for future work, many of the observations made about the results of individual experiments in this study lend themselves to systematic investigation. Perhaps, the effect of gamut difference is of most practical importance both from the point of view of end–users and from the point of view of those studying gamut mapping, as it might well be a cause for differences between the findings of different studies.

The results also suggest that the algorithms which make smaller changes perform better. Hence, it would be of interest to compare various clipping algorithms with GCUSP to see whether this principle holds in the extreme. These clipping algorithms should include the clipping, which minimises $\Delta E$ (as this has, by definition, the smallest possible colour difference on a pixel–by–pixel basis) and the algorithm proposed by Katoh and Ito (1996) (as its results are also in–line with the experimental gamut clipping study by Ebner and Fairchild (1997)).

A number of choices in this study were made by trial and error (most notably, the function determining the percentage of lightness compression in GCUSP) and it would be of interest to determine them on a systematic basis. A further area of future work would be to incorporate some ideas into GCUSP which were published after GCUSP was developed. An example of this are the results of the investigation of lightness compression done by Montag and Fairchild (1997) or some of the mapping methods proposed by Herzog and Müller (1997).

Another area of future work could be to focus on issues, which were not investigated at all in this study, e.g. the use of image gamuts *versus* media gamuts, how well results from actual *versus* simulated colour gamuts correlate, how the spatial characteristics of images could be utilised when gamut mapping them, how well image difference metrics (like S–CIELAB (Zhang and Wandell, 1996)) predict the experimental results of this study and how they could be used for gamut mapping etc. Further, the influence of image contents on gamut mapping is of particular interest. Here it would be useful to see whether images with similar image statistics (e.g. image gamut, colour histogram, etc.) but different image contents perform differently when gamut mapped.

The work of the above mentioned CIE TC on Gamut Mapping also follows on from the present study and (as is said in its Terms of Reference) has as its aim:

*To recommend a standard solution to the gamut mapping problem, which could be applied to the areas of colour reproduction in general and colour imaging in particular. This solution would consist of (a) a standard way for calculating colour gamuts and (b) a gamut mapping algorithm or a set of gamut mapping algorithms and rules for deciding when each of them is to be used.*

To achieve this aim, the TC has the following work programme:

1. *Review current gamut mapping algorithms and algorithms for calculating gamut boundaries.*
2. *Provide guidelines for the evaluation of gamut mapping algorithms.*
3. *Review results of gamut mapping algorithm evaluation done according to guidelines.*
4. *Recommend a standard gamut mapping algorithm or a small number of algorithms and rules for deciding when each of them is to be used.*

The arrival at such a standardised, universal algorithm is of great practical importance as it will enable a consistent quality of image reproduction to be obtained from a variety of computer platforms and across a variety of media.

Clearly, the potential for future work in this field is vast and varied.

# References

*All things were made by him;*
*and without him was not any thing made*
*that was made.*

*John (1:3)*

ANSI (1993) *ANSI IT8.7/1 Color Transmission Target for Input Scanner Calibration*, ANSI

Appel J. J., Durbin J. A. and Lehman R. F. (1994) *Methods for Matching Color Prints to Color Images on a Monitor Screen*, Xerox Corporation, US Patent 5,313,291

Balasubramanian R. (1994) Color Transformations for Printer Color Correction, *Proceedings of 2nd IS&T/SID Color Imaging Conference*

Balasubramanian R. and Maltz M. S. (1996) Refinement of printer transformations using weighted regression, *SPIE Proceedings*, **2658**:334–340

Bartleson C. J. (1984) *Optical Radiation Measurement. Vol. 5 – Visual Measurements*, Bartleson C. J. and Grum F. (eds.), Academic Press Inc.

Bartleson C. J. and Breneman E. J. (1967) Brightness Perception in Complex Fields, *Journal of the Optical Society of America*, **57**/7:953–957

Bell I. E. and Cowan W. (1994) Device Characterisation Using Spline Smoothing and Sequential Linear Interpolation, *Proceedings of 2nd IS&T/SID Color Imaging Conference*

Berns R. S. (1996) Methods for Characterising CRT displays, *Displays. Special Issue: 'To Achieve WYSIWYG Colour'*, 173–182

Berns R. S. and Choh H. K. (1995) Cathode–Ray–Tube to Reflection–Print Matching Under Mixed Chromatic Adaptation Using RLAB, *Journal of Electronic Imaging*, **4**/4:347–359

Berns R. S., Motta R. J. and Grozynski M. E. (1993a) CRT Colorimetry. Part I: Theory and Practice, *Color Research and Application*, **18**/5:299–314

Berns R. S., Grozynski M. E. and Motta R. J. (1993b) CRT Colorimetry. Part II: Metrology, *Color Research and Application,* **18**/5:315–325

Braun G. J. and Fairchild M. D. (1997) Techniques for Gamut Surface Definition and Visualization, *Proceedings of 5th IS&T/SID Color Imaging Conference*, 147–152

Braun K. M., Fairchild M. D. and Alessi P. J. (1996) Viewing Techniques for Cross–Media Image Comparisons, *Color Research and Application*, **21**:6–17

Brill M. H. (1992) Tradeoffs in VDU Monitor Calibration and in Color Correction, *TAGA Proceedings*, 903–916

Bristow J. A., Klaman M. and Hoc M. (1994) The Comparison of Colour Gamuts, *IARAIGAI Conference Proceedings. Advances in Printing Science and Technology*, **24**:311–332

Budin J. P. (1995) Emissive Displays: the Relative Merits of ACTFEL, Plasma and FEDs, *Getting The Best from State–of–the–Art Display Systems. SID Conference Proceedings*, London

CARISMA (1992) Colour Appearance Research for Interactive System Management and Application – CARISMA, Work Package 2 – Device Characterisation, *Report WP2–19 Colour Gamut Compression*

Chau W. W. K and Cowan W. B. (1996) Gamut Mapping Based on the Fundamental Components of Reflective Image Specifications, *Proceedings of 4th IS&T/SID Color Imaging Conference*, 67–70

CIE (1986) CIE Publication 15.2, *Colorimetry*, Second Edition

CIE (1981) CIE Publication 51, *A Method for Assessing the Quality of Daylight Simulators for Colorimetry*

Clapper F. R. (1961) An Empirical Determination of Half–tone Colour Reproduction Requirements, *TAGA Proceedings*, 31–41

Clarke F. J. J., MacDonald R. and Rigg B. (1984) Modification of the JPC79 Colour–Difference Formula, *Journal of the Society of Dyers and Colourists*, **100**:117

Ebner F. and Fairchild M. D. (1997) Gamut Mapping from Below: Finding the Minimum Perceptual Distances for Colors Outside the Gamut Volume, *Color Research and Application*, 22:402–413

Ebner F. and Fairchild M. D. (1998) Finding Constant Hue Surfaces in Color Space, *SPIE Proceedings*, **3300**:107–117

Engeldrum P. G. (1986) Computing Color Gamuts of Ink–jet Printing Systems, *SID Proceedings*, **27**:25–30

Engeldrum P. G. and Ingraham J. L. (1990) Analysis of White Point and Phosphor Set Differences of CRT Displays, *Color Research and Application*, **15**:151–155

Evans R. M. (1943) Visual Processes and Color Photography, *Journal of the Optical Society of America*, **33**/11:579

Evans R. M. (1974) *The Perception of Color*, Wiley–Interscience, New York, 97 & 205

Fairchild M. D. (1992) Chromatic Adaptation to Image Displays, *TAGA/ISCC Proceedings,* **2**

Fairchild M. D. (1994) Visual Evaluation and Evolution of the RLAB Color Space, *Proceedings of 2nd IS&T/SID Color Imaging Conference*, 9–13

Fairchild M. D. (1998) *Color Appearance Models*, Addison–Wesley

Fairchild M. D. and Berns R. S. (1993) Image Color – Appearance Specification Through Extension of CIE LAB, *Color Research and Application*, **18**/3:178–190

Gentile R. S., Walowitt E. and Allebach J. P. (1990) A comparison of techniques for color gamut mismatch compensation, *Journal of Imaging Technology*, **16**:176–181

Gescheider G. A. (1976) *Psychophysics, Method and Theory*, Lawrence Erlbaum Associates, 84–102

Gondek, J. (1996) *Private communication*, November 1996

Gordon J., Holub R. and Poe R. (1987) On the Rendition of Unprintable Colors, *TAGA Proceedings*, 186–195

Granger E. M. (1995) Gamut Mapping for Hard Copy Using the ATD Color Space, *SPIE Proceedings*, **2414**:27–35

Guth S. L. (1989) Unified Model for Human Color Perception and Visual Adaptation, *SPIE Proceedings*, **1077**:370

Haneishi H., Miyata K., Yaguchi H. and Miyake Y. (1993) A New Method for Color Correction in Hardcopy from CRT Images, *Journal of Imaging Technology*, **37**/1:30–36

Harrington S. J. (1994) *Methods and Apparatus for Performing Real Time Color Gamut Compressions,* Xerox Corporation, U.S. Patent 5,319,473

Hering E. (1920) *Outlines of a Theory of the Light Sense,* Harvard University Press, Cambridge (Translation Hurvich L. M. and Jameson D. (1964))

Herzog P. G. (1996) Analytical Color Gamut Representations, *Journal of the IS&T*, **40**:516–521

Herzog P. G. (1997) A New Approach to Printer Calibration Based on Nested Gamut Shells, *Proceedings of 5th IS&T/SID Color Imaging Conference*, 245–249

Herzog P. G. (1998) Further Development of the Analytical Color Gamut Representations, *SPIE Proceedings*, **3300**:118–128

Herzog P. G. and Müller M. (1997) Gamut Mapping Using an Analytical Color Gamut Representation, *SPIE Proceedings*, **3018**:117–128

Herzog P. G. and Roger T. (1998) Comparing Different Methods for Printer Characterisation, *ICPS Conference Proceedings*, **2**:23–30

Heuberger K. J. and Jing Z. M. (1991) Colour Transformations from RGB to CMY, *IARAIGAI Conference Proceedings. Advances in Printing Science and Technology*, **21**:76-90

Heuberger K. J., Jing Z. M. and Persiev S. (1992) Color Transformations from Lookup Tables, *TAGA Proceedings*

Hoshino T. (1991) A Preferred Color Reproduction Method for the HDTV Digital Still Image System, *IS&T Proceedings: Symposium on Electronic Photography*, 27–32

Hoshino T. (1994) *Color Estimation Method for Expanding a Color Image for Reproduction in a Different Color Gamut,* U.S. Patent 5,317,426

Hoshino T. and Berns R. S. (1993) Color Gamut Mapping Techniques for Color Hard Copy Images, *SPIE Proceedings*, **1909**:152–164

Hung P. C. (1995) Gamut Mapping Using Lightness Adaptation, *Electronic Imaging*, SPIE, July 1995

Hung P. C. and Berns R. S. (1995) Determination of Constant Hue Loci for a CRT Gamut and Their Predictions Using Color Appearance Spaces, *Color Research and Application*, **20**:285–295

Hunt R. W. G. (1982) A Model of Colour Vision for Predicting Colour Appearance, *Color Research and Application*, **7**:95–112

Hunt R. W. G. (1987) *The Reproduction of Colour in Photography, Printing & Television*, Fourth Edition, Fountain Press, England

Hunt R. W. G. (1991) Revised Colour Appearance Model for Related and Unrelated Colours, *Color Research and Application*, **16**:146–165

Hunt R. W. G. (1994) An Improved Predictor of Colourfulness in a Model of Colour Vision, *Color Research and Application*, **19**:23–26

Hunt R. W. G. (1995) *Measuring Colour*, Second Edition, Ellis Horwood

Hunt R. W. G. and Luo M. R. (1994) Evaluation of a Model of Colour Vision by Magnitude Scalings: Discussion of Collected Results, *Color Research and Application*, **19**:27–33

ICC (1998) *ICC Profile Format Specification*, http://www.color.org

Inui M. (1993) Fast Algorithm for Computing Color Gamuts, *Color Research and Application*, **18**:341–348

ISO (1997) *ISO 3664: Viewing Conditions for Graphic Technology and Photography*, Working Draft of 3/3/1997

Ito M. and Katoh N. (1995) Gamut Compression for Computer Generated Images, *Extended Abstracts of SPSTJ 70th Anniversary Symposium on Fine Imaging*, 85–88

Jackson R., MacDonald L. W. and Freeman K. (1994) *Computer Generated Colour,* John Wiley & Sons, New York

Jennings E. and Thompson Pearce B. (1993) Monitor Color Gamut Changes under White Point Simulation, *TAGA Proceedings*, 85–97

Johnson A. J. (1979) *Perceptual Requirements of Digital Picture Processing,* Paper presented at IARAIGAI symposium and printed in part in *Printing World* 6 February 1980

Johnson A. J. (1996) Methods for Characterising Colour Scanners and Digital Cameras, *Displays Special Issue: 'To Achieve WYSIWYG Colours'*, 183–192

Johnson A. J. and Birkenshaw J. W. (1978) The Influence of Viewing Conditions on Colour Reproduction Objectives, *IARAIGAI Conference Proceedings – Advances in Printing Science and Technology*, **14**:48–72

Johnson A. J., Luo M. R., Lo M. C., Xin J. H., Rhodes P. A. (1998a) Aspects of Colour Management. Part I – Characterisation of Three–Colour Imaging Devices, *Color Research and Application*, **23**:000–000

Johnson A. J., Luo M. R., Lo M. C., Xin J. H., Rhodes P. A. (1998b) Aspects of Colour Management, Part II Characterisation of Four–Colour Imaging Devices and Colour Gamut Compression, *Color Research and Application*, **23**:000–000

Kang H. R. and Anderson P. G. (1992) Neural Network Applications to the Color Scanner and Printer Calibrations, *Journal of Electronic Imaging*.

Kasson J. M., Nin S. I., Plouffe W., Hafner J. L., (1995) Performing Color Space Conversions with Three–Dimensional Linear Interpolation, *Journal of Electronic Imaging*, **4**/3:226–250

Katoh N. (1994) Practical Method for Appearance Match Between Soft Copy and Hard Copy, *SPIE Proceedings*, **2170**:170–181

Katoh, N. (1998) *Private Communication*, March 1998

Katoh N. and Ito M. (1996) Gamut Mapping for Computer Generated Images (II), *Proceedings of 4th IS&T/SID Color Imaging Conference*, 126–129

Kavsek M. J. (1993) Methoden psychophysikalischer Messung im Überblick: I. Direkte Skalierverfahern, Die Farbe, **38**:127–139

Kim S. D., Lee C. H., Kim K. M., Lee C. S. and Ha Y. H. (1998) Image Dependent Gamut Mapping Using a Variable Anchor Point, *SPIE Proceedings*, **3300**:129–137

Kress W. and Stevens M. (1994) Derivation of 3–Dimensional Gamut Descriptors for Graphic Arts Output Devices, *TAGA Proceedings*, 199–214

Laihanen P. (1987) Colour Reproduction Theory based on the Principles of Colour Science, *IARAIGAI Conference Proceedings – Advances in Printing Science and Technology*, **19**:1–36

Laihanen P. (1994) Exact Soft Proofing, *Journal of the IS&T*, **38**/5:432–440

Lamming M. G. and Rhodes W. L. (1990) A Simple Method for Improved Color Printing of Monitor Images, *ACM Transactions on Graphics*, **9**/4:345–375

Liang Z. (1994) *Method for Reproducing Color Images Having One Color Gamut With a Device Having a Different Color Gamut*, U.S. Patent 5,323,249

Lo M. C. (1995) *The LLAB Model for Quantifying Colour Appearance*, PhD. Thesis, University of Loughborough

Lo M. C., Luo M. R. and Rhodes P. A. (1996) Evaluating Colour Models' Performance Between Monitor and Print Images, *Color Research and Application*, **21**/4:277–291

Luo M. R. (1995) A Review of Colour–Difference Formulæ, *Colour Control for Surface Industries*, Autumn School '95, Derby

Luo M. R. and Hunt R. W. G. (1998) The Structure of the CIE 1997 Colour Appearance Model (CIECAM97s), *Color Research and Application.*, **23**:138–146

Luo M. R., Lo M. C. and Kuo W. G. (1996) The LLAB(l:c) Colour Model, *Color Research and Application*, **21**:412–429

Luo M. R. and Morovic J. (1996) Two Unsolved Issues in Colour Management – Colour Appearance and Gamut Mapping, *Proc. 5th International Conference on High Technology: Imaging Science and Technology – Evolution & Promise*, Chiba, Japan, 136:147

MacDonald L. W. (1993) Gamut Mapping in Perceptual Colour Space, *Proceedings of 1st IS&T/SID Color Imaging Conference*, 193–196

MacDonald L. W., Luo M. R. and Scrivener S. A. R. (1990) Factors Affecting the Appearance of Coloured Images on a Video Display Monitor, *Journal of Photographic Science*, **38**:177–186

MacDonald L. W. and Morovic J. (1995) Assessing the Effects of Gamut Compression in the Reproduction of Fine Art Paintings, *Proceedings of 3rd IS&T/SID Color Imaging Conference*

MacDonald L. W., Morovic J. and Saunders D. (1995) Evaluation of Colour Fidelity for Reproductions of Fine Art Paintings, *Journal of Museum Management and Development*

MacDonald L. W., Deane J. M. and Rughani D. N. (1994) Extending the Colour Gamut of Printed Images, *Proceedings of AIC/RPS Symposium 'Images in Colour'*, Cambridge

Mahy M. (1997) Calculation of Color Gamuts Based on the Neugebauer Model, *Color Research and Application*, **22**:365–374

Mahy M. (1998) Insight Into the Solutions of the Neugebauer Equations, *SPIE Proceedings*, **3300**

Mahy M. and Delabastita P. (1996) Inversion of the Neugebauer Equations, *Color Research and Application,* **21**/6

Marcu G. and Abe S. (1994) CRT and Ink Jet Models for Device Independent Color Reproduction in Image Transmission, *Proceedings of 2nd IS&T/SID Color Imaging Conference*

Marcu G. and Abe S. (1995a) Ink Jet Printer Gamut Visualisation, *Proceedings of 11th IS&T International Congress on Advanced Non–Impact Printing Technology*, 459–462

Marcu G. and Abe S. (1995b) Three–Dimensional Histogram Visualisation in Different Color Spaces and Applications, *Journal of Electronic Imaging*, **4**:330–346

Marcu G. and Abe S. (1996) Gamut Mapping for Color Simulation on CRT Devices, *Electronic Imaging '96 Color Hard Copy and Graphic Arts*, San Jose

Meyer G. (1990) The Importance of Gun Balancing in Monitor Calibration, *SPIE Proceedings*, **1250**:69–79

Meyer G. W. and Robertson C. A. (1997) A Data Flow Approach to Color Gamut Visualization, *Proceedings of 5th IS&T/SID Color Imaging Conference*, 209–214

Meyer J. and Barth B. (1989) Color Gamut Matching for Hard Copy, *SID 89 Digest*, 86–89

Milton J. S. and Arnold J. C. (1990) *Introduction to Probability and Statistics*, McGraw–Hill Publishing Company, Second Edition, 204–221

Montag E. D. and Fairchild M. D. (1997) Psychophysical Evaluation of Gamut Mapping Techniques Using Simple Rendered Images and Artificial Gamut Boundaries, *IEEE Trans. Image Proc.*, **6**:977–989

Morovic J. (1995) *Soft Proofing – The Influence of Viewing Conditions on Colour Appearance*, B. A. (Hons.) Dissertation, London College of Printing

Morovic J. (1998) Colour Management for the Graphic Arts, *Colour Image Processing Handbook,* Sangwine S. J. and Horne R. E. N. (eds.), Chapman & Hall, 332–357

Morovic J. and Luo M. R. (1996); Characterising Desktop Colour Printers Without Full Control Over All Colorants, *Proceedings of 4th IS&T/SID Color Imaging Conference*, 70–74

Morovic J. and Luo M. R. (1997a) Cross–media Psychophysical Evaluation of Gamut Mapping Algorithms, *Proc. AIC Color 97 Kyoto*, **2**:594–597

Morovic J. and Luo M. R. (1997b) Gamut Mapping Algorithms Based on Psychophysical Experiment, *Proceedings of the 5th IS&T/SID Color Imaging Conference*, 44–49

Morovic J. and Luo M. R. (1998a) A Universal Algorithm for Colour Gamut Mapping, *Proceedings of CIM '98 Conference*

Morovic J. and Luo M. R. (1998b) The Pleasantness and Accuracy of Gamut Mapping Algorithms, *ICPS Conference Proceedings*, **2**:39–43

Morovic J. and Luo M. R. (1998c) Verification Of Gamut Mapping Algorithms In CIECAM97s Using Various Printed Media, *Proceedings of the 6th IS&T/SID Color Imaging Conference*

Morovic J. and Luo M. R. (1998d) Developing Algorithms for Universal Colour Gamut Mapping, *Colour Engineering: Vision and Technology*, MacDonald L. W. (*ed.*), John Wiley & Sons

Motomura H., Yamada O. and Fumoto T. (1997) Categorical Color Mapping for Gamut Mapping, *Proceedings of the 5th IS&T/SID Color Imaging Conference,* 50–55

Murch G. M. and Taylor J. M. (1989) Color in Computer Graphics: Manipulating and Matching Color, *Eurographics Seminar: Advances in Computer Graphics V*, Springer Verlag, 41–47

Murray A. (1936) Monochrome Reproduction in Photoengraving, *Journal of the Franklin Institute*, **221**:721–744

Musgrave F. K. (1989) Prisms and Rainbows: A Dispersion Model for Computer Graphics, *Graphics Interface '89*, 227–234

Nakauchi S., Imamura M. and Usui S. (1996) Color Gamut Mapping by Optimizing Perceptual Image Quality, *Proceedings of the 4th IS&T/SID Color Imaging Conference*, 63–67

Nayatani Y., Takahama K. and Sobagaki H. (1986) Prediction of Color Appearance under Various Adapting Conditions, *Color Research and Application*, **11**:62–71

Nayatani Y., Hashimoto K., Takahama K. and Sobagaki H. (1987) A Nonlinear Color Appearance Model using Estévez–Hunt–Pointer Primaries, *Color Research and Application,* **12**:231–242

Nayatani Y., Takahama K., Sobagaki H. and Hashimoto K. (1990) Color–Appearance Model and Chromatic–Adaptation Transform, *Color Research and Application*, **15**:210–221

Nayatani Y. (1995) Revision of the Chroma and Hue Scales of a Nonlinear Color–Appearance Model, *Color Research and Application*, **20**:143–155

Neugebauer H. (1937) Die theoretischen Grundlagen des Mehrfarbenbuchdrucks, *Zeitschrift für wissenschaftliche Photographie, Photophysik und Photochemie*, **36**/4: 73–89

Oittinen P., Autio H. and Saarelma H. (1992) Color Gamut in Halftone Printing, *Journal of the IS&T,* **36**:496–501

Pariser E. G. (1991) An Investigation of Color Gamut Reduction Techniques, *IS&T's 2nd Symposium on Electronic Publishing*, 105–107

Pham B. and Pringle G. (1995) Color Correction for an Image Sequence, *IEEE Computer Graphics and Applications,* May 1995, 38–42

Pobboravsky I., Pearson M. and Yule J. A. C. (1971) The Relationship Between Photomechanical Color Reproductions and the Original Copy, *Inter–Society Color Council Proceedings*, 186–195

Post D. L. and Calhoun C. S. (1989) An Evaluation of Methods for Producing Desired Colors on CRT Monitors, *Color Research and Application.*, **14**:172–186

Rhodes P. A. and Luo M. R. (1996) A System for WYSIWYG Colour Communication, *Displays Special Issue: To Achieve WYSIWYG Colour,* **16**/4:213–221

Ruetz B. (1994) *Color Printing Method and Apparatus Using an Out–of–Gamut Color Table*, Canon Information Systems, U.S. Patent 5,299,291

Sara J. J. (1984) *The Automated Reproduction of Pictures with Nonreproducible Colors*, PhD. Thesis, Massachusetts Institute of Technology (MIT)

Schläpfer K. (1990) How to Test Colour Monitors, *IARAIGAI Conference Proceedings. Advances in Printing Science and Technology*, **20**:118–130

Schläpfer K. (1994) *Color Gamut Compression – Correlations Between Calculated and Measured Values*, IFRA Project, EMPA, 8 August 1994

Schläpfer K. and Widmer E. (1993) Which Color Gamut Can Be Achieved in Multicolor Printing and in Television?, *TAGA Proceedings*, 41–49

Selhuber L. and Parker A. (1995) Optical Characterisation of Colour LCDs: Pitfalls and Solutions, *Getting The Best from State–of–the–Art Display Systems. SID Conference Proceedings,* London

Shepard D. (1968) A two–dimensional interpolation function for irregularly spaced data, *Proceedings of 23rd National Conference of the ACM*, ACM Press, 517–524

Sluyterman S. A. A. (1995) The CRT as the Display of the Future, *Getting The Best from State–of–the–Art Display Systems, SID Conference Proceedings*, London

Spaulding K. E., Ellson R. N. and Sullivan J. R. (1995) UltraColor: A New Gamut Mapping Strategy, *SPIE Proceedings*, **2414**:61–68

Spence J. P., Granger E. M. and Rinehart C. E. (1994) *Technique for Use in Conjunction with an Imaging System for Providing an Appearance Match Between Two Images and for Calibrating the System Thereto*, Eastman Kodak Company, US Patent 5,317,425

Spence J. P. (1994) *Technique for Use in Conjunction with an Imaging System for Providing an Appearance Match Between Two Images and for Calibrating the System Thereto*, Eastman Kodak Company, US Patent 5,333,069

Stevens S. S. (1975) *Psychophysics*, John Wiley & Sons, New York

Stokes M., Fairchild M. D. and Berns R. S. (1992) Colorimetrically Quantified Visual Tolerances for Pictorial Images, *TAGA/ISCC Proceedings,* **2**:757–777

Stone M. C., Cowan W. B. and Beatty J. C. (1988) Color Gamut Mapping and the Printing of Digital Color Images, *ACM Transactions on Graphics*, **7**:249–292

Stone M. C. and Wallace W. E. (1991) Gamut Mapping Computer Generated Imagery, *Graphics Interface '91*, 32–39

Taylor J. M., Murch G. M. and McManus (1989) Tektronix HVC: A Uniform Perceptual Color System, *SID Digest of Technical Papers*

Thurstone L. L. (1927) A Law of Comparative Judgment, *Psychological Review*, **34**:273–286

Torgerson W. S. (1954) A Law of Categorical Judgment, *Consumer Behaviour*, Clark L. H. (ed.), New York University Press, New York, 92–93

UGRA (1995) *UGRA GAMCOM Version 1.1 – Program for the Color Gamut Compression and for the comparison of calculated and measured values*, UGRA, St. Gallen, 17 July 1995

Viggiano J. A. S. and Wang J. (1992) A Comparison of Algorithms for Mapping Color Between Media of Differing Luminance Ranges, *TAGA Proceedings*, **2**:959–974

Voicu L. I., Myler H. R. and Weeks A. R. (1997) Practical considerations on color image enhancement using homomorphic filtering, *Journal of Electronic Imaging*, **6**/1:108–113

Wei R. Y. C., Shyu M. J. and Sun P. L. (1997) A New Gamut Mapping Approach Involving Lightness, Chroma and Hue Adjustment, *TAGA Proceedings*, 685–702

Wolski M., Allebach J. P. and Bouman C. A. (1994) Gamut Mapping. Squeezing the Most out of Your Color System, *Proceedings of the 2nd IS&T/SID Color Imaging Conference*, 89–92

Xerox Corporation (1989) *Xerox Color Encoding Standard* XNSS 288811, Xerox Corporation

Yendrikhovskij S. N. (1998) *Color Reproduction and the Naturalness Constraint*, PhD. Thesis, Technische Universiteit Eindhoven, The Netherlands, 109–111

Yule J. A. C. (1938) The Theory of Subtractive Colour Photography. I. The Conditions for Perfect Colour Rendering, *Journal of the Optical Society of America*, **28**:419–430

Yule J. A. C. (1967) *Principles of Colour Reproduction*, John Wiley & Sons Inc., 205–232

Yule J. A. C. and Colt R. S. (1951) Colorimetric Investigations in Multi–Colour Printing, *TAGA Proceedings*, 77–82

Yule J. A. C. and Nielsen W. J. (1951) The Penetration of Light into Paper and its Effect on Halftone Reproduction, *TAGA Proceedings*, 65–76

Zhang X. M. and Wandell B. A. (1996) A spatial extension to CIELAB for digital color image reproduction, *Proceedings of the SID Symposiums*

# Appendix A

# Device Characterisation

*Time flies like the wind, fruit flies like the banana.*

*Groucho Marx*

# Printer Test Chart

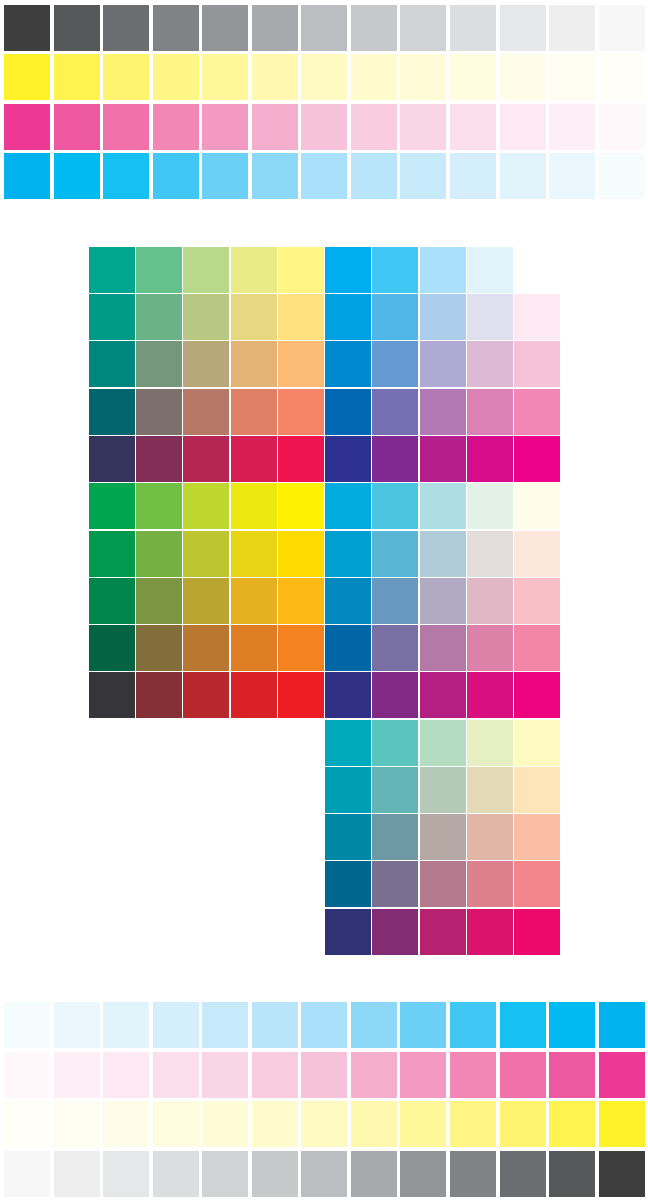

***Figure A.1*** *Printer test chart.*

The two sets of 4×14 patches at the top and bottom of Figure A.1 were used for the evaluation of spatial uniformity and the central set is the 5×5×5 training cube described in Chapter 3, which was used for evaluating the differences between individual inkjet cartridges.

# XYZ to CMY Transformation

All the values shown here are CMC(1:1) colour differences (Section 2.1.3.1) between predicted and target values with the adopted white being the printing substrate.

## *Mean*

| **model \ cube size** | **3** | **4** | **5** | **9** |
|---|---|---|---|---|
| **3rd order** | 11.45 | 6.68 | 6.46 | 6.68 |
| **4 sector** | 22.42 | 13.67 | 10.84 | 6.32 |
| **4th order** | 14.55 | 6.71 | 6.03 | 5.47 |
| **interpolation** | 7.39 | 6.58 | 6.09 | 5.79 |

*Standard deviation*

| model \ cube size | 3 | 4 | 5 | 9 |
|---|---|---|---|---|
| 3rd order | 12.02 | 4.46 | 4.37 | 5.03 |
| 4 sector | 21.44 | 11.83 | 18.67 | 6.09 |
| 4th order | 20.10 | 5.53 | 4.63 | 3.13 |
| interpolation | 4.54 | 4.41 | 3.35 | 3.86 |

*Median*

| model \ cube size | 3 | 4 | 5 | 9 |
|---|---|---|---|---|
| 3rd order | 8.06 | 5.25 | 5.35 | 5.41 |
| 4 sector | 18.75 | 10.20 | 5.36 | 5.04 |
| 4th order | 9.73 | 5.62 | 4.51 | 5.08 |
| interpolation | 6.30 | 5.59 | 5.62 | 5.14 |

*95th percentile*

| model \ cube size | 3 | 4 | 5 | 9 |
|---|---|---|---|---|
| 3rd order | 29.11 | 14.20 | 14.04 | 16.09 |
| 4 sector | 59.91 | 38.90 | 40.71 | 16.48 |
| 4th order | 36.11 | 15.41 | 12.67 | 11.06 |
| interpolation | 15.77 | 15.63 | 12.59 | 13.63 |

*Maximum*

| model \ cube size | 3 | 4 | 5 | 9 |
|---|---|---|---|---|
| 3rd order | 87.15 | 24.89 | 27.62 | 29.65 |
| 4 sector | 146.20 | 56.96 | 139.09 | 49.20 |
| 4th order | 166.85 | 39.43 | 25.88 | 16.47 |
| interpolation | 23.80 | 22.64 | 17.12 | 19.66 |

# CMY to XYZ Transformation

*Mean*

| model \ cube size | 3 | 4 | 5 | 9 |
|---|---|---|---|---|
| 3rd order | 7.88 | 6.55 | 6.61 | 7.38 |
| 4th order | 10.10 | 6.28 | 6.40 | 7.16 |
| interpolation | 13.40 | 10.74 | 9.42 | 8.36 |

*Standard deviation*

| model \ cube size | 3 | 4 | 5 | 9 |
|---|---|---|---|---|
| 3rd order | 4.01 | 3.60 | 3.73 | 4.55 |
| 4th order | 6.27 | 3.63 | 3.80 | 4.99 |
| interpolation | 9.21 | 8.83 | 6.05 | 5.65 |

*Median*

| model \ cube size | 3 | 4 | 5 | 9 |
|---|---|---|---|---|
| 3rd order | 7.28 | 6.21 | 6.17 | 7.05 |
| 4th order | 9.34 | 5.39 | 5.86 | 6.75 |
| interpolation | 10.69 | 8.89 | 8.67 | 7.40 |

*95th percentile*

| model \ cube size | 3 | 4 | 5 | 9 |
|---|---|---|---|---|
| **3rd order** | 14.80 | 12.64 | 12.41 | 15.28 |
| **4th order** | 21.08 | 12.00 | 12.35 | 15.70 |
| **interpolation** | 32.21 | 25.86 | 21.59 | 18.02 |

*Maximum*

| model \ cube size | 3 | 4 | 5 | 9 |
|---|---|---|---|---|
| **3rd order** | 21.01 | 21.84 | 21.64 | 27.13 |
| **4th order** | 38.42 | 21.37 | 21.10 | 33.52 |
| **interpolation** | 43.23 | 62.05 | 28.21 | 25.60 |

# Appendix B

# Test Images

*Time wounds all heels.*
*Groucho Marx*

# Test Images

DOL


BUS


MUS

SKI

NAT

As it is not possible to reproduce the appearance of the original test images exactly, the reproductions shown here were obtained by using the CARISMA algorithm in CIECAM97s to gamut map the original CRT images to the inkjet gamut for the glossy substrate from Experiment 3. The resulting gamut mapped values were transformed to CIELAB sent to the Postscript™ printer on which these reproductions were made. CIELAB to CMYK conversion was then carried out on the basis of its *Color Rendering Dictionary* (CRD). The purpose of these reproductions is only to give a better idea of what was used in this study and they are not intended for critical examination.

## Test Image Gamuts

Note, that the lightness ranges of all the test images used here were equal to the lightness range of the CRT monitor on which they were displayed. Their gamuts in terms of chroma (i.e. projections onto the *a*b** or *a'b'* plane) are shown in Figures B.1 and B.2.

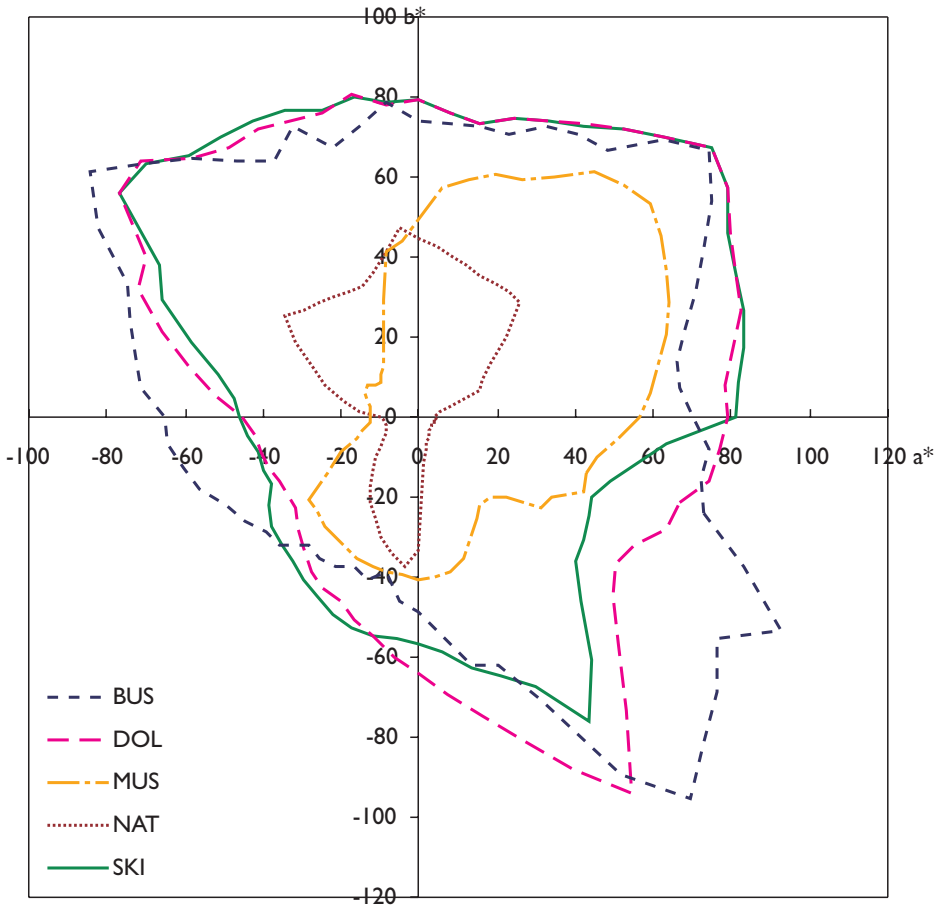


***Figure B.1*** *Gamuts of test images on Barco Reference Calibrator in CIELAB.*

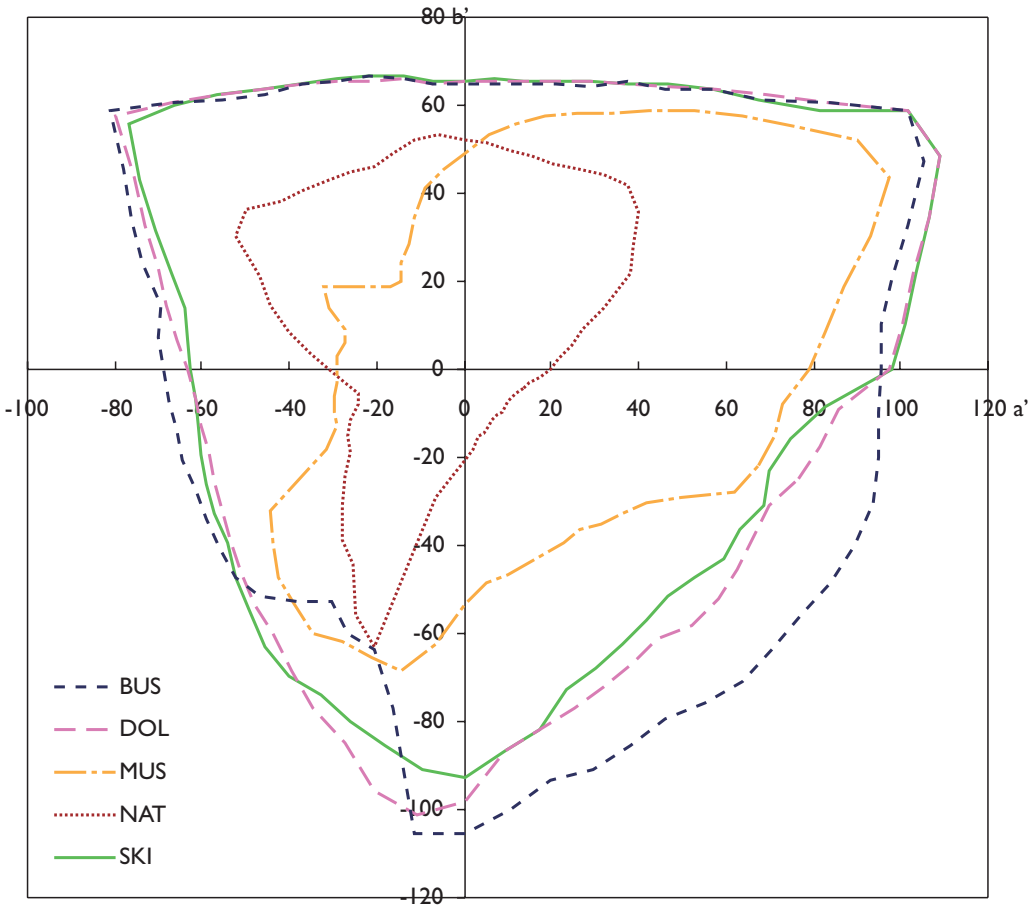


***Figure B.2*** *Gamuts of test images on Barco Reference Calibrator in CIECAM97s.*

# Test Image Statistics

## *Out–of–Gamut Pixels (per cent)*

| gamut \ image | BUS | DOL | MUS | NAT | SKI |
|---|---|---|---|---|---|
| **E1** | 72.32 | 64.42 | 55.93 | 31.12 | 73.13 |
| **E2&4** | 66.78 | 48.51 | 44.90 | 27.62 | 61.25 |
| **E3g** | 62.67 | 51.01 | 51.73 | 32.97 | 64.32 |
| **E3p** | 73.48 | 67.97 | 64.17 | 46.44 | 72.80 |

The values given here are the percentages of out–of–gamut pixels in the five test images relative to the printed media used in the four experiments whereby E*n* denotes Experiment *n* and *g* and *p* stand for glossy and premium inkjet paper respectively.

## *Relative Chroma Ranges*

| gamut \ image | BUS | DOL | MUS | NAT | SKI |
|---|---|---|---|---|---|
| **E1,2&4 CRT** | 82.36% | 78.22% | 27.71% | 9.70% | 70.95% |
| **E1 inkjet** | 97.36% | 92.46% | 32.76% | 11.46% | 83.87% |
| **E2&4 inkjet** | 78.51% | 74.56% | 26.41% | 9.24% | 67.63% |
| **E3 CRT** | 92.47% | 86.19% | 44.39% | 20.72% | 82.65% |
| **E3 inkjet g** | 81.71% | 76.17% | 39.23% | 18.31% | 73.03% |
| **E3 inkjet p** | 98.36% | 91.68% | 47.22% | 22.04% | 87.91% |

Again the values are the chroma ranges of the test images relative to the media gamuts used in the four experiments whereby the absolute chroma ranges were the following (note that these values are areas in the a**b** or *a'b'* plane).

*Absolute Chroma Ranges*

| image | BUS | DOL | MUS | NAT | SKI |
|---|---|---|---|---|---|
| **chroma range (CIELAB)** | 18063 | 17155 | 6077 | 2126 | 15560 |
| **chroma range (CIECAM97s)** | 22438 | 20915 | 10772 | 5029 | 20055 |

## Colour Regions

The following are colour regions for which judgements were made in Experiment 1. Note that slight alterations were made to some of these in subsequent experiments (e.g. the three skin tones in the MUS image were later judged together and the cyan region in SKI was not considered anymore).

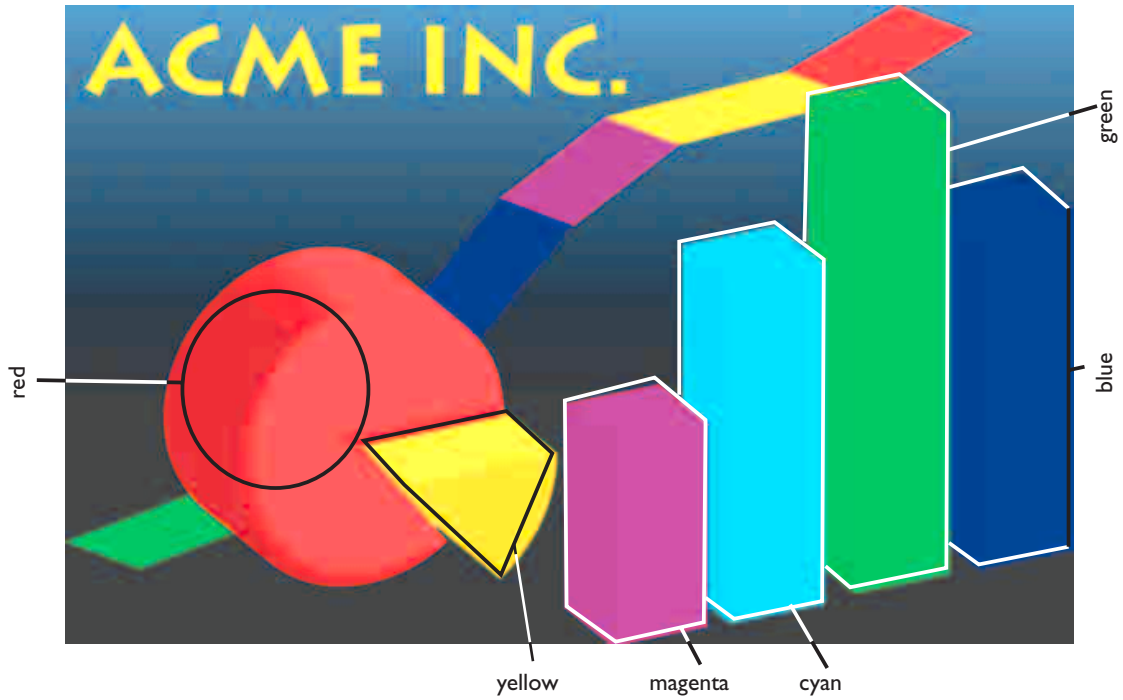


***Figure B.3*** *BUS colour regions.*

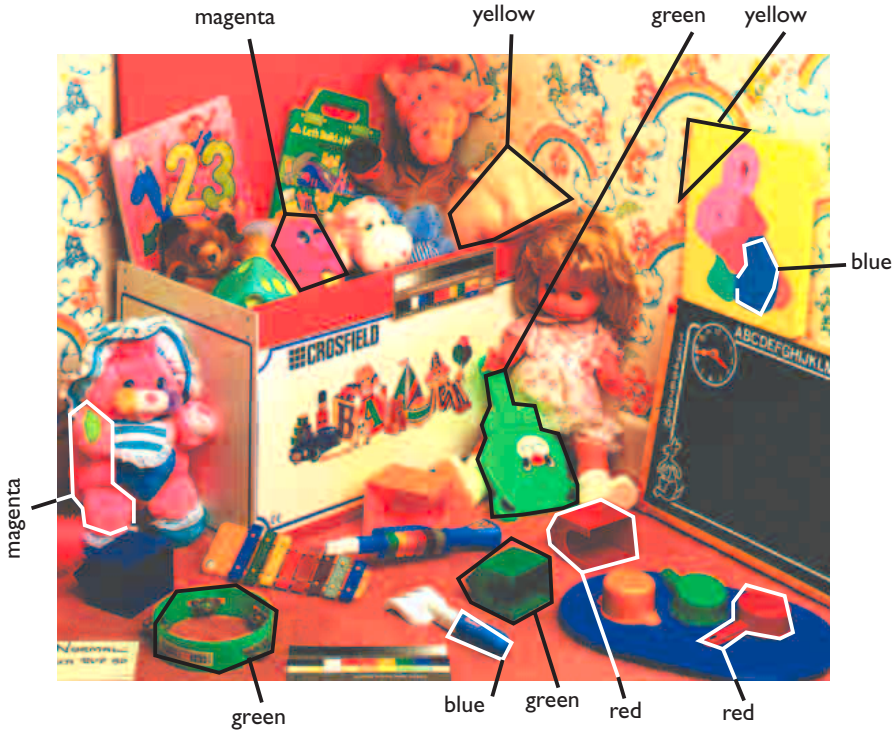


***Figure B.4*** *DOL colour regions.*

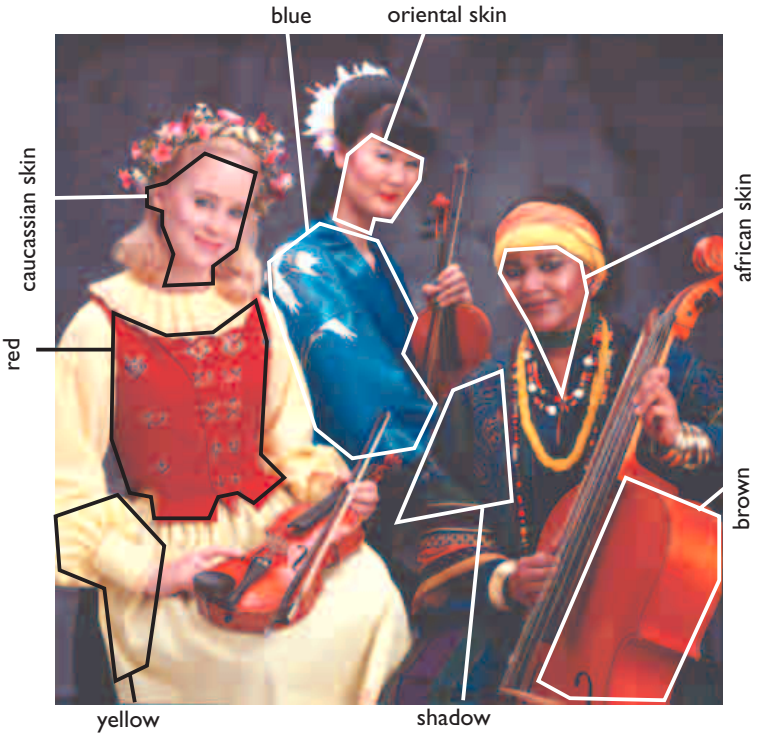


***Figure B.5*** *MUS colour regions.*

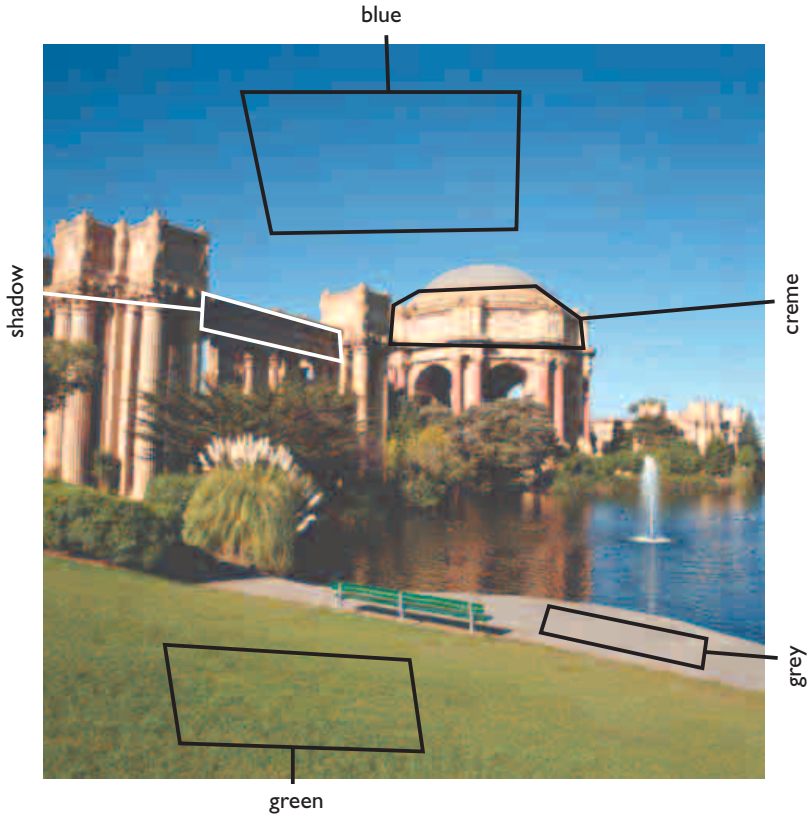


***Figure B.6*** *NAT colour regions.*


***Figure B.7*** *SKI colour regions.*

# Appendix C

# Data Analysis of Psychophysical Experiments

*A man at the dinner table dipped his hands in the mayonnaise*
*and then ran them through his hair.*
*When his neighbour looked astonished, the man apologised:*
*"I'm so sorry. I thought it was spinach."*

*Siegmund Freud*

# Worked Example of Pair Comparison Data Analysis

The following is an example of the data analysis of an experiment in which four observers judge the accuracy of three reproductions. Note that the values used here are arbitrary and only serve the purpose of demonstrating the data analysis procedure described in Chapter 5.

**Observer 1 (O1)**

| | A | B | C |
|---|---|---|---|
| A | | 0 | 0 |
| B | 1 | | 0 |
| C | 1 | 1 | |
| Average | 1 | 0.5 | 0 |

**Observer 2 (O2)**

| | A | B | C |
|---|---|---|---|
| A | | 0 | 0.5 |
| B | 1 | | 0 |
| C | 0.5 | 1 | |
| Average | 0.75 | 0.5 | 0.25 |

**Observer 3 (O3)**

| | A | B | C |
|---|---|---|---|
| A | | 0.5 | 0.5 |
| B | 0.5 | | 0 |
| C | 0.5 | 1 | |
| Average | 0.5 | 0.75 | 0.25 |

**Observer 4 (O4)**

| | A | B | C |
|---|---|---|---|
| A | | 0 | 0.5 |
| B | 1 | | 0 |
| C | 0.5 | 1 | |
| Average | 0.75 | 0.5 | 0.25 |

**Frequency Matrix (FM)** FM=O1+O2+O3+O4

| | A | B | C |
|---|---|---|---|
| A | | 0.5 | 1.5 |
| B | 3.5 | | 0 |
| C | 2.5 | 4 | |

**Percentage Matrix (PM)** PM=FM/4

| | A | B | C |
|---|---|---|---|
| A | | 0.125 | 0.375 |
| B | 0.875 | | 0 |
| C | 0.625 | 1 | |
| Average | 0.75 | 0.563 | 0.188 |
| Stdev | 0.204 | 0.125 | 0.125 |

**LG Matrix (LGM)** LGM=LN((FM+0.5)/(4-FM+0.5))

| | A | B | C |
|---|---|---|---|
| A | | -1.386 | -0.405 |
| B | 1.386 | | -2.197 |
| C | 0.405 | 2.197 | |

**z–score Matrix (zM)** zM=LGM*0.9244

| | A | B | C |
|---|---|---|---|
| A | | -1.281 | -0.375 |
| B | 1.281 | | -2.031 |
| C | 0.375 | 2.031 | |

| | | | |
|---|---|---|---|
| **mean** | 0.828 | 0.375 | -1.203 |
| **95% interv.** | 0.693 | | =1.96*(1/SQRT(2))/SQRT(4) |

**Inter–Observer Variance**

Mean Stdev. 0.151

Max. Stdev. 0.204

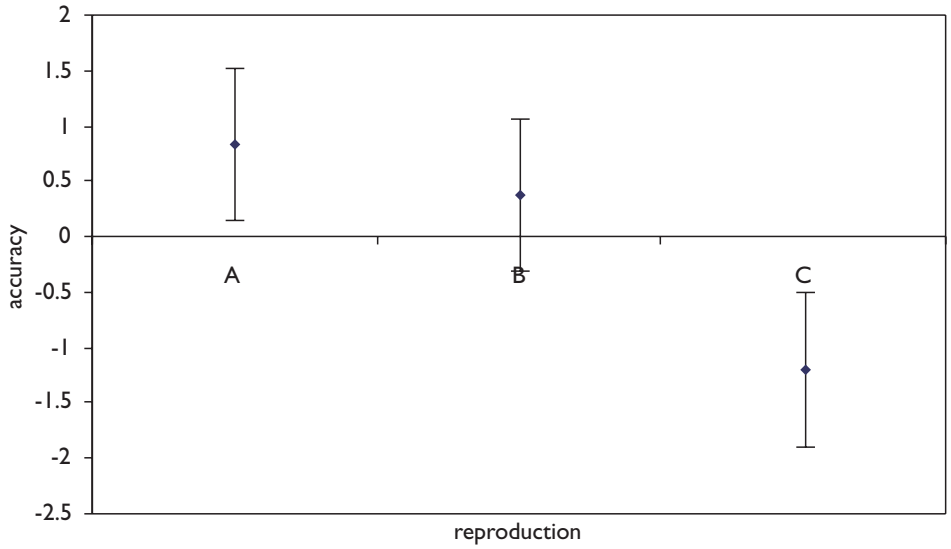


***Figure C.1*** *Accuracy scores for reproductions A, B and C and their 95 per cent confidence intervals.*

The 0.9244 parameter in the LG to z–score transformation is obtained by calculating an equation to fit the z–score v. LG data (Figure C.2). For the present example, 41 percentages (0.005, 0.995 and 39 percentages at equal intervals between 0.025 and 0.975) were chosen for which the corresponding LG and z–score values were calculated. Percentages are converted to LG values using Equation 5.4.3 and to z–scores using the inverse of the standard normal cumulative distribution (this is available in *Microsoft Excel*™ as the NORMSINV() function which takes a percentage as its input and returns the corresponding z–score for a normal distribution with a mean of zero and a standard deviation of one).

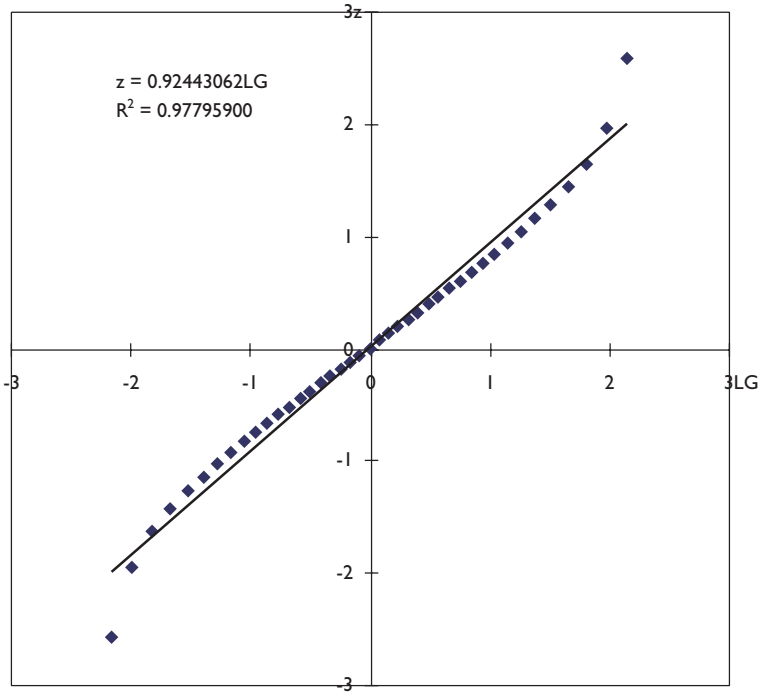


***Figure C.2*** *Z–score v. LG plot including least–squares fit line.*

# Worked Example of Category Judgement Data Analysis

The following is an example of data analysis of an experiment where four observers made judgements on the pleasantness of three reproductions in terms of seven categories (the experiment was repeated twice, i.e. eight observations were made for each image). For details of how to calculate the individual steps see Chapter 5 and note that the data in this example is again arbitrary.

**Observer 1 (01)**

| | 7 | 6 | 5 | 4 | 3 | 2 | 1 | Avg. categ. | Diff | % diff. |
|---|---|---|---|---|---|---|---|---|---|---|
| A | 0 | 0 | 0 | 0 | 2 | 0 | 0 | 3 | 0.125 | 4% |
| B | 0 | 0 | 0 | 1 | 1 | 0 | 0 | 3.5 | 0.25 | 7% |
| C | 1 | 1 | 0 | 0 | 0 | 0 | 0 | 6.5 | 1 | 18% |

**Observer 2 (02)**

| | 7 | 6 | 5 | 4 | 3 | 2 | 1 | Avg. categ. | Diff | % diff. |
|---|---|---|---|---|---|---|---|---|---|---|
| A | 0 | 0 | 0 | 0 | 2 | 0 | 0 | 3 | 0.125 | 4% |
| B | 0 | 0 | 0 | 1 | 1 | 0 | 0 | 3.5 | 0.25 | 7% |
| C | 0 | 0 | 2 | 0 | 0 | 0 | 0 | 5 | 0.5 | 9% |

**Observer 3 (03)**

| | 7 | 6 | 5 | 4 | 3 | 2 | 1 | Avg. categ. | Diff | % diff. |
|---|---|---|---|---|---|---|---|---|---|---|
| A | 0 | 0 | 0 | 0 | 2 | 0 | 0 | 3 | 0.125 | 4% |
| B | 0 | 0 | 1 | 1 | 0 | 0 | 0 | 4.5 | 0.75 | 20% |
| C | 0 | 2 | 0 | 0 | 0 | 0 | 0 | 6 | 0.5 | 9% |

**Observer 4 (04)**

| | 7 | 6 | 5 | 4 | 3 | 2 | 1 | Avg. categ. | Diff | % diff. |
|---|---|---|---|---|---|---|---|---|---|---|
| A | 0 | 0 | 0 | 0 | 1 | 1 | 0 | 2.5 | 0.375 | 13% |
| B | 0 | 0 | 0 | 1 | 1 | 0 | 0 | 3.5 | 0.25 | 7% |
| C | 0 | 0 | 1 | 1 | 0 | 0 | 0 | 4.5 | 1 | 18% |

**Frequency Matrix**

| | 7 | 6 | 5 | 4 | 3 | 2 | 1 | Avg. categ. | Avg. di | % diff. |
|---|---|---|---|---|---|---|---|---|---|---|
| A | 0 | 0 | 0 | 0 | 7 | 1 | 0 | 2.875 | 0.188 | 7% |
| B | 0 | 0 | 1 | 4 | 3 | 0 | 0 | 3.75 | 0.375 | 10% |
| C | 1 | 3 | 3 | 1 | 0 | 0 | 0 | 5.5 | 0.75 | 14% |
| | | | | | | | | | Mean | 10% |
| | | | | | | | | | Max | 14% |

**Cumulative Frequency Matrix**

| | 7 | 6 | 5 | 4 | 3 | 2 |
|---|---|---|---|---|---|---|
| A | 0 | 0 | 0 | 0 | 7 | 8 |
| B | 0 | 0 | 1 | 5 | 8 | 8 |
| C | 1 | 4 | 7 | 8 | 8 | 8 |

**Cululative Percentage Matrix**

| | 7 | 6 | 5 | 4 | 3 | 2 |
|---|---|---|---|---|---|---|
| A | 0 | 0 | 0 | 0 | 0.88 | 1 |
| B | 0 | 0 | 0.13 | 0.63 | 1 | 1 |
| C | 0.13 | 0.5 | 0.88 | 1 | 1 | 1 |

**LG Matrix**

| | 7 | 6 | 5 | 4 | 3 | 2 |
|---|---|---|---|---|---|---|
| A | -2.8 | -2.8 | -2.8 | -2.8 | 1.6 | 2.8 |
| B | -2.8 | -2.8 | -1.6 | 0.5 | 2.8 | 2.8 |
| C | -1.6 | 0.0 | 1.6 | 2.8 | 2.8 | 2.8 |

**z–score Matrix**

| | 7 | 6 | 5 | 4 | 3 | 2 |
|---|---|---|---|---|---|---|
| A | -2.2 | -2.2 | -2.2 | -2.2 | 1.2 | 2.2 |
| B | -2.2 | -2.2 | -1.2 | -0.2 | 2.2 | 2.2 |
| C | -1.2 | 0.0 | 1.2 | 2.2 | 2.2 | 2.2 |

**Difference Matrix**

| | 7 | 6 | 5 | 4 | 3 |
|---|---|---|---|---|---|
| A | 0.0 | 0.0 | 0.0 | 3.4 | 0.9 |
| B | 0.0 | 0.9 | 1.1 | 2.4 | 0.0 |
| C | 1.2 | 1.2 | 0.9 | 0.0 | 0.0 |
| mean | 0.4 | 0.7 | 0.7 | 1.9 | 0.3 |

**Category Boundary Estimates**

| T1 | T2 | T3 | T4 | T5 | T6 |
|---|---|---|---|---|---|
| 0 | 0.4 | 1.1 | 1.8 | 3.8 | 4.1 |

| **Scale values** | | | | | **mean** | **rank** | **category** |
|---|---|---|---|---|---|---|---|
| A | 2.2 | 2.6 | 3.3 | 4.0 | 2.5 | 2.9 | 1 | 3 |
| B | 2.2 | 2.6 | 2.4 | 2.0 | 1.6 | 2.2 | 2 | 3 |
| C | 1.2 | 0.4 | -0.1 | -0.4 | 1.6 | 0.6 | 3 | 5 |

**Inter–Observer Variance**

Mean Precision 10 *per cent*

Maximum Precision 14 *per cent*

Note, that the LG to z–score conversion uses 0.7761 as the scaling parameter since the sample size is eight (rather than four as in the pair comparison example) and the confidence interval of these scores is smaller (by a factor of $\sqrt{2}$) than that of the pair comparison example also due to the larger sample size.

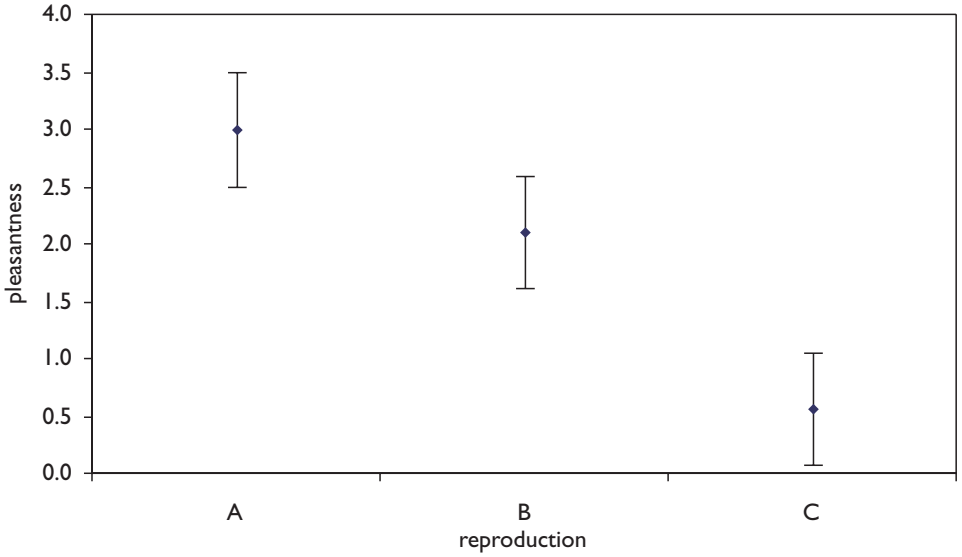


***Figure C.3*** *Pleasantness scores for reproductions A, B and C and their 95 per cent confidence intervals.*

# Appendix D

# Experiment 1: Supplementary Data

*If you wish to study a granfalloon*
*just remove the skin of a toy balloon.*

*Kurt Vonnegut (Cat's Cradle)*

# Sample–Size Dependent Parameters

| Sample Size | LG to z–score scaling factor | 95 per cent confidence interval |
|---|---|---|
| **12** | 0.7189 | ±0.40 |
| **24** | 0.6515 | ±0.28 |
| **36** | 0.6241 | ±0.23 |
| **48** | 0.6085 | ±0.20 |
| **60** | 0.5982 | ±0.18 |

# Overall Accuracy Scores

Note that in the following tables *N* represents the sample size on which a given row of values is based and that in the first column the number in brackets is the numbers of images from which results are pooled together.

## *Including SLINLLAB*

| | CUSP | SLIN | SLINLLAB | LSLIN | LLIN | LNLIN | LCLIP | N |
|---|---|---|---|---|---|---|---|---|
| **Overall (5)** | 1.00 | 0.92 | 0.91 | -0.49 | -1.13 | -0.61 | -0.60 | 60 |

## *Excluding SLINLLAB*

| | CUSP | SLIN | LSLIN | LLIN | LNLIN | LCLIP | N |
|---|---|---|---|---|---|---|---|
| **overall (5)** | 1.16 | 1.06 | -0.43 | -0.86 | -0.41 | -0.52 | 60 |
| **red (4)** | 1.85 | 1.77 | -0.29 | -1.14 | -1.12 | -1.07 | 48 |
| **green (4)** | 0.53 | 0.54 | 0.11 | -0.49 | -0.39 | -0.29 | 48 |
| **blue (5)** | 1.43 | 0.83 | -0.86 | -0.78 | -0.28 | -0.34 | 60 |
| **cyan (2)** | 0.58 | 0.58 | -0.05 | -0.36 | -0.33 | -0.42 | 24 |
| **magenta (3)** | 1.47 | 1.76 | 0.00 | -1.10 | -1.05 | -1.08 | 36 |
| **yellow (4)** | 0.64 | 0.28 | 0.35 | -0.31 | -0.36 | -0.60 | 48 |

# Accuracy Scores for Images and Colour Regions

## *BUS*

| | CUSP | SLIN | LSLIN | LLIN | LNLIN | LCLIP | N |
|---|---|---|---|---|---|---|---|
| **overall** | 1.95 | 1.47 | 0.74 | -1.46 | -1.34 | -1.37 | 12 |
| **red** | 1.90 | 1.64 | -0.55 | -0.95 | -0.97 | -1.06 | 12 |
| **green** | 1.36 | 1.60 | 1.03 | -1.37 | -1.31 | -1.32 | 12 |
| **blue** | 2.21 | 0.14 | -0.74 | -0.52 | -0.51 | -0.58 | 12 |
| **cyan** | 1.23 | 1.02 | 0.21 | -0.98 | -0.72 | -0.75 | 12 |
| **magenta** | 1.34 | 1.32 | 1.40 | -1.31 | -1.39 | -1.37 | 12 |
| **yellow** | 1.23 | 1.14 | 0.53 | -0.92 | -0.99 | -0.99 | 12 |

*DOL*

| | CUSP | SLIN | LSLIN | LLIN | LNLIN | LCLIP | N |
|---|---|---|---|---|---|---|---|
| **overall** | 1.41 | 1.25 | -0.20 | -0.66 | -0.82 | -0.98 | 12 |
| **red** | 1.64 | 1.51 | -0.87 | -0.82 | -0.60 | -0.87 | 12 |
| **green** | 0.91 | 0.91 | 0.33 | -0.74 | -0.72 | -0.68 | 12 |
| **blue** | 2.10 | 1.15 | -1.23 | -0.69 | -0.54 | -0.80 | 12 |
| **magenta** | 1.49 | 1.83 | -0.52 | -1.04 | -0.76 | -0.99 | 12 |
| **yellow** | 0.96 | 0.18 | 0.76 | -0.56 | -0.41 | -0.92 | 12 |

*MUS*

| | CUSP | SLIN | LSLIN | LLIN | LNLIN | LCLIP | N |
|---|---|---|---|---|---|---|---|
| **overall** | 0.67 | 1.81 | -0.55 | -0.52 | -0.58 | -0.84 | 12 |
| **red** | 1.71 | 1.99 | -0.81 | -0.97 | -0.84 | -1.08 | 12 |
| **yellow** | 0.26 | -0.55 | -0.12 | 0.39 | 0.00 | 0.02 | 12 |
| **shadow** | -0.32 | -0.23 | 0.25 | 0.18 | 0.13 | -0.02 | 12 |
| **brown** | 0.78 | 0.94 | 0.01 | -0.80 | -0.09 | -0.84 | 12 |
| **blue** | 1.81 | 1.79 | -0.65 | -1.01 | -0.90 | -1.03 | 12 |
| **Caucasian** | 1.22 | 1.55 | -0.29 | -0.71 | -0.82 | -0.94 | 12 |
| **Oriental** | 1.43 | 1.42 | -0.42 | -0.73 | -0.80 | -0.89 | 12 |
| **African** | 1.92 | 1.78 | -0.76 | -0.97 | -0.71 | -1.26 | 12 |

*NAT*

| | CUSP | SLIN | LSLIN | LLIN | LNLIN | LCLIP | N |
|---|---|---|---|---|---|---|---|
| **overall** | 1.26 | 0.24 | -1.37 | -1.73 | 0.63 | 0.97 | 12 |
| **blue** | 1.28 | 0.44 | -1.76 | -1.84 | 0.90 | 0.97 | 12 |
| **green** | -0.43 | -0.72 | -0.15 | -0.21 | 0.68 | 0.83 | 12 |
| **creme** | 0.85 | 0.75 | -0.79 | -0.38 | -0.23 | -0.21 | 12 |
| **shadow** | 1.17 | 0.51 | -1.24 | -1.34 | 0.60 | 0.30 | 12 |
| **grey** | -0.04 | -0.33 | 0.07 | 0.22 | 0.02 | 0.07 | 12 |

*SKI*

| | CUSP | SLIN | LSLIN | LLIN | LNLIN | LCLIP | N |
|---|---|---|---|---|---|---|---|
| **overall** | 1.66 | 1.87 | -0.49 | -1.04 | -0.85 | -1.14 | 12 |
| **red** | 1.78 | 1.92 | 0.02 | -1.15 | -1.49 | -1.08 | 12 |
| **green** | 1.61 | 1.75 | -0.67 | -0.68 | -1.14 | -0.87 | 12 |
| **blue** | 0.84 | 1.99 | -0.87 | -0.62 | -0.66 | -0.69 | 12 |
| **cyan** | 0.30 | 0.32 | -0.20 | -0.07 | -0.11 | -0.24 | 12 |
| **magenta** | 1.85 | 1.85 | -0.77 | -0.99 | -0.99 | -0.95 | 12 |
| **yellow** | 0.86 | 0.82 | 0.61 | -0.61 | -0.41 | -1.28 | 12 |
| **skin** | 1.71 | 0.64 | -0.75 | -0.67 | -0.41 | -0.52 | 12 |

# Inter–Observer Variance

| Image | Mean Stdev. | Max. Stdev. |
|---|---|---|
| **BUS** | 0.12 | 0.26 |
| **DOL** | 0.13 | 0.26 |
| **MUS** | 0.15 | 0.31 |
| **NAT** | 0.14 | 0.28 |
| **SKI** | 0.12 | 0.24 |

# Appendix E

# Experiment 2: Supplementary Data

***Attila the Hun:*** *That's right, yes. A. T. Hun.*
*My parents were Mr and Mrs Norman Hun,*
*but they had a little joke when I was born.*
***Chief Constable:*** *Yes well, Mr Hun …*
***Attila:*** *Oh! Call me 'The' for heaven's sake!*

*Monty Python's Flying Circus (Episode Thirteen)*

# Sample–Size Dependent Parameters

| Sample Size | LG to z–score scaling factor | 95 per cent confidence interval |
|---|---|---|
| **13** | 0.7094 | ±0.38 |
| **39** | 0.6195 | ±0.22 |
| **52** | 0.6047 | ±0.19 |
| **65** | 0.5949 | ±0.17 |

# Nature of Changes Made by GMAs in Experiment 2

| Original | | | GCUSP | | CLLIN | | CARISMA | | |
|---|---|---|---|---|---|---|---|---|---|
| **L*** | **C*** | **$h_{ab}$** | **$\Delta$L*** | **$\Delta$C*** | **$\Delta$L*** | **$\Delta$C*** | **$\Delta$L*** | **$\Delta$C*** | **$\Delta h_{ab}$** |
| **58.06** | **108.38** | **40.80** | -0.34 | -13.17 | 2.22 | -13.10 | -3.00 | -8.80 | -3.55 |
| **52.50** | **100.25** | **40.80** | 0.59 | -12.15 | -1.78 | -4.97 | -3.35 | -7.74 | -3.55 |
| **49.93** | **49.91** | **40.99** | 3.47 | -1.40 | 11.72 | -1.31 | 9.91 | -0.15 | -5.27 |
| **24.98** | **24.77** | **41.81** | 11.32 | -4.78 | 14.38 | -0.63 | 11.63 | -1.53 | -5.19 |
| **74.92** | **25.37** | **40.56** | 2.67 | 0.00 | 8.89 | -0.67 | 7.92 | -1.62 | -3.30 |
| **97.73** | **84.94** | **100.75** | -3.80 | -16.23 | -7.70 | -4.99 | -6.65 | -2.68 | -5.29 |
| **90.05** | **70.13** | **100.81** | 0.47 | 0.00 | -3.70 | 0.00 | -2.52 | -0.60 | -5.27 |
| **90.02** | **34.80** | **100.40** | 0.92 | -0.03 | 1.85 | 0.00 | 1.54 | -0.06 | -4.94 |
| **50.12** | **25.02** | **100.88** | 5.33 | 0.00 | 7.99 | 0.00 | 6.27 | 0.10 | -5.25 |
| **25.08** | **20.37** | **102.08** | 11.44 | -1.44 | 12.36 | 0.00 | 11.10 | -1.43 | -4.96 |
| **86.11** | **114.83** | **143.39** | -16.58 | -46.34 | -21.41 | -41.36 | -35.47 | -30.12 | 4.81 |
| **70.15** | **90.06** | **143.40** | -5.02 | -20.20 | -9.47 | -28.75 | -21.97 | -16.16 | 4.80 |
| **41.58** | **64.75** | **143.39** | 3.08 | 0.00 | 4.89 | -20.67 | -2.64 | -4.36 | 4.81 |
| **19.91** | **24.75** | **143.27** | 9.19 | -0.92 | 12.92 | -7.89 | 10.17 | 0.13 | 4.78 |
| **70.01** | **50.24** | **143.55** | -5.65 | -14.19 | -0.77 | -16.02 | -6.54 | -0.91 | 4.65 |
| **88.91** | **62.40** | **196.36** | -12.59 | -19.46 | -24.91 | -2.18 | -20.51 | -6.34 | 10.21 |
| **80.14** | **50.19** | **195.95** | -7.55 | -13.06 | -23.98 | 0.00 | -20.91 | -3.95 | 10.13 |
| **79.93** | **25.01** | **196.61** | -4.12 | -4.49 | -7.02 | 0.00 | -7.70 | 1.39 | 9.97 |
| **50.17** | **25.11** | **199.61** | 5.32 | 0.00 | -5.44 | 0.00 | -5.64 | 2.39 | 6.97 |
| **25.08** | **20.09** | **196.67** | 8.47 | 0.00 | 0.82 | 0.00 | 1.97 | 3.60 | 9.91 |
| **28.79** | **130.56** | **302.53** | -2.63 | -83.29 | 7.04 | -91.40 | 9.29 | -78.51 | -13.77 |
| **36.65** | **115.14** | **302.67** | -6.46 | -64.15 | 4.22 | -78.30 | 4.49 | -63.43 | -13.64 |
| **25.02** | **100.16** | **302.58** | 0.25 | -58.54 | 9.66 | -68.12 | 11.55 | -54.27 | -13.72 |
| **25.03** | **49.69** | **302.46** | 2.27 | -24.72 | 10.70 | -33.81 | 11.39 | -24.73 | -13.70 |
| **75.08** | **24.94** | **302.57** | -4.50 | -3.34 | 1.80 | -16.96 | -4.34 | -4.70 | -13.73 |
| **63.16** | **108.34** | **330.99** | -13.22 | -48.53 | -10.91 | -55.98 | -4.73 | -46.76 | 9.89 |
| **60.10** | **89.75** | **331.22** | -8.98 | -32.10 | -6.18 | -41.51 | -1.83 | -32.25 | 9.65 |
| **59.95** | **45.00** | **330.93** | -4.56 | -11.42 | 1.76 | -20.39 | 0.23 | -11.60 | 9.85 |
| **24.84** | **25.20** | **330.47** | 7.98 | -3.42 | 12.14 | -11.46 | 10.76 | -2.30 | 9.53 |
| **80.05** | **25.20** | **330.78** | -3.37 | -2.80 | -0.14 | -11.43 | -0.47 | -2.09 | 9.74 |

| Original | | | SLIN | | LLIN | | TRIA | |
|---|---|---|---|---|---|---|---|---|
| L* | C* | $h_{ab}$ | ΔL* | ΔC* | ΔL* | ΔC* | ΔL* | ΔC* |
| 58.06 | 108.38 | 40.80 | 0.00 | 0.00 | 5.43 | -21.93 | -8.80 | -17.76 |
| 52.50 | 100.25 | 40.80 | 0.00 | 0.00 | 6.15 | 0.00 | -5.97 | -15.93 |
| 49.93 | 49.91 | 40.99 | 0.00 | -1.26 | 6.48 | 0.00 | -0.11 | -6.03 |
| 24.98 | 24.77 | 41.81 | 8.00 | -7.93 | 9.71 | -3.99 | 6.37 | 0.57 |
| 74.92 | 25.37 | 40.56 | 0.00 | 0.00 | 3.25 | 0.00 | -0.14 | -3.07 |
| 97.73 | 84.94 | 100.75 | -5.49 | -9.77 | 0.29 | -84.66 | -20.21 | 15.02 |
| 90.05 | 70.13 | 100.81 | -2.40 | -4.19 | 1.29 | 0.00 | -15.69 | 12.85 |
| 90.02 | 34.80 | 100.40 | 0.00 | 0.00 | 1.29 | 0.00 | -6.88 | 7.06 |
| 50.12 | 25.02 | 100.88 | 0.00 | 0.00 | 6.45 | 0.00 | 0.38 | 7.63 |
| 25.08 | 20.37 | 102.08 | 7.06 | -5.77 | 9.69 | -0.97 | 4.48 | 8.03 |
| 86.11 | 114.83 | 143.39 | -15.32 | -48.72 | 1.80 | -82.88 | -41.42 | -41.39 |
| 70.15 | 90.06 | 143.40 | -4.99 | -22.32 | 3.86 | -30.43 | -30.05 | -31.20 |
| 41.58 | 64.75 | 143.39 | 0.00 | 0.00 | 7.56 | 0.00 | -10.74 | -20.45 |
| 19.91 | 24.75 | 143.27 | 9.15 | -7.53 | 10.37 | -2.60 | 1.04 | -3.77 |
| 70.01 | 50.24 | 143.55 | -6.73 | -16.89 | 3.88 | -16.76 | -15.16 | -16.38 |
| 88.91 | 62.40 | 196.36 | -12.45 | -19.97 | 1.44 | -45.25 | -41.74 | -2.12 |
| 80.14 | 50.19 | 195.95 | -8.70 | -14.50 | 2.57 | -22.15 | -32.18 | -1.05 |
| 79.93 | 25.01 | 196.61 | -5.70 | -4.77 | 2.60 | -10.83 | -14.70 | 0.28 |
| 50.17 | 25.11 | 199.61 | 0.00 | 0.00 | 6.45 | 0.00 | -10.83 | 3.36 |
| 25.08 | 20.09 | 196.67 | 0.00 | 0.00 | 9.70 | 0.00 | -1.05 | 3.90 |
| 28.79 | 130.56 | 302.53 | 12.57 | -77.37 | 9.22 | -76.36 | -4.63 | -94.92 |
| 36.65 | 115.14 | 302.67 | 7.33 | -63.21 | 8.20 | -62.06 | -4.16 | -83.62 |
| 25.02 | 100.16 | 302.58 | 12.61 | -50.57 | 9.70 | -52.18 | -0.97 | -71.45 |
| 25.03 | 49.69 | 302.46 | 9.43 | -18.77 | 9.70 | -26.03 | 4.36 | -32.91 |
| 75.08 | 24.94 | 302.57 | -4.65 | -4.63 | 3.23 | -10.62 | 0.57 | -17.38 |
| 63.16 | 108.34 | 330.99 | -6.40 | -52.66 | 4.77 | -60.58 | -30.40 | -66.11 |
| 60.10 | 89.75 | 331.22 | -4.01 | -35.60 | 5.16 | -45.34 | -23.97 | -53.96 |
| 59.95 | 45.00 | 330.93 | -3.58 | -16.17 | 5.18 | -22.84 | -9.41 | -25.83 |
| 24.84 | 25.20 | 330.47 | 7.65 | -7.66 | 9.73 | 0.00 | 1.62 | -11.03 |
| 80.05 | 25.20 | 330.78 | -4.19 | -3.51 | 2.58 | -12.55 | -5.57 | -14.65 |

Note, that the Δ values in the above table were obtained by subtracting the original's values (shown in the first three columns) from the gamut mapped values.

# Overall Accuracy Scores

Note, that the same notation is used here as in Appendix D.

## *Including CLLINLLAB*

| | GCUSP | CLLIN | CLLINLLAB | CARISMA | SLIN | LLIN | TRIA | DEF | N |
|---|---|---|---|---|---|---|---|---|---|
| **Overall (5)** | 0.59 | 0.52 | 0.59 | 0.65 | 0.22 | 0.09 | -1.37 | -1.29 | 65 |

*Excluding CLLINLLAB*

| | GCUSP | CLLIN | CARISMA | SLIN | LLIN | TRIA | DEF | N |
|---|---|---|---|---|---|---|---|---|
| **overall (5)** | 0.68 | 0.66 | 0.78 | 0.32 | 0.16 | -1.35 | -1.24 | 65 |
| **red (4)** | 0.40 | 0.89 | 0.19 | -0.38 | 0.61 | -0.85 | -0.85 | 52 |
| **green (4)** | 0.56 | 0.20 | -0.06 | 0.46 | -0.17 | -0.58 | -0.41 | 52 |
| **blue (5)** | 0.16 | -0.52 | 1.18 | 0.14 | -0.17 | -0.84 | 0.05 | 65 |
| **cyan (1)** | 1.67 | -0.01 | 0.65 | 1.34 | -0.71 | -1.38 | -1.56 | 13 |
| **magenta (3)** | 0.73 | -0.14 | 0.86 | 0.42 | 0.66 | -1.15 | -1.39 | 39 |
| **yellow (4)** | 1.00 | 0.37 | 0.87 | 0.22 | -0.44 | -1.40 | -0.63 | 52 |

# Accuracy Scores for Images and Colour Regions

*BUS*

| | GCUSP | CLLIN | CARISMA | SLIN | LLIN | TRIA | DEF | N |
|---|---|---|---|---|---|---|---|---|
| **overall** | 1.22 | 0.62 | 0.89 | 0.56 | -0.84 | -1.49 | -0.96 | 13 |
| **red** | 0.63 | 0.70 | 0.57 | 0.08 | -0.24 | -0.25 | -1.50 | 13 |
| **green** | 1.54 | 1.44 | -0.17 | 0.73 | -1.10 | -1.02 | -1.41 | 13 |
| **blue** | 0.12 | -1.04 | 1.02 | -0.99 | -1.05 | 0.32 | 1.62 | 13 |
| **cyan** | 1.67 | -0.01 | 0.65 | 1.34 | -0.71 | -1.38 | -1.56 | 13 |
| **magenta** | 1.12 | 0.65 | 1.36 | 0.78 | -0.10 | -2.06 | -1.75 | 13 |
| **yellow** | 1.49 | 0.53 | 0.71 | 0.00 | -1.03 | -1.53 | -0.17 | 13 |

*DOL*

| | GCUSP | CLLIN | CARISMA | SLIN | LLIN | TRIA | DEF | N |
|---|---|---|---|---|---|---|---|---|
| **overall** | 0.70 | 0.94 | 0.74 | 0.33 | 0.18 | -1.17 | -1.71 | 13 |
| **red** | 0.78 | 0.73 | 0.07 | -0.01 | 0.73 | -0.97 | -1.32 | 13 |
| **green** | 1.10 | 1.00 | -0.40 | 1.14 | -0.62 | -1.14 | -1.08 | 13 |
| **blue** | 0.15 | -0.51 | 1.78 | -0.69 | -0.60 | -1.03 | 0.90 | 13 |
| **magenta** | 0.67 | 0.07 | 0.99 | 0.37 | 0.89 | -1.03 | -1.97 | 13 |
| **yellow** | 1.15 | 0.15 | 0.92 | 0.37 | -0.48 | -1.55 | -0.56 | 13 |

*MUS*

| | GCUSP | CLLIN | CARISMA | SLIN | LLIN | TRIA | DEF | N |
|---|---|---|---|---|---|---|---|---|
| **overall** | 0.51 | 1.20 | 0.96 | -0.29 | 1.16 | -1.60 | -1.93 | 13 |
| **red** | -0.09 | 1.92 | 0.88 | -1.51 | 1.46 | -1.65 | -1.02 | 13 |
| **yellow** | 0.43 | 0.93 | 1.13 | 0.13 | 0.53 | -1.04 | -2.11 | 13 |
| **shadow** | 0.57 | 0.17 | 0.97 | -0.70 | 1.33 | -1.26 | -1.08 | 13 |
| **brown** | -0.89 | 1.48 | 0.10 | -0.80 | 1.64 | -1.36 | -0.16 | 13 |
| **cyan** | 0.50 | 0.11 | 1.12 | 1.15 | 0.34 | -2.17 | -1.05 | 13 |
| **skin** | 0.52 | 1.13 | 0.26 | -0.59 | 1.21 | -0.60 | -1.92 | 13 |

*NAT*

| | GCUSP | CLLIN | CARISMA | SLIN | LLIN | TRIA | DEF | N |
|---|---|---|---|---|---|---|---|---|
| **overall** | 0.28 | 1.16 | 1.70 | 0.26 | -0.28 | -1.16 | -1.95 | 13 |
| **blue** | 0.17 | 1.04 | 2.07 | 0.55 | -0.69 | -1.56 | -1.58 | 13 |
| **green** | -0.45 | -0.52 | 0.48 | -0.51 | -0.14 | 0.20 | 0.94 | 13 |
| **creme** | 0.30 | 0.94 | 0.62 | 0.33 | 0.27 | -0.12 | -2.34 | 13 |
| **shadow** | -0.17 | 0.55 | 0.48 | 0.11 | 0.45 | -0.38 | -1.03 | 13 |

*SKI*

| | GCUSP | CLLIN | CARISMA | SLIN | LLIN | TRIA | DEF | N |
|---|---|---|---|---|---|---|---|---|
| **overall** | 0.85 | -0.14 | 0.37 | 0.66 | -0.14 | -1.70 | -0.65 | 13 |
| **red** | 0.37 | 1.15 | -0.40 | -0.74 | 1.41 | -1.53 | -0.26 | 13 |
| **green** | 1.39 | -0.63 | -0.64 | 1.60 | 0.89 | -1.54 | -1.06 | 13 |
| **blue** | 0.39 | -1.08 | 1.36 | 0.87 | 0.30 | -1.69 | -0.15 | 13 |
| **magenta** | 0.57 | -0.91 | 0.45 | 0.21 | 1.40 | -0.82 | -0.89 | 13 |
| **yellow** | 1.41 | -0.23 | 1.16 | 0.60 | -0.94 | -1.49 | -0.51 | 13 |

# Inter–Observer Variance

| Image | Mean Stdev. | Max. Stdev. |
|---|---|---|
| **BUS** | 0.14 | 0.28 |
| **DOL** | 0.16 | 0.29 |
| **MUS** | 0.13 | 0.25 |
| **NAT** | 0.16 | 0.35 |
| **SKI** | 0.16 | 0.29 |

# Appendix F

# Experiment 3: Supplementary Data – Results

*Science without religion is lame,*
*religion without science is blind.*
*Albert Einstein (Science, Philosophy and Religion)*

# Sample–Size Dependent Parameters

| Sample Size | LG to z–score scaling factor | 95 per cent confidence interval |
|---|---|---|
| **10** | 0.7426 | ±0.44 |
| **20** | 0.6663 | ±0.31 |
| **30** | 0.6356 | ±0.25 |
| **40** | 0.6181 | ±0.22 |
| **50** | 0.6065 | ±0.20 |
| **60** | 0.5982 | ±0.18 |
| **80** | 0.5870 | ±0.15 |
| **100** | 0.5796 | ±0.14 |

# Overall Accuracy Scores

Note, that the same notation is used here as in Appendix D.

| | GCUSP | CARISMA | LCUSPH | UniGMA | LLIN | N |
|---|---|---|---|---|---|---|
| **overall (10)** | 0.22 | 0.24 | -0.15 | -0.08 | -0.22 | 100 |
| **red (8)** | 0.40 | -0.35 | -0.12 | -0.20 | 0.26 | 80 |
| **green (8)** | 0.09 | 0.26 | -0.23 | 0.12 | -0.24 | 80 |
| **blue (10)** | -0.09 | 0.20 | 0.05 | -0.12 | -0.04 | 100 |
| **cyan (2)** | 0.47 | 0.95 | 0.50 | 0.43 | -2.35 | 20 |
| **magenta (6)** | -0.01 | 0.31 | 0.28 | 0.04 | -0.63 | 60 |
| **yellow (8)** | -0.02 | 0.97 | 0.03 | 0.00 | -0.99 | 80 |

# Accuracy Scores for Plain Paper

## *Overall*

| | GCUSP | CARISMA | LCUSPH | UniGMA | LLIN | N |
|---|---|---|---|---|---|---|
| **overall (5)** | 0.36 | 0.18 | -0.02 | -0.19 | -0.33 | 50 |
| **red (4)** | 0.35 | -0.51 | 0.31 | -0.22 | 0.08 | 40 |
| **green (4)** | 0.17 | 0.28 | -0.18 | -0.06 | -0.21 | 40 |
| **blue (5)** | -0.13 | 0.34 | 0.17 | -0.36 | -0.03 | 50 |
| **cyan (1)** | 0.35 | 1.21 | 0.45 | 0.11 | -2.12 | 10 |
| **magenta (3)** | 0.03 | 0.41 | 0.20 | -0.03 | -0.61 | 30 |
| **yellow (4)** | 0.08 | 1.17 | 0.05 | -0.15 | -1.14 | 40 |

In the following tables, the *Range* column contains the difference between the largest and the smallest accuracy score in a row and the *Plain/Glossy* column contains the ratio of the accuracy score ranges for the plain and glossy substrates respectively (again for a given row).

*BUS*

| | GCUSP | CARISMA | LCUSPH | UniGMA | LLIN | Range | Plain/Glossy | N |
|---|---|---|---|---|---|---|---|---|
| **overall** | 1.44 | 0.27 | 0.13 | -0.10 | -1.74 | 3.19 | 1.29 | 10 |
| **red** | 1.99 | -1.49 | -0.45 | -0.84 | 0.79 | 3.48 | 1.99 | 10 |
| **green** | 0.40 | 2.09 | -0.37 | -0.32 | -1.81 | 3.90 | 1.16 | 10 |
| **blue** | 0.78 | 0.54 | 0.52 | 0.16 | -2.00 | 2.78 | 1.04 | 10 |
| **cyan** | 0.41 | 1.23 | 0.51 | 0.13 | -2.28 | 3.52 | 1.19 | 10 |
| **magenta** | 0.42 | 0.52 | 0.91 | 0.61 | -2.47 | 3.39 | 1.59 | 10 |
| **yellow** | 0.06 | 1.93 | 0.35 | -0.16 | -2.19 | 4.12 | 1.02 | 10 |

*DOL*

| | GCUSP | CARISMA | LCUSPH | UniGMA | LLIN | Range | Plain/Glossy | N |
|---|---|---|---|---|---|---|---|---|
| **overall** | 0.94 | 0.07 | -0.55 | -0.86 | 0.40 | 1.80 | 2.20 | 10 |
| **red** | 0.38 | -0.33 | 0.17 | -0.32 | 0.10 | 0.70 | 0.26 | 10 |
| **green** | 0.66 | 0.78 | -0.07 | -0.08 | -1.30 | 2.08 | 1.54 | 10 |
| **blue** | -1.35 | 0.33 | 1.44 | -1.37 | 0.95 | 2.81 | 1.79 | 10 |
| **magenta** | 0.43 | 0.80 | -0.33 | 0.27 | -1.16 | 1.96 | 4.06 | 10 |
| **yellow** | 0.44 | 2.19 | -0.46 | -0.27 | -1.90 | 4.09 | 1.23 | 10 |

*MUS*

| | GCUSP | CARISMA | LCUSPH | UniGMA | LLIN | Range | Plain/Glossy | N |
|---|---|---|---|---|---|---|---|---|
| **overall** | 0.07 | -0.68 | 0.86 | 0.11 | -0.35 | 1.54 | 1.96 | 10 |
| **red** | -0.15 | -0.74 | 1.55 | 0.26 | -0.92 | 2.47 | 3.08 | 10 |
| **yellow** | 0.05 | 0.18 | 0.20 | -0.25 | -0.18 | 0.45 | 1.22 | 10 |
| **shadow** | -0.33 | 0.00 | 0.35 | 0.42 | -0.43 | 0.85 | 4.91 | 10 |
| **brown** | 1.19 | -1.90 | 0.17 | -0.06 | 0.60 | 3.09 | 1.66 | 10 |
| **blue** | 0.32 | -0.71 | 0.14 | -0.11 | 0.36 | 1.07 | 1.08 | 10 |
| **skin** | -0.20 | -0.15 | 0.75 | 0.05 | -0.45 | 1.19 | 0.99 | 10 |

*NAT*

| | GCUSP | CARISMA | LCUSPH | UniGMA | LLIN | Range | Plain/Glossy | N |
|---|---|---|---|---|---|---|---|---|
| **overall** | 0.25 | 0.57 | -0.74 | -0.21 | 0.13 | 1.31 | 0.75 | 10 |
| **blue** | 0.06 | 1.71 | -1.15 | -0.49 | -0.13 | 2.87 | 0.91 | 10 |
| **green** | 0.27 | -0.52 | -0.69 | 0.09 | 0.84 | 1.53 | 1.00 | 10 |
| **highlight** | 0.17 | -0.20 | -0.31 | 0.03 | 0.31 | 0.61 | 1.11 | 10 |
| **shadow** | 0.26 | -0.07 | 0.10 | -0.13 | -0.16 | 0.42 | 2.02 | 10 |

*SKI*

| | GCUSP | CARISMA | LCUSPH | UniGMA | LLIN | Range | Plain/Glossy | N |
|---|---|---|---|---|---|---|---|---|
| **overall** | -0.10 | 0.90 | 0.33 | -0.17 | -0.95 | 1.85 | 1.50 | 10 |
| **red** | 0.00 | -0.13 | 0.16 | -0.43 | 0.40 | 0.83 | 0.99 | 10 |
| **green** | -0.43 | -0.35 | 0.31 | -0.14 | 0.61 | 1.04 | 1.02 | 10 |
| **blue** | -1.06 | 1.49 | 0.60 | -1.28 | 0.25 | 2.77 | 1.27 | 10 |
| **magenta** | -0.37 | 0.40 | 0.22 | -0.73 | 0.48 | 1.22 | 0.37 | 10 |
| **yellow** | -0.06 | 2.47 | -0.13 | -0.19 | -2.09 | 4.57 | 1.47 | 10 |

# Accuracy Scores for Glossy Paper

## *Overall*

| | GCUSP | CARISMA | LCUSPH | UniGMA | LLIN | N |
|---|---|---|---|---|---|---|
| **overall (5)** | 0.10 | 0.33 | -0.30 | 0.01 | -0.14 | 50 |
| **red (4)** | 0.50 | -0.24 | -0.57 | -0.19 | 0.50 | 40 |
| **green (4)** | 0.01 | 0.28 | -0.31 | 0.32 | -0.30 | 40 |
| **blue (5)** | -0.07 | 0.09 | -0.07 | 0.10 | -0.06 | 50 |
| **cyan (1)** | 0.46 | 0.67 | 0.43 | 0.70 | -2.26 | 10 |
| **magenta (3)** | -0.05 | 0.24 | 0.40 | 0.13 | -0.71 | 30 |
| **yellow (4)** | -0.12 | 0.88 | 0.02 | 0.16 | -0.95 | 40 |

## *BUS*

| | GCUSP | CARISMA | LCUSPH | UniGMA | LLIN | Range | N |
|---|---|---|---|---|---|---|---|
| **overall** | 0.78 | 0.76 | -0.43 | 0.58 | -1.69 | 2.47 | 10 |
| **red** | 0.81 | -0.19 | -0.93 | -0.32 | 0.64 | 1.74 | 10 |
| **green** | 0.60 | 1.38 | -0.10 | 0.11 | -1.99 | 3.36 | 10 |
| **blue** | 0.98 | 0.69 | -0.60 | 0.64 | -1.70 | 2.68 | 10 |
| **cyan** | 0.46 | 0.67 | 0.43 | 0.70 | -2.26 | 2.96 | 10 |
| **magenta** | 0.17 | 0.83 | -0.01 | 0.31 | -1.29 | 2.12 | 10 |
| **yellow** | -0.42 | 1.92 | 0.00 | 0.62 | -2.12 | 4.05 | 10 |

## *DOL*

| | GCUSP | CARISMA | LCUSPH | UniGMA | LLIN | Range | N |
|---|---|---|---|---|---|---|---|
| **overall** | 0.29 | -0.32 | -0.32 | -0.14 | 0.50 | 0.82 | 10 |
| **red** | 1.40 | -1.30 | -1.12 | -0.23 | 1.24 | 2.71 | 10 |
| **green** | 0.62 | 0.58 | -0.44 | -0.03 | -0.73 | 1.35 | 10 |
| **blue** | -0.25 | -0.96 | 0.61 | -0.01 | 0.60 | 1.57 | 10 |
| **magenta** | -0.14 | -0.24 | 0.24 | 0.00 | 0.14 | 0.48 | 10 |
| **yellow** | -0.36 | 2.04 | -0.44 | 0.04 | -1.28 | 3.31 | 10 |

## *MUS*

| | GCUSP | CARISMA | LCUSPH | UniGMA | LLIN | Range | N |
|---|---|---|---|---|---|---|---|
| **overall** | 0.07 | -0.14 | -0.14 | -0.29 | 0.50 | 0.78 | 10 |
| **red** | 0.21 | 0.17 | -0.28 | -0.45 | 0.35 | 0.80 | 10 |
| **yellow** | 0.16 | -0.19 | 0.18 | -0.14 | 0.00 | 0.37 | 10 |
| **shadow** | -0.07 | 0.07 | -0.03 | -0.07 | 0.10 | 0.17 | 10 |
| **brown** | 0.41 | -0.57 | -0.50 | -0.60 | 1.27 | 1.87 | 10 |
| **blue** | 0.09 | -0.70 | 0.29 | 0.21 | 0.10 | 0.99 | 10 |
| **skin** | 0.35 | 0.21 | -0.27 | -0.75 | 0.45 | 1.21 | 10 |

*NAT*

| | GCUSP | CARISMA | LCUSPH | UniGMA | LLIN | Range | N |
|---|---|---|---|---|---|---|---|
| **overall** | -0.08 | 1.03 | -0.71 | 0.17 | -0.42 | 1.74 | 10 |
| **blue** | -0.06 | 1.97 | -0.94 | 0.20 | -1.17 | 3.14 | 10 |
| **green** | -0.65 | -0.27 | -0.47 | 0.88 | 0.51 | 1.53 | 10 |
| **highlight** | 0.15 | 0.21 | -0.22 | -0.35 | 0.21 | 0.55 | 10 |
| **shadow** | -0.07 | 0.14 | 0.03 | -0.03 | -0.07 | 0.21 | 10 |

*SKI*

| | GCUSP | CARISMA | LCUSPH | UniGMA | LLIN | Range | N |
|---|---|---|---|---|---|---|---|
| **overall** | -0.32 | 0.91 | -0.27 | -0.07 | -0.25 | 1.23 | 10 |
| **red** | 0.18 | -0.06 | -0.49 | 0.03 | 0.35 | 0.85 | 10 |
| **green** | -0.26 | -0.21 | -0.41 | 0.61 | 0.26 | 1.02 | 10 |
| **blue** | -1.19 | 0.49 | -0.02 | -0.27 | 0.99 | 2.18 | 10 |
| **magenta** | -0.12 | 0.48 | 1.36 | 0.18 | -1.90 | 3.26 | 10 |
| **yellow** | -0.21 | 1.34 | 0.37 | 0.26 | -1.76 | 3.10 | 10 |

# Inter–Observer Variance

*Plain*

| Image | Mean Stdev. | Max. Stdev. |
|---|---|---|
| **BUS** | 0.13 | 0.37 |
| **DOL** | 0.18 | 0.42 |
| **MUS** | 0.20 | 0.35 |
| **NAT** | 0.21 | 0.41 |
| **SKI** | 0.19 | 0.37 |

*Glossy*

| Image | Mean Stdev. | Max. Stdev. |
|---|---|---|
| **BUS** | 0.17 | 0.30 |
| **DOL** | 0.17 | 0.32 |
| **MUS** | 0.21 | 0.38 |
| **NAT** | 0.17 | 0.24 |
| **SKI** | 0.20 | 0.32 |

Appendix G

# Experiment 3: Supplementary Data – Changes Caused by GMAs

*The word 'good' has many meanings.*
*For example, if a man were to shoot his grandmother*
*at a range of five hundred yards, I should call him a good shot,*
*but not necessarily a good man.*

*G. K. Chesterton*

# Nature of Changes Made by GMAs in Experiment 3

Note, that the Δ values in the following tables were obtained by subtracting the original's values (shown in the first three columns) from the gamut mapped values.

## *Plain Paper*

| Original | | | CARISMA | | | GCUSP | | LCUSPH | | |
|---|---|---|---|---|---|---|---|---|---|---|
| J | C | h | ΔJ | ΔC | Δh | ΔJ | ΔC | ΔJ | ΔC | Δh |
| 52.09 | 125.16 | 28.17 | 3.42 | -27.63 | -6.00 | 0.14 | -21.83 | 3.57 | -27.81 | -6.00 |
| 45.38 | 122.18 | 27.68 | 6.29 | -17.91 | -5.84 | 1.23 | -15.23 | 6.44 | -18.25 | -5.84 |
| 40.43 | 70.47 | 33.16 | 8.62 | 0.02 | -5.90 | 4.97 | -13.85 | 8.57 | 0.00 | -5.90 |
| 16.95 | 45.20 | 33.86 | 13.55 | -3.45 | -5.88 | 14.11 | -10.54 | 13.38 | -3.17 | -5.88 |
| 68.90 | 35.72 | 36.69 | 4.82 | -0.08 | -5.82 | 3.18 | 0.00 | 4.48 | 0.00 | -5.82 |
| 96.40 | 69.04 | 104.27 | -6.05 | -2.03 | -4.43 | -3.26 | -13.39 | -2.17 | -13.29 | -4.43 |
| 86.58 | 62.07 | 103.20 | 0.24 | -0.44 | -4.45 | 0.83 | 0.00 | 1.93 | 0.00 | -4.45 |
| 86.90 | 36.01 | 98.81 | 4.24 | -0.16 | -4.54 | 1.33 | 0.00 | 1.83 | -1.03 | -4.54 |
| 38.51 | 35.80 | 99.08 | 13.75 | -0.46 | -4.54 | 10.78 | -4.14 | 11.90 | -2.77 | -4.54 |
| 16.28 | 32.32 | 101.37 | 17.19 | -1.20 | -4.49 | 15.83 | -3.92 | 16.50 | -2.50 | -4.49 |
| 77.65 | 100.34 | 143.88 | -23.96 | -18.14 | 8.37 | -9.10 | -30.92 | -11.19 | -34.82 | 8.37 |
| 58.52 | 92.83 | 144.65 | -8.53 | -10.45 | 8.47 | 0.00 | -8.77 | 0.56 | -19.32 | 8.47 |
| 28.27 | 83.99 | 145.98 | 10.32 | -1.05 | 8.64 | 6.21 | -20.94 | 10.32 | 0.00 | 8.64 |
| 12.54 | 42.64 | 145.49 | 15.17 | -0.30 | 8.57 | 14.50 | -11.18 | 13.92 | -4.57 | 8.57 |
| 59.68 | 60.62 | 144.44 | -4.50 | -2.24 | 8.44 | -1.33 | -14.88 | -2.53 | -18.89 | 8.44 |
| 81.96 | 67.65 | 197.74 | -15.12 | -4.95 | 15.30 | -10.03 | -14.78 | -8.15 | -14.20 | 15.30 |
| 71.40 | 62.32 | 197.29 | -8.00 | -2.94 | 15.24 | -4.64 | -9.81 | -2.08 | -9.14 | 15.24 |
| 72.55 | 40.17 | 196.92 | -3.94 | 0.40 | 15.19 | -4.16 | -6.38 | -2.32 | -5.83 | 15.19 |
| 37.45 | 48.00 | 200.34 | -0.14 | -0.72 | 14.64 | 5.17 | 0.00 | 9.00 | 0.00 | 14.64 |
| 15.73 | 43.41 | 198.40 | 5.36 | 0.15 | 15.13 | 7.58 | 0.00 | 12.13 | 0.00 | 15.13 |
| 18.55 | 115.01 | 265.26 | -1.34 | -39.93 | -1.71 | 0.65 | -40.60 | 6.96 | -42.05 | -1.71 |
| 25.83 | 103.93 | 274.68 | -6.97 | -33.76 | -0.01 | -1.15 | -35.35 | 4.36 | -37.44 | -0.01 |
| 16.41 | 101.57 | 272.84 | 1.95 | -30.27 | -0.35 | 2.18 | -30.32 | 8.91 | -32.39 | -0.35 |
| 16.71 | 68.94 | 286.98 | 5.11 | -16.29 | 2.20 | 4.26 | -21.45 | 9.75 | -19.56 | 2.20 |
| 68.34 | 34.57 | 296.66 | -3.30 | -3.62 | 3.95 | -3.29 | -4.56 | -2.55 | -4.84 | 3.95 |
| 58.41 | 99.88 | 335.13 | -16.65 | -20.49 | 10.88 | -9.90 | -33.44 | -4.90 | -30.53 | 10.88 |
| 53.82 | 90.30 | 334.93 | -10.90 | -14.34 | 10.85 | -6.64 | -25.65 | -1.68 | -23.69 | 10.85 |
| 51.46 | 57.09 | 333.60 | -2.60 | -2.66 | 10.61 | -3.91 | -14.59 | 0.16 | -12.97 | 10.61 |
| 16.84 | 44.75 | 332.40 | 10.39 | -0.25 | 10.39 | 7.63 | -7.22 | 11.97 | 0.00 | 10.39 |
| 75.32 | 33.63 | 333.19 | -2.25 | 0.49 | 10.53 | -3.90 | -4.24 | -1.34 | -3.25 | 10.53 |

| **Original** | | | **UniGMA** | | | **LLIN** | |
|---|---|---|---|---|---|---|---|
| **J** | **C** | **h** | **ΔJ** | **ΔC** | **Δh** | **ΔJ** | **ΔC** |
| **52.09** | **125.16** | **28.17** | -0.77 | -19.80 | -6.00 | 6.89 | -35.35 |
| **45.38** | **122.18** | **27.68** | 0.67 | -8.44 | -5.84 | 7.86 | -19.57 |
| **40.43** | **70.47** | **33.16** | 3.31 | -3.90 | -5.90 | 8.57 | -7.29 |
| **16.95** | **45.20** | **33.86** | 12.22 | -9.54 | -5.88 | 11.95 | -12.80 |
| **68.90** | **35.72** | **36.69** | 3.18 | 0.00 | -5.82 | 4.48 | 0.00 |
| **96.40** | **69.04** | **104.27** | -2.27 | -14.17 | -4.43 | 0.52 | -46.35 |
| **86.58** | **62.07** | **103.20** | 0.83 | 0.00 | -4.45 | 1.93 | 0.00 |
| **86.90** | **36.01** | **98.81** | 1.05 | -1.28 | -4.54 | 1.89 | 0.00 |
| **38.51** | **35.80** | **99.08** | 10.93 | -4.68 | -4.54 | 8.85 | -1.67 |
| **16.28** | **32.32** | **101.37** | 16.04 | -3.85 | -4.49 | 12.05 | -9.14 |
| **77.65** | **100.34** | **143.88** | -12.21 | -34.24 | 8.37 | 3.22 | -51.51 |
| **58.52** | **92.83** | **144.65** | -2.21 | -17.02 | 8.47 | 5.97 | -16.91 |
| **28.27** | **83.99** | **145.98** | 3.57 | -11.44 | 8.64 | 10.32 | -10.52 |
| **12.54** | **42.64** | **145.49** | 12.62 | -11.84 | 8.57 | 12.59 | -14.89 |
| **59.68** | **60.62** | **144.44** | -4.33 | -19.47 | 8.44 | 5.80 | -12.15 |
| **81.96** | **67.65** | **197.74** | -8.68 | -13.39 | 15.30 | 2.60 | -32.77 |
| **71.40** | **62.32** | **197.29** | -3.02 | -7.62 | 15.24 | 4.11 | -17.21 |
| **72.55** | **40.17** | **196.92** | -3.12 | -5.61 | 15.19 | 3.95 | -11.92 |
| **37.45** | **48.00** | **200.34** | 5.17 | 0.00 | 14.64 | 9.00 | 0.00 |
| **15.73** | **43.41** | **198.40** | 7.58 | 0.00 | 15.13 | 12.13 | 0.00 |
| **18.55** | **115.01** | **265.26** | 1.47 | -39.11 | -1.71 | 11.72 | -44.53 |
| **25.83** | **103.93** | **274.68** | -1.51 | -39.22 | -0.01 | 10.67 | -39.34 |
| **16.41** | **101.57** | **272.84** | 2.07 | -32.72 | -0.35 | 12.03 | -32.75 |
| **16.71** | **68.94** | **286.98** | 4.48 | -21.62 | 2.20 | 11.99 | -20.15 |
| **68.34** | **34.57** | **296.66** | -3.23 | -4.50 | 3.95 | 4.56 | -12.01 |
| **58.41** | **99.88** | **335.13** | -6.75 | -27.99 | 10.88 | 5.98 | -48.81 |
| **53.82** | **90.30** | **334.93** | -4.19 | -21.91 | 10.85 | 6.65 | -39.29 |
| **51.46** | **57.09** | **333.60** | -1.55 | -12.17 | 10.61 | 6.99 | -23.59 |
| **16.84** | **44.75** | **332.40** | 8.95 | -9.22 | 10.39 | 11.97 | -0.65 |
| **75.32** | **33.63** | **333.19** | -1.59 | -3.08 | 10.53 | 3.55 | -14.10 |

## *Glossy Paper*

| **Original** | | | **CARISMA** | | | **GCUSP** | | **LCUSPH** | | |
|---|---|---|---|---|---|---|---|---|---|---|
| **J** | **C** | **h** | **ΔJ** | **ΔC** | **Δh** | **ΔJ** | **ΔC** | **ΔJ** | **ΔC** | **Δh** |
| **52.09** | **125.16** | **28.17** | -1.53 | -5.60 | -4.51 | -0.08 | -10.06 | 2.42 | -13.99 | -4.51 |
| **45.38** | **122.18** | **27.68** | 4.18 | -0.50 | -4.39 | 0.53 | 0.00 | 4.57 | -1.22 | -4.39 |
| **40.43** | **70.47** | **33.16** | 7.11 | 0.34 | -4.41 | 2.08 | -2.17 | 5.08 | 0.00 | -4.41 |
| **16.95** | **45.20** | **33.86** | 8.26 | -0.73 | -4.39 | 7.32 | -4.59 | 7.57 | -0.94 | -4.39 |
| **68.90** | **35.72** | **36.69** | 8.39 | -1.97 | -4.33 | 1.89 | 0.00 | 2.65 | 0.00 | -4.33 |
| **96.40** | **69.04** | **104.27** | -4.89 | -1.26 | -2.85 | -3.54 | -17.56 | -2.51 | -17.22 | -2.85 |
| **86.58** | **62.07** | **103.20** | -0.90 | -0.38 | -2.88 | 0.49 | 0.00 | 1.14 | 0.00 | -2.88 |
| **86.90** | **36.01** | **98.81** | 2.98 | -0.18 | -2.97 | 0.79 | 0.00 | 1.12 | 0.00 | -2.97 |
| **38.51** | **35.80** | **99.08** | 6.25 | -0.21 | -2.97 | 4.75 | -0.80 | 5.24 | 0.00 | -2.97 |
| **16.28** | **32.32** | **101.37** | 8.04 | -0.50 | -2.92 | 8.01 | -1.35 | 8.86 | -0.85 | -2.92 |
| **77.65** | **100.34** | **143.88** | -24.56 | -16.33 | 5.88 | -11.10 | -31.13 | -12.34 | -31.52 | 5.88 |
| **58.52** | **92.83** | **144.65** | -10.16 | -9.18 | 5.92 | -1.30 | -10.07 | -0.75 | -13.81 | 5.92 |
| **28.27** | **83.99** | **145.98** | 6.12 | -1.09 | 5.99 | 1.88 | -2.50 | 6.12 | 0.00 | 5.99 |
| **12.54** | **42.64** | **145.49** | 7.66 | -0.07 | 5.96 | 7.10 | -4.60 | 7.46 | 0.00 | 5.96 |
| **59.68** | **60.62** | **144.44** | -7.88 | -1.68 | 5.91 | -4.11 | -16.50 | -4.40 | -16.03 | 5.91 |
| **81.96** | **67.65** | **197.74** | -16.19 | -5.20 | 8.68 | -10.00 | -15.12 | -8.84 | -15.07 | 8.68 |
| **71.40** | **62.32** | **197.29** | -9.88 | -3.20 | 8.66 | -4.64 | -9.49 | -3.01 | -9.17 | 8.66 |
| **72.55** | **40.17** | **196.92** | -6.31 | 0.34 | 8.64 | -4.73 | -6.46 | -3.61 | -6.27 | 8.64 |
| **37.45** | **48.00** | **200.34** | -4.18 | -1.04 | 8.19 | 3.06 | 0.00 | 5.33 | 0.00 | 8.19 |
| **15.73** | **43.41** | **198.40** | -0.47 | -0.09 | 8.56 | 4.49 | 0.00 | 7.19 | 0.00 | 8.56 |
| **18.55** | **115.01** | **265.26** | -1.40 | -37.30 | -4.20 | -0.99 | -39.39 | 2.87 | -37.69 | -4.20 |
| **25.83** | **103.93** | **274.68** | -3.98 | -33.00 | -2.44 | -2.64 | -33.99 | 0.66 | -34.64 | -2.44 |
| **16.41** | **101.57** | **272.84** | 0.30 | -29.16 | -2.78 | 0.59 | -28.15 | 4.57 | -29.72 | -2.78 |
| **16.71** | **68.94** | **286.98** | 1.13 | -17.05 | -0.13 | 2.14 | -18.41 | 5.35 | -19.03 | -0.13 |
| **68.34** | **34.57** | **296.66** | -6.67 | -0.13 | 1.69 | -4.38 | -4.26 | -4.01 | -4.47 | 1.69 |
| **58.41** | **99.88** | **335.13** | -16.15 | -17.40 | 8.90 | -9.72 | -31.03 | -5.80 | -27.67 | 8.90 |
| **53.82** | **90.30** | **334.93** | -10.91 | -11.92 | 8.86 | -6.79 | -23.85 | -2.80 | -20.54 | 8.86 |
| **51.46** | **57.09** | **333.60** | -4.08 | -1.95 | 8.61 | -4.65 | -13.46 | -1.44 | -11.40 | 8.61 |
| **16.84** | **44.75** | **332.40** | 5.93 | -0.12 | 8.39 | 4.62 | -3.44 | 7.09 | 0.00 | 8.39 |
| **75.32** | **33.63** | **333.19** | -2.72 | 0.58 | 8.54 | -4.23 | -3.76 | -2.27 | -2.95 | 8.54 |

| Original | | | UniGMA | | | LLIN | |
|---|---|---|---|---|---|---|---|
| J | C | h | ΔJ | ΔC | Δh | ΔJ | ΔC |
| 52.09 | 125.16 | 28.17 | -0.22 | -7.64 | -4.51 | 4.08 | -17.35 |
| 45.38 | 122.18 | 27.68 | 0.53 | 0.00 | -4.39 | 4.66 | 0.00 |
| 40.43 | 70.47 | 33.16 | 1.82 | 0.00 | -4.41 | 5.08 | 0.00 |
| 16.95 | 45.20 | 33.86 | 6.86 | -4.42 | -4.39 | 7.08 | -4.68 |
| 68.90 | 35.72 | 36.69 | 1.89 | 0.00 | -4.33 | 2.65 | 0.00 |
| 96.40 | 69.04 | 104.27 | -2.28 | -15.99 | -2.85 | 0.31 | -42.36 |
| 86.58 | 62.07 | 103.20 | 0.49 | 0.00 | -2.88 | 1.14 | 0.00 |
| 86.90 | 36.01 | 98.81 | 0.79 | 0.00 | -2.97 | 1.12 | 0.00 |
| 38.51 | 35.80 | 99.08 | 4.49 | -0.63 | -2.97 | 5.24 | 0.00 |
| 16.28 | 32.32 | 101.37 | 8.26 | -1.46 | -2.92 | 7.14 | -1.03 |
| 77.65 | 100.34 | 143.88 | -12.72 | -30.94 | 5.88 | 1.91 | -52.70 |
| 58.52 | 92.83 | 144.65 | -2.55 | -13.02 | 5.92 | 3.54 | -15.64 |
| 28.27 | 83.99 | 145.98 | 1.61 | 0.00 | 5.99 | 6.12 | 0.00 |
| 12.54 | 42.64 | 145.49 | 6.38 | -3.78 | 5.96 | 7.46 | -1.22 |
| 59.68 | 60.62 | 144.44 | -5.89 | -17.60 | 5.91 | 3.44 | -11.36 |
| 81.96 | 67.65 | 197.74 | -12.18 | -11.11 | 8.68 | 1.54 | -31.82 |
| 71.40 | 62.32 | 197.29 | -3.96 | -8.20 | 8.66 | 2.44 | -15.58 |
| 72.55 | 40.17 | 196.92 | -4.37 | -5.99 | 8.64 | 2.34 | -10.84 |
| 37.45 | 48.00 | 200.34 | 3.15 | 0.00 | 8.19 | 5.33 | 0.00 |
| 15.73 | 43.41 | 198.40 | 4.52 | 0.00 | 8.56 | 7.19 | 0.00 |
| 18.55 | 115.01 | 265.26 | -1.63 | -38.66 | -4.20 | 6.95 | -41.60 |
| 25.83 | 103.93 | 274.68 | -4.33 | -35.03 | -2.44 | 6.32 | -36.98 |
| 16.41 | 101.57 | 272.84 | 0.04 | -31.05 | -2.78 | 7.13 | -30.07 |
| 16.71 | 68.94 | 286.98 | 0.10 | -21.42 | -0.13 | 7.10 | -17.52 |
| 68.34 | 34.57 | 296.66 | -4.72 | -3.91 | 1.69 | 2.70 | -10.78 |
| 58.41 | 99.88 | 335.13 | -7.78 | -25.58 | 8.90 | 3.55 | -43.85 |
| 53.82 | 90.30 | 334.93 | -4.48 | -17.34 | 8.86 | 3.94 | -33.46 |
| 51.46 | 57.09 | 333.60 | -3.06 | -10.69 | 8.61 | 4.14 | -19.88 |
| 16.84 | 44.75 | 332.40 | 4.49 | -2.98 | 8.39 | 7.09 | 0.00 |
| 75.32 | 33.63 | 333.19 | -2.51 | -2.73 | 8.54 | 2.11 | -12.76 |

# Statistics of Changes Caused by GMAs

*Plain Paper*

| GMA | median ($\Delta E_{97s}$) | median (\|ΔJ\|) | median (\|ΔC\|) | Δ(C/J) | (\|ΔC\|/\|ΔJ\|) |
|---|---|---|---|---|---|
| GCUSP | 15.02 | 4.21 | 12.29 | -0.30 | 2.45 |
| CARISMA | 15.81 | 6.17 | 2.45 | -0.03 | 0.43 |
| LCUSPH | 17.23 | 5.67 | 7.48 | -0.32 | 2.22 |
| UniGMA | 16.75 | 3.27 | 10.49 | -0.28 | 2.23 |
| LLIN | 17.60 | 6.94 | 14.50 | -0.61 | 2.56 |

## *Glossy Paper*

| GMA | median ($\Delta E_{97s}$) | median ($\lvert\Delta J\rvert$) | median ($\lvert\Delta C\rvert$) | $\Delta$(C/J) | ($\lvert\Delta C\rvert$/$\lvert\Delta J\rvert$) |
|---|---|---|---|---|---|
| **GCUSP** | 8.55 | 4.17 | 5.53 | -0.18 | 1.35 |
| **CARISMA** | 9.67 | 6.19 | 1.18 | -0.01 | 0.24 |
| **LCUSPH** | 11.22 | 4.48 | 5.37 | -0.23 | 1.50 |
| **UniGMA** | 9.82 | 3.56 | 5.20 | -0.16 | 1.00 |
| **LLIN** | 11.49 | 4.11 | 11.10 | -0.44 | 3.65 |

# Appendix H

# Experiment 4: Supplementary Data

*Well, art is art, isn't it? Still, on the other hand, water is water!*
*And east is east and west is west and if you take cranberries*
*and stew them like applesauce they taste much more like prunes than rhubarb does.*
*Now, uh... Now you tell me what you know.*

*Groucho Marx*

# Sample–Size Dependent Parameters

| Sample Size | LG to z–score scaling factor | 95 per cent confidence interval |
|---|---|---|
| **8** | 0.7761 | ±0.49 |
| **13** | 0.7094 | ±0.38 |
| **17** | 0.6811 | ±0.34 |
| **24** | 0.6515 | ±0.28 |
| **39** | 0.6195 | ±0.22 |
| **51** | 0.6055 | ±0.19 |

# Pleasantness Results

## *Category Judgement Pleasantness Scores*

| Image | GCUSP | CARISMA | SLIN | CLLIN | LLIN | DEF | TRIA | N |
|---|---|---|---|---|---|---|---|---|
| **Overall (3)** | 2.57 | 2.55 | 2.40 | 2.21 | 1.93 | 1.41 | 1.38 | 51 |
| **MUS** | 2.31 | 2.63 | 2.01 | 2.29 | 2.86 | 0.60 | 1.20 | 17 |
| **NAT** | 2.52 | 2.92 | 2.51 | 2.57 | 2.35 | 1.24 | 1.64 | 17 |
| **SKI** | 3.06 | 2.23 | 2.66 | 2.01 | 1.02 | 2.36 | 1.37 | 17 |

## *Category Judgement Pleasantness Categories*

| Image | GCUSP | CARISMA | SLIN | CLLIN | LLIN | DEF | TRIA | N |
|---|---|---|---|---|---|---|---|---|
| **Overall (3)** | 3 | 3 | 3 | 4 | 4 | 5 | 5 | 51 |
| **MUS** | 3 | 3 | 4 | 3 | 3 | 5 | 4 | 17 |
| **NAT** | 3 | 3 | 3 | 3 | 3 | 4 | 4 | 17 |
| **SKI** | 2 | 3 | 3 | 4 | 5 | 3 | 4 | 17 |

## *Inter–Observer Variance (CJ)*

| Image | Mean % difference | Max. % difference |
|---|---|---|
| **MUS** | 0.22 | 0.31 |
| **NAT** | 0.23 | 0.35 |
| **SKI** | 0.22 | 0.31 |

## *Pair Comparison Pleasantness Scores*

| Image | GCUSP | CARISMA | SLIN | CLLIN | LLIN | DEF | TRIA | N |
|---|---|---|---|---|---|---|---|---|
| **Overall (3)** | 0.20 | 0.58 | 0.15 | 0.29 | -0.12 | -0.54 | -0.57 | 24 |
| **MUS** | 0.17 | 0.56 | -0.06 | 0.52 | 0.74 | -1.55 | -0.37 | 8 |
| **NAT** | -0.12 | 1.30 | -0.22 | 0.39 | -0.34 | -0.72 | -0.30 | 8 |
| **SKI** | 0.73 | 0.46 | 0.88 | 0.15 | -0.89 | 0.18 | -1.51 | 8 |

## *Inter–Observer Variance (PC)*

| Image | Mean Stdev. | Max. Stdev. |
|---|---|---|
| **MUS** | 0.24 | 0.38 |
| **NAT** | 0.20 | 0.44 |
| **SKI** | 0.20 | 0.28 |

# Accuracy Results

## *Pair Comparison Accuracy Scores*

| Image | GCUSP | CARISMA | SLIN | CLLIN | LLIN | DEF | TRIA | N |
|---|---|---|---|---|---|---|---|---|
| **Overall (3)** | 0.55 | 0.81 | 0.26 | 0.60 | 0.51 | -1.31 | -1.43 | 39 |
| **MUS** | 0.51 | 0.96 | -0.29 | 1.20 | 1.16 | -1.93 | -1.60 | 13 |
| **NAT** | 0.28 | 1.70 | 0.26 | 1.16 | -0.28 | -1.95 | -1.16 | 13 |
| **SKI** | 0.85 | 0.37 | 0.66 | -0.14 | 0.61 | -0.65 | -1.70 | 13 |

Note, that these accuracy results are a subset of the results of Experiment 2 and that the same inter–observer variance values apply.